Università degli studi di Genova

Doctorate in Sciences and Technologies of Chemistry and Materials

Curriculum: Chemical Sciences and Technologies

(XXXVI cycle)

Crystallization of recycled polyolefin blends: molecular characterization and surface nucleation

Magdalena Góra

Tutors: Prof. Dario Cavallo and Dr. Andreas Albrecht

Thesis defense day: 26 March 2024

Acknowledgements

A PhD is always a collaborative endeavor, especially when it is part of an international, multi-institutional research project. In my case, it was certainly shaped by the unwavering support of numerous individuals.

First and foremost, I am grateful to my supervisors, Dario Cavallo and Andreas Albrecht. Their constant direction and assistance throughout the REPOL EID project have been invaluable. This thesis and investigation could not have been completed without their thoughtful suggestions and support.

I also want to thank my laboratory colleagues, Wei, Seif, and Enrico, as well as my University and Borealis desk peers, Andrea and Sebastian, for making every day better. I am furthermore thankful to Marlena, Kasia, Vishal, Juan, Raquel, Christopher and the rest of "the Genova team" for making my days in Genova far more interesting than they could have been. Thank you for all the hikes, BBQs, support and talks about our PhDs and beyond. A special thanks to Bianka and Emilia for guiding me in various aspects of life, for your support and for believing in me.

Acknowledgements are also due to all the individuals involved in the REPOL project, particularly Davide Tranchida, Vitor Barroso, Susanne Kahlen, Alejandro Müller and Mónica Moreno. I appreciate their dedication, not only in securing funding but also in actively contributing to the project. Here, I would like to express my appreciation for the support I received during my three-year doctoral research, sponsored by the European Union. This research endeavor was made possible through the Marie Skłodowska-Curie scholarship.

Thanks to Stefanie, Gudrun, Pia, Lili and Floran at Borealis Linz for the enjoyable conversations and for making me feel like a valued member of the team. Special acknowledgements to Polish colleagues - Ania, Karolina, Oskar, Ewelina and Martyna - for insightful coffee breaks and discussions.

Last but not least, heartfelt thanks to my family members in Austria and Poland. Your enduring positivity and support have been crucial. Dominic, your ability to bring a smile to my face during challenging times is deeply appreciated.

This PhD would not have been possible without all of you. Your encouragement, honest criticism and simply being there for me meant everything. Thank you so much, everyone.

Table of contents

1 SUMMARY AND OUTLINE

1.1 Processing-structure-properties relationship

The intricate interplay of processing-structure-properties in recycled polyolefin blends underscores the complexity of their lifecycle, from synthesis to their eventual application. Figure 1.1–1 illustrates the schematic connection between feedstock, molecular structure, processing and crystallization and the resulting properties.

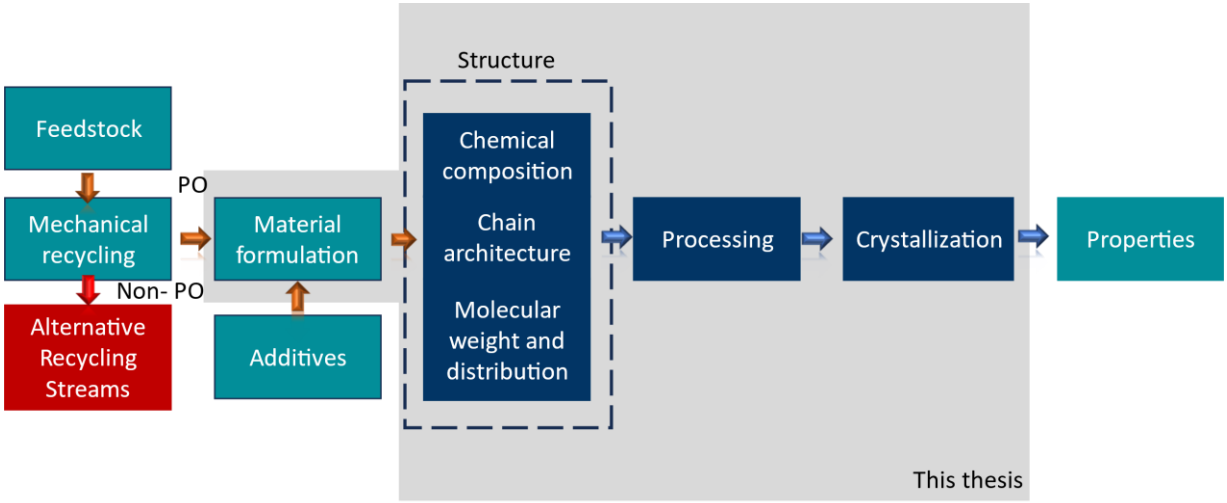

Figure 1.1–1 Flow chart describing the process-structure-properties relationship in recycled polyolefin blends.

Recent research has concentrated on identifying key parameters influencing these relationships, with a special focus on recycled polymers. In an era prioritizing sustainability, recycled polyolefins, derived from cost-effective and widely available monomers, have emerged as a sustainable choice for various industrial and consumer applications[1]. Their utilization would be particularly relevant in sectors like packaging, construction and automotive, where the balance of durability and recyclability is crucial. However, understanding the process-properties relationship in these recycled materials, especially considering their molecular heterogeneities, remains challenging. Deciphering these complexities is essential for customizing the properties of recycled polyolefins to suit specific applications. The measurement of these molecular heterogeneities is central to developing structure-property relationships, elucidating the material formulation and enhancing processing-property correlations. The performance of polyolefins in real-world applications is heavily dependent on these molecular variations. As a result, there is an increasing demand for

reliable, precise and inexpensive ways to examine the microstructure of recycled polyolefin blends, which aligns with the desire to use them in more demanding applications with targeted architectures and the best properties.

1.2 Advancements in polyolefin technology: Historical perspectives

The history of polyethylene and polypropylene can be traced back to the early 20th century, when chemists first discovered the possibility of transforming simple hydrocarbons into complex macromolecules. However, it was not until the 1930s and 1950s that these polymers were successfully synthesized and commercialized by different researchers and companies around the world[2–4].

Polyethylene was the first polyolefin to be discovered and produced. In 1898, the German chemist Hans von Pechmann accidentally obtained a waxy substance by heating diazomethane, which he called polymethylene[5,6]. However, he did not pursue further studies on this material. In 1933, two British chemists, Reginald Gibson and Eric Fawcett, working at Imperial Chemical Industries (ICI), repeated von Pechmann's experiment and obtained a similar substance, which they analyzed and identified as polyethylene. They also found that the polymer could be molded into various shapes by applying heat and pressure. However, they did not realize the potential of their discovery[7–10].

The breakthrough in polyethylene production came in 1935, when another British chemist, Michael Perrin, also working at ICI, developed a high-pressure process that could produce large quantities of polyethylene. This process involved the polymerization of ethylene gas under pressures of ~50 to 120 MPa and temperatures of 150 to 250°C, using oxygen or peroxide as initiators. The resulting polymer was a low-density polyethylene (LDPE), which had a highly branched structure and a melting point of about 120°C[10]. Polyethylene was used by the Allies for the insulation of radar cables, as it had excellent electrical and thermal properties, as well as resistance to moisture and chemicals[11]. After the war, polyethylene became widely available for civilian applications, such as packaging and film[12].

In the 1950s, two new processes for polyethylene production were developed, which led to the creation of different types of polyethylene with improved properties. The first process was the Ziegler-Natta process, named after the German chemist Karl Ziegler and the Italian chemist Giulio Natta. They both discovered the use of transition metal catalysts, such as titanium and chromium, for the polymerization of polyethylene. Karl Ziegler used solid $TiCl_3$,

for polymerization of polypropylene Giulio Natta used $TiCl_4$[13–16]. The process operated at low pressures of ~101.3 kPa and temperatures of 50 to 70 °C, and produced a high-density polyethylene (HDPE), which had a linear structure and a melting point of about 135 °C. HDPE had higher strength, stiffness, and hardness than LDPE, and was suitable for applications such as bottles, containers, and pipes[17].

The second process was the Phillips process, named after the Phillips Petroleum Company, where two American chemists, J. Paul Hogan and Robert L. Banks, discovered a new catalyst for the polymerization of ethylene in 1951[18]. The catalyst was based on chromium oxide supported on silica, and it operated at moderate pressure in the range 0.7 to 3.4 MPa and temperatures of 65 to 230 °C. The resulting polymer was also a high-density polyethylene (HDPE), but it had a broader molecular weight distribution and a lower degree of crystallinity than the Ziegler-Natta HDPE. The Phillips HDPE had better processability and environmental stress cracking resistance than the Ziegler-Natta HDPE, and was suitable for applications such as film, injection molding and blow molding [13,19,20].

Polypropylene was the second polyolefin to be discovered and produced. In 1954, Giulio Natta and his assistant Paolo Chini, working in association with the Montecatini Company (now LyondellBasell), discovered the polymerization of propylene using a Ziegler-type catalyst based on titanium[21,22]. They obtained a crystalline polypropylene, which had an isotactic structure, meaning that all the methyl groups attached to the carbon backbone were oriented on the same side with respect to the plane containing the chain. This gave the polymer a high degree of crystallinity and a melting point of about 165 °C. Isotactic polypropylene had higher strength, stiffness, and heat resistance than polyethylene, and was suitable for applications such as fibers, films, and pipes[7]. In 1963, Karl Ziegler and Giulio Natta were jointly awarded the Nobel Prize in Chemistry for their respective contributions to the development of polyethylene (PE) and polypropylene (PP), pioneering advancements that revolutionized the field of polymer chemistry and the plastics industry[23].

In 1957, Karl Ziegler and Erhard Holzkamp, working at the Max Planck Institute for Coal Research, discovered another type of polypropylene, which had an atactic structure, meaning that the methyl groups attached to the carbon backbone were randomly oriented [24]. This gave the polymer a low degree of crystallinity and a soft and rubbery texture[7]. Atactic polypropylene was not useful as a plastic, but it was a valuable precursor for the production of propylene oxide, a chemical intermediate for the synthesis of other polymers, such as polyurethanes and polyesters.

In 1964, Natta and his co-workers discovered a third type of polypropylene, which had a syndiotactic structure, meaning that the methyl groups attached to the carbon backbone were oriented alternately on opposite sides[25]. This gave the polymer a high degree of stereoregularity and a melting point of about 130 °C. Syndiotactic polypropylene had higher heat resistance and transparency than isotactic polypropylene and was suitable for applications such as packaging, medical devices and optical discs. However, syndiotactic polypropylene was not commercially available until the 1990s, when new catalysts based on metallocenes were developed[26].

1.3 Characterization of polyolefins

Polymer characterization is an essential analytical approach that explores the intricate properties and structures of polymers, with a special focus on their molecular composition [27]. This examination is crucial in understanding the relationship between a polymer's molecular structure and its macroscopic behavior, which is key to advancing current applications and pioneering new ones[28]. Among the diverse array of techniques employed for polymer characterization, methods such as molecular weight determination[29], molecular and structural characterization[30–32], morphology analysis[33] and thermal analysis[34] stand out for their ability to provide a comprehensive understanding of polymer properties.

When it comes to polyolefins—a distinct subgroup of polymers—the characterization principles remain consistent but are tailored to address the unique properties of polyolefins [35,36]. Known for their versatile applications, polyolefins demand a nuanced analysis to fully grasp their behavior under a variety of conditions [37–40]. This is particularly true for polyolefin blends, which may combine different polyolefins or integrate them with other polymers[41]. The characterization of these blends is pivotal, focusing on aspects like component types, composition and processing conditions[33]. Techniques specific to polyolefin blends include, but are not limited to, thermal analysis, rheological analysis, mechanical testing and structural and morphological analysis[36,42].

Polyolefin blends, especially when recycled, present unique challenges in characterization. These recycled blends frequently incorporate a mixture of additives, fillers, and stabilizers, which introduces additional complexity[43–45]. Advanced characterization techniques are essential in navigating this complexity effectively. For example, spectroscopic analysis like fourier-transform infrared (FTIR)[46] and nuclear magnetic resonance (NMR)[47] spectroscopy are crucial for identifying the chemical composition of blends. Thermal analysis

methods, such as differential scanning calorimetry (DSC) and thermogravimetric analysis (TGA)[48], provide insights into thermal transitions of blend components and thermal stability, respectively. Rheological assessments offer deep insights into the flow behavior of polymer blends, crucial for processing and end-use performance, particularly in recycled materials where property variability is increased[49–51]. Recycling processes can introduce changes in molecular weight and bring contaminants, affecting the blends' properties[52,53]. Techniques like gel permeation chromatography (GPC) and mechanical testing are vital for assessing the molecular weight distribution and durability of recycled blends[54]. Temperature rising elution fractionation (TREF) and successive self-nucleation and annealing (SSA) have been recognized for their specialized applications in solution and thermal fractionation of polyolefins[55].

In conclusion, characterizing mixed and recycled polyolefin blends is a multifaceted and essential area of study. It addresses complexities absent in virgin polymers, requiring a range of methodologies and analytical techniques to optimize these blends' properties and applications.

1.4 Processing of polyolefins

Polyolefins, including polypropylene (PP) and polyethylene (PE), are predominantly processed in their molten state, utilizing specific flows and temperature gradients. The method utilized here aimed to understand the interactions between PP and PE in the blend. Designing a manufacturing process for polyolefins, particularly recycled blends, requires a thorough understanding of molecular weight (M_w), molecular weight distribution (MWD), interaction between blend components and their crystallization behavior. This thesis looks into the molecular characterization of various grades of PP and PE. Furthermore, the study delves into the intricacies of surface nucleation in polyolefin blends, specifically the impact of self-nucleated PP on different PE grades.

Recent advancements have demonstrated that cooling rate, particularly ballistic cooling, during processing significantly alters the crystallization rate in recycled polyolefin blends[56]. An acceleration of the kinetics of one phase can be found, due to the formation of nuclei of the molten phase on top of the previously crystallized phase[57], but also the rate of crystallization of blend components is different[56], which consequently changes the material's final morphology, impacting its mechanical, optical and transport properties[58]. Importantly, the final

morphology is heavily influenced by nuclei formed during the early stages of crystallization. These precursors, while initially showing an undetectable degree of crystallinity, possess a degree of order and can become spontaneously growing crystallites under specific conditions[59].

Heterogeneous nucleation is especially pertinent in recycled blends. In recycled polyolefin blends, contaminants and degradation products can act as nucleation or anti-nucleation agents, due to the transfer of heterogeneously nucleating impurities between the blend's components. In these blends, morphologies resulting from static interactions can significantly influence the material's properties[60]. In mechanically recycled melt-mixed polypropylene, nucleation is critical. The slower nucleation rate often necessitates the use of nucleating agents (NAs). These NAs not only affect polymer morphology but also influence stress distribution during loading[61].

Recent studies on the effects of different PE grades in polyolefin mixed blends have shown how blend composition, processing conditions and the presence of NAs can influence material properties[57,62,63]. These insights are pivotal for optimizing the mechanical recycling process, tailoring it to specific applications, and enhancing the performance of recycled polyolefin products.

1.5 Aim of the thesis

The aim of this thesis is to develop and refine methodologies for the enhanced characterization and fractionation of recycled polyolefin blends, focusing on the impact of molecular characteristics and processing conditions (surface nucleation) on their crystallization behaviors. This objective is pursued by examining three key aspects:

1) the application of fast successive self-nucleation and annealing (SSA) thermal fractionation protocol for rapid and efficient characterization of polyolefin blends, significantly reducing analysis time while maintaining accuracy;

2) advancing the precision of cross fractionation chromatography (TREFxGPC) for accurate determination of polyethylene and polypropylene content in complex blends and recyclates; and

3) exploring surface-enhanced nucleation in immiscible polypropylene and polyethylene blends, particularly focusing on the effects of polyethylene chain regularity on crystallization dynamics.

These studies collectively aim to provide a comprehensive understanding of the crystallization behavior in recycled polyolefin blends and establish methodologies that can be applied for the optimization of recycled polyolefin materials for various applications.

1.6 Outline of the thesis

The dissertation is divided into the following chapters:

Chapter 1 introduces the relationship between processing, structure, and properties in recycled polyolefin blends, emphasizing the need for precise methods to assess their microstructure.

A brief literature review is given in **Chapter 2**, focusing on molecular characterization techniques and interactions between the blend's components in processing conditions.

Chapters 3 and **4** focus on polyolefin characterization utilizing advanced approaches such as successive self-nucleation and annealing (SSA) and TREFxGPC, respectively. These techniques are crucial for understanding the complex chemical compositions and crystallization behaviors of polyolefins, particularly from recycling streams. The chapters also delve into additional characterization approaches, broadening the analytical scope.

Chapter 5 covers the topic of surface nucleation and polyolefin crystallization, emphasizing the importance of correctly assessing the molecular composition of the polyolefin blend for advancing polyolefin recycling and processing technologies.

In **Chapter 6**, the research findings of the work reported in Chapters 3, 4 and 5 are given in a concise summary and recommendations for future work are presented.

2 INTRODUCTION

2.1 Advancements in polyolefin technology

By 2019, global plastic production reached 368 million tons, with polyolefins, derived from vinyl hydrocarbons (C_nH_{2n}), making up roughly one-third to one-half of the total production. These statistics highlight growth and demand for plastics, underscored by a report from PlasticsEurope[64,65]. The most common polyolefins are polyethylene and polypropylene, made mostly or entirely from ethylene and propylene monomers. This can be attributed to their generally low cost in combination with a wide variety of chemical and mechanical materials' properties. They can be adapted to meet a spectrum of application requirements such as rigid applications like pipes and containers made from high-density polyethylene (HDPE), or flexible ones, like films and coatings made from low-density polyethylene (LDPE)[66–73].

As the synthesis of polyolefins advances, it now faces more and more complex challenges when it comes to their recycling, thanks to the greater material variety in recyclates. Incorporating recycled polyolefins introduces issues like contaminant management, control of molecular weight distribution and microstructure[74,75]. The ongoing research to comprehend crystallization behavior, thermal properties and processability of recycled blends is crucial for a sustainable approach to polymer science[55,76–83]. The subsequent section will delve into the nuanced complexities and innovative techniques within polyolefin recycling, specifically mechanical recycling of polyolefins.

2.2 Recycling of polyolefin materials

Global recycling efforts, including polyolefin recovery, are driven by a variety of factors, such as a more efficient use of natural resources, reducing the dependency on raw material imports, reducing waste that ends up in the environment[84]. The more efficient use of natural resources furthermore reduces the carbon dioxide emissions related to the use of this materials. The recycling efforts are therefore integral to the international drive for climate neutrality. The European Union champions the circular economy within its broader strategy to reach net-zero greenhouse gas emissions by 2050, aligning with the Paris Agreement and actualized through the European Green Deal[85,86]. The circular economy seeks to minimize CO_2 emissions by promoting the reuse and recycling of polyolefins, crucial in global environmental protection efforts[1].

Early scientific studies, notably one by J. Murray Mitchell Jr., accurately forecasted climate trends[87,88], including the rise in CO_2 levels and global temperatures. These insights highlight the critical need for the clear and consistent application of scientific data in policy formulation, underscoring sustainable material management's role. Given their environmental footprint associated with large-scale use, polyolefins have come to the forefront of the sustainability agenda[1]. While their uniformity and chemical resistance suggest ideal recyclability, their diverse compositions designed for specific uses add complexity to the process[89]. There are several recycling methods, including mechanical recycling and solvent-assisted recycling, among different recycling schemes. Recycling technologies for polyolefins are broadly categorized into primary (re-extrusion), secondary (mechanical), tertiary (chemical), and quaternary (energy recovery) schemes, encompassing a wide range of processes and methodologies tailored to the specific properties and applications of these polymers[90].

Mechanical recycling, the predominant method for polyolefin reprocessing, involves grinding, melting, and re-pelletizing[91–95]. While energy-efficient, it often leads to polymer degradation, limiting the end-product's applications. Advanced techniques and digitalization have evolved mechanical recycling, enhancing precision and reducing contamination. However, despite these advancements, mechanically recycled materials can suffer compromised properties due to thermomechanical deterioration[96,97] and waste heterogeneity[98]. The benefits and drawbacks of mechanical recycling are well-documented, highlighting both its role in reducing emissions and the challenges it faces, such as property degradation and economic feasibility. Solvent-assisted recycling emerges as an advanced alternative capable of recovering plastics with near-virgin qualities, potentially suitable for high-end applications such as food packaging and medical devices. Research indicates that this process can yield plastics with purity and properties comparable to virgin materials, essential for a closed-loop plastic system[99,100]. The digital integration into recycling, known as "smart recycling" is poised to transform the industry. Innovations such as sensors, smart bins (connected by the Internet of Things (IoT)) and artificial intelligence (AI) algorithms could further optimize recycling processes, potentially reducing contamination rates significantly[101–103].

The general environmental impact of plastics is context-dependent[104]. For example, the use of plastic bags can result in lower environmental impacts than paper or cotton bags when considering the full life cycle[105,106]. However, the increase in plastic production has not been

paralleled by advancements in waste management. By 2015, only a fraction of plastic waste was recycled, with the rest contributing to landfill accumulation or incineration, indicating a need for improved global waste management practices[107].

2.2.1 Mechanical recycling

It's been reported that mechanical recycling can conserve up to 60 MJ/kg of energy[108] when compared to producing virgin plastics and reduce CO_2 emissions by as much as 20%. Despite this, the market for mechanically recycled polyolefins is sometimes constrained by the quality of the recyclate. The European Union has set ambitious recycling targets, pushing for 50% of all plastic packaging to be recycled by 2025, which is driving innovation in the sector. Mechanical recycling employs a physical methodology to break polymer products down into smaller pieces or flakes, without altering their basic molecular structure. This process unfolds through several key stages, each critical to the integrity and success of recycling:

A. Pre-sorting: Starting with the collecting of recyclable materials, this stage focuses on sorting by polymer type and color.
B. Shredding: After pre-sorting, plastics are shredded into flakes. This phase is critical in lowering the size of the materials, making them easier to handle and treat in later steps.
C. Sorting: After shredding, a further sophisticated sorting process occurs. This stage employs innovative technology to further separate polymers.
D. Washing: After sorting, the plastics are washed to eliminate any leftover contaminants such as dirt, food remnants, or labels. This cleaning phase is critical to ensuring the quality of the recycled material.
E. Sorting: A last sorting step can assure the plastic material is pure and homogeneous. This stage fine-tunes the sorting process by removing any impurity or non-ideal materials missed in previous stages.
F. Extrusion: After cleaning and sorting, polymers are melted and extruded. This phase converts the plastics into a new form, such as pellets or fibers, which can then be used to manufacture new items.

The first generation of mechanical recycling revealed inherent limitations, specifically material quality, prompting the development of advanced mechanical recycling techniques[94,109–111]. These advancements primarily concentrate on enhancing the efficiency of key stages such as sorting, washing, purification and compounding in recycling processes. The integration of digital technologies in these stages facilitates more accurate and efficient operations. As a result, this leads to the production of recyclates and compounds characterized by reduced smell, lighter colors, consistent quality and superior mechanical properties[109,112,113]. Figure 2.2.1–1 depicts examples of current research and development activities in mechanical recycling compared to the state-of-the-art[109].

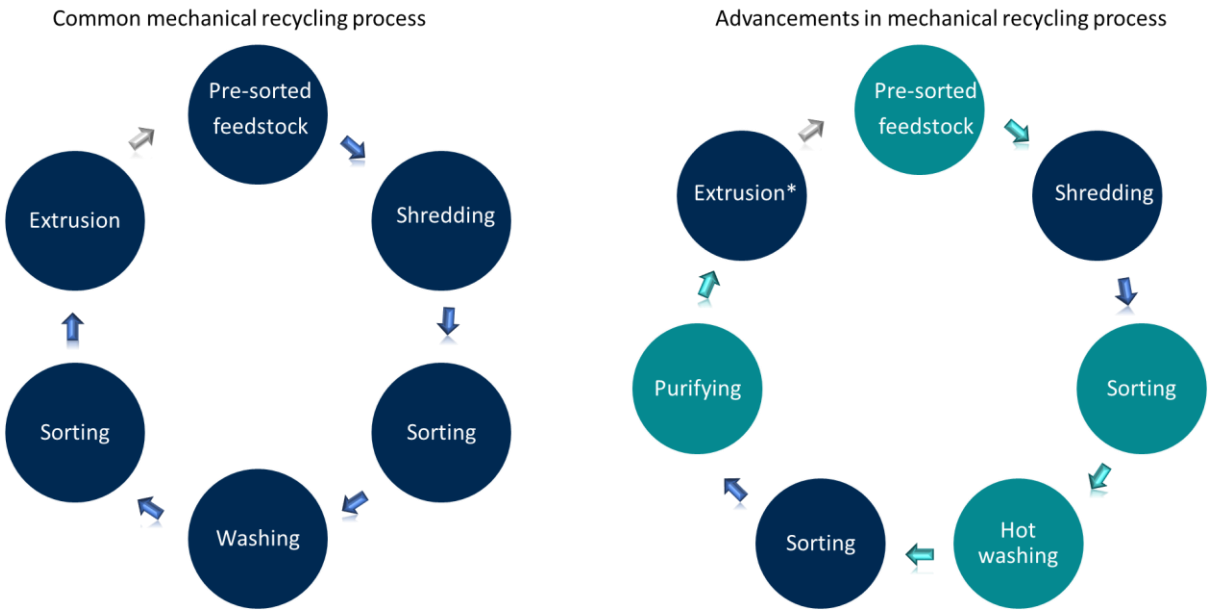

Figure 2.2.1–1 On the left, a step-by-step representation of the common mechanical recycling process is shown, while on the right, additional steps integrated into the conventional mechanical recycling process are depicted. Newly introduced steps are highlighted in light blue, contrasting with the existing process steps depicted in dark blue.

** - Additional changes are in the compounding step.*

Conventional sorting mechanisms like flotation and optical sorting may not suffice due to the similar densities and chemical compositions of these polymers. For instance, PP caps often end up with PE bottles, necessitating manual sorting or advanced automated systems that use near-infrared (NIR) technology to differentiate materials based on their specific infrared signature. However, advanced sorting can be costly. The industry is seeing innovations for example AMP Robotics, which uses AI to identify and sort recyclables more accurately and at a lower cost than traditional systems[114]. The shredding stage reduces the size of plastic waste to prepare it for reprocessing. One of the main challenges here is the potential for material

loss[115]. The current research focuses on minimizing this loss by optimizing shredder blade designs and configurations. Companies like WEIMA have developed shredders with customizable screens that control particle size, ensuring consistent quality in the output[116]. The washing stage aims to remove contaminants from the plastic waste. Contaminants often include food residue, adhesives and paper labels, which can adversely affect the quality of the recycled material. The industry has been exploring enzymatic detergents that can target and break down specific contaminants more effectively than conventional washes, thereby improving the purity of the recyclate. For example, a study has explored the use of fungi to degrade adhesives such as those used in labels from PP waste[117]. During extrusion, plastic flakes are melted and formed into pellets. This stage is critical as it can introduce thermal and mechanical stress, leading to polymer degradation. Often melt filtration is employed to remove any remaining contaminants. However, standard screens can clog, leading to downtime and increased costs. Technologies like Ettlinger's continuous melt filters operate under high pressure and can handle a higher level of contamination[118]. Another technology offered by Erema uses the laserfilter, which works by filtering contaminated plastic melt through two laser-bored screen discs arranged in parallel. A rotating scraper disc between these screens removes contaminants immediately and conveys them to a discharge system[119]. Thermal degradation is a persistent issue in mechanical recycling. To combat this, additives like stabilizers and chain extenders are added[120]. Companies such as Riverdale Global specialize in additives that can enhance the performance of recycled polyolefins, improving their resistance to degradation during processing. Among the notable advancements in the recycling industry, the Danish company Plastix is making significant contributions. Plastix specializes in recycling post-use maritime fibers, such as fishing nets and ropes, transforming them into high-quality Green Plastics. This innovative approach not only repurposes waste materials but also helps reduce the reliance on virgin plastics by 58%, demonstrating a practical application of circular economy principles. Currently, Plastix is actively engaged in the market, offering these recycled products to various industries[121].

The research is ongoing to address the inherent limitations of mechanical recycling. Studies are looking into improving the crystallinity of recycled polymers, which is a key determinant of their mechanical properties. Organizations like the National Renewable Energy Laboratory (NREL) in the United States are actively developing chemical recycling methods, specifically, they catalytically depolymerize plastic packaging[122]. This enables the repositioning of well-characterized, post-consumer recycled materials into new market

segments, extending beyond traditional low-grade applications such as flowerpots and waste containers[123–125]. However, it is crucial to note that advanced characterization methods, while providing detailed insights into polymer structure and composition, require significant financial investments[126]. This often makes them unfeasible for cost-sensitive recycling facilities that predominantly handle polyolefins. Consequently, these facilities typically resort to more traditional, economically viable quality control methods. Although these methods are less costly, they may not offer the comprehensive molecular insights of advanced techniques but are considered sufficient for basic processing requirements. This is demonstrated in Table 2.2.2–1's SWOT analysis, which compares the cost and value of mechanical recycling. This economic constraint significantly impacts the ability to accurately evaluate the degree of crystallinity and the distribution of crystalline and amorphous phases in recycled polyolefin blends [127]. The degree of crystallinity is a critical factor influencing the thermal and mechanical properties of polymers, especially in blends that include various types of polyethylene (PE) — such as high-density polyethylene (HDPE), low-density polyethylene (LDPE), linear low-density polyethylene (LLDPE), and medium-density polyethylene (MDPE) — as well as polypropylene (PP), including nucleated PP variants [128]. These polymers exhibit distinct crystalline behaviors due to differences in their molecular structures, which in turn affect the blend's overall properties. The varying crystallinity levels among these polymers can lead to challenges in processing and inconsistency in the end-use properties of the recycled material.

In light of these considerations, future research should focus on strategies to enhance the compatibility and interfacial adhesion within these diverse polyolefin blends[129]. Developing cost-effective and efficient compatibilization methods and recycling techniques is essential[33,83,130]. Such advancements would not only help in optimizing the mechanical and thermal performance of these complex blends but also in expanding their range of applications, overcoming the limitations imposed by economic and technical constraints[131,132].

Table 2.2.2–1 SWOT analysis of mechanical recycling of polyolefins benefits and drawbacks of mechanical recycling[133].

Strengths	**Weaknesses**
Energy Efficiency: lower energy use than producing new polyolefins.	Quality Degradation: recycled polyolefins may have inferior properties.
Environmental Impact: contributes to waste reduction and lower emissions.	Technical Limitations: difficulties in sorting and processing can lead to inefficiency.
Resource Conservation: less reliance on virgin resources.	Economic Challenges: costs of sorting and decontamination can be prohibitive.
Economic Growth: potential for new job creation within the recycling industry.	Limited Lifespan: polyolefins can only be recycled a finite number of times.
Scalability: adaptable existing infrastructure for recycling processes.	Market Acceptance: perceived lower quality can affect demand.
Opportunities	**Threats**
Technological Innovation: advances could improve recycling efficiency and output quality.	Raw Material Price Fluctuations: makes recycled polyolefins less competitive.
Legislative Support: policies incentivizing recycling can enhance market dynamics.	Contamination: increased contamination complicates recycling processes.
Consumer Trends: rising demand for sustainable products can increase market share.	Disparity in Global Waste Management: affects the consistency of recycled material supply.
Corporate Responsibility: company commitments to sustainability can drive recycling.	Alternative Materials: development of new materials could decrease polyolefin recycling demand.
Circular Economy Focus: mechanical recycling is essential to this economic model.	Public Perception: negative views on recycled products could limit their use.

*chain scission and crosslinking are possible if reprocessing done under uncontrolled conditions

2.3 Characterization techniques

Beyond providing a better understanding of the structure and behavior of polymers, characterization has practical significance in processing, regulation and standardization of polymers[134,135]. Polyolefin characterization is a challenging operation that requires a multi-modal analytical approach for understanding the material's complex molecular and microscopic architectures[136]. This is especially true for recycled polyolefins, where the material's past might add complications. Concurrent with these theoretical advancements, there was a growing impetus for developing analytical techniques capable of characterizing these complex macromolecules[137]. This led to the emergence of thermal and solution fractionation methods, each addressing different aspects of polymer behavior and structure.

Nuclear magnetic resonance (NMR) and fourier transform infrared spectroscopy (FTIR) are pivotal for chemical compositional analysis[138]. While FTIR has seen recent advancements extending its capabilities to quantitative analysis through the use of calibration curves generated from model blends, NMR, traditionally known for its qualitative insights into molecular structures, also offers quantitative applications[139]. However, NMR typically relies on direct spectral data analysis rather than external calibration curves. These methods are generally not adapted to elucidating structure-property relationships, which are crucial for understanding material performance[140]. For NMR, a significant limitation is its cost-effectiveness. NMR spectroscopy is often prohibitively expensive, making it less feasible for routine analysis in many contexts. Furthermore, NMR tends to provide average results regarding the chemical composition of materials. On the other hand, FTIR is more cost-effective compared to NMR, making it accessible for a wider range of applications. However, like NMR, FTIR also typically yields average information about the material's composition. It fails to offer detailed insights into the distribution of chemical components within the material. This limitation is crucial because the heterogeneity in material composition can significantly influence its macroscopic properties and understanding this distribution is key to establishing reliable structure-property relationships. In the domain of thermal analysis[141], the introduction of differential scanning calorimetry (DSC) in the 1960s marked a significant milestone[142]. DSC provided a method for precise thermal characterization of polymers, enabling the analysis of melting and crystallization behaviors, which are crucial for understanding polymer morphology and physical properties[143]. DSC serves as a complementary tool, providing critical data on thermal transitions such as melting and crystallization temperatures. Its widespread

availability makes it a staple in analytical laboratories[144]. For a nuanced understanding of the crystallization behavior, critical in determining the mechanical and thermal properties of recycled materials, advanced thermal fractionation methods are employed[145]. Techniques such as temperature rising elution fractionation (TREF) and crystallization analysis fractionation (CRYSTAF) are specialized for polyolefin characterization, offering detailed insights into their crystallizability and compositional distribution[146]. While highly informative, these methods are often time-consuming and require the use of solvents and sample pre-treatment[147]. Alternatively, techniques like step crystallization (SC) and successive self-nucleation and annealing (SSA) are employed for similar purposes but offer certain advantages[148]. Performed using DSC on bulk samples, SC and SSA are solvent-free, which reduces both environmental impact and cost[149]. SSA, in particular, is notable for its efficiency in fractionating molecules through dynamic crystallization ramps, providing a faster alternative to the more elaborate TREF and CRYSTAF methods[150]. Alongside chromatography advancements, gel permeation chromatography (GPC) has become crucial in polymer analysis. Originally for molecular weight and size separation, GPC now offers nuanced insights into polymer structures, including molar mass distribution and chain branching. Its role is pivotal in characterizing recycled materials, aiding sustainability efforts[151,152].

In summary, the comprehensive characterization of polyolefins, especially recycled variants, requires an integrated approach employing multiple analytical techniques. Each method provides unique but partial insights, and their collective interpretation is indispensable for advancing both academic research and industrial applications. The progression from theoretical understanding to practical analytical techniques highlights the dynamic interplay between conceptual advancements and technological innovations in polymer science. Thermal and solution fractionation emerged not merely as analytical methodologies but as pivotal tools that enabled a deeper understanding of the complexities inherent in polymer systems. This introduction aims to delineate this scientific trajectory, tracing the evolution of these techniques from their theoretical underpinnings to their practical applications in contemporary polymer analysis.

2.3.1 Thermal fractionation techniques based on crystallinity

Differential Scanning Calorimetry (DSC) technology effectively bridged the gap between theoretical understanding of polymer behavior and practical applications in materials engineering. DSC has since established itself as a critical tool in the arsenal of thermal analysis, playing a dual role in both quality control and advanced research settings[153,154].

The core strength of DSC lies in its capacity to precisely quantify enthalpy changes during phase transitions, such as crystallization and melting processes in polymers[155]. This capability is particularly crucial in the study of polyolefins, where DSC provides comprehensive insights into their thermal behavior and morphological characteristics[156]. By enabling a detailed analysis of phase transitions, DSC offers a window into the thermal history of these materials, contributing significantly to our understanding of their structural evolution and performance characteristics[157]. The continuous refinement of DSC methodologies and its integration with other analytical techniques have further enhanced its role in elucidating the complex nature of polymer systems.

Modern DSC techniques, including heat flux DSC and power compensation DSC, have significantly advanced in their capabilities, allowing for the identification of both endothermic and exothermic events during thermal cycling. The direct control of the rate of heating and controlled cooling has been instrumental in measuring a range of physical and chemical properties, such as melting transitions, crystallization temperatures and enthalpy of fusion and crystallization [158]. The continuous improvement and optimization of DSC, with the aid of technological innovations, have made it one of the most common and versatile techniques in material characterization. The introduction of modulated temperature DSC, has enabled to study deeply the chemical reactions, glass transitions and melting, due to the possibility of deconvolution of non-reversing and reversing heat flow and heat capacity[159–161]. DSC has not only sustained its historical significance but has also adapted to meet the demands of contemporary polymer science, making it an essential instrument for the in-depth study of polyolefins, especially in the context of recycling processes and material engineering[162].

The increasing complexity of polyolefin grades, driven by advancements in reactor technologies and polymer architecture, has necessitated a more detailed interpretation of Differential Scanning Calorimetry (DSC) data. Polypropylene (PP), for instance, can exist in

various grades, such as atactic, syndiotactic and isotactic, each with distinct thermal properties. Atactic PP is amorphous and exhibits a glass transition temperature (T_g) rather than crystallization (T_c) or melting temperatures (T_m). In contrast, syndiotactic and isotactic PP have different melting points, 165°C and 130°C, respectively. Polyethylene (PE) introduces another layer of complexity, characterized by distinct chain structures influenced by factors such as comonomer type and content (branching) and chain length. This variability results in a diverse range of densities and thermal properties with melting temperatures ranging from 106°C to 135°C[163], depending on the type of polyethylene. The interplay between these structural variations and material characteristics underscores the intricate nature of polyolefin analysis, highlighting the need for a comprehensive understanding of polymer architecture in interpreting DSC data.

The challenge of characterizing mixed materials is exacerbated by overlapping thermal transitions, especially in recycled blends[164]. This complicates quality monitoring, which is generally straightforward for neat materials. It is crucial to understand that melting temperature is influenced by the lamellar thickness, in turn, a function of molecular weight and chemical architecture, as described by the Thomson-Gibbs equation (1).

$$T_m = T_m^\circ \left(1 - \frac{2\sigma_e}{l\rho_c \Delta H_f^\circ}\right) \quad (1)$$

T_m – Melting temperature of the particle or crystallite [K].

T_m° – Equilibrium melting temperature of the bulk material [K].

σ_e – Surface free energy or interfacial energy of the particle or crystallite[$\frac{J}{m^2}$].

l – Thickness of the crystallite or particle [m].

ρ_c – Density of the crystalline phase [$\frac{g}{cm^3}$].

ΔH_f° – Heat of fusion per unit volume of the bulk material [$\frac{J}{g}$].

To address the complexities in characterizing polymers, particularly polyolefins, which arise from the distribution of polymeric chains with overlapping melting points, the successive self-nucleation and annealing (SSA) technique has been developed. The foundational concept of self-nucleation (SN), integral to SSA, originated from Keller et al.[165], who initially devised it to aid in the preparation of single crystals from solution. This concept was expanded upon by Fillon et al.[166], who employed differential scanning calorimetry (DSC) to advance the study

of self-nucleation. Building on this groundwork, the SSA technique was specifically designed and implemented by Müller et al. in 1997[167]. This innovative technique combined sequential self-nucleation and annealing steps applied to polymer specimens, a methodology distinct from previous thermal fractionation protocols. Notably, the acronym 'SSA' was first introduced in the publication by Müller et al. While earlier publications had reported designing thermal fractionation protocols similar to SSA[168,169], these did not incorporate the unique combination of self-nucleation and annealing steps that are central to the SSA technique.

In SSA, molecular segregation is achieved through a series of dynamic and isothermal steps. Initially, the sample undergoes a melting and cooling phase, followed by heating to a specific temperature or seeding temperature (T_s) that allows for partial melting. Subsequent crystallization leverages the self-nucleation of unmelted crystallites. This process is repeated with decreasing T_s values, each followed by an isothermal annealing phase for the remaining lamellae. The final heating run manifests the material's fractionation, a result of the preceding thermal protocol. This methodology has proven effective in molecular segregation, particularly in polyethylene[69–73] and later in polypropylene[175–177] .

The PE chain regularity can be represented by the value of the methylene sequence length (MSL), calculated from the melting point of the polyethylene grade. As melting temperatures of ethylene copolymers decrease with the increase in branch content but are independent of the branch length[178,179], it is convenient to consider this parameter. MSL could be calculated in relation to the change in melting temperature of polyethylene grade according to empirical relations such as the one reported in equation (2)[172,180,181].

$$MSL = \frac{2}{e^{\left(\frac{142.2}{T_m[K]} - 0.3451\right)} - 1} \tag{2}$$

Carmeli et al. were the first to apply SSA to complex recycled blends, successfully quantifying the composition of specific phases[55]. Recent advancements in SSA focus on the utilization of fast heating and cooling rates to reduce measurement time. Pijpers et al. proposed mass compensation to maintain data resolution when employing these rapid rates[182]. Varga et al. corroborated this by conducting experiments at constant rates, finding negligible differences in results when altering the final heating rate[183,184]. Lorenzo et al. extended this concept to hydrogenated polybutadiene, confirming its viability[181]. However, the case study presented in Chapter 4.1 explores the usage of the fast rates in complex systems, specifically focusing on recycled polyolefin blends, thereby filling a gap in existing studies.

The inherent rapid crystallization behavior of polyolefins, with PE crystallizing faster than PP, yet both crystallizing rather fast in comparison to other polymers, allows for the use of high heating and cooling rates in SSA. However, there is still a necessity to reduce the mass of the sample to compensate for the increased rates, thereby reducing the overall thermal fractionation time[181,185]. This is further explained by the graph in Figure 2.3.1–1.

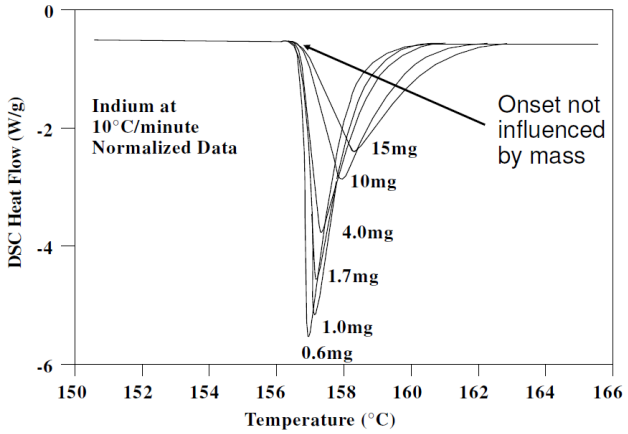

Figure 2.3.1–1 The principles of the loss of accuracy associated with a sample mass reduction is compensated by the increase in accuracy associated with the application of a higher rate [182].

2.3.2 Solution fractionation techniques based on crystallinity

The 1950s and 1960s were pivotal decades in polymer science, marked by a growing awareness of the need for techniques capable of separating polymers based on crystalline properties. This was driven by the understanding that crystallinity plays a crucial role in determining a polymer's functional attributes. TREF emerged as a robust technique, allowing for the study of polymers and significantly impacting both academic research and industrial applications. The key theoretical concepts underpinning TREF include solubility and crystallinity and fractionation process. TREF has since become a pivotal method for polyolefin separation, with its development attributed to Wild, who built upon the seminal work of Shirayama et al. and Desreux and Spiegels[186]. This technique has significantly advanced the field, offering a more precise and effective means of studying polymer crystallinity and composition[187]. Wild TREF operates on the thermodynamic principles governing selective precipitation and elution, utilizing a controlled temperature gradient to fractionate crystalline polymer chains[188].

Central to the TREF technique is the Flory–Huggins theory, which provides a fundamental understanding of the thermodynamics of polymer solutions. This theory is essential for understanding how polymers interact with solvents, a cornerstone of the TREF process[189]. It explains the behavior of polymer chains in solution, particularly how these interactions influence the crystallization and dissolution of polymers, which are key to TREF's fractionation capability[190].

The Flory–Huggins equation expresses the relationship between the equilibrium dissolution temperature of a polymer in a solvent and the melting temperature of the homopolymer. The equation takes into account the heat of fusion per repeating unit, the molar volumes of the homopolymer repeating unit and the diluent, and the polymer-solvent interaction parameter[191–193]. The equation (3) is as follows:

$$\frac{1}{T_m} - \frac{1}{T_m^\circ} = \left(\frac{R}{\Delta H_u}\right)\left(\frac{V_u}{V_1}\right)\left[-\frac{ln(V_2)}{x} + \left(1 - \frac{1}{x}\right)v_1 - \chi_1 {v_1}^2\right] \quad (3)$$

T_m – Melting temperature of the polymer in the presence of the solvent [K].

T_m° – Equilibrium melting temperature of the pure polymer [K].

ΔH_u – Heat of fusion per repeating unit of the polymer [$\frac{J}{mol}$].

V_u and V_1 – Molar volumes of the polymer repeating unit and the solvent, respectively [$\frac{m^3}{mol}$] or [$\frac{L}{mol}$].

v_1 and v_2 – Volume fractions of the polymer and the solvent, respectively[$-$].

x – Degree of polymerization of the polymer [$-$].

χ_1 – Polymer-solvent interaction parameter, a measure of the interaction between polymer chains and solvent molecules[$-$].

R – Universal gas constant [$\frac{J}{mol \cdot K}$].

Applying the Flory–Huggins theory to TREF involves understanding how variations in polymer features, such as molecular weight, comonomer content and chain branching, affect their solubility and crystallization behavior in a given solvent. This understanding is essential for optimizing TREF conditions, such as solvent choice, temperature range, cooling and heating rate, to achieve effective fractionation. The equation for the free energy of mixing in a polymer solution assumes a uniform distribution of solvent and polymer segments[192]. It accounts for the depression in the equilibrium dissolution temperature of the homopolymer due to the solvent's presence.

The TREF process involves two main cycles[194,195]:

1. Dissolution and Cooling Cycle: the sample is initially dissolved in a thermodynamically favorable solvent at high temperature. The solution is then subjected to a slow cooling process without flow, allowing polymer fractionation based on decreasing crystallinity.
2. Elution Cycle: in this stage, fresh solvent is pumped through the column while gradually raising the temperature. This results in the dissolution of polymer fractions with increasing crystallinity (i.e., decreasing short-chain branching (SCB) content).

The solvent's role is pivotal, as it dissolves the polymer at elevated temperatures and allows for crystallization upon cooling[196]. Solvents that are used in this method need to meet the criteria: thermal stability, solubility and IR compatibility[140]. 1,2,4-Trichlorobenzene (TCB) is considered the gold standard due to its thermal stability, allowing for its use in a wide temperature range from 16°C to 214°C and its solvation properties. However, for materials that crystallize at temperatures below 30°C, ortho-dichlorobenzene (o-DCB) may be preferred due to its lower melting point of -18°C to -17°C and a boiling point of 178°C to 180°C, accommodating substances that crystallize in colder solvents[197]. The chemical inertness of the

solvent is imperative to prevent reactions that could alter polymer properties and distort TREF results. Additionally, a high boiling point ensures process consistency and minimizes evaporative loss, affecting solvent concentration[198,199]. Infrared (IR) compatibility is also crucial; the solvent should not absorb in the same IR regions as the polymer to avoid spectral interference[200]. Specifically, the IR used in TREF detects the concentration of the eluted polyolefins by measuring the absorption of the IR signal[54]. Absorption is measured after the signal goes through the filter tailored for the C-H bond absorption around 2900cm^{-1}. Sustainability practices, such as solvent recycling, are increasingly being adopted in laboratories to reduce environmental impact and costs, provided the solvent retains its essential properties[201].

Crystallization, the most crucial step in TREF, is significantly influenced by the cooling rate; lower rates yield higher resolution[202]. While the choice of support materials, like glass beads or stainless steel particles and solvents such as xylene, o-DCB and TCB[203], play a role, they do not significantly impact the fractionation process[202,204]. Recent research, however, have revealed how column packing particles affects separation processes[205]. TREF's methodology has been reviewed and improved upon by several researchers, establishing correlations between elution temperature and SCB content.

TREF can be conducted on both analytical and preparative mode. Analytical TREF (a-TREF) utilizes a stable concentration detector like an infrared detector to monitor polymer concentration during the elution cycle[206], whereas preparative TREF (p-TREF) involves collecting polymer fractions, at selected temperature ranges, for further analysis using techniques like high-temperature size-exclusion chromatography (HT-SEC), NMR, or infrared spectroscopy[207].

Polyolefins, due to their varied applications and properties, require precise analytical techniques for their characterization. TREF stands out by providing detailed insights into their chemical composition distribution (CCD), crucial for applications ranging from consumer products to advanced materials engineering. The ability of TREF to fractionate polyolefins based on crystallinity and molecular structure makes it an indispensable tool in polymer science[208]. TREF is primarily used for characterizing linear low-density polyethylene (LLDPE) and other complex polyolefins[209]. It is instrumental in investigating microstructure-properties relationships, such as branching and tacticity[210]. However, for highly isotactic or stereoregular

structures, crystallization analysis fractionation (CRYSTAF) may offer better resolution[211,212]. For comprehensive characterization of complex polyolefins, cross-fractionation chromatography (CFC) provides three-dimensional distribution interrelating molar mass, chemical composition and concentration, essential for understanding complex materials[213,214]. In the context of increasing demand for recycled polyolefins, TREF's role is not just confined to academic research but extends to industrial applications. Understanding its nuances is essential for scientists and engineers working in material development and quality control[215].

Despite its utility and significant advancement, TREF faces challenges related to throughput and experiment duration, driving the development of alternative techniques like CEF and SSA[216]. TREF's potential contribution to the circular economy in polymer science, particularly for recycled polyolefin blends, remains a vital area for further research[186,217]. The need for solvents in TREF also poses some environmental challenges as solvents like TCB pose some environmental hazards[218]. Therefore, circulation of the used solvents TREF is highly recommended. This research gap underscores the need to enhance TREF's capabilities for analyzing the chemical composition distribution of recycled polyolefin materials, crucial for qualifying the feedstock providers and recycled polyolefin compounds design.

2.3.3 Chromatographic techniques

The technique discussed in the preceding sub-chapter for assessing molecular weight distribution (MWD) is gel permeation chromatography (GPC). This method is fundamentally driven by thermodynamic interactions, primarily entropy, and its significance in evaluating macromolecular structures is well-documented in the literature[219].

GPC's roots can be traced back to the early 20th century, but its application to polymers gained prominence in the late 1950s, thanks to the seminal work of J.C. Moore at Dow Chemical Company[220–222]. Initially designed for poly(styrene) characterization, the technique extended its applicability to polyolefins by the 1970s. Subsequent advancements in multi-detector systems and computational models have considerably expanded GPC's analytical scope.

SEC, which stands for size-exclusion chromatography (or GPC), operates on a principle of chromatography methods[223]. All forms of chromatography, including SEC, are based on the principle of separating components of a mixture based on differences in their interaction with

a stationary phase and a mobile phase[224]. However, in SEC, this separation is not based on adsorption or chemical affinity, but rather on the size and shape of the molecules[225]. This unique approach allows SEC to effectively separate molecules based on their physical dimensions, making it an essential technique in fields like biochemistry and polymer science[226].

In chromatography, solute molecules move within the column, alternating between the mobile and stationary phases[227]. This movement is driven by the need to maintain thermodynamic balance, ensuring that solutes distribute across both phases[228]. This state of equilibrium is typically reached during chromatographic processes, a fact supported by both flow-rate studies and static mixing experiments in size exclusion chromatography (SEC)[229]. The principle of thermodynamic equilibrium in solute distribution indicates that each solute component maintains consistent chemical potential across both phases[230]. In dilute solutions, when equilibrium is attained, the solute distribution is linked to the difference in standard free energy (ΔG°) between phases, maintained at a constant temperature and pressure[231]. The following equation (4) represents this relationship:

$$\Delta G^\circ = -RT \ln K \quad (4)$$

ΔG_m – Gibbs free energy difference between the phases [kJ].

R – Gas constant [$\frac{kJ}{mol \cdot K}$].

T – Temperature [K].

K – Solute partition coefficient, and ln signifies the natural logarithm [-].

ΔG° is further broken down into ΔH° (standard enthalpy difference) and TΔS° (temperature times standard entropy difference) between phases. So, it can be represented as equation (5):

$$\Delta G^\circ = \Delta H^\circ - T\,\Delta S^\circ \quad (5)$$

ΔG_m – Gibbs free energy difference between the phases [kJ].

ΔH_m – Change of the enthalpy [$\frac{kJ}{mol}$].

T – Temperature [K].

ΔS_m – Change of the entropy [$\frac{kJ}{K}$].

In other liquid chromatography (LC) techniques, solute partitioning predominantly occurs due to interactions between the solute and the stationary phase[232]. These interactions, whether they involve absorption or adsorption, bring about significant enthalpy alterations,

while the entropy changes are generally minimal and often negligible[233]. Consequently, by applying the aforementioned equations and disregarding the ΔS° factor, one can deduce the formula (6) for K_{LC} as:

$$K_{LC} = e^{-\frac{\Delta H}{RT}} \quad (6)$$

When retention is governed by entropic transformations, the size exclusion mode is active, but when retention is governed by enthalpic interactions, the adsorption mode is active. In the ideal case of GPC, where no enthalpic interaction i.e. (ΔH=0), K_{SEC} is then represented as equation (7):

$$K_{SEC} = e^{\frac{\Delta S^0}{R}} \quad (7)$$

The GPC process involves dissolving polymers in a solvent and passing the solution through a column packed with porous beads[234]. The beads serve as the stationary phase and are typically made of an inert copolymer of polystyrene (usually crosslinked poly (styrene-divinylbenzene) (PS-DVB) gels) where the porosity can vary[235]. When in solution, the polymers serve as the mobile phase. Polymer chains curl up into balls in solution and the size or hydrodynamic volume of the balls varies with the molecular weight of the polymer chain[236]. As the solution is injected into the column and passes through the beads the molecule enters the pore, it becomes confined and hence unable to acquire all potential conformations, resulting in a loss of conformational entropy[237]. The larger molecules are either not entering pores at all or are eluted first and hence have the shortest retention time in the column. The smallest chains have more possibilities to enter the pores therefore are retained for longer in the column and are eluted later[238]. Detectors at the point of exit measure the concentration of the sample eluted against time. This allows the segregation of the polymer samples according to their molecular weight[239]. At its core, GPC operates on thermodynamic principles, specifically the partitioning of the solute between a mobile and a stationary phase[240].

GPC has proven very effective in determining the molecular weight distribution[241]. The process involves the separation of pure polymer samples into different molecular weights. However conventional GPC systems do not provide direct information on crystallinity or other chemical identity of the polymers. It is crucial to recognize that macromolecules with identical hydrodynamic volumes can exhibit variations in chemical composition[242,243]. Therefore, it is possible for polymers of different chemical identities to be eluted together so long as they have the same hydrodynamic volume, presented in equation (8), meaning the same size in solution.

This proves ineffective in separating different forms of the same polyolefins within a sample of recyclates.

$$V_H = \eta \cdot M \tag{8}$$

V_H – Hydrodynamic volume [mL].

η – Viscosity [$\frac{mL}{g}$].

M – Molecular weight [$\frac{g}{mol}$].

To address this, GPC analysis of polyolefins has been augmented by the integration of multiple detectors. These include molar mass-sensitive detectors such as multi-angle light scattering detectors[244,245] online-viscosity detectors[246–249], and chemical-sensitive detectors like FTIR[250–254] or NMR spectroscopy[255,256]. This multi-detector approach, coupled with the precise molecular weight distribution data generated, provides invaluable insights into the chemical structure variations across the molecular weight spectrum in ethylene and propylene-based polymers[257].

2.3.4 Spectroscopic techniques

Spectroscopic techniques offer a comprehensive molecular understanding of polyolefins, crucial for advancing the field of recycled polyolefin blends and their crystallization kinetics[199]. Fourier-transform infrared (FTIR) spectroscopy excels in identifying functional groups, thereby providing insights into copolymer composition and the presence of side branches or defects[258]. However, its sensitivity to non-polar functional groups like C-H and C-C is limited, constraining its utility for quantifying low concentrations of structural defects in polyolefins[259].

Raman Spectroscopy, sensitive to molecular vibration symmetry, offers valuable data on crystallinity and orientation[260]. It effectively measures factors influencing the thermal and mechanical properties of polyolefins[261]. However, fluorescence interference can mask the Raman signal in certain samples.

Nuclear magnetic resonance (NMR) is particularly effective for detailed molecular structure elucidation, including stereochemistry and sequence distribution in copolymers[262]. Both ^{1}H and ^{13}C NMR are invaluable for understanding tacticity and comonomer distribution, key parameters for crystallization behavior in polyolefins[199]. Despite its high-resolution

capabilities, NMR requires extensive sample preparation and is less suited for high-throughput analysis[263].

Emerging techniques like two-dimensional correlation spectroscopy (2D-COS) and terahertz spectroscopy could further enrich polyolefin characterization[264]. Given the rapid advancements in spectroscopic methodologies, a continuous update of this theoretical framework is advised.

2.3.5 Morphological and structural analysis techniques

Scanning electron microscopy (SEM) and wide-angle X-ray scattering (WAXS) are critical tools for the characterization of polyolefins, each playing a complementary role in polymer science[265]. SEM has been a pivotal technique for morphological studies in polymer analysis. It offers high-resolution imagery that reveals the surface topography and composition of materials, including polyolefins[266]. Hagège et al.[267] demonstrated the method's usefulness in characterizing the size and shape of catalyst and polyethylene prepolymer particles. Park et al. [268] furthered this by introducing a chemical etching technique for investigating the microstructure of melt-crystallized polyethylene, particularly banded spherulites. Wilkes et al.[269] and Tagawa et al.[270] both utilized SEM to study the fine structure of polymers, with Wilkes focusing on spherulitic segmented polyurethanes and Tagawa on the fine lamellar structure of polyethylene. These studies collectively highlight the significant leap in polymer analysis made possible by SEM. However, it is important to note the potential challenges of SEM analysis, such as radiation damage and the need for proper controls[271]. The advent of modern SEM techniques, capable of 3D imaging and energy-dispersive X-ray spectroscopy (EDS), has further enhanced our understanding of the surface characteristics and the distribution of additives within polyolefins, thus providing insights into their macroscopic to nanometric features[272].

WAXS, in conjunction with SEM, has been pivotal in understanding the atomic arrangements in the crystalline domains of polyolefins, and how these arrangements impact their mechanical properties. It has provided crucial data on unit cell dimensions, crystallinity degrees, and crystallite orientations, which are essential for comprehending the intrinsic properties of polyolefins and their potential engineering for specific uses[273]. Furthermore, WAXS has been used to monitor the structural and morphological developments during the

crystallization of isotactic polypropylene, revealing the presence of oriented crystallites and their dependence on molecular weight distribution [274].

The use of SEM and WAXS in the study of polyolefins has significantly advanced our understanding of their microstructural features and macroscopic behavior. These techniques have been particularly valuable in predicting material behavior based on structural data for virgin materials[275]. In the realm of recycled polyolefins, they have revealed the complex interplay between processing, degradation, and material properties[79]. For instance, advanced WAXS has provided insights into the restructuring of crystalline phases during recycling, which is crucial for developing recycling methods that preserve material properties[275]. Similarly, SEM has shed light on the morphology of recycled polyolefins, highlighting the impact of impurities and blend miscibility on recycled product quality[276]. These findings underscore the importance of these techniques in both understanding and improving the properties of polyolefins.

Together, SEM and WAXS have catalyzed a comprehensive understanding of polyolefins. The integration of these techniques with thermal and chromatographic methods has established a multi-faceted approach to polymer characterization. SEM delivers the morphological narrative, while WAXS deciphers the subtleties of the crystalline structure. Their synergistic application offers a holistic vista of polyolefins, enriching our knowledge of their processing, behavior and ultimate application in a diverse array of industries. This harmonized approach continues to advance our understanding and opens pathways for the ongoing refinement of both virgin and recycled polyolefin grades.

2.3.6 Hyphenated techniques

Hyphenated techniques in analytical chemistry refer to methods where two (or more) different analytical techniques are combined in a single analysis[277,278]. This combination is usually done to enhance the capabilities of the analytical process, allowing a more detailed and accurate analysis of complex samples.

In the field of polyolefin characterization, hyphenated techniques represent a significant advancement, providing more comprehensive, accurate, and efficient analysis than traditional methods. These techniques combine various analytical methods, each contributing its strengths to overcome the limitations of standalone approaches. For instance, techniques like GPC-IR

(gel permeation chromatography with infrared detection) and TREF (temperature rising elution fractionation) have revolutionized the understanding of polyolefins[279,280], by combining these 2 techniques, the analysis acquires a multidimensional perspective, significantly elevating the information about the analyzed polymer sample[281].

The GPC-IR technique combined with TREF is called cross-fractionation chromatography (CFC) or TREFxGPC[282]. This technique is an advanced analytical method used in polyolefin science. It is designed to provide detailed characterization of polymers, particularly in understanding their composition and structure[283]. CFC is highly valued for its ability to analyze complex polymer systems[284].

The inception of CFC was driven by the need for a more comprehensive analysis of polymers[285]. Traditional chromatographic technique like size exclusion chromatography (SEC) or crystallization based technique like temperature rising elution fractionation (TREF) provided limited information, focusing either on molecular size or chemical composition separately[286,287]. CFC emerged as a solution to integrate these dimensions, offering a more holistic view of polymer properties.

CFC operates on the principle of combining multiple fractionation techniques, usually involving a sequential process. In a typical CFC setup[288]:

- First dimension - Chemical Composition Analysis: the polymer sample is first fractionated based on its chemical composition. Techniques like TREF (described in Chapter 2.3.2) or crystallinity analysis are employed. This step separates the polymer chains based on their chemical heterogeneity, such as the distribution of comonomers.
- Second dimension - Molecular Size Analysis: the fractions obtained from the first step are then passed through a second dimension, typically using SEC/GPC (described in Chapter 2.3.3). This stage separates the polymer chains based on their molecular weight or size.
- Detection and Analysis: the final step involves detecting and analyzing the fractions using detectors like infrared (IR), refractive index (RI), viscometry, or light scattering. This provides comprehensive data on molecular weight distribution, composition distribution, short-chain branching and other crucial polymer properties[289].

Notable combinations like TREFxGPC offer simultaneous insights into chemical composition distribution (CCD) and molecular weight distribution (MWD), addressing the intricate microstructural complexities of contemporary polyolefin resins[290].

The genesis of these techniques was primarily to enhance the characterization of linear low-density polyethylene (LLDPE). These hyphenated methods have been instrumental in elucidating synthesis-structure relationships. For example, W. Yau employed a Hybrid 3D-GPC-TREF instrument with three online detectors to characterize various polyolefins[246]. Ortín et al. further innovated by developing a fully automated cross-fractionation instrument (TREF-GPC)[291], expanding the analytical capabilities for polyolefins, including the study of catalytic systems in high-density polyethylene (HDPE) intended for pipes[292].

These advancements have also facilitated the investigation of thermomechanical degradation in polyolefin blends, such as polypropylene and polystyrene[293]. For complex syntheses or degradation products, integrating multiple methods for a comprehensive understanding of molecular architecture[209]. Bungu and Pasch proposed constructing libraries correlating molecular weight and branching across different polyolefin materials[294].

In summary, the characterization of virgin polyolefins is an ensemble of multiple analytical techniques. Each one contributes unique insights into the molecular or morphological attributes of the material. The amalgamation of these techniques provides a comprehensive understanding, particularly crucial for recycled polyolefins, which present additional challenges due to impurities, additives, and heterogeneities.

2.4 Impact of processing on crystallization behavior

In the realm of polyolefin research, the processing of neat polypropylene (PP) and polyethylene (PE), as well as their blends, is a critical aspect that directly influences their crystallization behavior, and consequently, their final properties[132]. The processing of these polymers, encompassing a range of techniques such as extrusion, injection molding, and blow molding, plays a pivotal role in determining the microstructure and hence the mechanical and thermal characteristics of the final product[295].

The crystallization of PP and PE during processing is not merely a function of their inherent molecular structures but is also significantly modulated by the processing

conditions[296]. Variables such as temperature gradients, cooling rates and shear forces encountered during processing can profoundly alter the crystalline morphology[297,298]. For instance, faster cooling rates can lead to higher degrees of supercooling, resulting in finer spherulitic structures, which in turn influence properties like toughness, clarity and barrier performance. In the context of blends, the interaction between different polyolefin types during processing further complicates the crystallization behavior, introducing additional variables like blend composition, compatibility and the presence of any compatibilizers or nucleating agents[299,300].

The goal of this section is to explain how processing conditions influence the crystallization behavior of PP, PE and their mixtures. Processing-induced crystallization has a substantial impact on the feasibility and performance of recovered materials. Understanding these relationships is critical for increasing the possible applications of recycled polyolefins, which are usually blends of the aforementioned polymers

2.4.1 Insights into the crystallization of neat polypropylene and polyethylene

Polyethylene (PE) and polypropylene (PP) are polymers with diverse structural and molecular weight characteristics, each imparting unique crystallization behaviors that significantly influence their properties[301].

PE variants range from low-density (LDPE)[302], high-density (HDPE), to linear low-density (LLDPE)[303]. LDPE, with its highly branched structure, exhibits lower crystallinity and melting temperatures compared to HDPE, which has a more linear structure with minimal branching[304]. LLDPE, on the other hand, combines aspects of both LDPE and HDPE, providing unique properties like enhanced tensile strength and puncture resistance[305]. These structural differences impact not only the crystallization and melting behavior but also the chemical resistance of these materials[306]. LDPE, with its lower crystallinity, is more susceptible to chemical attack, while HDPE offers better chemical resistance due to its higher crystallinity [307]. In processing, these variations necessitate different temperature and cooling rate controls to achieve the desired crystalline structure, which in turn affects the mechanical properties such as toughness, rigidity and transparency[308]. The applications of these PE types are vast, ranging from flexible films in packaging (LDPE), to rigid containers and piping systems (HDPE), and films requiring a balance of flexibility and strength (LLDPE). The crystal structure of PE is the

orthorhombic form[309]. Polymers with bulky side chains and branches generally have lower crystallinity compared to unbranched ones. Hence HDPE has higher crystallinity compared to LDPE or LLDPE which are more branched[310]. Branching length and distribution along the polymer chain affect the crystallinity and these can be controlled during the polymerization process. Such that polyethylenes can exist with varying degrees of crystallinity.

PP exists in various forms including atactic, syndiotactic and isotactic configurations, each presenting distinct crystallization characteristics[311]. Isotactic PP, with its regular and uniform chain structure, exhibits higher crystallinity and melting points, translating to greater stiffness and heat resistance[312]. In the case of PP, this characteristic is exemplified by the existence of multiple crystalline forms, including α-, β-, γ-phases and a mesomorphic phase[313]. Each of these phases represents a different arrangement of the PP chains, which all maintain a three-fold helical conformation but differ in their packing within the crystal lattice[314], while atactic PP, with its random methyl placement with respect to the backbone chain's plane, is largely amorphous and has lower strength[315].

In addition to homopolymers, there are heterophasic PP copolymers (HECOs), essential in applications requiring improved properties, such as automotive components. The glass transition of PP around 0°C necessitated the development of toughened grades[316]. Initially, these were produced as compounds with ethylene-propylene (EPR) or ethylene-propylene-diene elastomers (EPDM)[317,318]. However, more cost-effective solutions emerged with "block copolymers" from multi-reactor plants, like the Novolen or Spheripol process. These copolymers combine a crystalline PP matrix with embedded particles of EPR and PE, offering enhanced impact resistance and low-temperature performance. The development of 2nd and 3rd generation ZN catalysts in the 1970s and 1980s enabled the reliable synthesis of HECOs with high impact strength. HECO's are also called "PP impact copolymers".

In summary, the structural and molecular weight diversity of PE and PP has profound implications on their crystallization, melting behavior and chemical resistance. These factors need to be carefully considered during processing to tailor the mechanical properties of the final product to specific industry requirements. Understanding these nuances is crucial for optimizing the use of these materials, particularly in the context of recycling and creating sustainable polyolefin products.

2.4.2 Impact of nucleation on crystallization forms in neat PP and PE

Nucleation, the initial step in the crystallization of polymers like polypropylene (PP) and polyethylene (PE)[319], sets the stage for the transition from a disordered melt to an ordered crystalline structure, dictating the formation of crystallites that significantly influence the polymer's properties[320]. While homogeneous nucleation, occurring in ideal, impurity-free systems, is less common in PP and PE due to high energy requirements, heterogeneous nucleation, where impurities or added nucleating agents act as catalysts, predominates, thereby reducing the energy barrier and facilitating crystallization. This process is intricately linked to the molecular characteristics of PP and PE, such as molecular weight and branching, which affect chain mobility and thus the rate and nature of nucleation, with higher molecular weights or greater branching often impeding nucleation[321].

The Gibbs free energy has been the main parameter used to quantify the nucleation and growth stages in polymer crystallization. It implies a balance between decreasing the enthalpy and trying to limit the entropy losses. This free energy of crystallization can be easily explained by Gibbs thermodynamic equation (9)[322]:

$$\Delta G = \Delta H - T\Delta S \quad (9)$$

ΔG – Gibbs free energy [kJ].

ΔH – Change of the process enthalpy [$\frac{kJ}{mol}$].

T – Temperature [K].

ΔS – Change of the process entropy [$\frac{kJ}{K}$].

In the crystallization of polyolefins, nucleation is a critical step that requires a particular molecular chain arrangement to form a new phase. From a thermodynamic perspective, this involves close packing of chain segments to distances characteristic of the crystalline unit cell, aligning with crystal symmetry. During nucleation, the Gibbs free energy (ΔG) initially increases due to the energy required to form a new interface between the crystalline and amorphous phases.

As molecules get incorporated into the embryo, there is a reduction in Gibbs free energy, driving the crystallization process forward. The overall energy balance during the formation of a crystal involves both surface and bulk contributions, as represented by (10) :

$$\Delta G = V\Delta g + \sum_i A_i\,\sigma_i \quad (10)$$

ΔG – Gibbs free energy [J].

V – Volume [m^3].

Δg – Bulk free energy change per unit volume [$\frac{J}{m^3}$].

A_i – Surface area [m^2].

σ_i – Surface free energy per unit area [$\frac{J}{m^2}$].

Nucleation in polyolefins is influenced by both the molecular characteristics of the polymers and the external processing conditions, such as cooling rate and shear. These factors collectively determine how nucleation occurs[323]; for example, rapid cooling tends to increase the nucleation rate, leading to a higher number of smaller crystallites, while slower cooling allows for the growth of larger crystallites and shear can align polymer chains, promoting uniform crystalline structures[324]. In this context, the introduction of nucleating agents into PP and PE proves to be a pivotal control mechanism, providing additional nucleation sites and thus refining the crystalline structure, with the choice and dispersion of these agents within the polymer matrix being critical for achieving the desired mechanical and thermal properties. Nagarajan et al.[325] and Mubarak et al.[326] both highlighted the effectiveness of specific nucleating agents in increasing crystallization temperature and the number of nuclei formed in PP. Mubarak et al.[326] noted the impact of nucleating agents on the mechanical properties of PP, with higher crystallinity and α-crystal content leading to increased stiffness and yield stress.

Transitioning from neat polymers to blended systems, the foundational understanding of nucleation in PP and PE becomes vital[327], as the blending of different polymers introduces additional complexity to nucleation behavior, making the prediction and control of crystallization more challenging but also more intriguing, paving the way for tailored material properties through meticulous molecular and processing condition optimization[328].

2.4.3 Crystallization in processing conditions of neat PP and PE

The crystallization of neat polypropylene (PP) and polyethylene (PE) under various processing conditions is a key factor determining their final properties[329]. The primary processing parameters that significantly influence the crystallization behavior of these polymers are temperature, cooling rate and pressure[330].

The crystallization of PP and PE is highly temperature-dependent[331]. The crystallization temperature range for each polymer is determined by its specific molecular structure. During processing, maintaining the temperature within the optimal crystallization range is crucial. Temperatures that are too high can delay crystallization, leading to more amorphous regions and less rigidity in the final product. Conversely, temperatures that are too low can lead to uneven crystallization, affecting properties like clarity and impact strength[332].

The cooling rate is another critical factor in the crystallization process. Rapid cooling can lead to a higher degree of supercooling, resulting in smaller spherulites and a less opaque product with potentially higher impact strength but lower stiffness[333]. Slow cooling allows for the formation of larger, more perfect spherulites, which can enhance stiffness and thermal resistance but may reduce impact strength and transparency. The cooling rate must be carefully controlled to achieve the desired balance of properties.

Pressure, particularly in processes like injection molding, can significantly influence the crystallization behavior of PP and PE[334]. The relationship between processing parameters and the crystalline structure developed in PP and PE is complex and interdependent[335]. For instance, the combination of high temperature and slow cooling might be ideal for achieving a certain degree of crystallinity in PP, but the same conditions might not be suitable for PE due to its different molecular structure[299]. Similarly, the optimal pressure settings for injection molding might vary significantly between PP and PE[336].

In summary, understanding the relationship between processing conditions and the crystallization behavior of PP and PE is essential for tailoring their properties. This understanding allows for the optimization of processing parameters to achieve the desired mechanical, thermal and optical properties in the final product, which is especially crucial for applications requiring specific performance characteristics.

2.4.4 Crystallization in binary and ternary blends of PP and PE

The crystallization behavior of binary and ternary blends of polypropylene (PP) and polyethylene (PE) is a complex interplay of the individual components' characteristics, influenced significantly by their interactions under various processing conditions[337].

In binary blends of PP and PE, the interaction between these polymers is predominantly dictated by their respective molecular structures and crystallization kinetics. PP and PE exhibit different crystallization temperatures and spherulitic growth rates. When blended, these differences can lead to either synergistic or antagonistic effects on the crystallization behavior. For instance, in some blends, PE can act as a nucleating agent for PP, enhancing its crystallization rate. Conversely, the presence of PP can induce the crystallization of PE[56,83,338]. This interplay affects the final microstructure of the blend, influencing properties like tensile strength, impact resistance and thermal stability. The processing conditions, such as cooling rate and shear, further modulate these effects, making the prediction of the final properties more complex[339].

The complexity increases with ternary blends, where an additional polyolefin component is introduced. These blends offer a broader spectrum of property manipulation but require a more intricate understanding of the interactions among the constituents[340,341]. The crystallization behavior in such systems is affected not only by the individual polymers' characteristics but also by their relative proportions and compatibilization strategies. For example, the addition of a third component, such as a linear low-density polyethylene (LLDPE), into a PP/HDPE blend, can result in improved impact properties and processability. However, it can also lead to a more heterogeneous nucleation environment, affecting the overall crystallization kinetics and morphology[342].

In both binary and ternary blends, the key lies in understanding how the different components' crystallization behaviors interact under specific processing conditions. This includes analyzing how factors like blend ratio, molecular weight distribution and the presence of compatibilizers or nucleating agents influence the overall crystallization process[306]. By manipulating these variables, it is possible to tailor the mechanical and thermal properties of the blends for specific applications, such as in packaging, automotive components, or consumer goods.

Immiscibility and crystallization of PP/PE blends

The dynamics of crystallization within polyethylene (PE)/polypropylene (PP) blends are profoundly influenced by the blend components' compatibility or lack thereof, a characteristic governed by their inherent properties and the specific conditions under which the blending process is executed. A study by Lovinger et al. offers insights into the blends' morphology and

tensile properties, highlighting the pivotal role that the composition of the blend plays in defining the mechanical and structural attributes of the resulting materials. The tendency of these blends to fail at low levels of elongation can be traced back to their biphasic structure, which is characterized by either interpenetrating networks or discrete islands of the minority component embedded within the matrix. Notably, incorporating a minimum of 10% PE into the blend leads to a significant reduction in the average size of PP spherulites, a phenomenon that is believed to enhance the tensile modulus, particularly in blends composed of approximately 80% PP. Furthermore, the introduction of specific nucleating agents into PP not only further reduces the average spherulite size but also results in modest improvements in the material's modulus. This sequence of adjustments and additions elucidates a complex interplay between blend composition, structural morphology and mechanical performance, underscoring the intricate balance required to optimize the properties of PE/PP blends[343]. Furthering the investigation into crystallization kinetics, Bartczak et al.[62] and Wenig and Meyer[344]collectively found that the growth rate of PP in PP/PE blends does not depend on the presence of the PE phase, challenging previous assumptions[345] and highlighting the complexity of polymer blend behavior. The role of PP in nucleating the crystallization of PE was proposed by Last[346], though this was speculative without direct proof. Meanwhile, studies by Lotz and Wittmann and others [347,347–350] have observed epitaxial overgrowth and morphological changes under specific conditions, indicating lattice matching and epitaxial crystallization despite the general immiscibility of PP and PE. Rybnikár et al.[351] concluded that the enhancement of linear PE crystallization rate was attributed to the nucleating action of crystallized PP phase, which was excluded by Nishio et al.[352] and Kojima and Satake[353]. Souza et al. investigated how the processing temperature and HDPE concentration affect the interfacial tension in PP/HDPE polymer mixtures, discovering a reverse relationship between interfacial tension and these variables[49]. In a recent paper of Samuel et al., different methods of quantifying the melt compatibility between polyolefins by surface/interfacial tensions are compared[354]. It suggests that the surface tension difference could be a useful parameter for evaluating and optimizing the melt compatibility in the absence of compatibilizers. Surface/interfacial tensions are a fundamental aspect that influences both liquid-liquid separation and crystallization-induced phase separation. High interfacial tension can exacerbate phase separation by making it more difficult for the polymers to mix. This is a distinct phenomenon primarily concerned with the energetic balance at interfaces, which impacts the overall morphology and properties of the blend, by determining the ease with which phases can separate or mix. Double morphologies

were explain by liquid-liquid[355] and crystallization-induced phase separation[356]. Liquid-liquid separation and crystallization-induced phase separation are connected through their influence on the morphology of the blend. However, liquid-liquid separation occurs in the molten state due to immiscibility, while crystallization-induced phase separation occurs as a result of different crystallization rates and temperatures. Crystallization-induced phase separation is driven by differences in crystallization behavior rather than by the initial immiscibility. This phenomenon is closely related to melt processing in that the thermal history and cooling rates can significantly impact the extent and nature of phase separation. Both phenomena lead to distinct phase domains but differ in their underlying causes and stages at which they occur. In the former, during melt mixing, the components in the blend do not mix uniformly, but instead form separate liquid domains before solidifying into crystals. PP and PE have different conformational structures in the crystalline state, with PE forming a zig-zag planar conformationand PP organizing in a helical conformation. This difference affects the crystallization kinetics, with PE crystallizing much faster due to its higher chain flexibility compared to PP. The presence of branches in PE can hinder chain movement and delay the self-organization process, affecting crystallization kinetics and final morphology. The content and type of branches or comonomers significantly influences the crystallization behavior of PE, with higher branch contents leading to easier phase separation in the melt and affecting the heterogeneous morphology upon crystallization. In PP/PE blends, the crystallization of each component can vary significantly compared to the neat components, depending on the blend's morphology. For instance, crystallinity does not significantly vary in droplet-matrix morphology, while in co-continuous systems, the crystallinity of each component might change up to 20% due to the addition of the other component. The presence of PE in a PP blend reduces the nucleation density, explained by the migration of nucleating heterogeneities from PP to PE domains during melt mixing, driven by the difference in interfacial free energy of the impurity between the two phases. Partial miscibility can occur upon cooling from the melt just with special PE grades, but segregation during the crystallization process is common. Miscibility among different types of PEs can lead to the co-crystallization phenomenon, where chains of two PE types intermix at the macromolecular level, leading to the formation of joint crystals. The extent of co-crystallization increases with the closeness of the crystallization rates of the components and is influenced by the concentration of the branched component and the crystallization conditions imposed[357–359].

The current trend is to improve PP/PE miscibility by adding compatibilizers. Compatibilizers essentially act as molecular bridges that improve the interaction between PP and PE[360]. The compatibilization of polyolefin blends leads to lowering of the interfacial tension in immiscible blends and formation of stable and desired morphology. Compatibilizers are usually block and graft copolymers or nanofillers with affinity for both components forming the blend[132,361,362]. Consequently, these species have a tendency to locate at the interface between the two phases, visualized on Figure 2.4.4–1[363]. These chain segments of the block or graft copolymers can be identical as those of the main polymers or they can be different, provided that the blocks are well miscible with the corresponding phases. Furthermore, the presence of compatibilizing agents in the blend suppresses the coalescence of the dispersed phase and hence reduces the size of the domains[364,365]. If the compatibilizer molecules penetrate the matrix and dispersion phase deeply enough to co-crystallize or become entangled with the polymer chains of both phases, they improve solid-state adhesion[366]. Good interfacial adhesion improves the stress transfer from one phase to another and prevents the growth of cracks initiated at the interface. Overall effective compatibilization leads to enhanced mechanical properties, stability and processability of the blend.

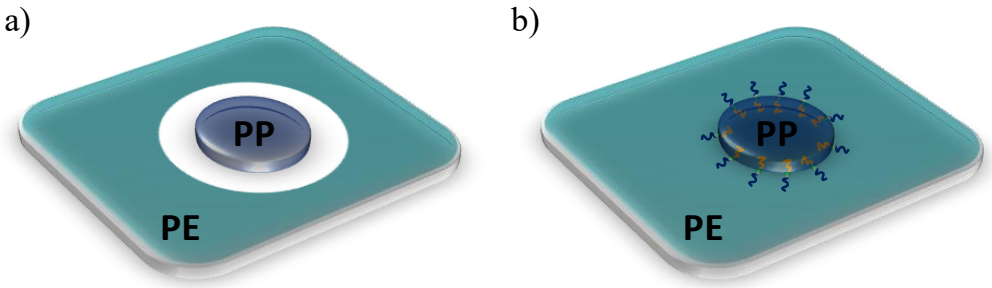

Figure 2.4.4–1 Illustration of PP/PE blend enhancement with compatibilizers: a) shows the phase separation in a PE matrix with PP droplet without compatibilizers; b) depicts compatibilizers as molecular bridges between the PE matrix and PP droplet.

The melt immiscibility and miscibility of PP/PE blends play a crucial role in determining the blend's final properties. Understanding the complex interactions between PP and PE during the blending and crystallization processes is essential for optimizing the properties of these blends for specific applications. The behavior of PP/PE blends in the melt and during crystallization is a fascinating area of study that combines aspects of thermodynamics, polymer science and materials engineering to create materials with tailored properties.

In conclusion, understanding the crystallization of binary and ternary blends of PP and PE is vital for advancing the application of these blends, particularly in recycling scenarios, where the ability to predict and control the properties of recycled materials is crucial for their effective reuse.

2.4.5 Impact of nucleation and surface nucleation on crystallization in polyolefins

Surface nucleation plays a crucial role in determining the crystallization behavior in polyolefins, such as PP and PE[367]. The process of nucleation, especially at surfaces, significantly influences the overall crystallization kinetics, morphology, and thus the final properties of these materials.

The characteristics of a surface, such as its chemical composition, roughness and energy, can profoundly influence the nucleation of polyolefins[368]. Surfaces with higher energy or roughness can induce heterogeneous nucleation more effectively than smoother, lower energy surfaces. For example, the introduction of certain fillers or fibers can provide additional nucleation sites, leading to a finer spherulitic structure in the polymer[369]. This change in morphology can enhance properties like mechanical strength, stiffness and clarity.

Additives are often used in polyolefins to modify their crystallization behavior. Nucleating agents[370], for instance, are added to increase the number of nucleation sites, thereby promoting faster crystallization and resulting in a finer and more uniform crystalline structure[371]. This is particularly useful in improving the optical clarity and heat resistance of PP and PE. Common nucleating agents include organic salts, pigments, and certain minerals[372].

The use of external nucleating agents is a strategic approach to control the crystallization behavior of polyolefins[373]. These agents can be specifically chosen to tailor the nucleation process, influencing factors like the crystallization temperature, rate of crystallization and the size of the crystallites. For example, talc is often used in PP to improve its rigidity and thermal properties by altering the crystallization process[374].

During processing, the interaction of these surface characteristics and additives with the polymer melt plays a critical role[375]. Processing conditions like temperature, shear rate and cooling rate can interact with the nucleation behavior, further influencing the crystallization process[376]. For instance, a higher shear rate in the presence of nucleating agents can lead to a

more pronounced nucleation throughout the polymer, enhancing the uniformity of the crystalline structure[319].

In conclusion, surface nucleation is a key factor in dictating the crystallization forms in polyolefins. By understanding and controlling the surface characteristics, the use of additives, and the application of external nucleating agents, it is possible to tailor the crystallization behavior of PP and PE during processing. This control is essential for achieving the desired material properties, particularly in applications where specific mechanical, thermal and optical properties are required.

2.4.6 Effect of processing conditions on crystallization of recycled polyolefins blends

This chapter culminates in an intricate exploration of how processing conditions distinctly impact the crystallization forms of recycled polyolefin blends[377], a subject that lies at the heart of this thesis, knitting together the insights gathered from the study of neat polyolefins. Recycled polyolefin blends, comprising materials like recycled polyethylene and polypropylene, present unique challenges in crystallization due to the variability in their molecular structures[378], a consequence of their previous life cycles and processing histories. The temperature, a critical factor in the crystallization of neat polymers, assumes an even more complex role in recycled blends; variations in thermal history and the presence of impurities or additives in recycled materials can lead to a wide range of crystallization behaviors, often resulting in less predictable crystalline structures[379].

Cooling rate, another pivotal processing condition, impacts these blends differently compared to their neat counterparts; the presence of mixed molecular weights and compositions in recycled blends can lead to diverse crystallization kinetics, affecting the material's overall mechanical and thermal properties. Similarly, the pressure and shear rate during processing, which can influence the orientation and size of crystallites in neat polyolefins, must be carefully managed in recycled blends to account for the added complexity of mixed polymers, with the goal of achieving a balance between material strength and ductility[375]. The interplay of these processing conditions with the inherent heterogeneity of recycled blends underscores the challenges in controlling and predicting their crystallization

behavior, making the optimization of processing parameters a key focus for researchers and industry practitioners alike.

This exploration of processing conditions and their effects on the crystallization of recycled polyolefins not only aligns with the core focus of this thesis but also bridges the gap between the fundamental understanding of neat polyolefin crystallization and the more nuanced scenarios presented by recycled materials. By tying in the previous sections on neat polyolefin crystallization, nucleation and the impact of processing conditions, this section offers a comprehensive perspective on the complexities and opportunities inherent in recycling polyolefin blends, highlighting the potential for advancing sustainable material practices in the polymer industry.

In conclusion, the study of crystallization in recycled polyolefins, influenced by diverse processing conditions, presents both a challenge and an opportunity, paving the way for more sustainable and efficient use of these ubiquitous materials in various applications, a theme that resonates throughout this thesis and represents a significant contribution to the field of polymer science.

2.5 Summary

Polyolefins, from their inception to their modern applications, have been shaped by a myriad of factors including chemical structure, processing techniques, and now, sustainability concerns. The characterization techniques, both traditional and emerging, offer a window into this complex world. Yet, there is still much to be explored, especially in the context of recycled materials and their intricate behaviors.

Adaptation of sophisticated R&D methods developed for virgin grades to study recycled materials is ongoing, there are intrinsic challenges due to the nature of recycled polyolefins. These include issues related to contamination, material heterogeneity, and the need for modifications in analytical techniques. This necessitates a re-evaluation and potentially the development of new methodologies or adaptations of existing ones to accurately characterize and analyze recycled polyolefins. This area represents a fertile ground for further research and innovation, particularly in advancing recycling and circular economy initiatives.

The roadmap is clear; there is a compelling need for more sophisticated characterization tools and advanced processing techniques, especially for recycled polyolefins. The ever-increasing demand for these materials, both in virgin and recycled forms, mandates a continuous and rigorous academic pursuit. It is this incessant quest for knowledge that will catalyze future advancements in polyolefin science and technology.

3 Fast successive self-nucleation and annealing (SSA) thermal fractionation protocol for the characterization of polyolefin blends from mechanical recycling

In the realm of polyolefin recycling, the industry faces significant challenges in efficiently analyzing and characterizing recycled blends, which is crucial for optimizing recycling processes and improving the quality of recycled materials. Traditional methods often fall short in providing detailed insights, particularly regarding the crystallization behavior of these complex blends. Chapter 3 of the thesis introduces a valuable approach using fast successive self-nucleation and annealing (SSA) protocol performed on differential scanning calorimetry (DSC) to fill this gap. This method allows a more detailed and rapid analysis of the melting of PP and PE (specifically HDPE) lamellae in recycled polyolefin blends. The method is based on comparison of the neat materials to recycled polyolefins. By leveraging the fast SSA technique, the analysis time is significantly reduced compared to traditional SSA, facilitating quicker turnaround times for material characterization in industrial settings.

3.1 Introduction

Plastic materials are part of our daily life and our economy. The EU commissions strategy aims to transform the way plastic products are designed, produced, used and recycled in the EU. The main recycling strategies are primary mechanical recycling, secondary mechanical recycling, tertiary or feedstock recycling, and quaternary recycling [380–382]. Not all materials can follow the same method of repurposing or recycling. Therefore, separating into different types is one of the key steps to recycle material for new products or components. Mixed materials cannot be reused and reprocessed easily, due to their structural differences.

In the mixed polyolefins (MPO) stream, we have mainly recycled polypropylene and polyethylene, which are incompatible in the melt phase, which leads to phase separation and inferior mechanical properties compared to neat materials [380,383–385].

Mixed polyolefins obtained by mechanical recycling consist of various grades, mainly LDPE, HDPE, PP [386,387]. Knowing the precise chemical composition of individual batches is essential for processing and compounding. Differential scanning calorimetry (DSC) provides

crucial material information, in particular melting and crystallization temperatures, which are valuable for processing. The chemical composition of semi-crystalline post-consumer recycled polyolefin blends can also be evaluated from DSC, on the basis of the melting enthalpy of the different phases [46,78]

The existence of branching in the polymer chain, the size of the chain, interactions between the chains, the presence of crystallization promoters (nucleating agents) and other factors all influence crystallization[388–390]. Industrially applied standard methods to analyze the chemical composition distribution of polyolefins are temperature rising elution fractionation (TREF)[190,194,391], crystallization analysis fractionation (CRYSTAF)[190] and crystallization elution fractionation (CEF)[392]. These techniques are based on changes of polymer concentration in solution during temperature reduction via precipitation (CRYSTAF) or after redissolution of the precipitated polymer during increasing the temperature (TREF, CEF)[36,393]. In these standard methods the dissolution step of the sample is typically time-consuming, uses hazardous solvents, and it is often necessary to pre-treat the sample (e.g., filtration of the recycled blend)[32]. Alternatives based on DSC of bulk samples, on the other hand, have several positive features that speak for them. Examples of these methods are Step crystallization (SC) and successive self-nucleation and annealing (SSA). These methods do not use solvents and are therefore cheaper, safer and typically quicker. The difference between SC and SSA is that, in the case of SSA, after each high-temperature treatment with an isothermal holding time of 5 min, non-isothermal crystallization ramps to room temperature are performed, which undercools the material and accelerates crystallization, speeding up the entire molecular fractionation process compared to SC[32]. Both methods can be used to characterize the crystallizable sequence length in the polymer chain (homopolymer or copolymer) and polymer blends, but there is better segregation and enhanced resolution with the SSA protocol[167].

Thermal fractionation using the SSA procedure differentiates the material into fractions that are formed as a result of polymer chain defects (branches, tacticity). This sensitivity to the low content of chain defects allows the study of polymer blend miscibility and co-crystallization, cross-linking, ageing, biodegradation, copolymerization, comonomer structure, and SCB distribution[394].

The molecular segregation in SSA is accomplished by several non-isothermal and isothermal stages. The sample is heated to a temperature (T_s) that assures partial melting after an initial melting and cooling phase [32]. With lowering T_s, these partial melting processes are

repeated and in particular followed by an isothermal phase during which the unmelted lamella anneals and some of the molten chains can isothermally crystallize according to their crystallizable chain length. The last heating run will disclose the thermal fractionation of the materials as a result of the previously applied thermal protocol[32]. As established for PE-copolymers, the approach results in remarkably effective molecular segregation[395,396]. Later it was also applied to other materials like polypropylene [175,397]. As for application to the determination of complex compositions of recycled blends, it was first done by Carmeli et al.[55]. In that study, the authors were able to quantitatively determine the amount of HDPE in the PE-phase and the entire amount of the PP phase.

Few publications have suggested the application of fast heating/cooling rates, which can result in shorter measurement time. This principle was suggested by the work of Pijpers et al.[182]. Varga et al. thermally fractionated by step crystallization low-density polyethylene and high-density polyethylene at a constant rate, but the last heating run was conducted at a different heating rate (20 and 40°C/min), without finding any significant differences in the obtained results[183,184]. The concept of using fast rates during the SSA protocol was used by Lorenzo et al., who investigated the application of fast scanning rates on hydrogenated polybutadiene[181]. Currently, there are no studies about the use of fast heating and cooling rates in complex systems like recycled polyolefin blends. The fast crystallization behaviour of polyolefins allows carrying out measurements on their blends at high heating/cooling rates. Applying fast scanning rates needs a mass reduction of the sample, to preserve the peak resolution and avoid superheating effects as much as possible. High scanning rates in the SSA protocol can substantially reduce the thermal fractionation time.

In this work, we investigate the applicability of faster SSA thermal protocols to the analysis of the chemical composition of recycled polyolefin blends. After exploring the self-nucleation behavior of selected blends at different rates to determine the optimal analysis conditions, we introduce a shortened SSA protocol which, while comprising a single fractionation step for the PE and PP phase, still allows the separation of the LDPE and non-crystallizable components from HDPE. Both the standard and the new SSA protocols are applied at different scanning rates, demonstrating no substantial difference in the obtained phase composition among the measurement methods. Finally, the recycled blends are analyzed with the fastest SSA protocol and the outcome, in terms of compositions, are compared with those of TREF, revealing excellent agreement in practically all cases.

3.2 Experimental

3.2.1 Materials

Eight materials were obtained from Borealis Polyolefine GmbH (see Table 3.2.1-1). Five materials are coming from post-consumer recycling sources, and are obtained from mechanical recycling. Materials marked with "*m*" are polyolefin mixed recyclates, while those containing "*pp*" in the name are polypropylene dominated recyclates. The approximate composition in percentage is also indicated in the sample code name, e.g., m-PE65PP35 indicates a mixed polyolefin recyclate with approximately 65% of high-density polyethylene and 35 % of polypropylene.

The other three materials are neat virgin grades of high-density polyethylene, heterophasic copolymer of polypropylene and polypropylene homopolymer, which were used as reference materials. Table 3.2.1–1 lists the essential physical parameters of the employed polymers. The thermal properties of the adopted materials are reported, in Table 3.3.1–1.

Table 3.2.1–1 List of the used materials in the investigation.

Post-consumer Recycled Blends	Melt Flow Rate (230 °C/2.16 kg)
m-PE65PP35	5.5g/10min
m-PE60PP40	5.5g/10min
m-PE40PP60	5.5g/10min
pp-PE30PP70	12.5g/10 min
pp-PE20PP80	20.0g/10 min
Neat Polymers (Virgin Materials)	**Melt Flow Rate (230 °C/2.16 kg)**
HDPE	0.3g/10 min*
Heterophasic copolymer PP	3.0g/10 min
Homopolymer PP	6.5g/10 min

* Melt Flow Rate (190 °C/2.16 kg)

3.2.2 Method of preparation

For some of the blends, a small amount of pellets (about 40 grams) was re-blended in a batch mixer (Brabender plastograph), to achieve a good homogeneity of the blend. Mixing was performed at 200°C for 10 min at 60 rpm.

3.2.3 Methods of investigation

Methodology

Equipment

The successive self-nucleation and annealing (SSA) protocol, as well as standard melting and crystallization runs, were applied using a TA Instruments Differential Scanning Calorimeter 250. Measurements were carried out at heating and cooling rates of 10 °C/min, 20 °C/min and 30 °C/min. The temperature limits of the linear ramps were 20 °C and 200 °C.
In order to compare the blend composition results obtained by the SSA protocols with a different quantification method, temperature rising elution fractionation (TREF) was used as an industrial standard. Measurements were performed using the Polymer Char device Crysaf-TREF 200+.

Sample preparation

Samples for the DSC measurement were firstly compression molded to obtain a thin film from the pellets. From that thin film, a small disk was made, with a 4-millimeters hole punch, to get a flat sample for the analysis. This sample size matches perfectly with the pan, which was used in the investigation, a T_{zero} pan, for having good contact with the sensor inside the device. To get a proper weight, needed for the mass compensation experiment, the sample was then cut to the required size (corresponding to weights of approximately 1, 2 and 3 mg).
Samples for TREF were used as received after sample preparation (2.2). In particular, to avoid injecting possible gels and/or polymers which do not dissolve in TCB at 160°C, like PET and PA, the weighed sample was packed into a stainless steel mesh MW 0,077/D 0,05mmm. About 50 mg of the polymer sample have been dissolved in 40 mL 1,2,4-trichlorobenzene (TCB), stabilized with 250 mg/L 2,6-di-tert-butyl-4-methyl-phenol (BHT), for 2 h at 160°C.

Measurement procedures

Standard runs

Standard DSC measurements were carried out at a heating and cooling rate of 10°C/min from 20°C to 200°C. Determination of melting and crystallization temperatures and enthalpies were measured from the second heating and cooling curves.

$T_{S,Ideal}$ selection

The previous thermal history was removed by heating the sample to 200°C. Then, the material was cooled down to 20°C with a chosen rate, to create a standard crystalline state. After cooling, the material was heated to a temperature T_s where the isothermal treatment was

applied for 5 minutes. This isothermal treatment can cause: (a) complete melting, if T_s is much higher than the melting point (T_m) (*Domain I* or complete melting *Domain*); (b) melting of most of the crystals but leaving small crystal fragments or ordered regions in the melt that act as self-nuclei (*Domain II* or self-nucleation *Domain*); (c) partial melting that will cause annealing of unmolten crystals during the 5 min of thermal treatment at T_s (*Domain III* or self-nucleation and annealing *Domain*). Then the material was cooled at a constant rate to 20°C. After that step, the material was finally heated to 200°C again. A final heating run will display any changes in the melting behavior of the material caused by the self-nucleation treatment. If the sample is in *Domain II* only minor changes are usually observed in the melting endotherm with respect to a sample in *Domain I*. However, if the sample is in *Domain III*, an additional high temperature melting peak will appear, due to the melting of the annealed crystals at T_s. Hence, this heating step is necessary to detect if the sample is in *Domain III* or not. Also, changes during the cooling run from the $T_{s,}$ will be observed. When the polymer changes its crystallization temperature (T_c) to a higher value, the material underwent self-nucleation during isothermal treatment at T_s. More nucleation centers increase the T_c, which is the desired effect. $T_{s,Ideal}$ is then found by knowing the boundary between *Domain III* (self-nucleation and annealing) and *Domain II* (exclusive self-nucleation). The ideal self-nucleation temperature ($T_{s,Ideal}$) is the lowest temperature within Domain II and it is defined as the temperature that produces the highest number of self-nuclei in the sample without causing any annealing.

Domain II is subdivided into two subdomains. *Domain IIa* occurs when the Ts temperature is high enough to melt all crystals in the sample (i.e., no latent heat of melting can be detected in *Domain IIa* but low enough to leave certain ordered regions in the melt that can act as self-nuclei upon following cooling. *Domain IIb* is defined by a Ts temperature that is high enough to nearly melt the entire sample but low enough to leave small crystal fragments unmolten, that can represent self-seeds (but are not annealed), as shown in Figure 3.2.3–1 [398,399].

For the recycled polyolefins blends containing polypropylene and polyethylene, the self-nucleation can be conducted as described above, without changes in the protocol, because the temperature treatment applied to PP, while slightly affecting the crystallization temperature of PE, does not meaningfully change the fractionation outcome of the low melting polymer [55]. The opposite, i.e., no effect of PE thermal treatment on PP fractionation, is also true, as demonstrated by Carmeli et al. (see Figure 5, ref [55]). The applied temperature during the self-nucleation protocol, for the polypropylene ($T_{s,Ideal}$ 163.0°C) corresponds to having polyethylene always in *Domain I*. On the contrary, when self-nucleation is applied to polyethylene ($T_{s,Ideal}$

=127.0°C) the polypropylene phase will be in *Domain III*. This concept is graphically represented in Figure 3.2.3–1, which reports representative temperature ranges for self-nucleation of the two phases with the respective self-nucleation Domains.

The steps of defining $T_{S,Ideal}$ needs to be conducted and repeated for every blend and cooling/heating condition used in this study. In fact, different ratios of the phases in the blend, as well as the used heating/cooling rates might change the values of the melting and crystallization temperature, and therefore $T_{S,Ideal}$ as well. The $T_{S,Ideal}$ for polypropylene and polyethylene defined in this stage, for the different compositions and cooling/heating rates, are then later used in the SSA protocol, see below.

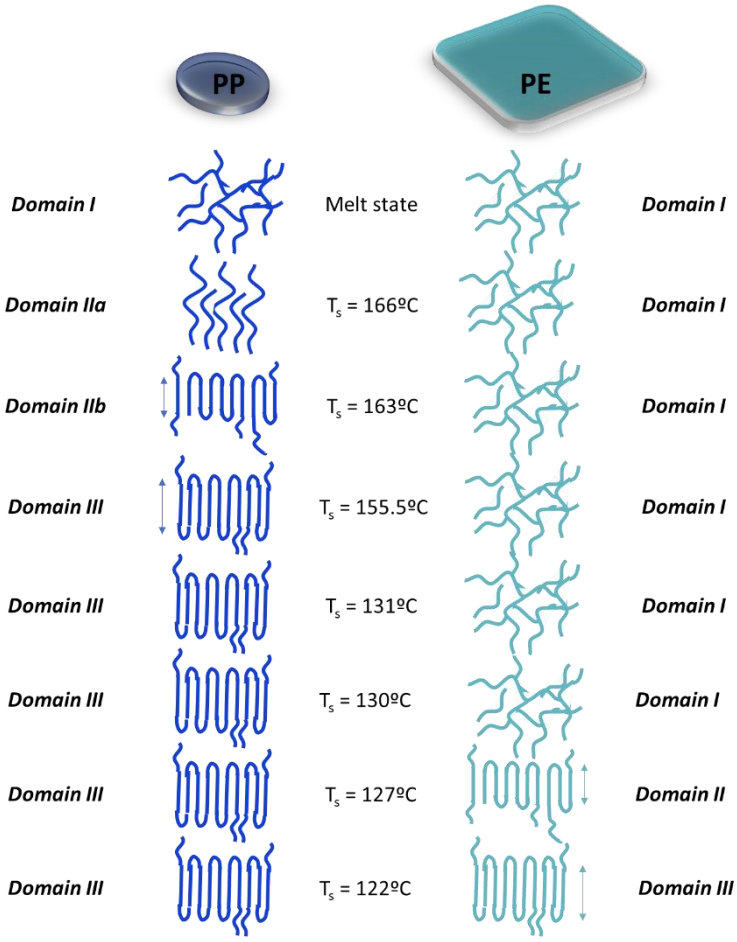

Figure 3.2.3–1 Graphical representation of the PP/PE blend under certain temperatures and related Domains of the two components. The presented temperatures are examples of typical values of a real blend.

SSA multi-fraction protocol ("coupled SSA protocol")

The sample was heated 30°C above the melting temperature to remove thermal history and then cooled down to room temperature under controlled cooling at the chosen rate. From this temperature, the sample was heated to the $T_{s,Ideal}$ (description of the $T_{s,Ideal}$ selection above), and

kept at this temperature for 5 min. As the next step, the temperature was lowered to room temperature to obtain the standard crystalline state. Following this step, the material was heated to T_{s1}^{PP}, which was 7.5°C lower than the $T_{s,Ideal}$ for the polypropylene fraction. The 7.5°C fractionation window was chosen on the basis of a previous optimization [55]. Then again, the sample was cooled down to room temperature. The fractionation window was lowered 4 times from the $T_{s,Ideal,}$ which allowed the production of 4 fractions from the PP phase. As for the polyethylene phase, the material is heated to the $T_{s,Ideal}$ of the polyethylene chosen before, and kept at this temperature for 5 min. From this temperature, it is cooled down to room temperature. The next step requires heating the sample to a temperature of 5°C lower than *TS* ideal for the polyethylene fraction (T_{s1}^{PE}), based on previous studies [32]. Later, the sample is cooled down to room temperature. The steps including lowering the temperature of 5°C and then cooling from that temperature to 20°C were repeated 8 times, which allowed the production of 8 fractions for the polyethylene phase. The last heating step, with the same rate as all the previous steps, goes to 200°C. In this measurement step, the melting points from the fractions produced during the applied protocol are observed. In this fractionation protocol, the material was fractionated into 12 thermal fractions.

SSA single-fraction protocol

The single fraction methodology follows the same measuring principles as the multi-fraction protocol previously mentioned. The difference is in the number of temperature steps. The single-fraction protocol creates only one fraction from each of the two materials under consideration, namely high-density polyethylene and polypropylene. This single fraction is obtained after thermal treatment at $T_{s,\mathrm{Ideal}}$ and $T_{s,1}$ for both materials. Furthermore, the fractionation window remains the same with respect to the multi-fraction protocol.

The protocol only uses a single fractionation step (i.e., isothermal treatment at $T_{s,1}$) for each component of the blend (apart from the self-nucleation step at $T_{s,\mathrm{Ideal}}$, which does not produce fractionation, only self-nucleation of the sample), as it has been demonstrated that the highest temperature fraction of the PE phase is unaffected by co-crystallization phenomena with LDPE [55]. Figure 3.2.3–2 shows the comparison between the abbreviated single fraction SSA thermal procedure and full treatment.

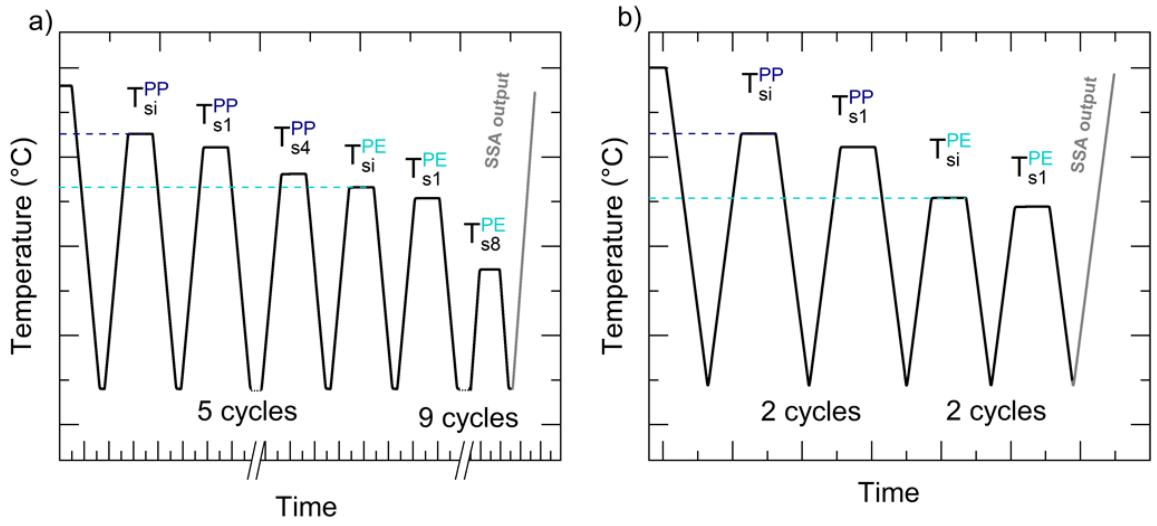

Figure 3.2.3–2 a) Fractionation program implemented and designed by Carmeli et al., which uses 14 cycles to obtain 8 fractions for polyethylene part and 4 fractions for the polypropylene phase [38]. b) Fractionation program designed for the calculation of the main types of the polyolefins: HDPE and PP, which uses 4 cycles of temperature treatments and results in 2 fractions, one for the polypropylene part and the second one for high-density polyethylene.

TREF measurement protocol

The a-TREF analysis was carried out using Crystef-TREF 200+ PolymerChar instrument, equipped with an infrared concentration detector. An aliquot of the prepared solution was injected onto the TREF column and stabilized for 30 minutes at 110°C. After the stabilization the temperature was lowered to 35°C after stabilization using a constant cooling rate of 0.1 °C/min. A flow rate of 0.5 mL/min at 35°C for 10 minutes was used to collect the soluble fraction, followed by a temperature ramp from 35°C to 140°C at a continuous heating rate of 0.5°C/min and flow rate of 0.5 ml/min. The concentration of the eluted fraction and the corresponding signal is determined with the detector and plotted as a function of temperature.

Data analysis

Data from the standard run

For the polypropylene, the crystallization and melting enthalpy were calculated from the baseline, which was chosen from the onset of the polyethylene phase melting till 180°C. On the other hand, for the polyethylene, the crystallization and melting temperature and enthalpy were calculated from the baseline starting from 40°C till the beginning of the polypropylene phase. In the neat materials, the baseline was fixed from 40°C to 180°C, except for neat polypropylene where the baseline ended at 200°C.

Area calculation

The heat flow rate values were divided by the heating/cooling rate to calculate the apparent heat capacity values. These normalized data points were imported into the OriginLab software. In the Origin Lab software, the data from the single fraction protocol was analyzed in the following way:

a) data was imported to the peak analyzer application,

b) baseline values were set to be 40°C to 180°C,

c) two highest peaks were selected manually,

d) boundaries for the area integration for polyethylene were set to be at the minima before and after the peak for polyethylene, and for polypropylene, constant temperature boundaries of 136-180°C were set.

The same methodology has been implemented for the characterization of all materials. The content of a given polymer in the recycled fraction was calculated using a proportion with respect to the area under the melting peak, with the maximum area constituted by the reference materials, i.e., virgin polymer. For polypropylene, the reference value was calculated as the average of heterophasic and homopolymer polypropylene melting peak area, given the different possible types of polypropylenes in real recycled grades. For the high-density polyethylene phase, a grade for film extrusion was used as reference material.

a-TREF analysis

From TREF analyses the normalized concentration plot (dW/dT) together with the cumulative concentration signal normalized to 100 along the temperature were retrieved. The different polymer types were assigned according to their elution temperature in a-TREF. The polymer fraction eluting between 35 and 90°C, which mainly comprises low-density polyethylene and PE fraction with a higher content of short chain branches but also low molar mass PE and PP, is defined as LDPE/LLDPE fraction. The fraction eluting between 90°C and 103°C, which mainly contains homo-PE chains and PE chains with low branching content, is named high-density polyethylene fraction where the fraction eluting above 103°C is defined as polypropylene fraction and the fraction below 35°C as soluble fraction. For materials with higher polypropylene content (*pp*-PE30PP70 and *pp*-PE20PP80), the temperature range was changed for the polypropylene fraction from 100°C to 130°C and for the high-density polyethylene fraction between 90 and 100°C because the elution of the polypropylene starts at lower temperatures. All the other fractions and their temperature ranges remain unchanged.

3.3 Results and discussion

3.3.1 Standard runs

When taken from different pellets, the Differential Scanning Calorimetry measurement showed differences in the enthalpy of fusion for the samples *m*-PE65PP35, *m*-PE40PP60, and *pp*-PE30PP70. Therefore, those blends were homogenized. After melting and blending in a batch internal mixer, 3 tests on the DSC were performed for each homogenized blend. Figure S1 (Appendix A) presents DSC results of blends before and after homogenization. The differences observed among the curves in Figure S1 a, b, c (Appendix A) plots are largely reduced after homogenization (Figure S1 d, e, f in Appendix A). The other two materials were homogeneous as supplied and did not need re-mixing.

Table 3.3.1–1 List of the used materials in the investigation with temperatures of crystallization and melting of the different phases. Measurements of non-fractionated materials were performed at 30°C/min.

Material	T_c **PE [°C]**	ΔH_c **PE [J/g]**	T_m **PE [°C]**	ΔH_m **PE [J/g]**	T_c **PP [°C]**	ΔH_c **PP [J/g]**	T_m **PP [°C]**	ΔH_m **PP [J/g]**
Homopolymer PP	-	-	-	-	124.2	113.5	165.0	113.3
Heterophasic copolymer PP	-	-	-	-	124.7	104.1	165.6	106.8
HDPE	113.1	177.8	127.6	182.2	-	-	-	-
m-PE65PP35	112.8	67.8	125.3	70.7	118.9	32.3	158.9	36.1
m-PE60PP40	114.0	73.8	126.4	72.9	119.4	34.5	159.2	38.8
m-PE40PP60	102.0	50.3	126.2	47.0	118.4	48.2	158.9	54.1
pp-PE30PP70	-	-	125.1	16.8	118.1	87.1	160.2	71.9
pp-PE20PP80	-	-	125.5	26.7	120.2	96.4	160.5	76.8

3.3.2 Self-nucleation and $T_{s,Ideal}$ selection

As an example, the DSC heating and cooling curves for *m*-PE65PP35, following isothermal treatments at T_s for 5 min are shown in Figure 3.3.2–1.

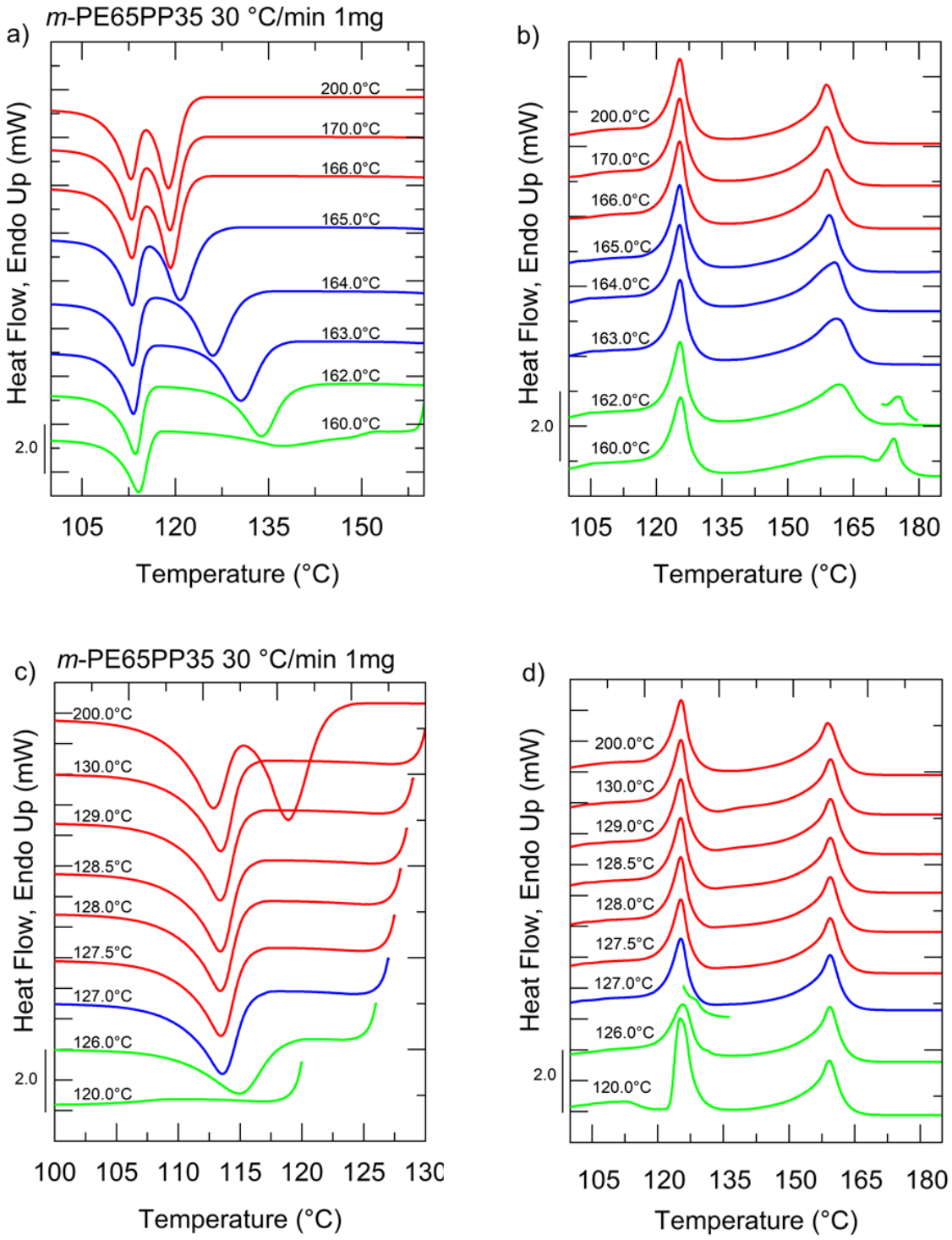

Figure 3.3.2–1 $T_{s,Ideal}$ selection for m-PE65PP35 a) DSC cooling scans at 30°C/min after 5 min at the indicated Ts for polypropylene in recycled polyolefin blend b) subsequent heating scans (at 10 °C/min) after cooling runs shown in a). c) DSC cooling scans at 30°C/min after 5 min at the indicated Ts for polyethylene in recycled polyolefin blend d) subsequent heating scans (at 30 °C/min) after cooling runs shown in c) Colors of the lines in the graphs indicating material under certain domains: red lines - Domain I, blue lines- Domain II, green lines - Domain III. The occurrence of an annealing peak in the PE and PP phase is highlighted as a separate inset next to the corresponding curve. The curves are color-coded to indicate the different SN Domains: red for Domain I, blue for Domain II, and green for Domain III.

In Figure 3.3.2–1a) cooling from 200°C, resulted in a crystallization temperature of the polypropylene phase at 119.0°C. Other experiments, where the isothermal treatment at T_s lays

between 165°C and 163°C, resulted in a significant increase in the crystallization temperatures, from 119.2°C to 130.7°C. Treatment at different T_s values did not change the melting peak significantly (Figure 3.3.2–1b), but slight changes in the shape of the peak were observed for T_s in *Domain II*. However, when T_s is equal to 162°C, the subsequent heating run revealed an additional melting peak around 175.7°C. As such, $T_{s,Ideal}$ can be defined as the lowest T_s value within *Domain II*, which for this specific case is 163°C.

Figure 3.3.2–1c) shows that the polypropylene crystallization peak does not appear when the material is crystallized from 130.0°C downwards, while it is still present if the cooling run starts from 200°C. No change in the crystallization temperature of the PE phase (113.4°C) was observed when experiments were done at T_s values between 130.0 and 127.5°C. However, T_c increased slightly after treatment at T_s =127.0°C from T_c =113.4 to T_c 113.6°C. Because the difference of 0.2°C is modest and within the measurement error range, *Domain II* in this mixed polyolefin system for the polyethylene phase is assumed to be absent.

In high-density polyethylene copolymers, Carmeli et al. found a narrow *Domain II* for high-density polyethylene [400]. In other studies, high-density polyethylene homopolymer and polyethylene blocks inside copolymers were shown to possess just *Domain I* and *Domain III* [401,402]. The authors attributed *Domain's II* complete absence to the high-density polyethylene extraordinarily high number of active heterogeneities, which prevent self-nucleation from causing any further increases in nucleation density. For T_s= 126.0°C there was a significant change in the T_c value which raised to 115.2°C. Therefore, the $T_{s,\,Ideal}$ was chosen as 127.0°C. This is the lowest temperature which does not cause annealing of the polymer lamellae.

In Figure 3.3.2–1d) the heating run after crystallization from 200.0°C results in a melting temperature at 125.4°C. The runs after treatment at selected T_s experiments did not show a significant trend in the melting point. However, after treatment at 126.0°C, an additional peak was obtained around 132.0°C. Therefore, $T_{s,Ideal}$ for the PE phase is identified as 127.0 °C.

Defining $T_{s,Ideal}$ might be a difficult task when the majority of the phase is polypropylene, whose tail might overlap with the melting temperature range of HDPE. In this case, the annealing peak appears on top of the low-temperature tail of polypropylene (see Figure S2 in Appendix A).

3.3.3 Influence of the scanning rate

Each adopted heating and cooling rate in the thermal protocol resulted in a different $T_{s,Ideal}$, see Figure 3.3.3–1. The polypropylene phase Ts ideal shifts from 166.0°C at 10 °C/min

at, to 163.0°C at 30 °C/min. For the polyethylene phase, the change is only minor, i.e., from 127.5°C at 10 °C /min to 127.0°C at 30°C/min. The obtained results for all the analyzed blends are in Figure S3 (Appendix A). The variation of $T_{s,Ideal}$ with cooling rate is associated to the corresponding variation of the crystalline standard state, as a consequence of the changes in crystallization temperature at different rates of cooling. Considering that the dependence of polypropylene and polyethylene crystallization kinetics on undercooling and the self-nucleation behavior of the two polymers are different, the observed different trend of $T_{s,Ideal}$ with cooling rate is understandable. In particular it must be reminded that PP has much less active nucleating heterogeneities than PE, so the crystallization kinetics is more sensitive to cooling rate. Moreover, in PP you can increase the crystallization temperature with self-nucleation much more than in the PE case, because of the lower density of active nuclei. So the small amount of change in crystallization temperature with self-nucleation for PE is reflected in the lower change in $T_{s,Ideal}$.

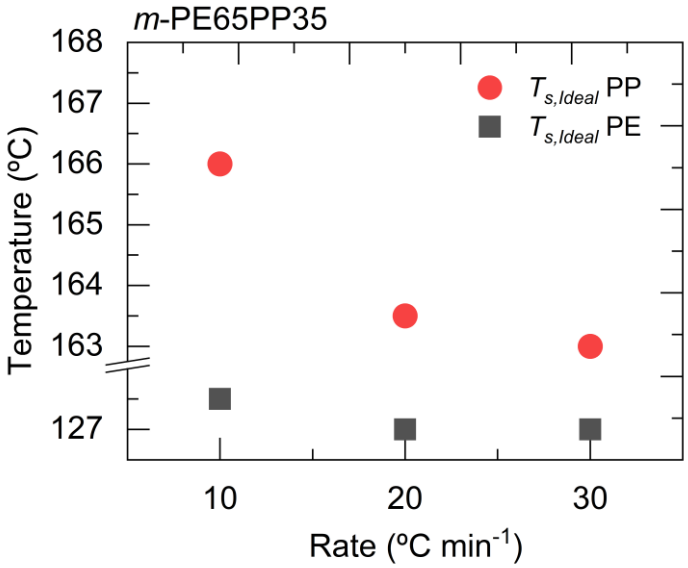

Figure 3.3.3–1 $T_{s,Ideal}$ values selected for the PE and PP fractions present in the recycled blend for m-PE65PP35, as a function of the change in the heating/cooling rate.

3.3.4 Comparison between the two SSA protocols employed

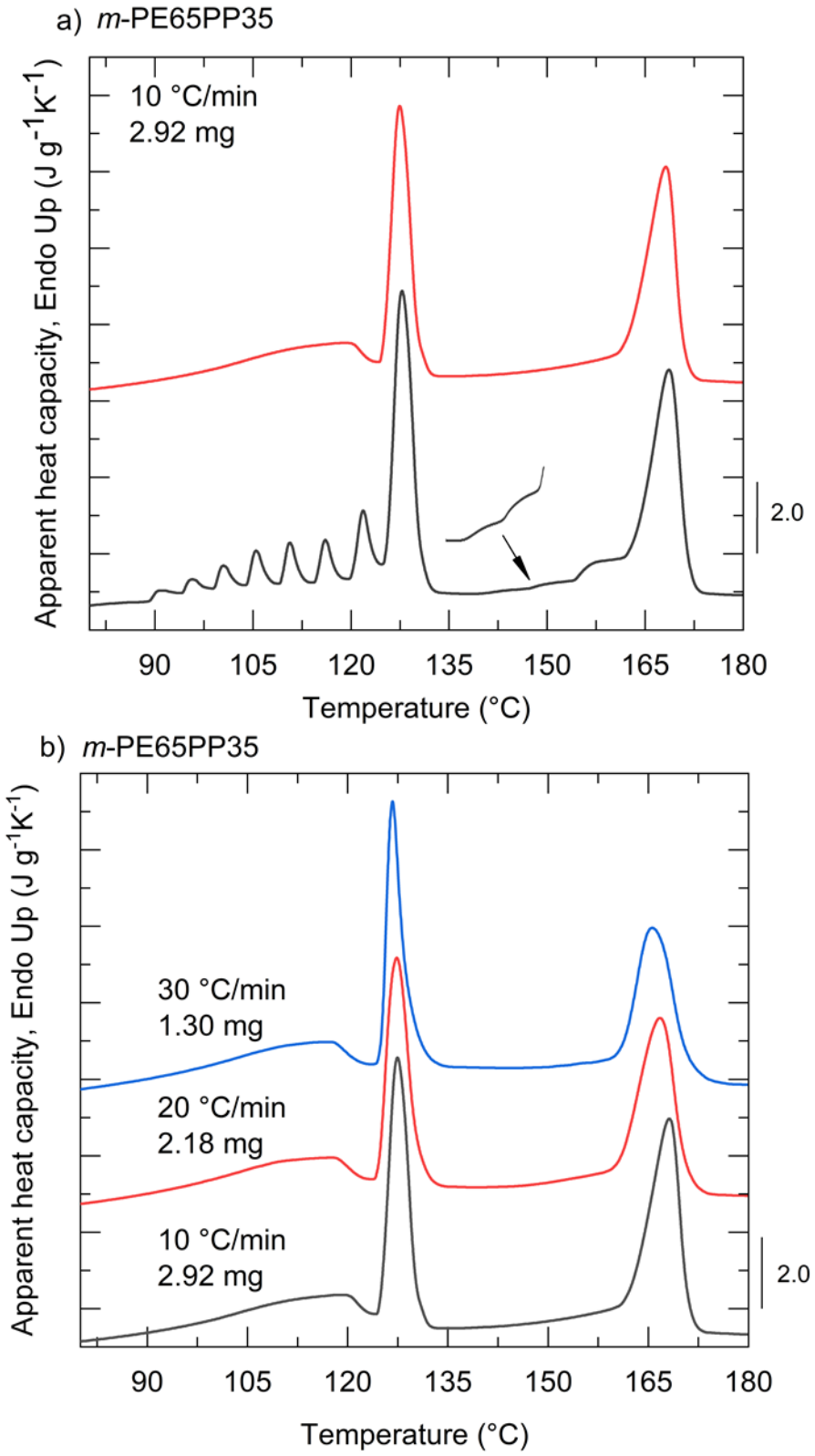

Figure 3.3.4–1 a) Comparison of the outcome of the two SSA fractionation protocols for m-PE65PP35: the DSC curve in red corresponds to the single-fraction and the one in black to the multi-fraction protocol. b) Comparison of single-fraction protocols under different heating/cooling rates, the rates and sample masses are indicated in the inner legend.

In Figure 3.3.4–1a) the black DSC trace represents data from the multi-fraction protocol (coupled SSA protocol). The result of the measurement shows 8 well-defined melting peaks between 90.0°C and 132.0°C corresponding to the 8 thermal fractions produced by SSA on the PE phase. The melting peaks appear every 5°C as expected (i.e., a fractionation window of 5 ºC was employed for the PE phase), and they have different heights and areas, according to the population of the respective crystallizable units in the fraction. Branches interrupt the linear crystallizable sequences in the chains leading to the formation of thinner lamellae that melt at lower temperatures. The higher the branch content, the lower the melting point of the corresponding fraction. Each fraction can be quantified by the area under each peak, or the corresponding melting enthalpy. Concerning polypropylene, there are four peaks between 136.0°C and 172.0°C that represent the four thermal fractions produced by the SSA protocol. The first two peaks at lower temperatures are not well pronounced, but the following ones at 158.5°C and 168.5°C stand out.

In Figure 3.3.4–1a) the red DSC curve represents the result of the single-fraction SSA protocol. The measurement shows a single broad peak in the lower temperature range between 80.0°C and 125.0°C, and a second sharp one at around 125.0°C-132.0°C. The sharp peak is produced by the thermal fractionation performed at $T_{s,1}$ for PE. The second, low-temperature broad peak corresponds to the melting of the unfractionated part of the PE phase. These two peaks probably correspond to the LDPE fraction (possibly co-crystallizing with HDPE) and to the neat HDPE, at low and high temperatures, respectively.

In the case of the PP phase, the single SSA fractionation protocol produces the sharp melting fraction in the range 160.0°C-172.0°C. The unfractionated part of the PP phase melts in the tail of the main fractionated peak located in between 136.0 and 160.0 °C.

Figure 3.3.4–1b) reports the results obtained after applying the SSA single fraction protocol at different cooling and heating rates. It can be seen that the overall appearance of the SSA fractionation curves keeps similar, despite the changes in the scanning rate. The melting peaks are slightly shifted to lower temperatures with a faster heating rate, indicating that the crystals might possess less time to reorganize themselves into thicker lamellae during the heating phase. This effect could also possibly be due to a lower crystallization temperature of the polymers in the cooling step. On the other hand, the area calculation results are not affected by the shift of the melting peak since the reference material was subjected to the same temperature program using same heating/cooling rate. Moreover, the resolution of the peaks

seems relatively unaffected using higher heating rates, as well as the relative area, which appears similar between the different runs, at a first qualitative inspection [403].

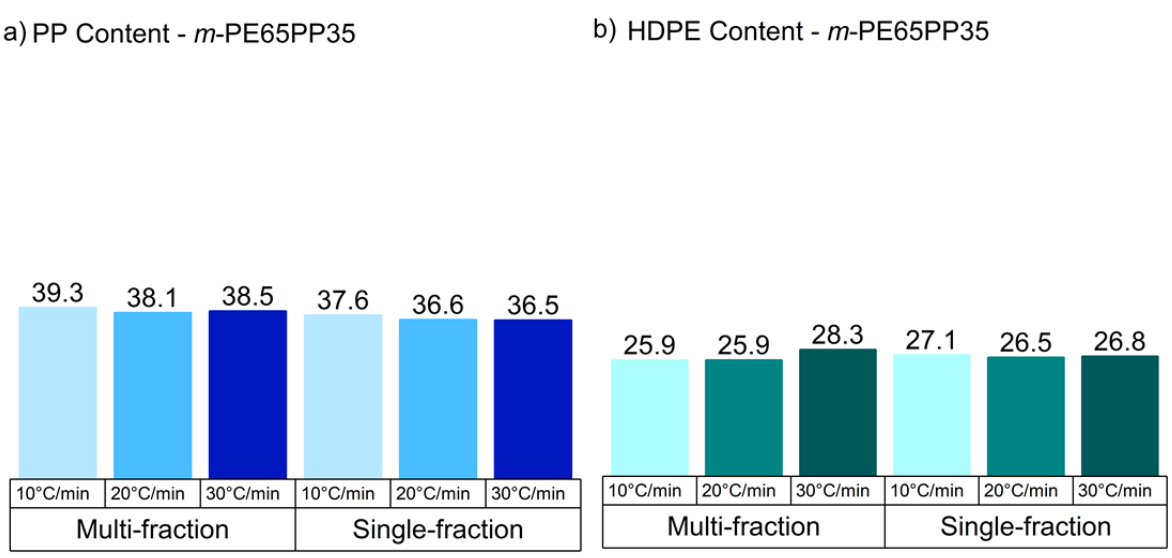

Figure 3.3.4–2 m-PE65PP35 a) content of the polypropylene and b) polyethylene calculated from different measurement rates and protocols (values of the bars are presented in % and the groups under the bars are related to the protocol used for the measurement, example: multi-fraction protocol at 10°C/min – 39.3% of polypropylene).

To confirm the qualitative indication regarding the area of the fractionation peaks, proportional to the content of PP and HDPE phases, the results obtained from calculating the areas under the peaks were pooled and compared together, among different SSA protocols and rates (Figure 3.3.4–2). The results from the multi-fraction SSA protocol were compared at different cooling and heating rates with the results from the single-fraction SSA protocol also at different rates.

For the selected blend, considered as an example, the calculated content is substantially independent of both the type of protocol selected and the heating/cooling rate adopted. This result validates the method and anticipates that meaningful timesaving can be gained by performing all the analyses with the single-fraction protocol and a rate of 30 °C/min.

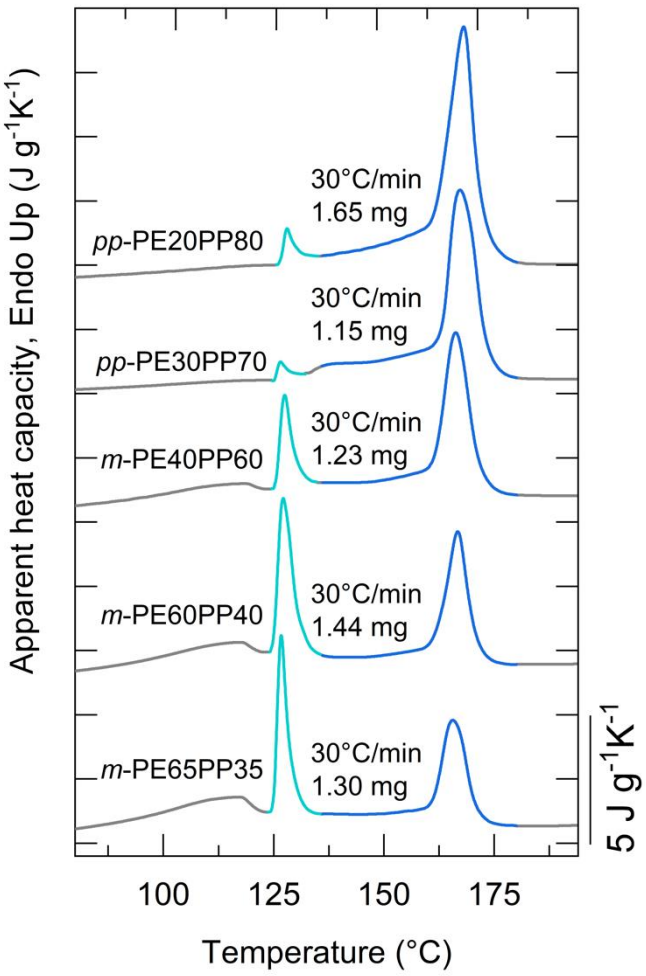

Figure 3.3.4–3 Fractionation output run results for the investigated materials. The content of PP decreases from top to bottom, while that of PE correspondingly increases in the same direction.

In Figure 3.3.4–3, the results of the single-fraction SSA protocol applied at 30°C/min are presented. The data are arranged with decreasing content of PP in the blends from top to bottom. The PE fraction correspondingly increases (notice the increase in melting peak areas of the PE phase in the temperature range of 80.0-135.0°C) in the same direction. It can be seen that only the materials with the highest PE fraction develop a third peak at low temperature upon fractionation, attributed to low-density polyethylene. Material with high PP content possesses a low-temperature melting tail of the polypropylene peak that partially overlaps with HDPE melting peak. For one material, *pp*-PE30PP70, besides this low melting tail, a distinct third fraction is found in between HDPE and PP, possibly generated upon the annealing at $T_{s,Ideal}$ of HDPE. This third fraction can be tentatively be ascribed to low-tacticity/high comonomer content PP chains [404].

The single-fraction SSA protocol was run 3 times on one of the blends at 30°C/min heating/cooling rate to calculate the repeatability of the area integration. The outcome is a precision of 1.3 % for the PP phase and 0.6 % for the HDPE phase. The data used for this calculation are shown in Figure S4 (Appendix A).

Comparison with TREF

Table 3.3.4–1 Results of the composition calculations from the single-fraction protocol (at 30 °C/min heating/cooling rate). All values are displayed as percentages.

Material	PP SSA [%]	PP a-TREF [%]	HDPE SSA [%]	HDPE a-TREF [%]	LDPE + others SSA [%]	LDPE a-TREF [%]	Soluble fraction a-TREF [%]
m-PE65PP35	36.5	35.9	26.8	27.1	36.7	29.7	7.3
m-PE60PP40	39.9	37.7	30.0	28.8	30.1	26.1	7.7
m-PE40PP60	58.0	55.1	16.0	19.8	29.0	16.3	8.7
pp-PE30PP70	71.8	80.8	3.4	5.3	24.8	3.8	10.1
pp-PE20PP80	83.5	82.4	5.7	7.6	10.8	0.0	10.0

All the results of the compositional analysis for the PP and HDPE contents obtained by the fastest SSA protocol (i.e., the single-fraction SSA protocol performed at 30 °C/min scanning rates) are summarized in Table 3.3.4–1, where they are compared with analytical TREF derived compositions on the same blends. The content of “LDPE+others” from SSA is simply derived by the complement to 100%, taking into account the percentages of PP and HDPE. In general, a very good agreement between the two techniques is found. To better visualize the discrepancies, the differences between TREF and SSA results are plotted as a histogram in Figure 3.3.4–4.

The differences in the obtained results between SSA and a-TREF are particularly small for *m*-PE65PP35 and are comprised within 4 % for all the blends, with one exception. In fact, an error of 10.9 % was obtained for *pp*-PE30PP70, in the content of polypropylene, which in turn caused a high error in the content of "LDPE + soluble" as well.

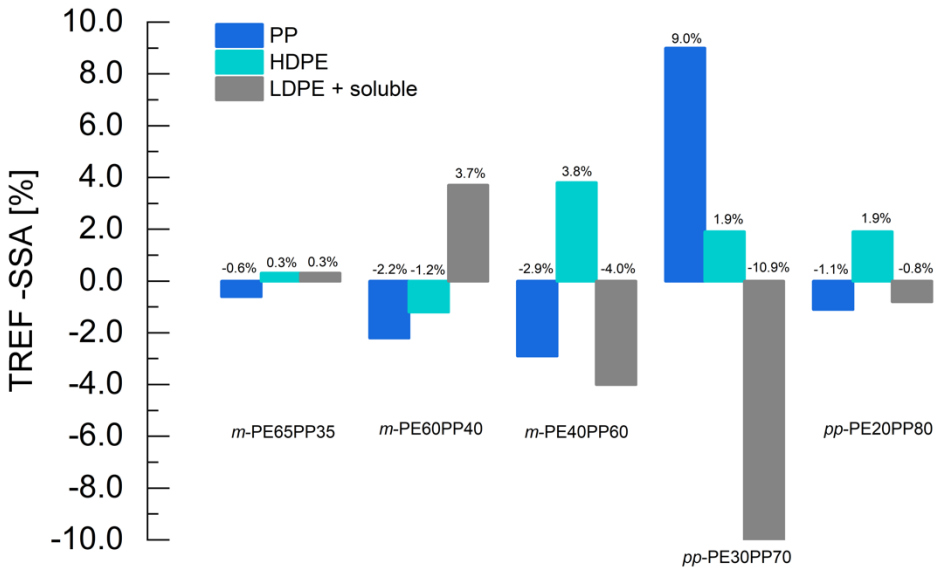

Figure 3.3.4–4 Difference between the TREF and SSA compositions. Each triplet of bars corresponds to a particular investigated material as indicated on the x-axis.

The reason behind the large discrepancy of *pp*-PE30PP70 might be found in the small peak between HDPE and PP fractionation peaks in the SSA results, see Figure 3.3.4–3. This peak cannot be detected in the standard run, which means that it arises during the lower temperature annealing steps of the SSA protocol. As previously described, the peak can be tentatively attributed to random propylene-ethylene copolymers, either crystallizing alone or co-crystallizing with the low-melting fraction of i-PP homopolymer [405]. Figure S5 (Appendix A) presents the result of the a-TREF measurement on the *pp*-PE30PP70 blend. Shorter chains of the low isotacticity polypropylene can elute at 60.0-80.0°C, and therefore there can be an underestimation from the a-TREF results of the polypropylene content [42]. A slight overestimation of the high-density polyethylene can also be produced by chains from the polypropylene, which might elute at the temperature of 90.0°C together with the high-density polyethylene fraction. In general, co-elution is a problem of a-TREF, which is influenced by the experimental conditions [202,291,406]. For most studied blends (except *m*-PE60PP40), the results of HDPE from a-TREF are estimating a higher content than from SSA. Where the polypropylene results from a-TREF present lower content concerning that obtained from the SSA protocol. Both effects of lower PP content and higher HDPE content can be explained partially by the co-elution of low molar mass PP with the HDPE and LDPE fraction in TREF. It is apparent that there is not a unique way of defining the blend composition, but each

technique, i.e., TREF and SSA, has its drawbacks and strengths. Nevertheless, even considering a general agreement within 10% as a worst-case scenario indicates that the faster single-fraction SSA protocol proposed in this work is a successful alternative to a-TREF, leading to faster results in less time and without the use of solvents.

3.4 Conclusions

Higher rates of heating/cooling during SSA thermal fractionation can be applied to commercial recycled polyolefin blends, provided that a mass compensation principle is adopted. Lowering the mass reduces the possibility of thermal inertia.

It is beyond the scope of the study to calculate the LDPE content in post-consumer blends since HDPE and LDPE can undergo partial co-crystallization in this system. This problem arises as well in the fractionation performed with other crystallization-based techniques, such as TREF, CRYSTAF and CEF.

In conclusion, the faster single-fraction SSA protocol proposed in this work is an easy and inexpensive method to be applied to recycled materials to characterize their crystallization properties and the chemical content of individual polymers in a blend. This study proved that the measurement results do not lose their quality if faster scanning rates (as applied in conventional DSC equipment) are used. Using faster cooling/heating rates allows conducting more measurements in the given time. In fact, the SSA protocol can be tailored according to the required outcome. A full fractionation using the rate of 10°C/min takes about 420 min, while the production of a single fraction for the two phases at the rate of 30 °C/min lasts about 75 min. SSA can be used to determine the composition of recycled materials faster than a-TREF, while the precision is comparable.

4 Accurate determination of polyethylene and polypropylene content in polyolefin blends and recyclates by cross-fractionation chromatography

Chapter 4 presents an advancement in the temperature rising elution fractionation coupled with gel permeation chromatography (TREFxGPC) technique. It introduces improvements in the quantification of both virgin and recycled PP/PE blends compositions, by estimating polymer-specific IR-detector response factors and correcting for the molecular weight-dependent amount of PP eluting in the TREF temperature range characteristic of PE. This refinement significantly reduces the error in composition determination from 8% to 2%, offering more accurate quantitative assessment capabilities for recycled blends. Moreover, the enhanced TREFxGPC method not only reliably determines the composition of PCR PP/PE blends but also elucidates their bivariate molecular weight and chemical composition distribution (MWD-CCD), which is essential for understanding their full microstructure. This knowledge is a necessity for their use in more demanding applications.

4.1 Introduction

Recyclates based on polyolefins obtained from post-consumer waste (PCW) or municipal solid waste (MSW) are attracting growing attention from both academia and industry[62,93,383–386]. Due to legislation, there has been an upswing in recycling efforts worldwide[411], driven by initiatives like the European Union's ambitious recycling targets[64,412,413], the evolving recycling policies in the United States[414], and the United Nations' advocacy for sustainable practices among its member nations[415]. This has favored the development to increase the application of recycled polyolefin (rec-PO) and compounds containing rec-PO into prime applications such as packaging or pipes[416–421].

In applications like packaging and pipes, where mechanical properties play a critical role, the characterization of these materials becomes of paramount importance. It is crucial to note that even during the initial material sourcing for rec-PO, a certain degree of consistency is essential. Representative samples must accurately reflect the chemical composition of the material. However, contamination remains a persistent concern[92,93,387,422–424]. For example, in

the pursuit of pure polypropylene (PP), traces of polyethylene (PE) may persist [78,409], and vice versa [95,425,426].

The importance of characterizing the structure extends beyond recyclates and applies to virgin polyolefins as well [35,55,77,185,427]. Fractionation and separation techniques, commonly used in polymer chemistry, are an ideal choice for characterizing the microstructure of polyolefins. These techniques delve deep into the molecular composition of polyolefins, offering profound insights into their properties. A precise understanding of molecular structure can drive advancements in designing high-performance materials, optimizing processing methods, and promoting sustainable practices [77,428,429]. Furthermore, characterizing recycled polyolefin materials becomes even more challenging in the age of growing sustainability demands, necessitating advanced analytical methods to unravel their complex molecular heterogeneities.

Size exclusion chromatography (SEC), also known as high-temperature gel permeation chromatography (HT-GPC or GPC), is an analytical technique developed by J.C. Moore in the 1960s. SEC separates polymers based on their molecular weight [220–222]. However, it is essential to note that macromolecules of the same size (hydrodynamic volume) may differ in chemical composition but co-elute in SEC. Therefore, the GPC of polyolefins has been enhanced by integrating various detectors, including molar mass-sensitive detectors such as multi-angle light scattering detectors [244,245], online-viscosity detectors [246–249], and chemical-sensitive detectors like FTIR [250–254] or NMR spectroscopy [255,256]. This combination of SEC separation with molecular and chemical sensitive detectors offers valuable insights into the variations in chemical structures across the molecular weight spectrum of ethylene and propylene-based polymers.

Temperature rising elution fractionation (TREF), has emerged as a powerful method for separating polyolefins based on their chemical composition. Unlike molecular weight distribution (MWD) based separation in GPC, TREF focuses on chemical composition distribution (CCD), providing insights into chemical composition. To increase TREF's capabilities, it has been combined with additional detectors similar to those commonly used in GPC [291,430,431]. These detectors enhance the depth of information, allowing for insights into average molar mass, intrinsic viscosity, and chemical composition along the elution temperature axis [246,428,432,433].

The development of these techniques was initially motivated by the need for improved characterization methods, particularly in the context of linear low-density polyethylene (LLDPE). Hyphenated methods have been frequently utilized to investigate synthesis-related properties, providing simultaneous data on chemical composition distribution in relation to molecular weight and vice versa. The increasing microstructural complexity of modern polyolefin resins has driven the adoption of more advanced techniques, involving multiple detectors and combining different separation methods. Pioneers in the field, such as Nakano and Goto [434], have paved the way for these hyphenated methods.

Yau et al. introduced the characterization of various polyolefins using a Hybrid 3D-GPC-TREF instrument equipped with three online detectors [246]. Ortín et al. developed a fully automated cross-fractionation instrument (TREFxGPC) to determine the bivariate distribution of polyolefins [291]. This innovation significantly expanded the capabilities of studying polyolefin materials, including the ability to investigate the impact of catalytic systems in the synthesis e.g., of high-density polyethylene (HDPE) intended for pipes [292] and the investigation of thermomechanical degradation of polypropylene within polypropylene/ polystyrene blends [293]. When examining molecular structures resulting from complex synthesis or degradation products, it is fair to use integrated analytical methods, as reported in previous studies [209]. This strategy necessitates the use of a variety of analytical techniques in order to gain a thorough understanding of molecular architecture. Another approach proposed by Bungu and Pasch [294] suggests constructing libraries of different polyolefin materials and their correlations between molecular weight and branching.

These examples highlight that in contemporary polymer research, understanding the molecular structure of polyolefins goes beyond simply considering molecular weight and chemical composition. Factors such as branching, stereochemistry, and tacticity significantly influence the material's properties and behavior[35,209,247,294,435–437]. Advanced analytical instrumentation has enabled researchers to delve deeper into these structural features, shedding light on previously unexplored relationships.

Moreover, in the context of recycling and circular economy initiatives, characterizing the molecular structure of recycled polyolefin materials becomes crucial for ensuring the quality and suitability of these materials for various applications [76,77,113,438]. Apart from the chemical structure of the main components, PE and PP, the amount and structure of impurities are crucial determinants. Pasch et al. demonstrated the capability to determine the amount of

different polyolefin types in mixed PP and PE blends containing HDPE, low-density polyethylene (LDPE), and PP mixtures by crystallization analysis fractionation (CRYSTAF) [439]. However, it is important to note that there were discrepancies of around 10% between experimental and nominal values. Monrabal et al. found that TREF offers better resolution for highly regular isotactic PP/ PE blends, while CRYSTAF is more suitable for PE blends with ethylene-propylene copolymers (EPC) or less regular resins [440]. Juan et al. investigated PE contaminated with 1-16 wt % PP and observed a relationship between differential scanning calorimetry (DSC) and TREF results [76]. Hashemnejad recently used crystallization elution fractionation (CEF) to analyze the compositions of blends of LLDPE and LDPE. His modification was efficient even for post-consumer recycled (PCR) LLDPE/LDPE [77].

None of the reported analytical methods provided satisfactory precision in determining PE and PP content or were developed for broader composition ranges. This study's primary aim is to discern the disparities between TREFxGPC outcomes and compounded (nominal) values of PP and PE. The methodology involved melt-mixing for blends, DSC for melting and crystallization temperatures, and TREFxGPC for concentrations and molecular weights. Blends of PE and PP with diverse concentrations, as well as different isotactic homo-polypropylenes characterized by varying molecular weight, were examined utilising cross-fractionation chromatography (CFC). This method improved analytical precision by taking the molecular weight of PP and polymer-specific detector response into account.

The developed approach was then validated with 3 different PE/PP virgin model blends and 3 commercially available PO-based recyclates.

4.2 Experimental

Materials. Seventeen blends (Table S 1) were created by blending neat virgin polyethylene (PE) and polypropylene (PP) at different concentrations using a twin-screw extruder to investigate variations between concentration values obtained from TREF and the provided values (obtained from processing). Concerning the polymers used in the 17 blends for composition investigation, the PE has a density of 945 kg/m³, a weight-average molecular weight (M_w) 206.0 kg/mol and dispersity (Đ) 19.8, while the PP is a homo PP with a M_w= 342.0 kg/mol and Đ= 8.4. The blend compositions were verified through nuclear magnetic resonance (NMR) spectroscopy, as indicated in Table S 2.

To assess the effectiveness of the method, both validation blends and post-consumer recycled (PCR) were employed in the evaluation. First, three validation blends, designated as

V1-PP/PE, V2-PP/PE and V3-PP/PE, were prepared using a solution blending technique. PP with M_w of 470.0, 342.0, and 124.0 kg/mol, along with the respective Đ 8.3, 8.4 and 5.2, were utilized for V1-PP/PE, V2-PP/PE, and V3-PP/PE. In V1-PP/PE and V3-PP/PE, polyethylene (PE) with M_w=158.5 kg/mol and Đ=16.0 was utilized, while PE with M_w=206.0 kg/mol and Đ=19.8 was incorporated into V2-PP/PE. Subsequently, the method's applicability was tested by evaluating three PCR.

To examine molar mass dependencies, 13 PP samples with varying molecular weights ranging from 31 to 412 kg/mol were utilised, see Table S 3. Furthermore, detector factor validation was carried out using ethylene-propylene copolymers (EPC) and the NIST standard of PE (EPC-10), as detailed in Table S 4.

TREFxGPC. Cross-fractionation chromatography (CFC or TREFxGPC) was carried out using a CFC instrument (PolymerChar, Valencia, Spain) [291]. The concentration was measured using an infrared detector (IR5 from PolymerChar, Valencia, Spain). 8 mg of the polymer sample was dissolved in 8 mL of 1,2,4-trichlorobenzene (TCB) at 150°C, and stabilized with 250 mg/L of 2,6-bis(1,1-dimethylethyl)-4-methylphenol. Once the material had been thoroughly dissolved, an aliquot was placed into the TREF column and stabilized at 95 °C for several minutes. For the first dimension TREF the sample was analyzed using the analytical parameters listed in Table 4.2–1.

Table 4.2–1 Experimental parameters for CFC analysis of PE and PP standards and blends. The table shows the dissolution temperature, dissolution time, stabilization temperature, stabilization time, cooling rate, and elution steps used for the CFC method.

Dissolution Temperature [°C]	**Dissolution Time [min]**	**Stabilisation Temperature [°C]**	**Stabilization Time [min]**	**Cooling rate [°C/min]**	**Elution steps**
150	150	95	45	0.2	27

A procedure of discontinuous elution was implemented, following the temperature increments outlined in Figure 4.2–1.

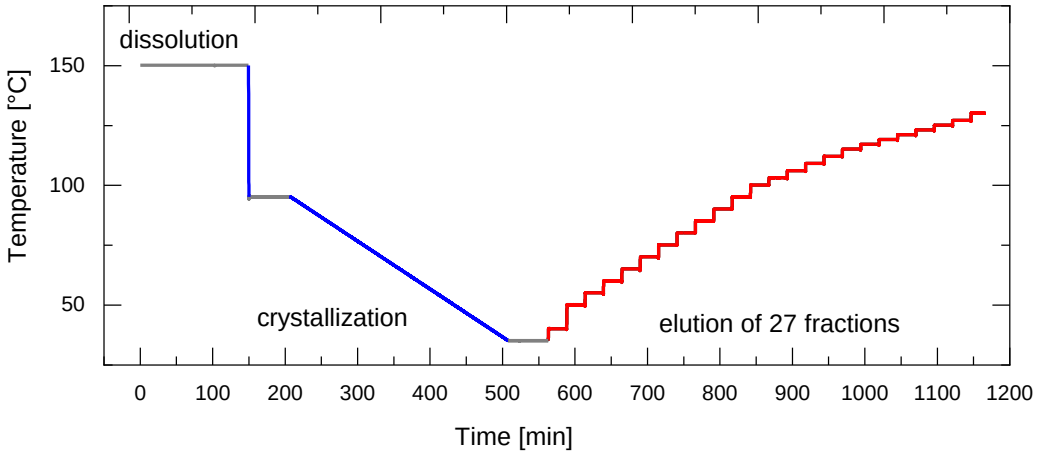

Figure 4.2–1 Schematic representation of the TREFxGPC method's temperature-time profile. The plot illustrates the sequential stages of dissolution (initiating at 150°C), crystallization, and subsequent elution of 27 distinct fractions.

In the second dimension (GPC) 3 PL Olexis columns 1x Olexis Guard columns from Agilent (Church Stretton, UK) were used as stationary phase. 1,2,4-trichlorobenzene (TCB) at 150 °C and a constant flow rate of 1 mL/min was used as the eluent. It was stabilized with 250 mg/L 2,6-Di tert-butyl-4-methyl-phenol. The column set was calibrated with 15 narrow MWD polystyrene (PS) standards in the range of 0.5 kg/mol to 11,500 kg/mol. Mark-Houwink constants for PS and PP used are as given in the literature [441]. The PP equivalent molecular weight distribution and the corresponding molecular weight averages M_n, M_v, M_w, and M_z are employed in this study for all CFC tests, regardless of the polymer composition.

DSC. Melting (T_m) and crystallization (T_c) temperatures were measured using a differential scanning calorimeter, Discovery series DSC2500, TA Instruments, according to ISO 11357/3. The measurements were carried out at a heating and cooling rate of 10 °C/min from 20 °C to 225 °C. The transitions were deduced from the second heating and cooling curves; the values of T_c and T_m are included in Table S 1.

Melt-mixing. The PE and PP materials were blended at various concentrations using a ZSK 18 MegaLAB twin-screw extruder (Coperion GmbH, Germany) operating at 220 °C. The blend compositions were verified by NMR spectroscopy (Table S 2).

NMR. Quantitative $^{13}C\{^1H\}$ NMR spectra were acquired using a Bruker Avance Neo 400 NMR spectrometer, operating at 400.15 MHz for ^1H and 100.62 MHz for ^{13}C. A ^{13}C -

optimised 10 mm extended temperature probe head was used to record all spectra at 125 °C while employing nitrogen gas for all pneumatics. Material (approx. 200 mg) dissolved in *1,2*-tetrachloroethane-d_2 (TCE-d_2, approx. 3 ml) alongside 3 mg of BHT (2,6-di-tert-butyl-4-methylphenol) and chromium-(III)-acetylacetonate resulted in a 60 mM relaxation agent solution[436]. Comonomer content in propene/ethylene copolymers was quantified according to Wang et al.[442]. To ensure a homogeneous solution, the NMR tube was heated in a rotatory oven for at least 1 hour following initial sample preparation in a heat block. The tube was spun at 10 Hz after being inserted into the magnet. This configuration was chosen primarily for the high resolution and quantitative requirements required for reliable ethylene content estimation. Without Nuclear Overhauser Effect (NOE), standard single-pulse excitation was used with an optimized tip angle, 1 s recycle delay, and a bi-level WALTZ16 decoupling technique as described in Zhou et al.[443] and Busico et al.[444] . Per spectrum, 6144 (6k) transients were collected. Spectra processing and integration yielded quantitative measures, with chemical shifts referenced to the central methylene group of the ethylene block at 30.00 ppm. This method enabled consistent referencing across various samples. Ethylene incorporation, identifiable via characteristic signals [445], was calculated as:

$$fE = \frac{E}{(P + E)}$$

Here, fE represents the fraction of ethylene relative to all monomers. The comonomer fraction calculation, adapted from W-J. Wang and S. Zhu[442], considered multiple signals across the spectral range. Integral regions were adjusted for broad comonomer content applicability. Mole percent comonomer incorporation was derived as:

$$E[mol\%] = 100 \cdot \text{fE}$$

4.3 Results and data analysis

GPC and DSC analysis of PE and PP blends

Prior to cross-fractionation chromatography (CFC) analysis, the 17 PE and PP blends were investigated with DSC and GPC-IR with an IR5 detector to gather fundamental information.

The molecular weight distribution (MWD) was determined from individual GPC (GPC-IR 5) analyses of all analytical TREF fractions obtained by CFC. The bulk MWD is calculated

from the bulk dw/dlogM at each specific molecular weight M_i, which is described in equation (10) below:

$$dw/dlogM_{Mi} = \frac{\sum_{35}^{140} w_i \cdot dw/dlogM_{Mi}}{\sum_{35}^{140} w_i} \quad (10)$$

where M_i is the molar mass of the polymer at a specific elution temperature [g/mol], w_i the weight fraction of the polymer at a specific elution temperature and i the index of the elution steps from 35 to 140 °C. It should be noted that 35°C was the lowest elution temperature and 140°C the highest one applied in the CFC analysis. Similarly, the total quantity of CH_3/1000 carbons across the molecular weight spectrum was determined utilizing the same approach employed for MWD analysis (GPC-IR5).

The resulting MWD data (GPC-IR5) for selected individual blends are depicted in Figure 4.3–1. Notably, discrepancies in MWD and peak shape (Figure 4.3–1a) were noted in the GPC profiles as the composition of the blend was altered. Notably, a significant distinction is observed in the dispersity of these materials. The selected PE displays broad dispersity, whereas PP exhibits a narrower distribution, resulting in a more uniform profile. These differences are evident in Figure 4.3–1 a, where a shift in peak shape can be seen. PE has a weight average molar mass of 245 kg/mol PP equivalent, while PP has a weight average molar mass of 374 kg/mol.

Relying solely on GPC or GPC-IR data to differentiate between PE and PP based on hydrodynamic volume can be complex due to the co-elution of PE and PP molecules of the same size. However, the distribution of chemical composition along the molecular weight spectrum is clear from the methyl units per 1000 total carbons (CH_3/1000TC) profiles (Figure 4.3–1b). The presence of both PE and PP in the blends is confirmed by CH_3/1000TC values ranging from 0 to 333. For neat grades, PE has a value near 18, while PP's value is approximately 330. These differences highlight the utility of combined GPC and CH_3/1000TC profiles for analyzing polyolefin blends. Still, it is challenging to discern from GPC-IR data whether a value of 200 CH_3/1000TC comes from a copolymer or a blend of PE and PP homopolymers, as shown in Figure 4.3–1b. The components of the specific PE/PP blends investigated in this study are well-defined, allowing a 200 value to be assigned to the simultaneous elution of PP and PE fractions. However, when dealing with unknown compositions, such as certain recycled polyolefins, determining the source of this value becomes difficult.

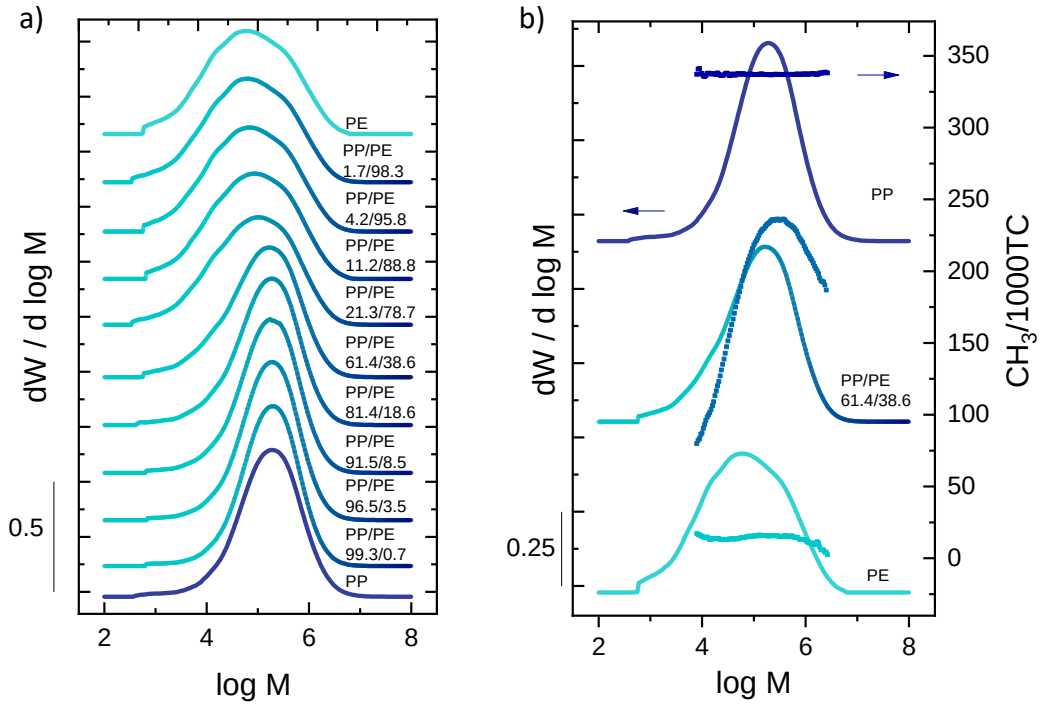

Figure 4.3–1 GPC and CH_3/1000TC profiles of selected PP and PE blends and neat grades. (a) GPC profiles show the variations in MWD and peak shape. (b) CH_3/1000TC profiles show the chemical composition distribution along the molecular weight.

Employing another fundamental technique, DSC, the differentiation of polymer blends based on their sizably different melting temperatures is effectively achieved. In examining PE/PP blends, it is noted that their melting points are 127.5°C and 161.1°C, respectively, as depicted in Figure 4.3–2. The recorded melting enthalpy curve for these blends displays characteristic dual peaks, clearly indicating the distinct separation in the melting peaks. Although the low content of PP and PE makes minor quantities challenging to discern, small traces of PP or PE remain identifiable against the neat (unmixed) material profiles, showcasing the sensitivity of thermal analysis. The intensities (enthalpy) change in accordance with the component content within the blends while the positions of the peaks remain unchanged, thus enabling an estimation of the PE and PP content. By utilizing the enthalpy of the neat specific polymer, it is possible to calculate the blend's composition accurately. The calculated content aligns well with the compounded composition, albeit with the lowest accuracy observed at PP/PE-61.4/38.6 and PP/PE-21.3/78.7 compositions, resulting in error bars of approximately 5-6%, as shown in Figure S1(Appendix B) . Nonetheless, differential scanning calorimetry (DSC) techniques remain a favored choice among researchers, for determining PP and PE content using calibration master curves [46,78], employing temperature-modulated DSC[446], fast scanning calorimetry (FSC) [427], or adhering to well-defined protocols to ensure the extraction of precise quantitative data accurate quantitative data [55,185,214,447].

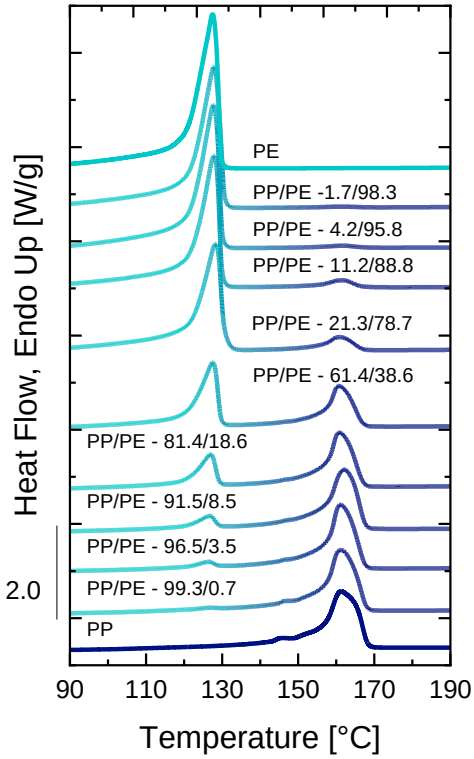

Figure 4.3–2 Melting behavior of neat PP, PE and selected blends indicating distinct thermal profiles of the two components.

TREF analysis of PE and PP blends

DSC provides insights into the content and melting properties of the studied material. On the other hand, GPC with infrared detection (GPC-IR) could be further investigated to gain insights not only on MWD but also on chemical content based on the CH_3/1000TC ratio. Fractionation techniques serve as tools to obtain chemical composition distribution and content. Among these methods, techniques for chemical composition distribution (CCD) based on crystallization of the polyolefins from polymer solution like TREF, CRYSTAF, and crystallization elution fractionation (CEF) have emerged as powerful tools for polyolefin separation.

TREF, an old but robust technique, has a good separation efficiency for semi-crystalline PE and PP [36,190,198,440,448]. The TREF results for selected PP/PE blends, neat PP, and PE are illustrated in Figure 4.3–3. This figure highlights distinct elution peaks for PP and PE, aligning with expectations from the literature. PP primarily elutes between 115-130°C and PE between 85-100°C. The soluble fraction is detected within the 30–35°C temperature range. However, its quantity is influenced by the specific blend of PP or PE being analyzed. In this study, the amount of the soluble fraction was found to correlate with the PP or PE content in the blend,

but this relationship was observed to be specific to the PE and PP variants that were examined. It must be emphasized that such behavior is not universally exhibited across all PE and PP types. For example, when the proportion of PP in the blend was increased, a decrease in the soluble fraction was observed, reflecting the inherent soluble fractions of 2.9% in the PP that was studied and 4.8% in the chosen PE. The designated quantification ranges of 35-103°C for PE and 103-140°C for PP enhance the measurement precision. In Figure 4.3–3, these elution temperature regions for PE and PP are represented using two distinct shades of blue.

A comprehensive overview of the results is presented in Figure 4.3–3, complemented by Figure 4.3–4 which displays a bar chart highlighting disparities between TREF-derived results and nominal blend composition values. Notably, when PP accounts for 61.4% of the blend, making PE the minority component, the overestimation of PE peaks remains stable at 4.9-7.3%. When PE is the main component, the content differences are small, ranging from 0.5 to 3.9%. Given the prominence of this trend and the acknowledged reliability of TREF as a technique within the field of polyolefin characterization, a more comprehensive investigation was carried out.

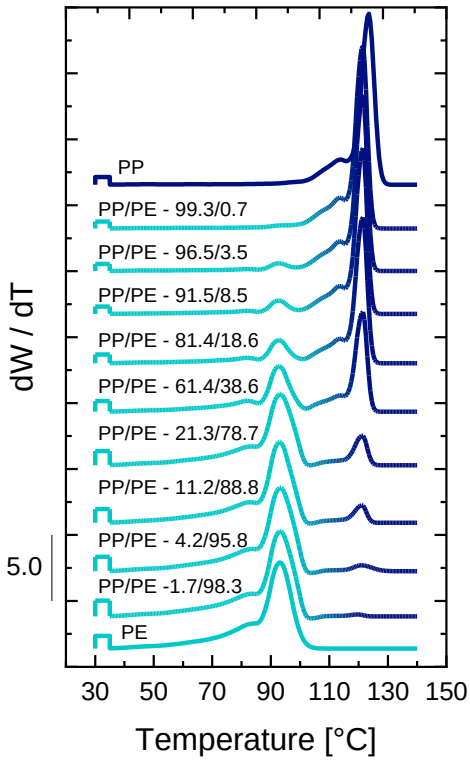

Figure 4.3–3 TREF profiles for selected blends of polypropylene (PP) and polyethylene (PE), as well as for neat grades of each polymer.

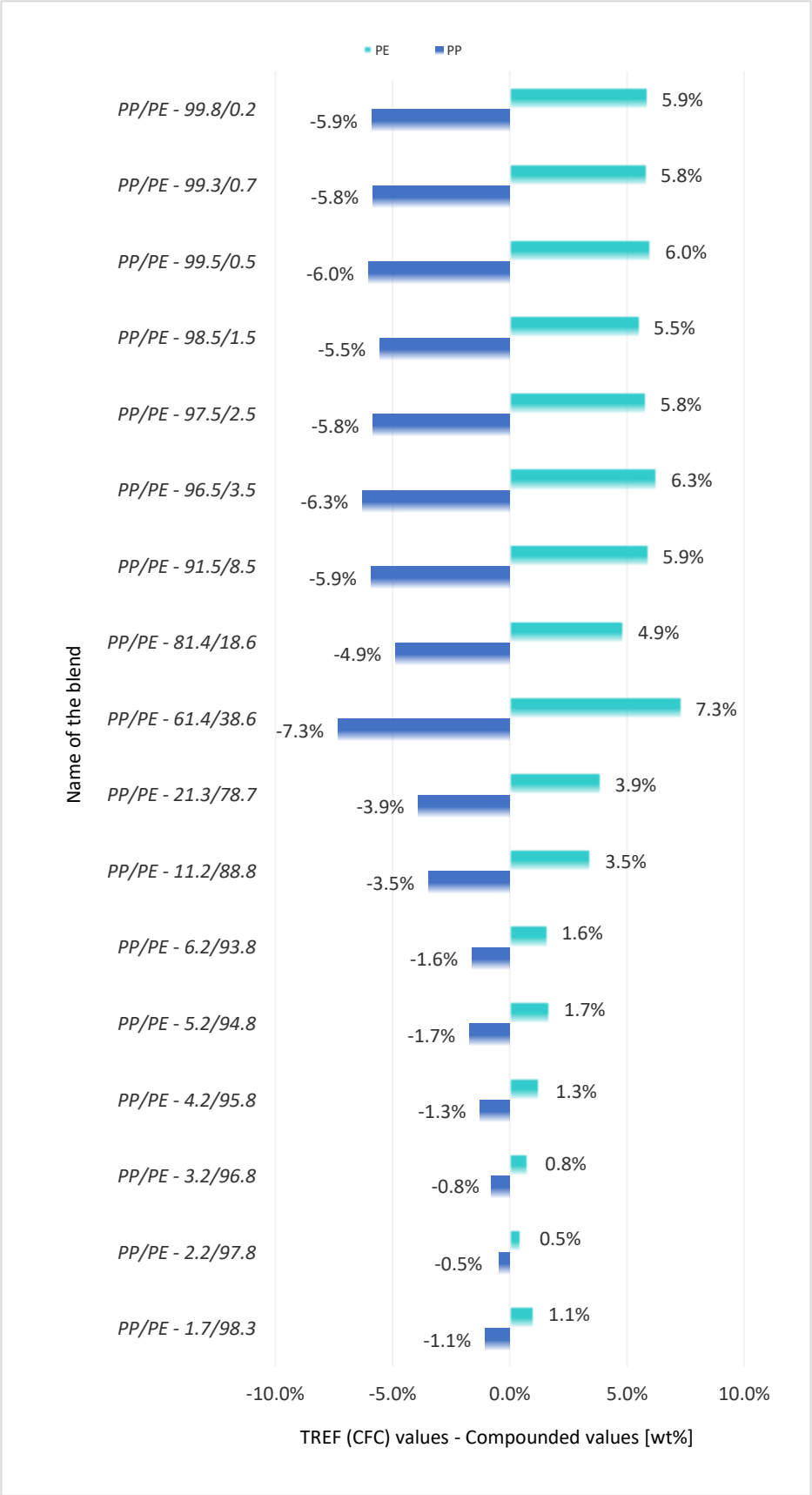

Figure 4.3–4 Bar chart representation of values of the concentration obtained from TREF measurement vs compounded values of PP/PE blends. The y-axis categorizes 17 different blends, designated by their respective PP and PE contents. The x-axis displays the percentage differences. The bars are color-coded, with polyethylene (PE) shown in light blue and polypropylene (PP) in blue.

The examination of the blends' MWD, illustrated in Figure 4.3–1, indicates the presence of a significant amount of low molecular weight fractions below 10 kg/mol. These fractions arise from standard industrial polymerization practices known for yielding diverse chain length distributions due to several active sites on the Ziegler-Natta catalyst [193,449–451] and/or from multimodal polymerization processes, where different polymer types are produced in different reactors [429,430]. Beyond the chemical structure, or more precisely, the longest chain sequences included in the crystals, it is now well documented that the quantity and molecular weight of the low molecular weight fraction below 10 kg/mol for PE [194] or 50 kg/mol for PP has an impact on the elution behavior in TREF [454]. To achieve exact elution at a selected temperature, a single chain length and precise chemical structures for all chains are required, an assumption that differs from the reality of polymers emerging from polymerization operations. Therefore, it is crucial to know the temperature region where co-elution of low molecular weight PP and PE is occurring.

Compensation for PP elution in the PE temperature range

In order to solve the issue of PP elution within the PE temperature range, it is necessary to define the region of co-elution of these two polymers. The matrix technique, as described by Bhati et al. [455], was used to define the region where both polymers coelute. As seen in Figure 4.3–5, the co-elution region is marked in grey, where the profiles of the neat materials overlap. This co-elution domain occurs within the PE elution temperature range, potentially leading to an overestimation of PE content and an underestimation of PP content. Specifically, the PP utilised in this study exhibited an elution of 4.2±0.3 wt% within the PE temperature range. For known neat grades of PP, the elution within the PE range can be isolated for separate measurement, thereby enabling adjustments to the quantity of PP eluting in the PE range within mixed blends. However, when unknown grades such as recycled materials are concerned, alternative strategies become necessary.

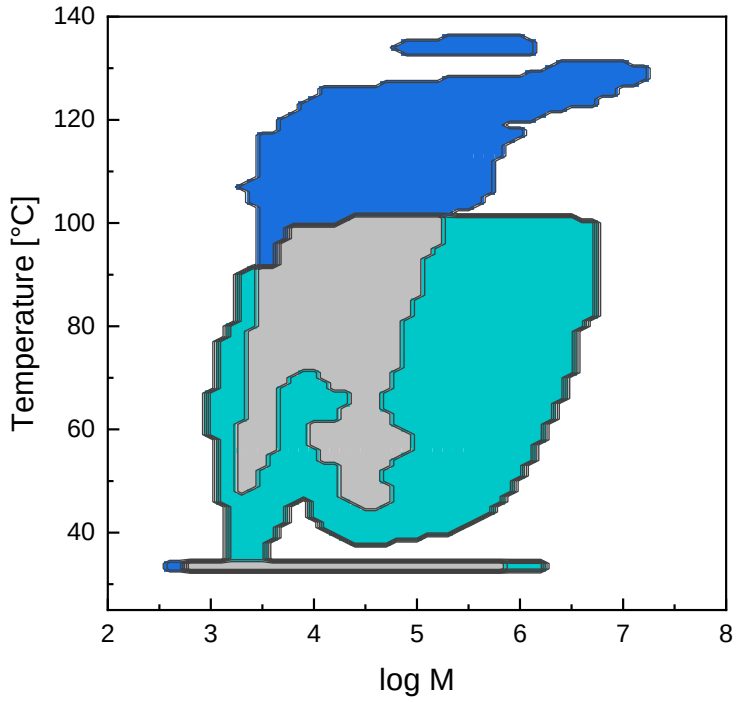

Figure 4.3–5 Contour plot of neat PP (blue area) and PE (light blue area), the overlay of the matrix of PP and PE reveals co-elution regions, indicated as grey area. The plot uses elution temperature (°C), as the y-axis and the logarithm of the molecular weight (g/mol), on the x-axis.

It is worth noting that addressing the PP fraction eluting within the PE regions is simpler compared to compensating for the elution of the PE component in the low molecular weight PP region. This complexity arises from the broader variety of comonomers, a wider distribution in molecular weights, and the intricate chemical structures that polyethylene (PE) can possess. In contrast, polypropylene exhibits a more uniform microstructure and chemical composition distribution, thereby simplifying the compensation process.

A correlation curve was therefore developed by measuring various grades of homopolymer PP and utilizing their viscosity average molecular weight (M_v). The goal of this correlation is to establish a connection between the M_v of a specific PP and the quantity of PP fraction present in the PE region. From the GPC part of TREFxGPC, the corresponding values for number-average molecular weight (M_n), weight-average molecular weight (M_w), viscosity average molecular weight (M_v), z-average molecular weight (M_z), and peak molecular weight (M_p) were obtained for each fraction. These individual values allowed the determination of corresponding molecular weight averages for the PP region.

A previous study set 103°C as a threshold, ensuring no PE fraction eluted above this temperature in the analyzed PE samples with a density range of 962-902 kg/m³ [338]. This was further supported by the overlay of PP and PE elution contours in Figure 4.3–5. Only the

fractions eluting above 103°C consist solely of PP and are used to evaluate the molecular weight dependence. In this case, M_v is employed to establish a connection between molecular weight and the PP fraction eluting in the PE temperature range. Equation (11) is utilized to calculate M_v from GPC data, serving as a valuable indicator, especially for smaller molecules exerting a higher influence on this average molecular weight compared to the M_w value.

$$M_v = \left[\frac{\sum_{i=1}^{\infty}(N_i \cdot M_i^{\alpha+1})}{\sum_{i=1}^{\infty}(N_i \cdot M_i)}\right]^{\frac{1}{\alpha}} \quad (11)$$

N_i – number of molecules

M_i – molecular weight [g/mol]

α – Mark-Houwink exponent

The established power-law correlation between the viscosity-average molecular weight (M_v) of polypropylene (PP) and the amount of PP eluting in the PE range enabled the adjustment of the PP content. An exponential decrease in elution within the PE range was observed with an increase in M_v. This correlation, represented by equation (12), was derived through the least square regression of the data (see Figure 4.3–6). The data includes the PP fraction eluting in the PE temperature range and M_v of PP calculated from polymer fractions eluting above 103°C. This analysis strongly suggests that M_v is suitable to be used as a predictive tool for quantifying the level of PP elution in the PE range, thereby enhancing the accuracy of TREFxGPC results for the content calculation of the homopolymers in the blends.

$$y = 9260.1x^{-0.977} \quad (12)$$

y – amount of the PP eluting in the PE range [wt%]

x – M_v of the fractions which elute above 103°C [g/mol]

The coefficient of determination (R^2) for this regression was found to be 0.97.

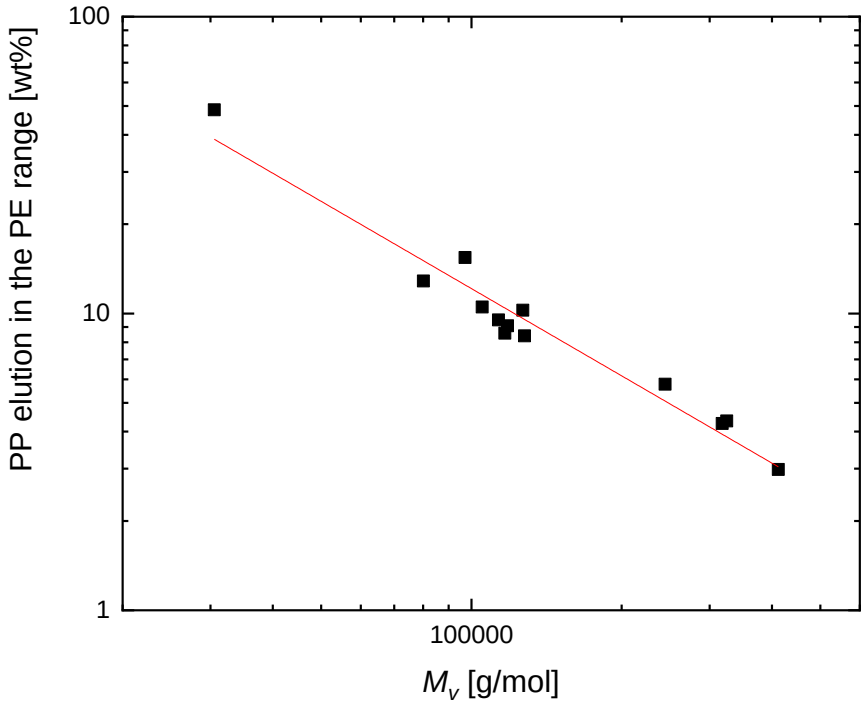

Figure 4.3–6 Scatter plot demonstrating an exponential correlation between viscosity-average molecular weight (M_v) of PP and the amount of PP eluting in the PE temperature range. A trend line fitting the data points is also included.

Unravelling detector factors for accurate composition calculation

Furthermore, beyond merely compensating for molecular weight discrepancies, it is imperative to account for the divergent responses of the IR5 infrared detector for PE and PP. This necessitates the introduction and exploration of the intricacies of the detector factor, a pivotal element in analytical chemistry that elucidates the interaction between a specific substance and the detector.

In accordance with the fundamental principle underlying analytical processes, the Beer-Lambert law, it was discovered that the absorbance of a solution is directly proportional to its concentration and the path length of the light, as expressed mathematically[456]:

$$A = \varepsilon \cdot c \cdot l \tag{4}$$

where A is the absorbance, ε is the molar absorptivity, c is the concentration of the solute, and l is the path length of the light.

This principle is indispensable in infrared (IR) spectroscopy, wherein the interaction of molecules with IR radiation is quantified. In the context of this study, such understanding was

deemed essential when interpreting responses from the IR5 detector, as varying molar absorptivities of PP and PE led to distinct absorbance values even at similar concentrations.

The relationship between concentration and absorption was investigated further, as shown in Figure 4.3–7, indicating a linear relationship between both parameters. Still, different slopes were found, indicating that PE had higher absorptivity with the employed filter set, whereas PP had lower absorptivity. This observation corroborated the findings of Frijns-Bruls et al.[457], wherein the newer generation of optical filters utilised in IR5 MCT detectors yielded more consistent results for the detection of PE, PP, polyethylene-1-butene (PB), and poly-1-hexene (PH). However, diverging signal values for PE compared to PP, PB, and PH were reported when older series filters were employed. Notably, the newer filters exhibited a 20% wider spectrum bandwidth, and they initiated transmission at higher wavelengths compared to their predecessors, resulting in different peak area values when older filters were utilized. Specifically, at equivalent concentrations, a larger peak area for PE compared to that for PP, PB, and PH was observed.

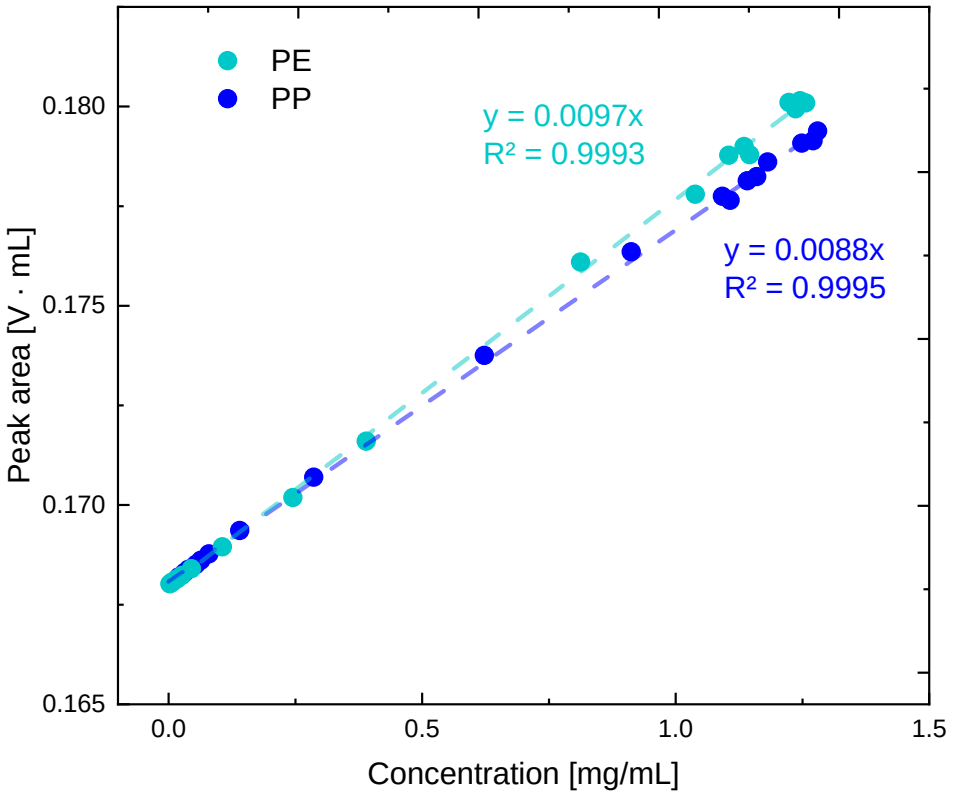

Figure 4.3–7 Peak area as a function of concentration for PE (light blue) and PP (blue).

The software that was used in this work quantifies detector factor values, making computations easier. The detector factor quantified the link between the electrical signal from the detector, the time recorded, and the mass of the sample, revealing how many millivolts of signal were collected for a given amount of sample in a particular time interval. Given the similarities between PP and PE, both being based on saturated hydrocarbons, investigations into differences in detector response were conducted, focusing on refractive index [437,458] and infrared detectors from the composition point of view [54,459]. It is essential to understand that the data from TREF and GPC had been corrected using the detector coefficient, which ensures the data's accuracy and reflects the polymer's properties at a specific concentration.

When analyzing a substance with two distinct components, like PP and PE, with different detector coefficients, errors in their proportions can arise. Due to the area-normalized spectrum, PE's relative absorption increases while PP's decreases, leading to potential data misinterpretation.

Detection coefficients for PP and PE, determined as detector factors that are directly proportional to the absorptivity of the concentration signal of the IR5 detector for the respective polymer, along with their mixtures, were systematically evaluated. Furthermore, to validate the results acquired, ethylene-propylene copolymers (EPC) encompassing a range of ethylene content from 0 to 70% by weight were measured. These coefficients played a pivotal role in ensuring the accuracy of concentration calculations. The detector factor was used to comply with the requirements for quantitative IR analysis, which state that individual responses to concentration must be linear [200].

Figure 4.3–8 shows a clear influence of polypropylene content, or CH_3/1000TC (Figure S 2 in Appendix B), on detector factor values. It was observed that the detector factor is directly proportional to the number of methyl groups, indicating that an increase in propylene content results in a decrease in the detector factor. Individual PP and PE evaluation gave average results of 73.7±2.2 $\frac{mV \cdot s}{mg}$ for PE and 67.3±2.0 $\frac{mV \cdot s}{mg}$ for PP. Equations (13) and (14) were then used to define detector factor compensations.

$$C^{TREF\ PP} = \frac{A^{TREF\ PP} \cdot d^{mat}}{d^{PP}} \quad (13)$$

$$C^{TREF\ PE} = \frac{A^{TREF\ PE} \cdot d^{mat}}{d^{PE}} \quad (14)$$

d^{PP} – detector factor for polypropylene $[\frac{mV \cdot s}{mg}]$

d^{PE} – detector factor for polyethylene $[\frac{mV \cdot s}{mg}]$

d^{mat} – detector factor for the material which was measured $[\frac{mV \cdot s}{mg}]$

$A^{TREF\ PP}$ – amount of PP [wt%]

$A^{TREF\ PE}$ – amount PE [wt%]

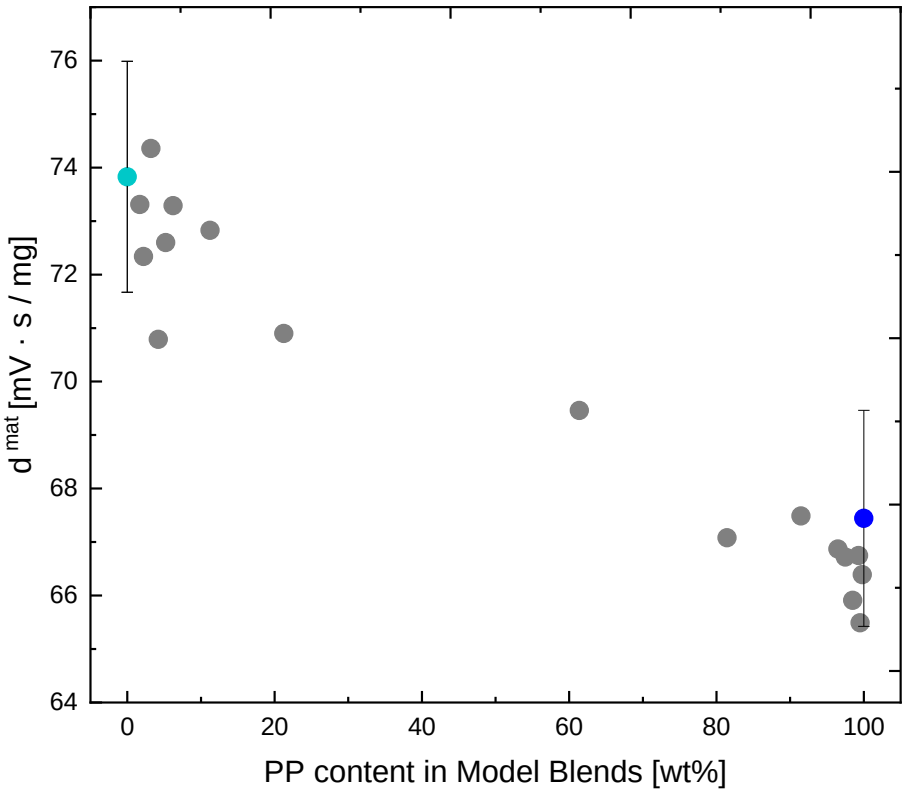

Figure 4.3–8 Scatter plot demonstrating a correlation between detector factor (d^{mat}) and PP content in model blends. The blends with a higher PP content exhibit lower detector factors. The x-axis represents the PP content in model blends in percentages, indicating the proportion of PP in the blend with PE. The y-axis presents the detector factor (d^{mat}).

Considering the detector factor and compensations for PP elution within the PE temperature range ensures accurate results. A comparison of CFC values for 17 compounded blends, after applying these corrections, showed reduced discrepancies with a maximum deviation of 2.5% in concentration (Figure 4.3–9). In Figure S4 (Appendix B) the results including the detector factor correction alone are reported.

To summarize, a novel CFC approach emerged for characterising PE/PP blends. The process involves three key steps: incorporating detector response factor corrections, determining high molecular weight PP fractions eluting above 103°C, and estimating the PP

fractions eluting below 103°C using calculated M_v of the TREF fraction. This integrated approach maximises the utility of bivariate MWDxCCD information for reliable PE and PP determination in polyolefin blends, accounting for the low molecular weight fraction in PP. Therefore, using our method, a more precise molar mass and chemical composition of the PE fraction within PP/PE blends was obtained.

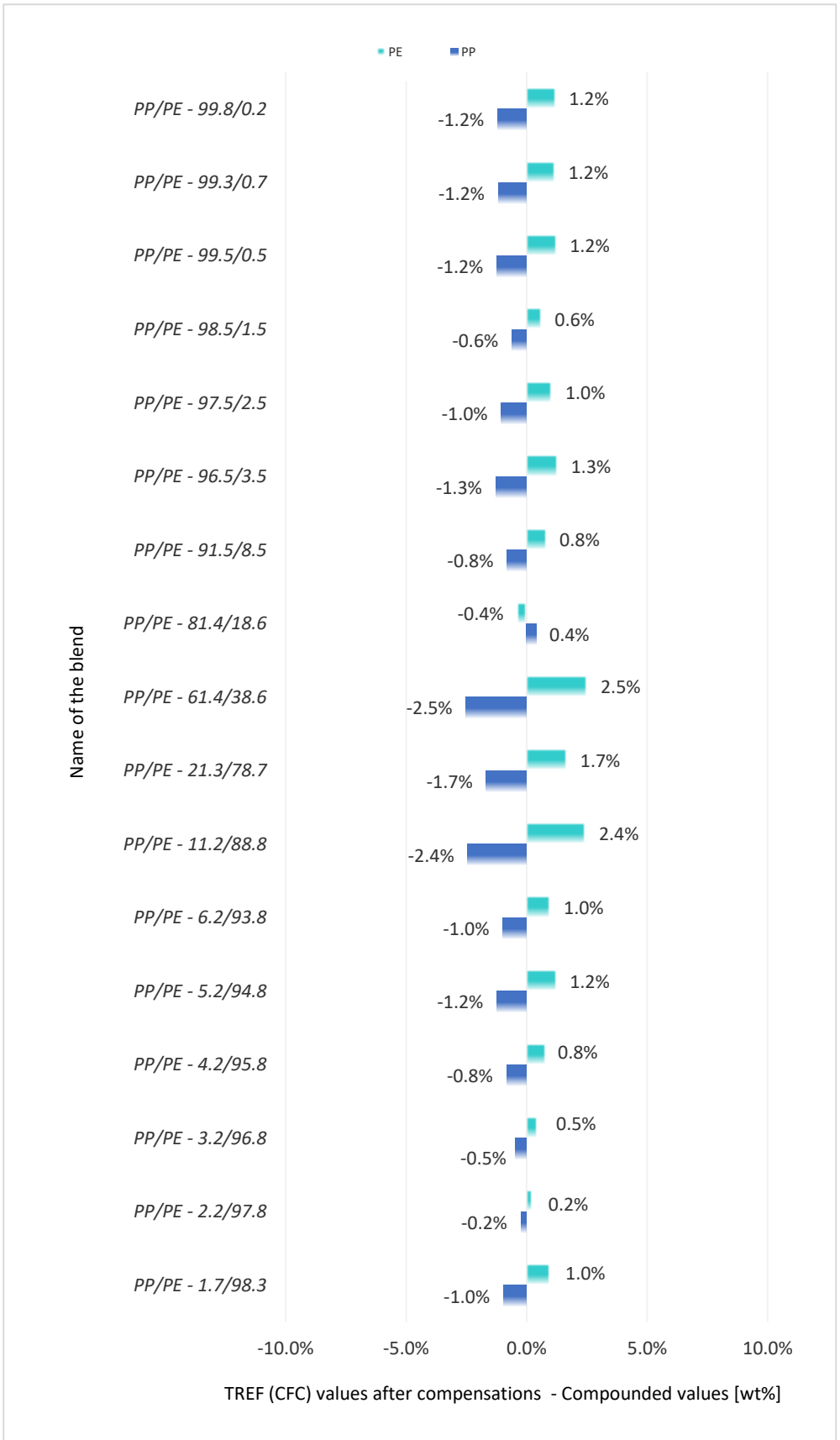

Figure 4.3–9 Bar chart comparing TREF (CFC) values after applied detector factor and PP elution in the PE temperature range compensations vs compounded values. The y-axis categorizes 17 different blends, designated by their respective PP and PE contents. The x-axis displays the percentage differences. The bars are color-coded, with polyethylene (PE) shown in light blue and polypropylene (PP) in blue.

Validation of the method with unknown blends and recyclates

The validation of the developed method was conducted through the examination of three blends: V1-PP/PE, comprising the same PE as in the primary blend albeit with a higher molecular weight PP component; V2-PP/PE, employing the same PP as in the primary blend, but with a different PE exhibiting lower density; and V3-PP/PE, encompassing the same PE as in the primary blend, with the PP component possessing a lower molecular weight relative to the primary blend, as listed in Table S5 (Appendix B). The outcomes, specifically the calculated concentrations of PP and PE, obtained from applying our method to these blends were compared to the compounded values. In the case of these validation blends, Figure 4.3–10a illustrates the significant discrepancies between the CFC values and the compounded values of three validation blends before applying any corrections. In Figure 4.3–10b, the disparities were significantly reduced after the detector factor correction and the PP elution in PE range adjustment were applied, demonstrating the efficiency of these corrections. The difference was within the same range as for the 17 model compounded blends (Figure 4.3–9), indicating that the approach is robust enough to analyze unidentified blends with the specified corrections.

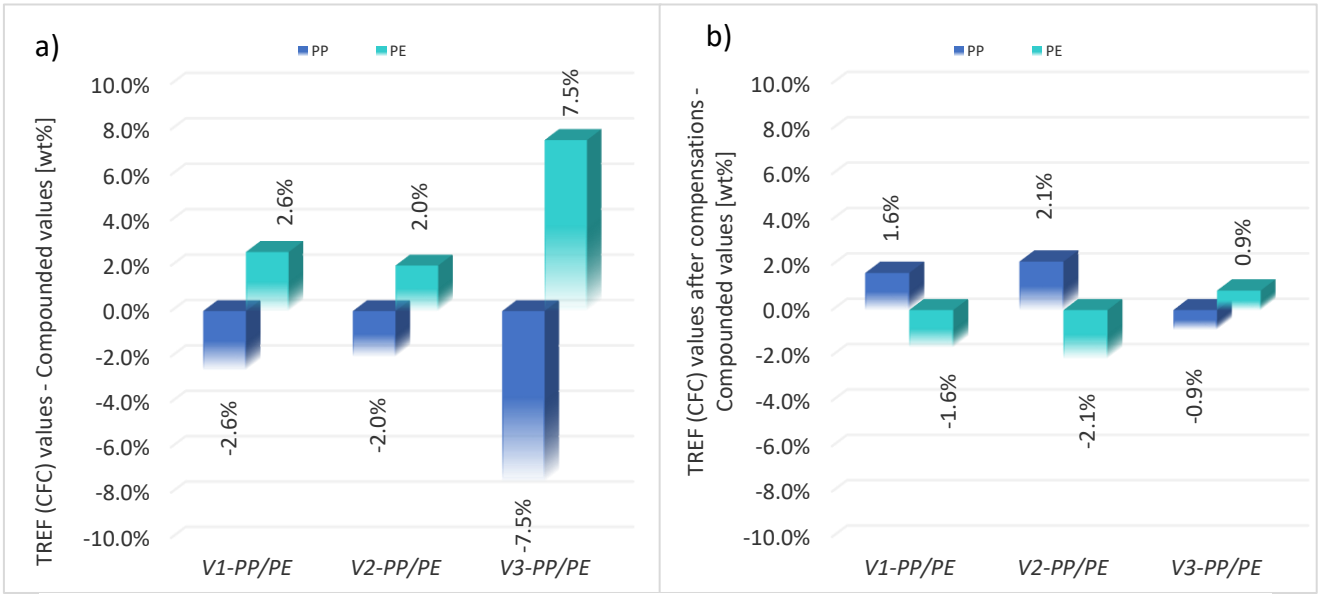

Figure 4.3–10 Bar chart comparing TREF (CFC) values a) before and b) after corrections in three validation blends. The x-axis lists the blends, while the y-axis shows the percentage difference between pre- and post-correction values. The bars, in shades of blue, represent polyethylene (PE) in light blue and polypropylene (PP) in blue.

In addition to the validation PE/PP, the accuracy of the newly developed CFC method for determining the composition of two-component blends of PE and PP was evaluated using three post-consumer recycled blends (PCR), as detailed in Table S6 (Appendix B). The results were compared to the NMR values. As illustrated in Figure 4.3–11a, significant differences

between the CFC values and the NMR values from the three PCR blends were obtained, in all cases between 7.0-8.2% overestimation of the PP amount in the PCR blends. This discrepancy between calculated and actual values before performing the correction may be attributed mostly to PP's lower molecular weight, with a minor effect from the detector factor which differs for PP and PE.

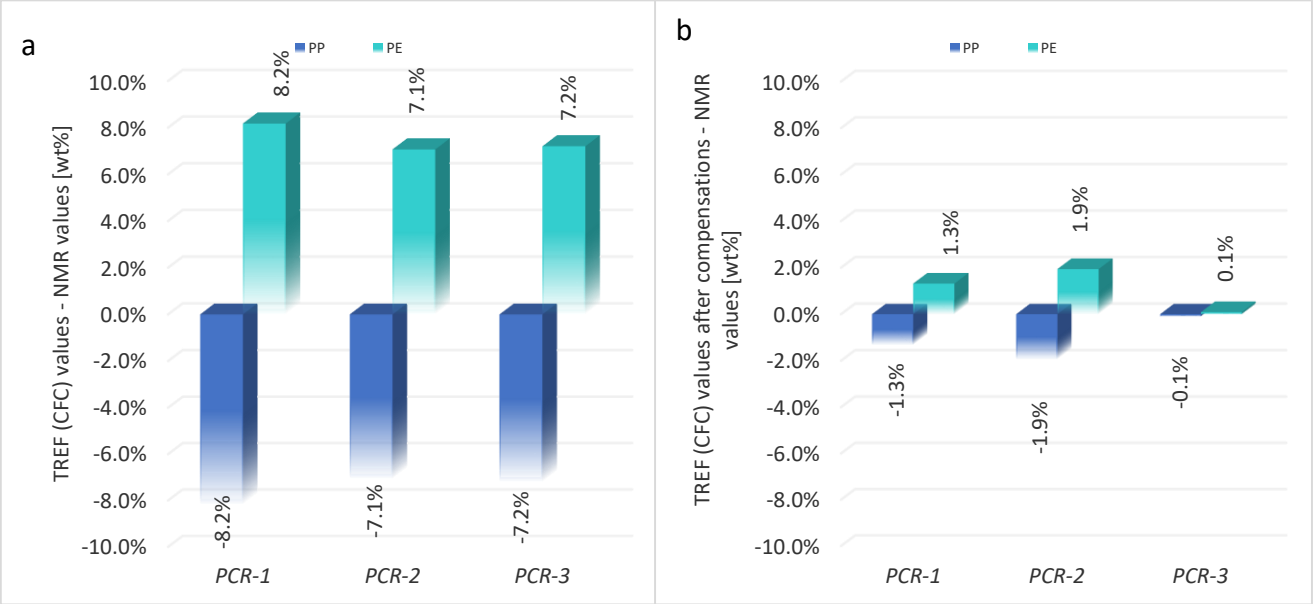

Figure 4.3–11 Bar chart comparing TREF (CFC) values a) before and b) after corrections in three PCR blends. The x-axis lists the blends, while the y-axis shows the percentage difference between pre- and post-correction values. The bars, in shades of blue, represent polyethylene (PE) in light blue and polypropylene (PP) in blue.

After implementing the necessary corrections, the discrepancies consistently stayed below 2.5% for all materials, namely PCR blends (Figure 4.3–11b), the validation PE/PP blends (Figure 4.3–10b) and the model 17 PE/PP blends (Figure 4.3–9). These results demonstrate that a substantial improvement in the accuracy of the CFC method for both types of PE/PP blends as well as for PCR samples was achieved by applying molar mass and detector corrections.

Furthermore, the measurement uncertainty for polypropylene (PP) was assessed, considering the molecular weight distribution (MWD) values of the fraction eluting in the temperature range of 103-130°C and the content of polypropylene eluting in the PE range (35-103°C). This evaluation was performed by conducting six repeated measurements of PP-12. The results indicate that the average molecular weight (M_v) for the temperature range of 103-130°C is 323.1±8.1 kg/mol at a 99.9% confidence level. For the elution of PP in the PE range (35-103°C), the value is 4.5±0.6 wt% at a 99.9% confidence level. The measurement uncertainty, represented by the standard deviation, is significantly lower than the observed 2

major factors of impact, i.e., PP/PE co-elution and detector response difference between PE and PP.

To further enhance the method's accuracy, it is essential to incorporate measurements of additional PP with varying MWD, along with their respective M_v values, to also account for different dispersity in the PP, which would also be beneficial for the PCR analysis. By doing so, a more comprehensive understanding of the impact of M_w can be achieved, resulting in more accurate forecasts that closely align with the compounded values.

4.4 Discussion

TREFxGPC offers a more comprehensive characterization of polyolefin blends compared to methods like DSC or GPC alone. The proposed correlation between the M_v of PP and the amount of PP eluting in the PE range is novel and can be used as a predictive tool for quantifying the composition of PP/PE blends.

However, this study has some limitations that should be considered. First, the correlation between M_v and PP elution was derived from a limited number of PP samples with different molecular weights. More measurements with a wider range of PP samples are needed to further validate and refine the correlation. It would also be beneficial to investigate a parameter that mirrors the MWD, such as $\frac{Mv}{Mw}$ or $\frac{Mv}{Mz}$, to better predict the low M_W PP fraction that elutes in the PE range. Second, the method may not be applicable to ethylene-propylene copolymers or blends with more complex chemical structures than isotactic PP and PE.

The correlation developed based on PP MWD will be effective for blends with homo-PP or heterophasic ethylene-propylene copolymers (HECO-PP) having a homo-PP matrix. However, it should be noted that this method will not be applicable to random-heterophasic copolymers (RAHECO-PPs) and random copolymer polypropylene (RACO-PP). While some literature [113,409,425,438,460,461] indicates the prevalence of RACO-PP in PP-based recyclates due to packaging applications, the materials most amenable to recycling within the PP family are homo-PP and HECO-PP with a homo PP matrix [424,462,463]. By analyzing the amount of CH_3/1000TC along the molecular weight for the PE fractions at around 100°C it is also possible to confirm that the PO based recyclates, used in this study, contain no or only in a minor amount crystalline EP copolymers, which would also co-elute in the PE region. Additionally, one could conduct a simple DSC test; a decrease of T_m would serve as a good indication of the ethylene

(C2) incorporation in PP. This DSC test might act as a preliminary check to determine whether to proceed with the detailed analysis described above.

Further studies are required to test the method on different types of polyolefin blends. Based on these observations, future research can explore the following directions: (1) measuring more PP samples with different molecular weights and dispersities to improve the accuracy of the M_v-PP elution correlation by including a broadness parameter (2) testing the method on ethylene-propylene copolymers or other types of polyolefin blends to deepen the understanding of its potential and limitations; (3) investigating the effects of degradation and reprocessing on the molecular structure and properties of polyolefin blends using TREFxGPC and other techniques.

4.5 Conclusions

A correlation linking the molecular weight of PP to the quantity of polymer eluting within the PE temperature range was established. Furthermore, it was concluded that variations in absorption factors between PP and PE, especially when using a broad band filter tuned to the absorption region 2800–3000 cm^{-1} for concentration signal analysis, could introduce a margin of influence on the results, amounting to 2%. In conclusion, implementing the detector response factor and compensating for PP elution in the PE range yielded results closely aligned with nominal blend values.

Additionally, this study reveals that the molecular weight and structure of PP influence its elution behavior in the PE range. These findings have implications for understanding the molecular composition and properties of polyolefin blends, especially those from mechanical recycling. Future research should focus on refining the M_v-PP elution correlation and testing the method on various polyolefin blends and copolymers. These improvements of a more precise PP and PE content determination, with the additional information which can be obtained from CFC like CCD and MWD of both components PE and PP of PCR, should be the focus of future work, as very detailed information of PCR can be obtained with this approach.

5 Surface-enhanced nucleation in immiscible polypropylene and polyethylene blends

The study of surface-enhanced nucleation in immiscible polypropylene (PP) and polyethylene (PE) blends, with a focus on the chain regularity of PE, offers significant implications for the recycling of polyolefins. Traditionally, the recycling industry has faced challenges in processing mixed polyolefin streams due to differences in the components' crystallization and melting behaviors. Chapter 5 introduces a novel approach to understanding how the molecular structure of PE influences its nucleation behavior when blended with PP, a common scenario in recycled polyolefin streams. The results demonstrated a threshold value of chain regularity required for effective surface nucleation of PE on PP. Polymers with a density above approximately 920 kg/m^3 and melting temperatures over 115 °C were found to nucleate efficiently onto the PP substrate. It is postulated that high amounts of branches or comonomers in PE chains impede the epitaxial matching between PE and PP, affecting the nucleation behavior.

5.1 Introduction

Nucleation is a fundamental step of crystallization, consisting of the aggregation of molecules to form supercritical size clusters, whose further growth into a macroscopic crystal is spontaneous [464,465]. In semicrystalline polymers, controlling nucleation is of great importance, for instance, to tune mechanical and optical properties [466]. Typically, polymer nucleation occurs on the surface of a heterogeneous substance due to the lower energy barrier in comparison with homogenous nucleation. Of particular interest is the nucleation of one polymer to another, which becomes extremely efficient if the two polymers exhibit some degree of lattice matching between their crystalline structures. This latter case is known as epitaxy. Systematic investigations about epitaxy in the polymer field have been reported by Lotz and Yan [348,467,468].

A well-studied example is the nucleation of high-density polyethylene (PE) on isotactic polypropylene surfaces (PP) [347,349,469,470]. It was shown for model systems in oriented thin films and blends that PE chains crystallize with an angle of 50° with respect to the PP chain axis.

This can be explained due to the alignment of the zig-zag PE chain along the rows of PP methyl groups having 0.5 nm intermolecular distances between the chain-row matches [469].
Yan and Petermann studied the effect of polyethylenes of various chain regularity and, therefore different PE densities on epitaxial nucleation onto an oriented PP substrate [350]. They analyzed the behaviour of high-density polyethylene (HDPE), linear low-density polyethylene (LLDPE) low-density polyethylene (LDPE). They found that all three PEs show epitaxial crystallization on PP according to the known crystallographic relationship for HDPE. However, the thickness of the epitaxially crystallized layer decreased from 250 nm to 30 nm as the polymer density lowered. This reduced thickness resulted from a competition between oriented and spherulitic growth in the film, although the authors did not suggest it, this effect could be explained by a slower epitaxial nucleation for more irregular polymers.

To study polymer-on-polymer nucleation kinetics, our group has devised a strategy applicable to binary polymer blends with two semicrystalline components and a droplet-in-matrix morphology[400,471]. The overall crystallization kinetics is dominated by nucleation in blends with a minor component dispersed as droplets in an immiscible matrix[59,472–474]. The method is based on differential scanning calorimetry (DSC) and consists in determining the relationship between the crystallization temperatures of the matrix and the dispersed phase when the matrix's T_c is varied through a self-nucleation thermal protocol[166]. The increase of matrix T_c due to self-nucleation enhances the dispersed phase T_c. This effect is attributed to the thicker crystalline lamellae of the matrix polymer, which provide a more favourable nucleation substrate to the droplet phase. The technique has been applied to various double semicrystalline polymer blends[400,471,475], including HDPE/PP[400], for which the epitaxial nucleation mechanism is active.

So far, the study is limited to the case of high-density polyethylene, and little is known about the applicability of such a method to PEs with different chain architecture (comonomer type and content and branching). Much information is available on the effect of blending different types of PE with polypropylene, especially from the point of view of the adhesion between the phases in blends and laminates[476–478]. It is known that better welding is obtained with metallocene PEs rather than with Ziegler-Natta type polymers due to the segregation of low molar mass and defective chains to the interface in the latter case[476]. Improved adhesion was obtained when interfacial entanglements were formed (for lower density metallocene PEs)[477] or when crystallization across the interface occurred[478].

Despite the body of literature on interfacial morphology in blends of different PE types with PP, a specific study on nucleation kinetics at the interface has yet to be performed. The aim of the present study is thus to extend our versatile DSC method to the investigation of surface nucleation of PE on PP in immiscible blends with droplets-in-matrix morphology, exploring polyethylenes with different chain regularity and composition [471].

5.2 Materials and Methods

An isotactic polypropylene produced with Ziegler-Natta catalyst technology with a molecular weight of 342.0 kg/mol was used as a matrix polymer for all investigated blends. The blends were prepared in a ratio of 80:20 polypropylene phase to polyethylene phase. The minor phase of each blend was composed of a different grade of polyethylene, including four Ziegler-Natta polyethylene (ZNPE) grades with varying density and molecular weight, three metallocene catalyst (mPE) grades with different comonomer types, and one low-density polyethylene (LDPE) from radical polymerization. The properties of all the used grades, measured as described below, are gathered in Table 5.2–1, together with the code names of the used PEs. In the sample name, the type of PE was followed by a number that represents the density of the material.

Table 5.2–1 List of the used materials in the investigation with material designation code, density and results from DSC and GPC measurements.

Material designation	**Density[a] [kg/m³]**	**Comonomer type**	**Comonomer content [wt %]**	**T_m [°C]**	**T_c [°C]**	**χ_c [%]**	**M_w [kg/mol]**	**$Đ$**
PP	905	-	-	161.1	112.4	52%	342.0	8.4
ZNPE962	962	C4	0.7	132.7	119.4	83%	67.8	3.8
ZNPE954	954	C4	1.1	128.7	116.2	74%	90.2	10.4
ZNPE945	945	C4	2.1	128.1	115.5	68%	158.5	16.0
ZNPE935	935	C4	4.8	127.3	114.8	57%	206.0	19.8
mPE927	927	C6	4.6	119.5	106.5	46%	77.7	3.8
LDPE922	922	-	-	112.7	97.8	45%	101.5	6.7
mPE918	918	C4/C6	0.6/7.5	121.9	107.0	41%	91.6	3.7
mPE902	902	C8	17.0	94.5	77.5	27%	52.8	3.5

[a] *Datasheet*
C4 = 1-butene
C6 = 1-hexene
C8= 1-octene

GPC. The molecular weight (M_w) was determined by Gel Permeation Chromatography (GPC) measurements using a GPC-IR chromatograph from PolymerChar (Valencia, Spain), equipped with an IR5 detector. The analysis was carried out at 160 °C and using three PLgel Olexis columns, each 300 × 7.5 mm (Agilent, Church Stretton, UK) as stationary phase. 1,2,4-Trichlorobenzene (TCB) was used as eluent with a flow rate of 1 mL/min. The column set was calibrated with narrow distributed polystyrene standards ranging from 500 to 11.5·106 g/mol. The PS equivalent molecular weight was converted into PE equivalent by using Mark Houwink constants [479].

a-TREF. The chemical composition distribution (CCD) was analyzed using a Crystaf-TREF 200+ PolymerChar instrument with an infrared concentration detector. 80 mg of sample was dissolved in 35 mL of trichlorobenzene (TCB), stabilized with 250 mg/L 2,6-bis(1,1-dimethylethyl)-4-methylphenol, at 160°C. 0.3 mL of the solution was injected into the TREF column. The column oven was cooled to 110 °C and held at 110 °C for 30 min for stabilization purposes. After stabilisation, the column oven was cooled to 35°C under a constant cooling rate (0.1 °C/min). The polymer was subsequently eluted from the column with 1,2,4-trichlorobenzene at a flow rate of 0,5 mL/min at 35 ºC for a period of 10 min followed by a temperature increase from 35 ºC to 135 ºC at a constant heating rate of 0.5 ºC/min with a flow rate of 0,5mL/min. The concentration of the eluted fraction was determined by the detector and plotted as a function of temperature. TREF plots can be found in Figure S1 (Appendix C) of the supporting information and the extracted contents for the various fractions are collected in Table S1 (Appendix C).

Self-nucleation thermal protocol (DSC). To investigate the crystallization of the PE phase in relation to the change in the crystalline state of PP, the blends underwent a specific thermal protocol with a heating/cooling rate of 10ºC/min [400,471]. The polypropylene crystalline structure was altered through this thermal treatment, conducted on a Differential Scanning Calorimeter at various self-nucleation temperatures (T_s), as its crystallization temperature can be elevated through self-nucleation. The thermal protocol used to study the self-nucleation of the polypropylene matrix (Figure 5.2–1) was adapted from Fillon et al. [166,398,480] as follows:

1. to erase thermal history, the sample was heated to 225 °C and held there for 5 minutes;
2. the sample was cooled to 20°C at 10 ºC/min to produce a standard crystalline state;

3. a heating scan at 10 ºC/min was performed to a temperature denoted as T_s or self-nucleation temperature. Depending on the applied T_s, the different self-nucleation *Domains* of the material are revealed;
4. the sample was held at T_s for 5 minutes;
5. a cooling scan at 10 ºC/min from T_s to 20 °C was performed;
6. a final heating scan at 10 ºC/min from 20°C to 225°C was carried out to investigate the melting behaviour of both phases.

An analogous protocol, with additional lower T_s temperatures, was applied to all the neat PE grades.

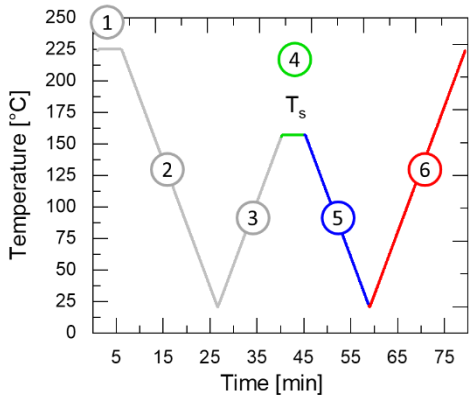

Figure5.2– 1 Thermal protocol for performing PP matrix self-nucleation and crystallization of the dispersed phase.

Standard thermal protocol (DSC). Melting (T_m) and crystallization (T_c) temperatures were measured using a Differential Scanning Calorimeter (DSC) Discovery series TA Instruments, according to ISO 11357/3. The measurements were carried out at a heating and cooling rate of 10 °C/min from 20 °C to 225 °C. The transitions were deduced from the second heating and cooling curves; the values of T_c and T_m are included in Table 5.2–1 and Table 5.3–1. The DSC curves are presented in Figure 5.3–1 a) and b) for the neat PE grades and Figure 5.3–1 c) and d) for the blends and neat PP.

Melt-mixing. Pellets from each selected PE grade were dry blended with polypropylene pellets in a weight ratio of PP/PE 80:20, and the resulting pellets mixtures were poured into the mixing chamber of a Brabender W50. Melt mixing was performed at a set temperature of 200ºC for 7 minutes at 100 rpm. The blends' composition code and basic thermal properties, measured by the DSC, are listed in Table 5.3–1 and presented in Figure 5.3–1 c) and d).

SEM. Scanning electron microscopy (SEM) was used to visualize the general morphology of the blends and the interface between PP and PE. At first, the samples were conditioned in

the DSC, applying annealing at the selected T_s and cooling to room temperature (i.e., steps 1 to 5 in Figure 5.2–1). The selected samples were cut via cryo-microtoming at -100°C on a Leica EM UC7 and then etched for 10 minutes in a 1% KMnO4 in 85% H_2SO_4 solution. After, the samples were washed with distilled water, stirred for 10 minutes in a 30% H_2O_2 solution, washed again, and finally rinsed with acetone. Before scanning electron microscope (SEM) analysis, the specimens were covered with a Pt layer using a Quorum Q150T S plus. SEM observations were performed on a Quanta 200F scanning electron microscope apparatus operating at an accelerating voltage of 5 kV.

WAXS. Wide angle X-ray scattering was employed to investigate the crystalline structure of the used materials and the created blend thereof. Prior to X-ray measurement, the samples were conditioned using DSC. They were subjected to heating at a controlled heating rate to 225°C and subsequently cooled to 0°C. X-ray diffraction measurements were conducted using a Bruker AXS D8 Discover diffractometer equipped with a two-dimensional GADDS detector and a Ni-filtered CuKα X-ray source. Each sample underwent three measurements with a scan duration of 300 s each, and the results were averaged. The angular range of the measurements (2θ) was set between 10° and 32.5°, with a step size of 0.02°.

Figure S5 (Appendix C) presents WAXS analysis of iPP, PE grades, and blends created thereof. The results in Figure S5 a) (Appendix C) show that the PE grades with higher crystallinity and well-ordered structures exhibit sharper and more intense diffraction peaks. Peaks with lower intensities or/and broader profiles may indicate reduced crystallinity and a higher presence of amorphous regions within the material. These peaks correspond to the reflections from different crystallographic planes such as the (110) at 21.2° and (200) at 23.5°. The results of PP in Figure S5 b) (Appendix C) the last curve (pink) show that PP crystallized in the usual α-form, as reflection at 2θ = 14.0°, 17°, 18.5°, 21.2°, 22°, 25.5°, 28.5° corresponding to the (110), (040), (130), (111), (131) and (041), (060), (220) planes. A small peak at 16° suggests that some crystals are crystallized in β-form, which comes from the plane (300), then the signal from the plane (301) is not visible because at 21.2° there is a strong signal from the plane (111) of the α-form.

For the 80:20 PP:PE blends (Figure S5 b) in Appendix C) with different PEs, it can be observed that both PP and PE crystallites contribute to the formation of the characteristic peaks. The PP peaks are dominant due to the higher concentration of PP, but the PE peaks are also

clearly distinguishable, especially for PE grades with a higher degree of crystallinity. In contrast, for low crystalline grades, the contribution from the PE to the XRD pattern is minor. This is because the lower degree of crystallinity in the PE means there are fewer ordered structures that can diffract the X-rays in a specific direction, which leads to a weaker or less distinct peak in the XRD pattern. This clearly illustrates the effect of the crystallinity of the PE on the overall structure of the blend. These results are consistent with those obtained from the DSC measurements, as depicted in Figure 5.3–1.

5.3 Results and discussion

The present study examines the crystallization effect in blends of polypropylene and different types of polyethylene. To better understand the properties of the PE grades before melt-mixing with PP, we first conduct a basic analysis of each neat material. The self-nucleation properties of the PP matrix are then discussed, followed by an examination of the behaviour of the PE grades as the minor phase in the blend. Finally, the study aims to establish a correlation between the PE crystallization temperature after the thermal treatment and its molecular characteristics, namely the T_m and the methylene sequence length.

In this study, we utilized different grades of PE within a wide range of densities (from 902 to 962 kg/m^3), also featuring diverse molecular architecture of the polymer chains. This is reflected by a distinct crystallization behaviour of the polymers that can be seen in Figures 5.3–1a and 2b, where the DSC cooling and subsequent heating curves of the various PE are reported. The crystallization and melting temperatures continuously drop 40 °C when decreasing the PE density from 962 to 902 kg/m^3. An exception to the observed trend is the behaviour of mPE918, which shows crystallization and melting temperatures higher than those of the LDPE with higher nominal density. The reason behind this observation will be discussed below.

Regarding the molecular features, ZNPE962 is characterized by a low weight-average molecular weight and extremely low comonomer content (T_m = 132.7°C, M_w= 67.8 kg/mol, $Đ$= 3.8) and therefore has higher crystallinity. The ZNPE962, ZNPE954, ZNPE945, and ZNPE935 are produced using the same catalyst technology, but the level of comonomer incorporation and the M_w differs. The radical polymerized grade LDPE922 has a high molecular weight and broad dispersity. The rest of the investigated grades are produced by single-site catalyst with a similar dispersity of ~ 3.7. Typical polymer chains produced under steady-state conditions by single-site catalysts (mPE927, mPE902) also possess an even comonomer concentration over

the molecular weight distribution and random comonomer incorporation. A different situation holds for grade mPE918, whose TREF trace is reported in Figure S1 (Appendix C). Two chain populations characterized by a different comonomer concentration and hence elution temperature are visible.

The estimation of crystallinity was based on equation 15, where ΔH_m^{ref} is a melting enthalpy of 100% crystalline polymer and ΔH_m is the experimental melting enthalpy. ΔH_m^{ref} for polypropylene is taken as 207 J/g [481,482] and for polyethylene 293 J/g [483,484], both generally accepted values.

$$\chi_c = \frac{\Delta H_m}{\Delta H_m^{ref}} \cdot 100 \quad (15)$$

Prepared blends with a ratio PP:PE equal to 80:20 were tested with the DSC, and the results are shown in Figures 5.3–1c and 2d. The standard cooling and heating runs revealed a single transition during cooling for most of the blends, indicating coincident crystallization of the PP and PE phases, while just two blends present two separated crystallization peaks for the two phases (PP/LDPE922 and PP/mPE902). Polypropylene and polyethylene are known to display mutual nucleation effects [56,485–487]. Nevertheless, Figure 5.3–1c shows that crystallization of the PP phase in the blends must occur at a higher temperature than for neat PP. The higher crystallization temperature of the PP phase in the blends can be explained by either a mild nucleating effect of the molten PE droplet for the PE grades whose density is below 935 kg/m^3 [56] or by nucleation onto the already formed PE crystals, especially for PEs with a density from 962 to 935 kg/m^3. Another possible explanation is the transfer of nucleating impurities from the PE to the PP phase during melt mixing, although the opposite transfer is more commonly observed [62,488,489]. It should be noted that for the blends for which the PE crystallization temperature could be measured during standard cooling, higher T_c values in comparison with neat polymers were detected. For example, mPE902 crystallization goes from 77.5°C in the neat polymer to 80.3°C in the blend and LDPE from 97.8°C to 98.8°C. This increase could indicate either nucleation of the PE phase at the interface with PP, the occurrence of which will

be discussed in detail further on, or the transfer of nucleating impurities from the matrix to the dispersed phase[489].

As expected, the melting scans revealed the presence of two components (Figure 5.3–1d). When comparing the melting temperature values of the PP and PE phases in the blend with respect to the neat polymers, it is observed that the values tend to be slightly lower in the blend, which can be attributed to the effect of processing or different crystallization conditions[490,491].

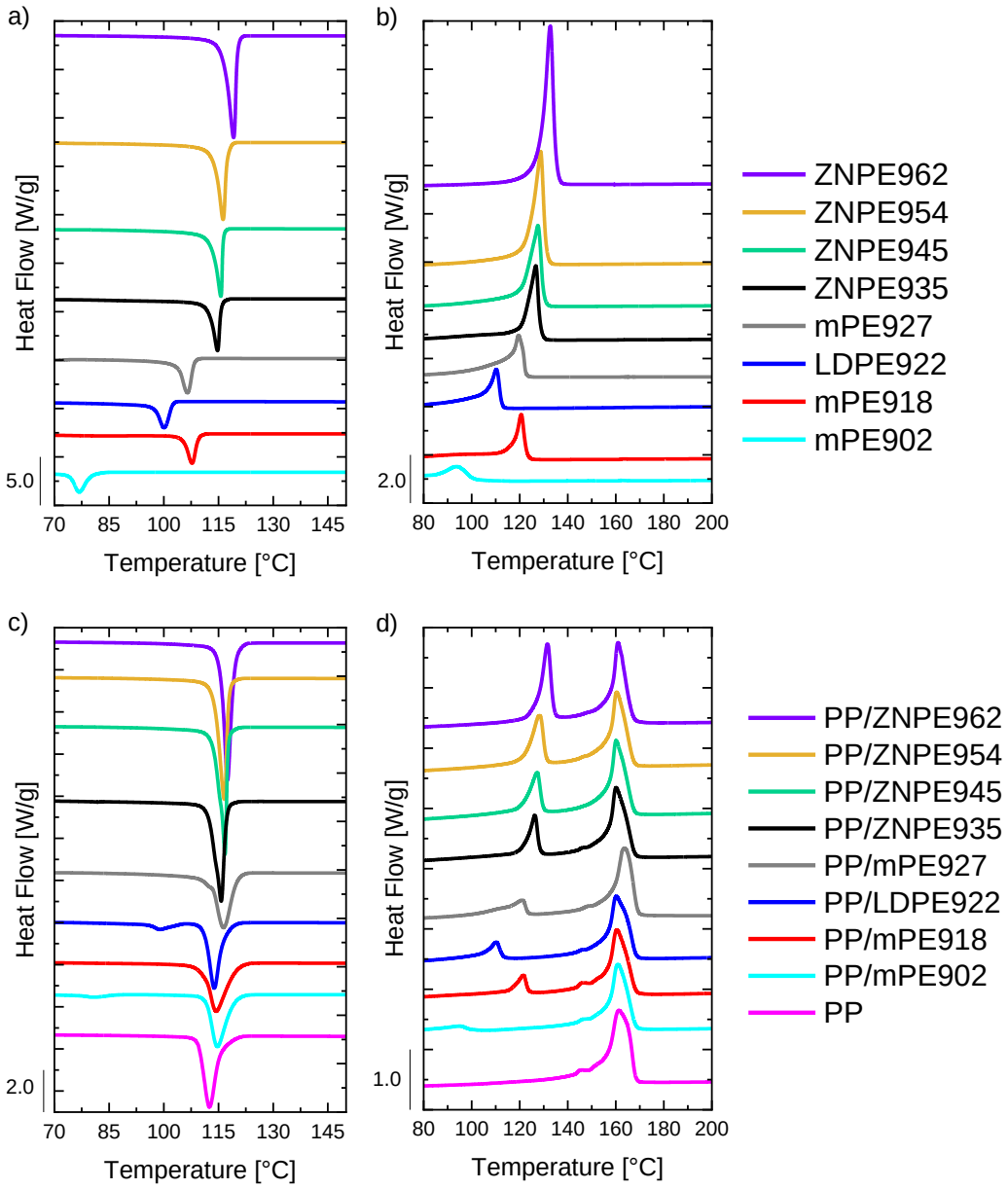

Figure 5.3–1 DSC cooling (a) and heating (b) scans of neat PE grades and blends (c and d) at scan rates of 10°C/min. The neat PE materials are arranged in order of increasing density from bottom to top and neat PP is added to the blends plot for comparison purposes.

In addition to these DSC results, we conducted the further analysis using Wide Angle X-ray Scattering (WAXS) to delve deeper into the crystalline structure of the blends and neat materials. These WAXS measurements, detailed in the supporting information (Figure S5 in Appendix C), offer complementary insights that reinforce our primary findings. In brief, these results align with the DSC data and contribute additional depth to our understanding of the crystalline behaviour of these blends.

Table 5.3–1 Thermal properties of blended materials obtained by DSC for each phase. The weight ratio in every blend is the same (80:20 PP:PE). The code of the blend therefore just indicates the difference in the type of PE.

Blend code	T_m^{PE} [°C]	T_c^{PE} [°C]	T_m^{PP} [°C]	T_c^{PP} [°C]
PP/ZNPE962	126.9	117.5	160.9	117.5
PP/ZNPE954	128.3	116.5	160.4	116.5
PP/ZNPE945	127.2	116.8	160.1	116.8
PP/ZNPE935	126.4	115.8	160.1	115.8
PP/mPE927	121.1	116.7	163.7	116.7
PP/LDPE922	110.2	98.8	160.2	113.9
PP/mPE918	121.5	114.4	160.5	114.4
PP/mPE902	94.7	80.3	160.9	114.7

SEM images (Figure 5.3–2) reveal that all blends display a sea-island morphology, with droplets of PE dispersed in the PP matrix. The PE droplet's size and size distribution (see Supporting Information, Figure S2 and Table S2 in Appendix C) vary only slightly. Still, it is important to note that the observed sizes are based on 2D images and may not accurately reflect the true size distribution of the 3D droplets. Even a monodisperse distribution of 3D particles would show a quite large distribution of sizes in a 2D image, with the largest diameter being the "true" diameter of the spheres. The differences in PE to PP viscosity ratio for the particular PE grades may contribute to the observed variation in droplet size. For instance, ZNPE935 generates a higher number of smaller droplets, while ZNPE945 yields a significant fraction of larger droplets. It is also worth noting that Figure 5.3–2h) shows a region of the sample where the mPE902 material has been removed during the etching process. In this area, there are no visible PE droplets, and the diameter of the etched hole has been considered equal to the size of the PE droplets.

The measurement of PE droplet sizes displayed in Table S2 (Appendix C) was performed according to Arnal et al. [492] and Chandrasekhar et al. [493]. It can be considered that the average diameter of the droplets in the blends is between approximately 1 and 2 µm. This suggests that

the dimension of the various droplets with different PE types, being almost constant, will not affect the interpretation of the subsequent crystallization results.

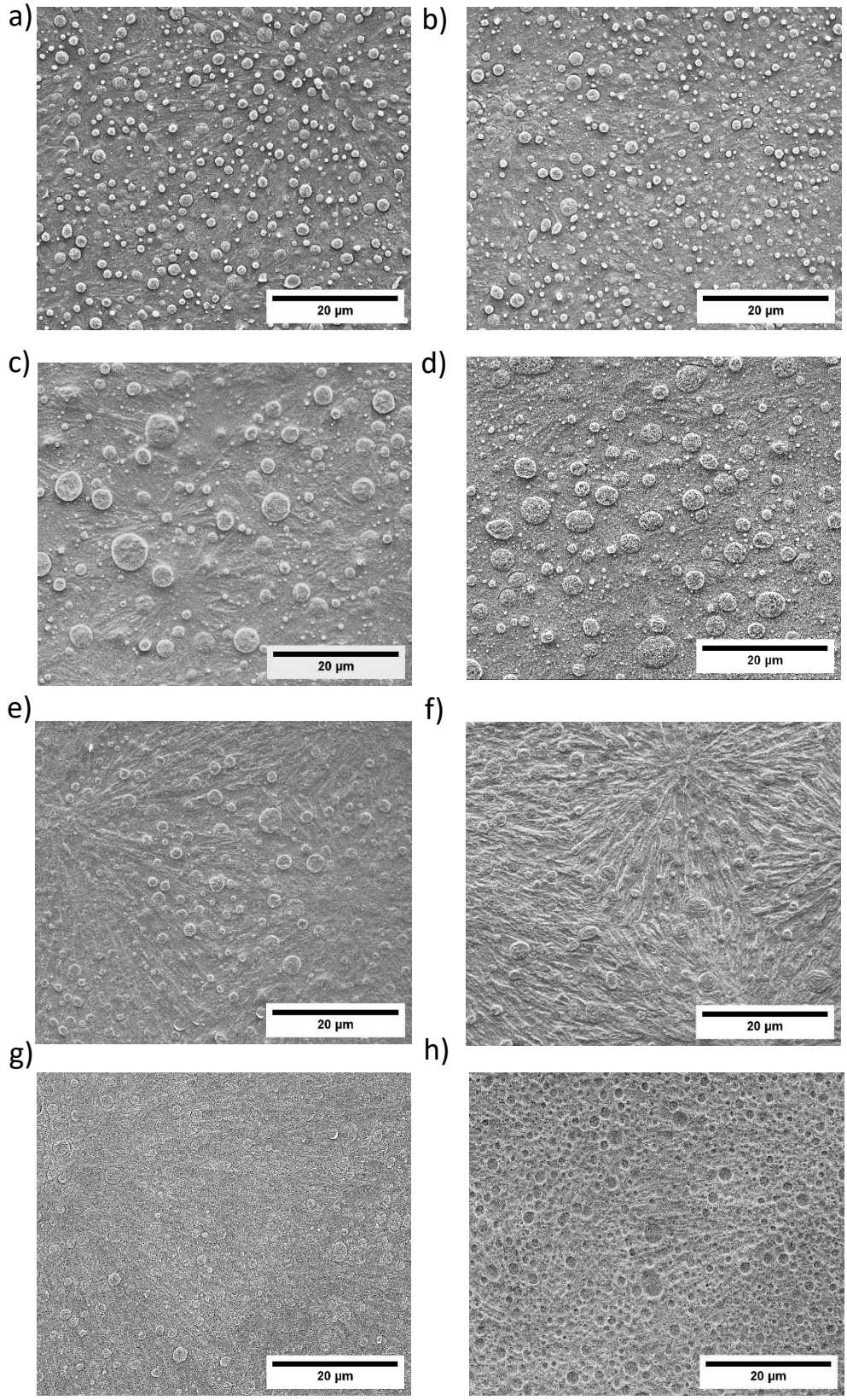

Figure 5.3–2 Scanning electron microscopy images of a) PP/ZNPE962 b) PP/ZNPE954 c) PP/ZNPE945 d) PP/ZNPE935 e) PP/mPE27 f) PP/LDPE922 g) PP/mPE918 h) PP/mPE902.

Next, we investigated the interfacial nucleation of PE droplets on the self-nucleated PP matrix. As mentioned in the method section, the different self-nucleation *Domains*, depending on the applied T_s, are identified as follows: *Domain I*, at high enough T_s, is characterized by no effect on the material's recrystallization due to the complete erasure of any memory of the previous crystalline order; *Domain II*, at intermediate T_s, occurs when an enhanced crystallization temperature is recorded due to the presence of residual self-nuclei; *Domain III*, at lower T_s, is found when unmolten crystals are left in the original sample and the lamellae thicken as an effect of the heat treatment. It was shown for PP/PE blends that applying T_s in *Domain II* and *III* causes an increase in the recrystallized PP lamellar thickness, which promotes epitaxial nucleation of PE droplets [400]. In particular, PP lamellae become thicker with the decrease of the self-nucleation temperature from 170°C to 161°C. At the T_s 161°C, the lamellar thickness of PP reached a maximum value, and consequently, the PE phase had the best nucleation substrate. However, depending on the PE type, a different nucleating effect of the PP matrix could be observed.

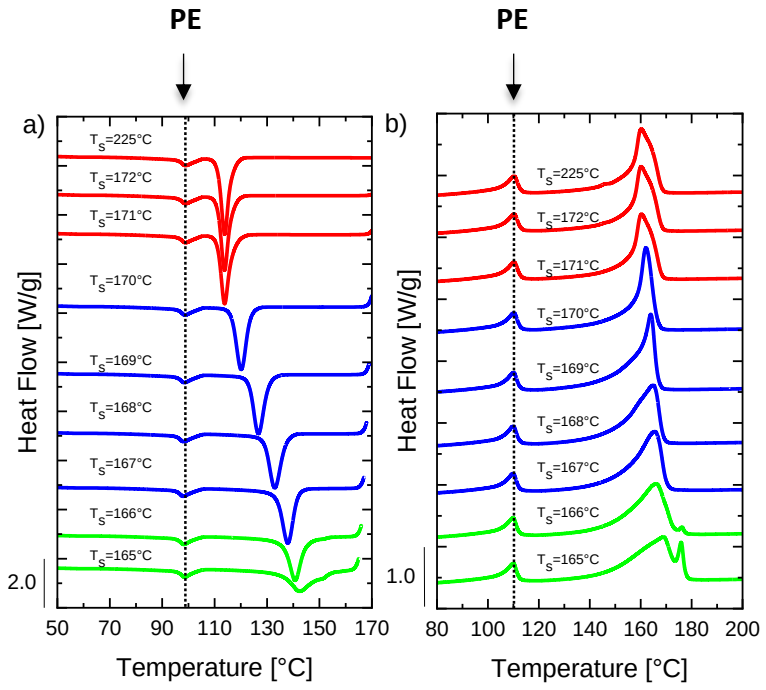

Figure 5.3–3 DSC scans of a) cooling and b) heating after thermal treatment at the indicated T_s for the blend PP/LDPE922-80/20. Domain I is represented in red color, Domain II in blue and Domain III in green. Vertical dashed lines are added as a guide to the eye, to highlight the lack of changes in the crystallization temperature of the PE phase.

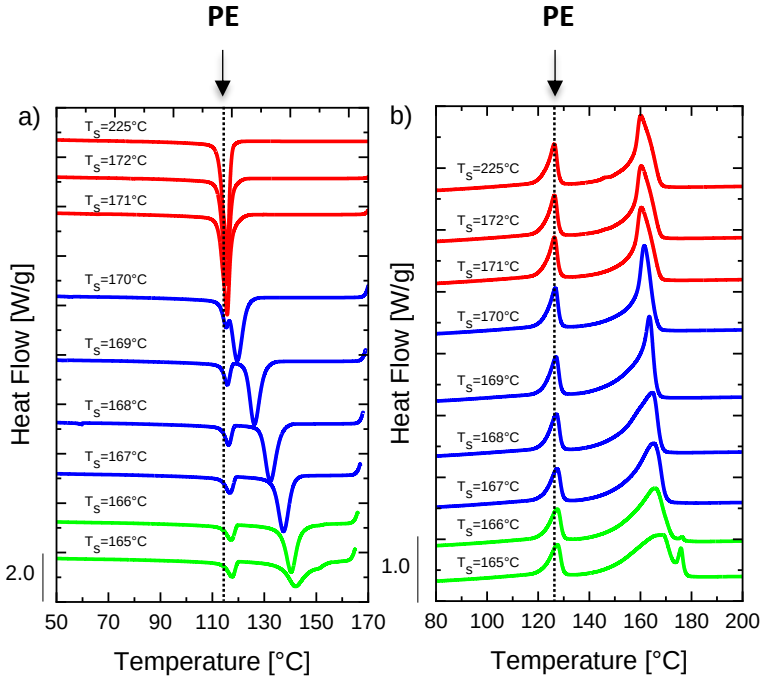

Figure 5.3–4 DSC scans of a) cooling and b) heating after thermal treatment at the indicated T_s for the blend PP/ZNPE935. Domain I is represented in red color, Domain II in blue and Domain III in green. Vertical dashed lines are added as a guide to the eye, to highlight the changes in the crystallization temperature of the PE phase.

The cooling and heating scans corresponding to steps 5 and 6 in the applied self-nucleation thermal protocol (see Figure 5.2–1) are shown in Figure 5.3–3a and 5.3–3b, respectively, for a

blend of PP with low-density polyethylene (LDPE922). The T_s range is selected to illustrate the temperature variations in the PP's crystallization and melting temperatures and to understand how the PE phase crystallization is influenced by the matrix self-nucleation. The self-nucleation domains of PP are identified by different curves' colors, i.e., *Domain I* red, *Domain II* blue and *Domain III* green. Figure 5.3–3a shows that while the crystallization temperature of PP has an obvious shift towards higher temperatures with decreasing T_s in *Domain II* and *III*, the peak from the PE minor phase remains approximately constant, at around 100 °C. Thus, enhanced surface nucleation does not seem particularly active for LDPE922, even when thicker PP lamellae (as judged by the higher melting point, Figure 5.3–3b) are available at the interface with the molten PE phase.

Analogously, Figures 5.3–4a and 5.3–4b report cooling and heating curves from various T_s for the PP/ZNPE935 blend. In this case, contrary to the previous example, the increase in PP crystallization temperature with decreasing T_s is accompanied by a significant increase in the crystallization temperature of the PE phase as well. As previously reported by our group, this behaviour indicates surface nucleation of PE on the PP matrix, which becomes more and more favourable with the thickening of the PP lamellae [400]. This surface nucleation mechanism is explained by the known epitaxial matching of PE crystals on PP substrates [347,494].

The recorded changes of PE phase crystallization temperature as a function of T_s for the two systems selected as examples (PP/LDPE922 and PP/ZNPE935) are reported in Figures 5.3–5a and 5.3–5b, respectively. They are compared with the behaviour of the neat PE material and with the variation of the PP matrix crystallization temperature. In Figure 5.3–5a, it can be seen that the increase of PE crystallization temperature (T_c) from T_s in PP *Domain I* (i.e., 225 °C) to *Domain III* (i.e., 161 °C) is practically negligible, although the shift in PP T_c is remarkable. On the other hand, the data for the blended PE present a characteristic trend displaying a minimum of T_c with T_s in the self-nucleation range of PP. The same trend is observed for all the materials that do not show meaningful surface nucleation effects, namely PP/mPE927, PP/mPE902 (see Supporting Information Figures S4d and S4f, respectively in Appendix C). We note that the magnitude of the decrease in crystallization temperature is minimal (within 1 °C), nevertheless, the data are consistent and reproducible. The reason behind this result is currently unknown. However, it could be tentatively attributed to the generation of a particular state of the PP surface induced by self-nucleation, which is unfavourable for the nucleation of low-chain regularity PE (resulting in an anti-nucleation

effect). The role of the interface here is deduced since the same dip in T_c values is not recorded for the neat PE material in the given T_s temperature range.

A different situation is depicted for high-chain regularity PEs (e.g., Figure 5.3–5b). In this case, the T_c of the dispersed ZNPE935 phase increases by about 3 °C for T_s temperatures within PP *Domain II* and *III*, in correspondence with the increase in T_c of PP. On the other hand, the neat material does not show such variation in the same T_s temperature range, and the crystallization temperature starts to increase only at much lower temperatures, when the self-nucleation *Domain II* or *III* of the neat PE is encountered. This clearly indicates an interfacial interaction between PP and ZNPE935 by means of the known epitaxial nucleation mechanism, as already demonstrated for a similar PP/ZNPE blend in a previous work [400].

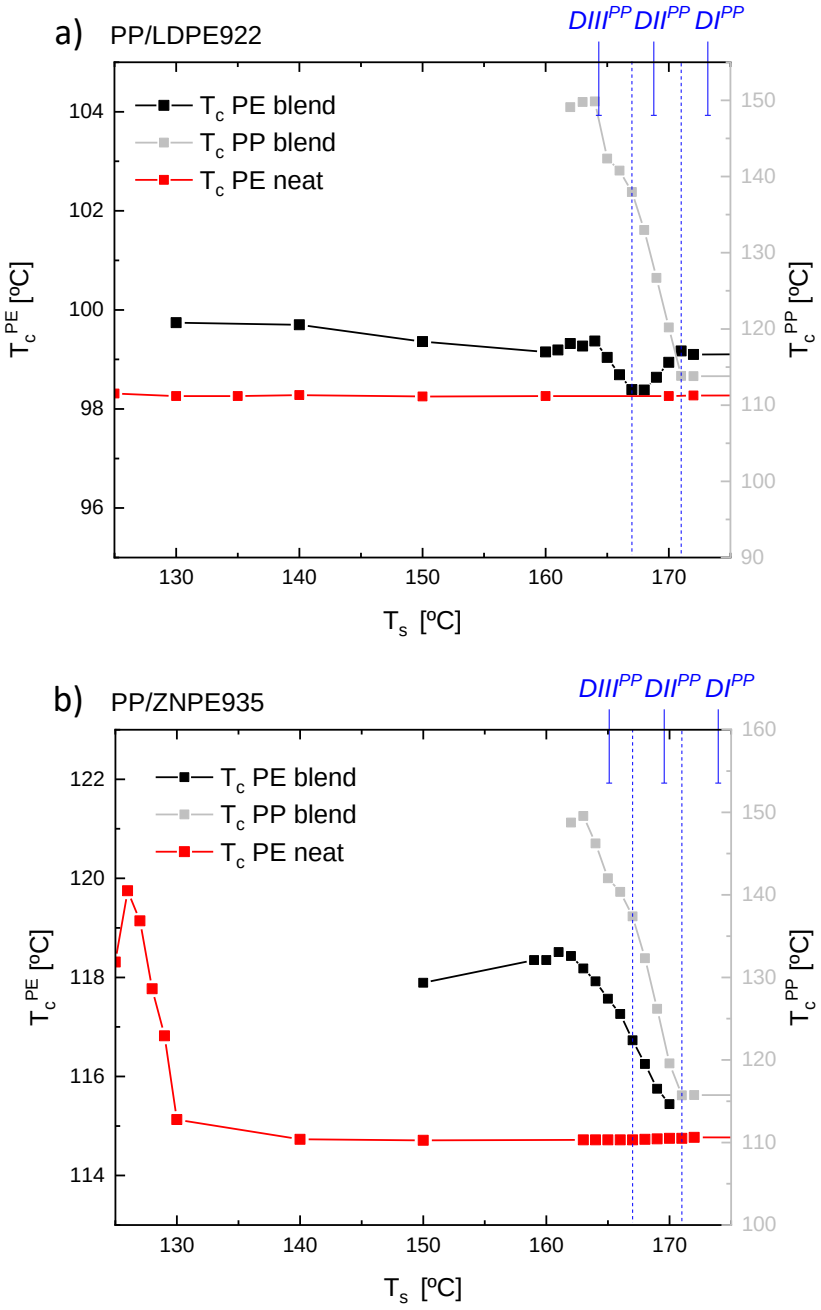

Figure 5.3–5 Crystallization temperature (T_c) values of PE phase in the blend (black symbols, left y-axis) and PP phase (grey symbols, right y-axis) and of neat PE (red symbols) as a function of T_s for a) PP/LDPE922; b) PP/ZNPE935; The different self-nucleation Domains of PP are also indicated.

Figure 5.3–6 reports the correlation between the dispersed phase's crystallization temperatures and the matrix with varying T_s in the PP self-nucleation domains for all the investigated blends. It can be observed that a linear relationship exists between the two T_c*s* for all the systems considered. However, the slope of the fitting lines is dependent on the PE chain regularity. In particular, the steepest slopes are obtained for the ZNPE with the higher densities, while the mPE and LDPEs are characterized by very low slopes. The data might be interpreted

as a measure of the sensitivity of PE phase nucleation kinetics (as crystallization in the minor droplet phase is dominated by nucleation [59,472–474]) to a change in the matrix T_c. More precisely, being the T_c related to the undercooling and thus inversely related to the lamellar thickness, the link provided in Figure 5.3–6 tells us how sensitive the crystallization of PE is to a change in PP lamellar thickness. In this respect, the largest effect on PE crystallization temperature is reported for ZNPE, while mPE and LDPE show almost no variation of their T_c with the change of PP's T_c. Therefore, mPE and LDPE are less sensitive to the PP surface. It is noteworthy that mPE918, despite the relatively low density, shows a mild surface nucleation effect. Therefore, density itself is apparently not the only controlling aspect for surface nucleation.

We underline that the found scale of surface nucleation activity, i.e., high-density PE > linear low-density PE > low-density PE, is the same reported by Yan and Petermann in thin-films experiments. In their case, the epitaxially grown crystalline layer thickness decreases with a decrease in the PE density [350]. To explain this behaviour, two hypotheses can be put forward. On the one hand, the results point to the existence of a certain minimum chain regularity to allow surface nucleation of PE on PP, notwithstanding the lamellar thickness of the substrate. When there are too many chain defects (comonomer and/or branches), their presence hinders the templating of PE chains onto the PP substrate, thus disfavouring the nuclei formation. This latter case is analogous to the findings of Petermann and Yan on thin films of HDPE, LLDPE, and LDPE onto oriented PP [350]. A decrease in the epitaxial layer thickness was observed with decreasing PE density and interpreted as a competition between epitaxial nucleation and bulk (spherulitic) crystallization. Similarly, in our immiscible blends, nucleation at the surface might still be possible for the low-density materials. Still, the nucleation rate might be much slower with respect to that of HDPE, so eventually, it becomes comparable to or slower than the nucleation rate in the bulk of the PE droplets. On the other hand, Chaffin et al. reported that low chain regularity PEs could form entanglements easier with PP at the interface, [476] and that such topological constraints hinder epitaxial nucleation of the PE phase. Both hypotheses might play a role in our observations.

The overall surface nucleation effect of the different PE types can be obtained by considering the maximum increase in non-isothermal crystallization temperature between the melt cooled from the first T_s at which the crystallization temperature of the two phases does not overlap, i.e., 170 °C (edge of PP *Domain II*) and from PP *Domain III*, i.e., 161 °C.

The increase in crystallization temperature difference, calculated as outlined above, is plotted as a function of the peak melting temperature in Figure 5.3–7a. T_m values and the surface nucleation effect of PE onto PP have a clear correlation. In particular, no enhanced nucleation effect is observed for T_m values lower than about 115 °C. When the T_m is larger than 120 °C, the increase in the T_c of the PE phase starts to be larger than 1 °C, and afterwards it increases approximately linearly with the melting temperature. Generally speaking, the higher the T_m value, the longer the uninterrupted crystallizable PE chain sequence is. Figure 5.3–7a suggests that a certain level of PE chain regularity is required to enable efficient surface-induced nucleation of PE onto PP in immiscible blends. The behaviour of mPE918 is noteworthy, as it displays a low density but melting temperature higher than grades with similar densities. This data is thus corroborating the fact that melting temperature is governing surface-nucleation of PE onto PP, rather than the sole density.

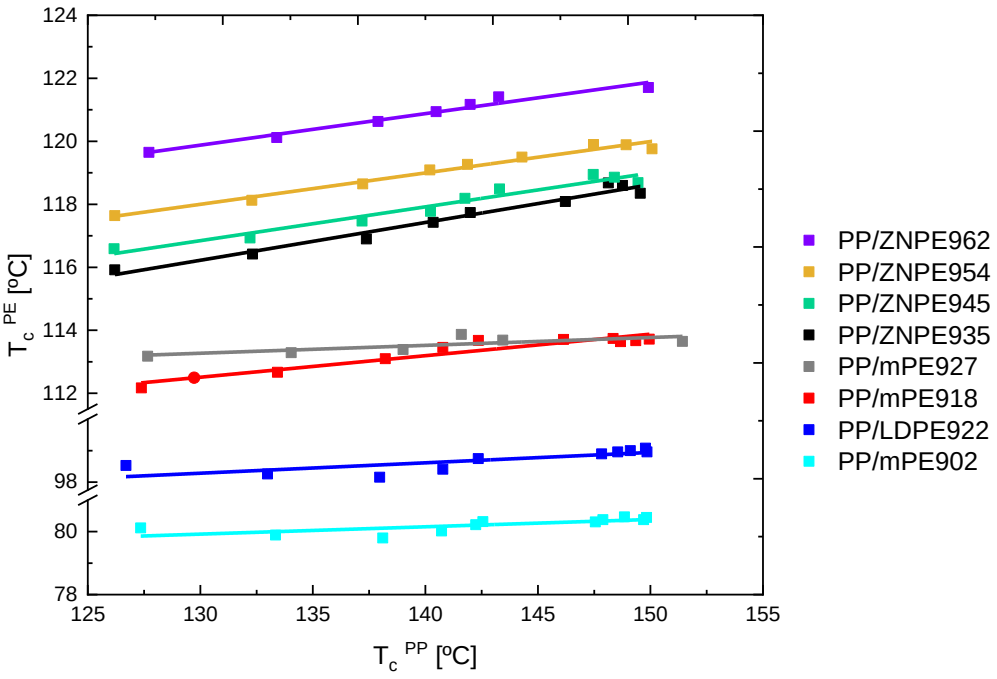

Figure 5.3–6 T_c values of the PE as a function of T_c values of PP in the different blends. The lines are linear fitting of the data.

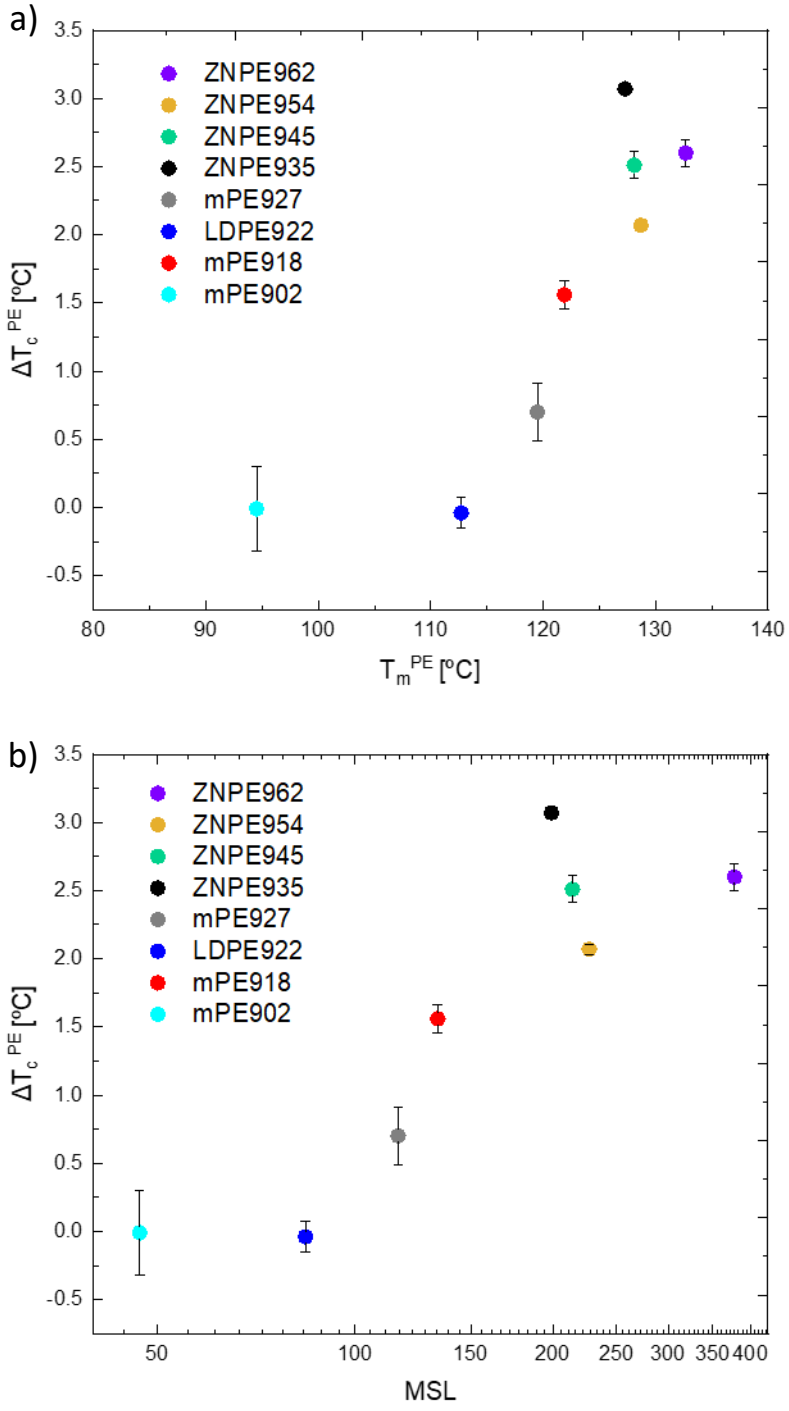

Figure 5.3–7 Maximum increase in crystallization temperature recorded as a consequence of PP matrix self-nucleation for the different blends as a function of a) peak melting temperature and b) methylene sequence length of the various PE grades. The measurement error was estimated by repeating the measurement 6 times and employing the Student's t-distribution at a confidence level of 0.99 to calculate the error associated with a small number of repetitions.

The PE chain regularity can be represented by the value of the methylene sequence length (MSL), calculated from the melting point of the polyethylene grade. As melting temperatures of ethylene copolymers decrease with the increase in branch content but are independent of the

branch length [178,179], it is convenient to consider this parameter. MSL could be calculated in relation to the change in melting temperature of the polyethylene grade according to empirical relations such as the one reported in equation 16 [172,180,181].

$$MSL = \frac{2}{e^{\left(\frac{142.2}{Tm[K]} - 0.3451\right)} - 1} \tag{16}$$

The relation between the maximum increase of crystallization temperature of the PE phase and MSL could be appreciated again in Figure 5.3–7b. No enhanced nucleation effect is observed for MSL values lower than about 100. After a threshold value of 200, the increase in T_c reaches a plateau. It should be noted that the reported MSL values, being related to the peak melting temperature, only represent the most probable MSL among the polymer chains and not the average or the maximum. It is also clear that, since it is based on an empirical relation derived for long alkanes (equation 16), the calculated MSL could deviate from the real values, as determined for instance via NMR. Nevertheless, the conclusions on chain regularity effect on surface nucleation of PE onto PP that can be grasped from Figure 5.3–7b can be considered as semi-quantitative.

In order to demonstrate that nucleation of PE droplets occurred at the interface with the PP matrix and to different extents for the PE grades of varying regularity, SEM analysis on thermally treated and etched samples was conducted. The results are shown in Figures 5.3–8 and 5.3–9. Figure 5.3–8 shows the detail of a single ZNPE935 droplet embedded in the PP matrix, crystallized starting from a T_s temperature in PP *Domain I* (Figure 5.3–8a) or *Domain III* (Figure 5.3–8b). In both cases, there is a relevant fraction of PE lamellar stacks which originate from the droplet interface. However, in the case of the lower seeding temperature (5.3–8b), the nucleation density at the droplet surface is higher, leading to the generation of a transcrystalline morphology. This indicates the promoted surface nucleation in the case of high-density ZNPE. The results are analogous to previous observations on a similar system, constituted by a blend of the same PP matrix and a Ziegler-Natta PE with a slightly higher density (945 kg/m^3)[400].

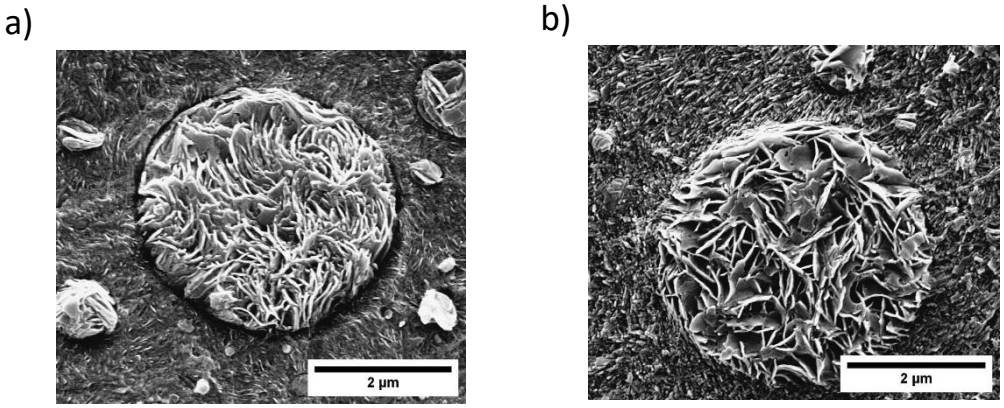

Figure 5.3–8 SEM images of the PP/ZNPE935 blend after cooling from selected T_s a) T_s 225°C, b) 161°C.

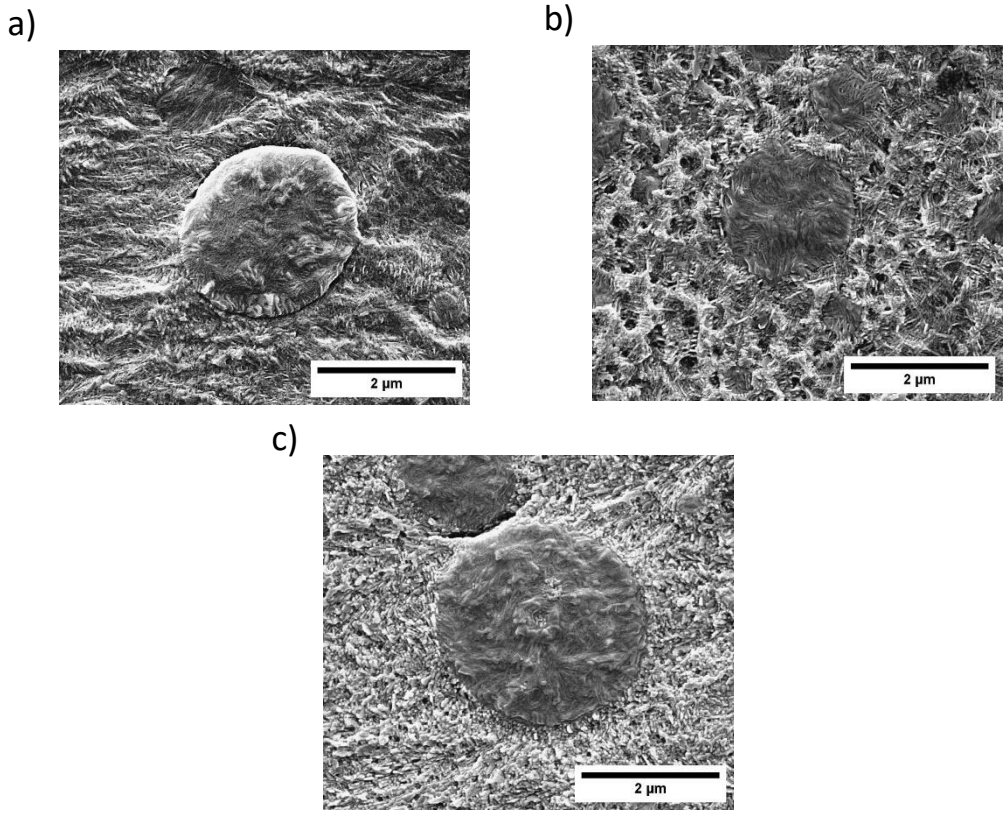

Figure 5.3–9 SEM images of the PP/LDPE922 blend after cooling from selected T_s first images (a) T_s 225°C b) 167°C, c) 161°C.

To investigate the peculiar minimum in T_c versus T_s for PP/LDPE922 blends, samples were pre-treated in the DSC to obtain PP in *Domain I*, *Domain II* and *Domain III* at 225 °C, 167 °C and 161°C, respectively. The droplets of LDPE appear to be darker than the PP matrix. In Figure 5.3–9a, a relatively smooth interface between the two phases can be appreciated, while the main nucleation sites of the LDPE are difficult to be detected since the lamellar stacks seem

to originate from both the bulk and the interface of the droplet. In Figure 5.3–9b, the phase boundary becomes rougher due to the higher amount of spherulites that were created during self-nucleation of the PP matrix. On the other hand, at T_s= 161 °C (Figure 5.3–9c), a smoother interface is again obtained because the PP matrix is just partially molten and annealed during the thermal treatment. Therefore, the observed minimum in T_c with T_s can be tentatively attributed to a change in the roughness state of the PP/PE surface. Similar changes can be highlighted in another system displaying the same minimum, i.e., PP/mPE902, see Figure S3f and S4 (Appendix C), where the very low-density PE phase has been etched away before the SEM measurement. We note that if the surface roughness plays a role in the observed decrease of the overall crystallization kinetics at intermediate T_ss, it must mean that nucleation occurs at the interface, at least to some extent, and also for the materials with lower chain regularity. However, the fact that the T_c is not increased when changing the lamellar thickness of the PP substrate points towards the fact that the surface nucleation mechanism is not dominant in these PEs, and it must be competing with nucleation in the bulk of the droplet.

In fact, by comparing Figure 5.3–8b and Figure 5.3–9c, it can be seen that a transcrystalline layer at the interface is clearly apparent for the ZNPE sample annealed at 161 °C, while it is practically absent for the LDPE sample. This is in agreement with the measurement by Petermann and Yan, which observed a large decrease of the PE epitaxial layer thickness onto PP substrates when passing from HDPE to LDPE[350].

5.4 Conclusions

We previously reported that surface nucleation of polyethylene droplets at the interface with polypropylene matrix is promoted by the self-nucleation of the PP matrix in PP/PE blends. In this work, we investigated the effect of the PE phase chain regularity on the mechanism of epitaxial crystallization onto the self-nucleated PP matrix. We found that the surface nucleation of PE droplets on self-nucleated PP matrices, strongly depends on chain regularity. Thus the increase in crystallization temperature observed for PE droplets (that correlates with an increase in nucleation effect) was maximum for HDPE samples, much less for metallocene-catalyzed LLDPE, and negligible for highly branched and comonomer-rich polymers.

The results were interpreted by considering polymer chain regularity, i.e., the average methylene sequence length (MSL), as a key parameter. It was noted that when the PE crystallizable sequence length is below ~ 100, corresponding to a melting temperature lower than approximately 115 °C, the epitaxial matching between the aligned PE chains and the rows

of PP methyl groups can not be efficiently attained, and the surface nucleation rate dramatically slows down. The increase in interfacial entanglement between PE and PP with decreasing PE regularity could also possibly hinder epitaxial crystallization among the two polymers.

Electron microscopy observations corroborate the DSC results, as a distinct interfacial morphology could be detected in HDPE and LDPE samples, with the latter lacking a clear transcrystalline layer, which is instead observed for the former polymer pair.

6 CONCLUSIONS & RECOMMENDATIONS

6.1 Conclusions

This thesis contains a collection of studies that have increased understanding of polyolefin blends in the context of recycling. While higher heating/cooling rates in the SSA thermal fractionation process can be applied to recycled polyolefin blends, restrictions exist due to co-crystallization processes in LDPE and HDPE, impacting the accuracy of content computation in post-consumer blends, as revealed in Chapter 31. The focus of Chapter 4 is on the relationship between PP low molecular weight and its elution behavior within the PE temperature range, which is critical in defining the accurate composition of polyolefin blends. The study emphasizes the need to include the detector response parameters to achieve accurate composition analysis, hence having the full microstructure distribution of the mixed blends and composition. The surface nucleation in PP and PE blends is discussed in Chapter 5, with an emphasis on the effect of PE chain regularity on epitaxial crystallization. These chapters collectively add significant expertise to the topic of polymer recycling, providing new insights and answers to industry difficulties.

The investigations given in this thesis in the field of polyolefin science and recycling technology provide insights into successive self-nucleation and annealing (SSA) thermal fractionation process, surface nucleation phenomena in PP and PE blends, and co-elution of PE with low molecular weight PP behavior. These findings are significant because they have substantial implications for R&D laboratories in terms of validating the feedstock suppliers of commercial mechanical recycled polyolefins and select recycled material for higher-demand application. This thesis not only addresses specific issues in polyolefin fractionation and nucleation, but it also lays the path for more precise composition determination and understanding of crystallization during processing, specifically static interactions between blend’s components.

The study demonstrates that higher heating/cooling rates in the SSA thermal fractionation process can be effectively applied to commercial recycled polyolefin blends, with the prerequisite of adopting a mass compensation principle to mitigate thermal inertia issues. The methodology, however, does not extend to calculating the content of low-density polyethylene (LDPE) and linear low-density polyethylene (LLDPE) in post-consumer blends

due to the partial co-crystallization phenomena observed between high-density polyethylene (HDPE) and LDPE, LLDPE. This issue is also present in other crystallization-based fractionation techniques like Temperature Rising Elution Fractionation (TREF), Crystallization Analysis Fractionation (CRYSTAF), and Crystallization Elution Fractionation (CEF).

Additionally, the surface nucleation phenomena in immiscible polypropylene (PP) and polyethylene (PE) blends are studied in this thesis. Central to our findings is the role of polyethylene chain regularity indictating the mechanism of epitaxial crystallization onto a self-nucleated PP matrix. This investigation reveal that the surface nucleation of PE droplets in self-nucleated PP matrices is intricately dependent on the chain regularity of the PE component. It was observed that the increase in crystallization temperature, an indication for the nucleation effect, varied notably across different PE types. The increase was most pronounced in high-density polyethylene (HDPE) samples. Conversely, the effect was considerably less in metallocene-catalyzed linear low-density polyethylene (LLDPE) and almost negligible in polymers that were highly branched or rich in comonomer, LDPE and LLDPE with high octene content. A pivotal aspect of our analysis focused on the average methylene sequence length (MSL) as a critical parameter in determining the nucleation behavior. It was established that when the PE crystallizable sequence length is below approximately 100 — correlating to a melting temperature under 115 °C — the epitaxial matching between the aligned PE chains and the PP methyl groups rows becomes inefficient. This mismatch leads to a dramatic decrease in the surface nucleation rate. Furthermore, our research suggests that increasing interfacial entanglement between PE and PP, particularly with decreasing PE regularity, could impede the epitaxial crystallization between these polymers. These conclusions are supported by electron microscopy observations, which corroborate the Differential Scanning Calorimetry (DSC) results. The HDPE samples displayed a pronounced interfacial morphology, characterized by a distinct phase boundary. However, this region where two phases are in contact, appeared less prominent in samples where PP underwent self-nucleation with the same PE. Conversely, both the low-density polyethylene (LDPE) and linear low-density polyethylene (LLDPE) samples exhibited a more subdued phase boundary, regardless of whether PP was in a self-nucleated state or in its standard state. This observation underscores the significant impact of polymer chain regularity on the phenomena of surface nucleation.

Moreover, there has successfully established a correlation between the molecular weight of polypropylene (PP) and its elution behavior within the polyethylene (PE) temperature range in TREF. This finding is crucial in the context of accurately determining the composition of polyolefin blends, particularly in mechanical recycling processes. On top of this, the aspect of the last study was the identification of variations in absorption factors between PP and PE. These variations, especially significant when using a broadband filter tuned to the absorption region of 2800–3000 cm^{-1} for concentration signal analysis, were found to potentially introduce a 2% margin of influence on the results. Implementing the detector response factor and compensating for PP elution in the PE range has proven to be effective, yielding results that closely align with the nominal blend values. The development is particularly relevant for the recycling enterprise, where material composition precision is critical to quality and understanding the microstructure of the blend might lead to an application of mix into products.

6.2 Recommendations for future work

Characterization of polyolefins, while fundamentally aimed at monitoring processes and understanding microstructures, presents several areas for future exploration.

A primary area of investigation is the refinement of quantitative analysis for low-density polyethylene (LDPE) in post-consumer blends. The challenge lies in accurately quantifying LDPE, particularly due to its co-crystallization with high-density polyethylene (HDPE). Refining the successive self-nucleation and annealing (SSA) technique and integrating it with infrared spectroscopy (IR), modulated differential scanning calorimetry (MDSC), or atomic force microscopy (AFM) could help developing a robust method for LDPE quantification, crucial for R&D departments with appropriate resources.

Expanding the SSA protocol's application to a broader range of recycled polymers is another critical research direction. This expansion could significantly improve recycling processes and material characterization, establishing SSA as a key tool in polymer recycling. Research into the long-term stability and ageing of materials processed via the SSA protocol is also interesting field to focus on. This will provide insights into material performance and durability, informing practical applications and ensuring reliability. Comparative studies with other crystallization-based fractionation techniques, like temperature rising elution

Fractionation (TREF), crystallization analysis fractionation (CRYSTAF), and crystallization elution fractionation (CEF), are vital. Integrating design of experiment or chemometrics for data analysis in the SSA protocol could enhance the gained information. This approach promises novel insights in recycled polymer blend characterization.

It is proposed that the impact of various polypropylene (PP) matrices with different polyethylene (PE) chain regularities on the nucleation and crystallization in immiscible polymer blends can be explored. An improved understanding of the behavior of these blends is anticipated from this research. The use of advanced characterization techniques such as atomic force microscopy (AFM), X-ray diffraction (XRD), and fourier transform infrared (FTIR) spectroscopy for the analysis of PP/PE blends is recommended. Comprehensive insights into the molecular structures and interfacial dynamics within the blends are expected to be yielded by these techniques.

Future TREFxGPC research should immediately focus on expanding the spectrum of polypropylene (PP) samples. By measuring more PP samples with varying molecular weights and dispersities, researchers can refine and enhance the accuracy of the M_v-PP elution correlation. This expansion is not just a quantitative increase but necessitates the inclusion of a broadness parameter, a vital factor that could significantly impact the correlation's applicability across different PP types. Such a study would not only validate the current findings but also extend its applicability, providing a more comprehensive understanding of PP behaviors in various contexts.

In parallel, there is a compelling need to test the established method on other types of polyolefin blends, particularly ethylene-propylene copolymers. This exploration is crucial for understanding the method's versatility and limitations. Since the current methodology is shown to be less effective for random polypropylene heterophasic copolymers (RAHECO-PPs) and random polypropylene copolymers (RACO-PP), exploring its application on these and other polyolefin blends can provide insights into potential modifications or alternative approaches. Such studies would greatly benefit the recycling industry, especially considering the prevalence of RACO-PP in PP-based recyclates due to packaging applications.

Additionally, the effects of degradation and reprocessing on the molecular structure and properties of polyolefin blends present another promising research avenue. Using techniques like temperature rising elution fractionation with gel permeation chromatography (TREFxGPC) and SSA, future studies can delve into how recycling processes impact the molecular integrity and subsequent usability of PP blends. This area of research is particularly pertinent given the increasing demand for sustainable and efficient recycling methods in the plastics industry.

In conclusion, these proposed future works aim to build upon the current research foundations, addressing both scientific and practical aspects of polyolefin recycling and blend characterization. These studies hold the promise of expanding our understanding of polymer blends, paving the way for novel applications and innovations in polymer science and engineering.

References

(1) *Polyolefin Circular Economy Platform*. European Circular Economy Stakeholder Platform. https://circulareconomy.europa.eu/platform/en/dialogue/existing-eu-platforms/polyolefin-circular-economy-platform (accessed 2023-11-14).

(2) Frey, H.; Johann, T. Celebrating 100 Years of "Polymer Science": Hermann Staudinger's 1920 Manifesto. *Polym. Chem.* **2020**, *11* (1), 8–14.

(3) Tomalia, D. A. Twenty-First Century Polymer Science After Staudinger: The Emergence of Dendrimers/Dendritic Polymers as a Fourth Major Architecture and Window to a New Nano-Periodic System. In *Hierarchical Macromolecular Structures: 60 Years after the Staudinger Nobel Prize I*; Percec, V., Ed.; Advances in Polymer Science; Springer International Publishing: Cham, 2013; Vol. 261, pp 321–389. https://doi.org/10.1007/12_2013_252.

(4) Ciolino, A. E.; de Freitas, A. G.; Satti, A. J.; Ninago, M. D. From Atoms to Macromolecules: 100 Years of Polymer Research. *Adv. Org. Synth. Vol. 16* **2022**, *16*, 212.

(5) Pechmann, H. V. Ueber Diazomethan. *Berichte Dtsch. Chem. Ges.* **1894**, *27* (2), 1888–1891. https://doi.org/10.1002/cber.189402702141.

(6) Bamberger, Eug.; Tschirner, F. Ueber Die Einwirkung von Diazomethan Auf β-Arylhydroxylamine. *Berichte Dtsch. Chem. Ges.* **1900**, *33* (1), 955–959. https://doi.org/10.1002/cber.190003301166.

(7) Kaminsky, W. Polyolefins. In *Handbook of Polymer Synthesis*; CRC Press, 2004.

(8) Dobbin, C. An Industrial Chronology of Polyethylene. In *Handbook of Industrial Polyethylene and Technology*; Spalding, M. A., Chatterjee, A. M., Eds.; Wiley, 2017; pp 1–23. https://doi.org/10.1002/9781119159797.ch1.

(9) Ballard, D. G. H. The Discovery of Polyethylene and Its Effect on the Evolution of Polymer Science. In *History of Polyolefins*; Seymour, R. B., Cheng, T., Eds.; Springer Netherlands: Dordrecht, 1986; pp 9–53. https://doi.org/10.1007/978-94-009-5472-4_2.

(10) Improvements in or Relating to the Polymerisation of Ethylene, February 4, 1936. https://patents.google.com/patent/GB471590A/en (accessed 2023-11-14).

(11) *GriffsNotes: How polyethylene won the war*. plasticstoday.com. https://www.plasticstoday.com/griffsnotes-how-polyethylene-won-war (accessed 2023-11-15).

(12) Atiqullah, M.; Al-Asiri, H. S. Polyolefin Catalyst Research: A Product-Driven Industrial Perspective. *Chem. Rec.* **2022**, *22* (7), e202100321. https://doi.org/10.1002/tcr.202100321.

(13) Cheng, R.; Liu, Z.; Zhong, L.; He, X.; Qiu, P.; Terano, M.; Eisen, M. S.; Scott, S. L.; Liu, B. Phillips Cr/Silica Catalyst for Ethylene Polymerization. In *Polyolefins: 50 years after Ziegler and Natta I*; Kaminsky, W., Ed.; Advances in Polymer Science; Springer Berlin Heidelberg: Berlin, Heidelberg, 2013; Vol. 257, pp 135–202. https://doi.org/10.1007/12_2013_222.

(14) Goodall, B. L. Chapter 1 - Polypropylene; Catalysts and Polymerization Aspects. In *Polypropylene and other Polyolefins*; Ven, S. van der, Ed.; Studies in Polymer Science; Elsevier, 1990; Vol. 7, pp 1–133. https://doi.org/10.1016/B978-0-444-88690-3.50006-X.

(15) Natta, G.; Pino, P.; Corradini, P.; Danusso, F.; Mantica, E.; Mazzanti, G.; Moraglio, G. Crystalline High Polymers of α-Olefins. *J. Am. Chem. Soc.* **1955**, *77* (6), 1708–1710. https://doi.org/10.1021/ja01611a109.

(16) Ziegler, K.; Holzkamp, E.; Breil, H.; Martin, H. Polymerisation von Äthylen Und Anderen Olefinen. *Angew. Chem.* **1955**, *67* (16), 426–426. https://doi.org/10.1002/ange.19550671610.

(17) Maddah, H. A. Polypropylene as a Promising Plastic: A Review. *Am. J. Polym. Sci.* **2016**.

(18) *Poylpropylene and High-Density Polyethylene - National Historic Chemical Landmark*. American Chemical Society. https://www.acs.org/education/whatischemistry/landmarks/polypropylene.html (accessed 2023-11-15).

(19) Paul, H. J.; Banks, R. L. Polymers and Production Thereof. US2825721A, March 4, 1958. https://patents.google.com/patent/US2825721A/en (accessed 2023-10-13).

(20) Hogan, J. P. Ethylene Polymerization Catalysis over Chromium Oxide. *J. Polym. Sci. [A1]* **1970**, *8* (9), 2637–2652. https://doi.org/10.1002/pol.1970.150080929.

(21) Martin, H. *Polymers, Patents, Profits: A Classic Case Study for Patent Infighting Karl Ziegler, the Team, 1953-1998*; Wiley-VCH: Weinheim, 2007.

(22) *Patentlösung aus dem Einmachglas*. https://www.mpg.de/8355774/rueckblende-ziegler (accessed 2023-11-16).

(23) *The Nobel Prize in Chemistry 1963*. NobelPrize.org. https://www.nobelprize.org/prizes/chemistry/1963/summary/ (accessed 2023-11-14).

(24) Ziegler, K. Historische Stätten der Chemie.

(25) Natta, G.; Peraldo, M.; Allegra, G. Crystalline Modification of Syndiotactic Polypropylene Having a Zig-Zag Chain Conformation. *Makromol. Chem.* **1964**, *75* (1), 215–216. https://doi.org/10.1002/macp.1964.020750120.

(26) De Rosa, C.; Auriemma, F. Structure and Physical Properties of Syndiotactic Polypropylene: A Highly Crystalline Thermoplastic Elastomer. *Prog. Polym. Sci.* **2006**, *31* (2), 145–237. https://doi.org/10.1016/j.progpolymsci.2005.11.002.

(27) Lovell, R. J. Y., Peter A. *Introduction to Polymers*, 3rd ed.; CRC Press: Boca Raton, 2013. https://doi.org/10.1201/9781439894156.

(28) Sperling, L. H. The Crystalline State. In *Introduction to Physical Polymer Science*; John Wiley & Sons, Ltd, 2005; pp 239–323. https://doi.org/10.1002/0471757128.ch6.

(29) Billmeyer, F. W. *Textbook of Polymer Science*; John Wiley & Sons, 1984.

(30) Coates, J. Interpretation of Infrared Spectra, A Practical Approach. In *Encyclopedia of Analytical Chemistry*; Meyers, R. A., Ed.; Wiley, 2000. https://doi.org/10.1002/9780470027318.a5606.

(31) Malik, M. I.; Pasch, H. Characterization of Polyolefins. In *Molecular Characterization of Polymers*; Elsevier, 2021; pp 173–222. https://doi.org/10.1016/B978-0-12-819768-4.00016-6.

(32) Müller, A. J.; Arnal, M. L. Thermal Fractionation of Polymers. *Prog. Polym. Sci.* **2005**, *30* (5), 559–603. https://doi.org/10.1016/j.progpolymsci.2005.03.001.

(33) Utracki, L. A.; Wilkie, C. A. *Polymer Blends Handbook*; Kluwer academic publishers Dordrecht, 2002; Vol. 1.

(34) *Thermal Analysis of Polymers: Fundamentals and Applications*; Menczel, J. D., Prime, R. B., Eds.; John Wiley: Hoboken, N.J, 2009.

(35) deGroot, A. W.; Gillespie, D.; Cong, R.; Zhou, Z.; Paradkar, R. Molecular Structural Characterization of Polyethylene. In *Handbook of Industrial Polyethylene and Technology*; Spalding, M. A., Chatterjee, A. M., Eds.; John Wiley & Sons, Inc.: Hoboken, NJ, USA, 2017; pp 139–216. https://doi.org/10.1002/9781119159797.ch5.

(36) Monrabal, B. Polyolefin Characterization: Recent Advances in Separation Techniques. In *Polyolefins: 50 years after Ziegler and Natta I*; Kaminsky, W., Ed.; Advances in Polymer Science; Springer Berlin Heidelberg: Berlin, Heidelberg, 2013; Vol. 257, pp 203–251. https://doi.org/10.1007/12_2013_216.

(37) Gahleitner, M.; Paulik, C. Polypropylene and Other Polyolefins. In *Brydson's Plastics Materials*; Elsevier, 2017; pp 279–309. https://doi.org/10.1016/B978-0-323-35824-8.00011-6.

(38) Kaminsky, W. Polyolefins. In *Handbook of Polymer Synthesis*; CRC Press, 2004.

(39) Chum, P. S.; Swogger, K. W. Olefin Polymer Technologies—History and Recent Progress at The Dow Chemical Company. *Prog. Polym. Sci.* **2008**, *33* (8), 797–819. https://doi.org/10.1016/j.progpolymsci.2008.05.003.

(40) Kim, Y. The Use of Polyolefins in Industrial and Medical Applications. In *Polyolefin Fibres*; Elsevier, 2009; pp 133–153. https://doi.org/10.1533/9781845695552.1.133.

(41) Charfeddine, I.; Majesté, J.; Carrot, C.; Lhost, O. Surface Tension and Interfacial Tension of Polyolefins and Polyolefin Blends. *J. Appl. Polym. Sci.* **2022**, *139* (14), 51885. https://doi.org/10.1002/app.51885.

(42) Pasch, H.; Malik, M. I. Crystallization-Based Fractionation Techniques. In *Advanced Separation Techniques for Polyolefins*; Springer Laboratory; Springer International Publishing: Cham, 2014; pp 11–73. https://doi.org/10.1007/978-3-319-08632-3_2.

(43) Pfaendner, R. Restabilization – 30 Years of Research for Quality Improvement of Recycled Plastics Review. *Polym. Degrad. Stab.* **2022**, *203*, 110082. https://doi.org/10.1016/j.polymdegradstab.2022.110082.

(44) Vilaplana, F.; Karlsson, S. Quality Concepts for the Improved Use of Recycled Polymeric Materials: A Review. *Macromol. Mater. Eng.* **2008**, *293* (4), 274–297. https://doi.org/10.1002/mame.200700393.

(45) Stoian, S. A.; Gabor, A. R.; Albu, A.-M.; Nicolae, C. A.; Raditoiu, V.; Panaitescu, D. M. Recycled Polypropylene with Improved Thermal Stability and Melt Processability. *J. Therm. Anal. Calorim.* **2019**, *138* (4), 2469–2480. https://doi.org/10.1007/s10973-019-08824-2.

(46) Camacho, W.; Karlsson, S. NIR, DSC, and FTIR as Quantitative Methods for Compositional Analysis of Blends of Polymers Obtained from Recycled Mixed Plastic Waste. *Polym. Eng. Sci.* **2001**, *41* (9), 1626–1635. https://doi.org/10.1002/pen.10860.

(47) Kahlen, S. M.; Shutov, P.; Tran, T. A. Polypropylene Polyethylene Mixture Upgrading. WO2022008434A1, January 13, 2022. https://patents.google.com/patent/WO2022008434A1/en?q=(%22ZSK+18+MegaLAB%22+%22mixing%22+%22Borealis%22)&oq=%22ZSK+18+MegaLAB%22+%22mixing%22+%22Borealis%22 (accessed 2023-09-30).

(48) Hasanah, T. I. T. N.; Wijeyesekera, D. C.; Lim, A. J. M. S.; Ismail, B. Recycled PP/HDPE Blends: A Thermal Degradation and Mechanical Properties Study. *Appl. Mech.*

Mater. **2014**, *465–466*, 932–936. https://doi.org/10.4028/www.scientific.net/AMM.465-466.932.

(49) de Souza, A. M. C.; Caldeira, C. B. An Investigation on Recycled PET/PP and Recycled PET/PP-EP Compatibilized Blends: Rheological, Morphological, and Mechanical Properties. *J. Appl. Polym. Sci.* **2015**, *132* (17). https://doi.org/10.1002/app.41892.

(50) Al-Mulla, A.; Shaban, H. Study on Compatibility of Recycled Polypropylene/High-Density Polyethylene Blends Using Rheology. *Polym. Bull.* **2014**, *71* (9), 2335–2352. https://doi.org/10.1007/s00289-014-1191-5.

(51) Miller, P.; Sbarski, I.; Kosior, E.; Masood, S.; Iovenitti, P. Correlation of Rheological and Mechanical Properties for Blends of Recycled HDPE and Virgin Polyolefins. *J. Appl. Polym. Sci.* **2001**, *82* (14), 3505–3512. https://doi.org/10.1002/app.2212.

(52) Saikrishnan, S.; Jubinville, D.; Tzoganakis, C.; Mekonnen, T. H. Thermo-Mechanical Degradation of Polypropylene (PP) and Low-Density Polyethylene (LDPE) Blends Exposed to Simulated Recycling. *Polym. Degrad. Stab.* **2020**, *182*, 109390. https://doi.org/10.1016/j.polymdegradstab.2020.109390.

(53) Santos, A. S. F.; Agnelli, J. A. M.; Trevisan, D. W.; Manrich, S. Degradation and Stabilization of Polyolefins from Municipal Plastic Waste during Multiple Extrusions under Different Reprocessing Conditions. *Polym. Degrad. Stab.* **2002**, *77* (3), 441–447. https://doi.org/10.1016/S0141-3910(02)00101-5.

(54) Ortín, A.; Montesinos, J.; López, E.; Del Hierro, P.; Monrabal, B.; Torres-Lapasió, J. R.; García-Álvarez-Coque, M. C. Characterization of Chemical Composition along the Molar Mass Distribution in Polyolefin Copolymers by GPC Using a Modern Filter-Based IR Detector. *Macromol. Symp.* **2013**, *330* (1), 63–80. https://doi.org/10.1002/masy.201300060.

(55) Carmeli, E.; Tranchida, D.; Albrecht, A.; Müller, A. J.; Cavallo, D. A Tailor-Made Successive Self-Nucleation and Annealing Protocol for the Characterization of Recycled Polyolefin Blends. *Polymer* **2020**, *203*, 122791. https://doi.org/10.1016/j.polymer.2020.122791.

(56) Carmeli, E.; Kandioller, G.; Gahleitner, M.; Müller, A. J.; Tranchida, D.; Cavallo, D. Continuous Cooling Curve Diagrams of Isotactic-Polypropylene/Polyethylene Blends: Mutual Nucleating Effects under Fast Cooling Conditions. *Macromolecules* **2021**, *54* (10), 4834–4846. https://doi.org/10.1021/acs.macromol.1c00699.

(57) Carmeli, E.; Fenni, S. E.; Caputo, M. R.; Müller, A. J.; Tranchida, D.; Cavallo, D. Surface Nucleation of Dispersed Polyethylene Droplets in Immiscible Blends Revealed by

Polypropylene Matrix Self-Nucleation. *Macromolecules* **2021**, *54* (19), 9100–9112. https://doi.org/10.1021/acs.macromol.1c01430.

(58) Silvestre, C.; Di Lorenzo, M. L.; Di Pace, E. Crystallization of Polyolefins. *Plast. Eng.-N. Y.*- **2000**, *59*, 223–248.

(59) Fenni, S. E.; Müller, A. J.; Cavallo, D. Understanding Polymer Nucleation by Studying Droplets Crystallization in Immiscible Polymer Blends. *Polymer* **2023**, *264*, 125514. https://doi.org/10.1016/j.polymer.2022.125514.

(60) Aumnate, C.; Rudolph, N.; Sarmadi, M. Recycling of Polypropylene/Polyethylene Blends: Effect of Chain Structure on the Crystallization Behaviors. *Polymers* **2019**, *11* (9), 1456. https://doi.org/10.3390/polym11091456.

(61) Balkaev, D.; Neklyudov, V.; Starshinova, V.; Stolov, M.; Amirova, L. M.; Ziyatdinova, A.; Amirov, R. R. Novel Nucleating Agents for Polypropylene and Modifier of Its Physical-Mechanical Properties. *Mater. Today Commun.* **2021**, *26*, 101783. https://doi.org/10.1016/j.mtcomm.2020.101783.

(62) Bartczak, Z.; Galeski, A.; Pracella, M. Spherulite Nucleation in Blends of Isotactic Polypropylene with High-Density Polyethylene. *Polymer* **1986**, *27* (4), 537–543. https://doi.org/10.1016/0032-3861(86)90239-9.

(63) Blom, H. P.; Teh, J. W.; Bremner, T.; Rudin, A. Isothermal and Non-Isothermal Crystallization of PP: Effect of Annealing and of the Addition of HDPE. *Polymer* **1998**, *39* (17), 4011–4022. https://doi.org/10.1016/S0032-3861(97)10305-6.

(64) *Plastic waste and recycling in the EU: facts and figures | News | European Parliament*. https://www.europarl.europa.eu/news/en/headlines/society/20181212STO21610/plastic-waste-and-recycling-in-the-eu-facts-and-figures (accessed 2022-01-26).

(65) PlasticsEurope. Plastics – the Facts 2020: An Analysis of European Plastics Production, Demand and Waste Data, 2021. https://plasticseurope.org/wp-content/uploads/2021/09/Plastics_the_facts-WEB-2020_versionJun21_final.pdf.

(66) Yeh, C.-L.; Nikolić, M. A. L.; Gomes, B.; Gauthier, E.; Laycock, B.; Halley, P.; Bottle, S. E.; Colwell, J. M. The Effect of Common Agrichemicals on the Environmental Stability of Polyethylene Films. *Polym. Degrad. Stab.* **2015**, *120*, 53–60. https://doi.org/10.1016/j.polymdegradstab.2015.06.007.

(67) Setnickova, K.; Petrychkovych, R.; Reznickova, J.; Uchytil, P. A Novel Simple and Efficient Procedure for the Pervaporation Transport Study of Binary Mixtures through

Polymeric Membranes: Tested Systems Propanol Isomers—Water–Polyethylene Membrane. *J. Taiwan Inst. Chem. Eng.* **2016**, *58*, 49–56. https://doi.org/10.1016/j.jtice.2015.05.043.

(68) Kircheva, N.; Outin, J.; Perrier, G.; Ramousse, J.; Merlin, G.; Lyautey, E. Bio-Electrochemical Characterization of Air-Cathode Microbial Fuel Cells with Microporous Polyethylene/Silica Membrane as Separator. *Bioelectrochemistry* **2015**, *106*, 115–124. https://doi.org/10.1016/j.bioelechem.2015.05.016.

(69) Kindsfater, K. A.; Pomeroy, D.; Clark, C. R.; Gruen, T. A.; Murphy, J.; Himden, S. In Vivo Performance of Moderately Crosslinked, Thermally Treated Polyethylene in a Prospective Randomized Controlled Primary Total Knee Arthroplasty Trial. *J. Arthroplasty* **2015**, *30* (8), 1333–1338. https://doi.org/10.1016/j.arth.2015.02.041.

(70) So, K.; Goto, K.; Kuroda, Y.; Matsuda, S. Minimum 10-Year Wear Analysis of Highly Cross-Linked Polyethylene in Cementless Total Hip Arthroplasty. *J. Arthroplasty* **2015**, *30* (12), 2224–2226. https://doi.org/10.1016/j.arth.2015.06.053.

(71) Tajeddin, B.; Arabkhedri, M. Chapter 16 - Polymers and Food Packaging. In *Polymer Science and Innovative Applications*; AlMaadeed, M. A. A., Ponnamma, D., Carignano, M. A., Eds.; Elsevier, 2020; pp 525–543. https://doi.org/10.1016/B978-0-12-816808-0.00016-0.

(72) Kahlen, S.; Jerabek, M.; Wallner, G. M.; Lang, R. W. Characterization of Physical and Chemical Aging of Polymeric Solar Materials by Mechanical Testing. *Polym. Test.* **2010**, *29* (1), 72–81. https://doi.org/10.1016/j.polymertesting.2009.09.007.

(73) Wang, Y.; Feng, G.; Lin, N.; Lan, H.; Li, Q.; Yao, D.; Tang, J. A Review of Degradation and Life Prediction of Polyethylene. *Appl. Sci.* **2023**, *13* (5), 3045. https://doi.org/10.3390/app13053045.

(74) Singh, M. K.; Mohanty, A. K.; Misra, M. Upcycling of Waste Polyolefins in Natural Fiber and Sustainable Filler-Based Biocomposites: A Study on Recent Developments and Future Perspectives. *Compos. Part B Eng.* **2023**, *263*, 110852. https://doi.org/10.1016/j.compositesb.2023.110852.

(75) Cecon, V. S.; Da Silva, P. F.; Curtzwiler, G. W.; Vorst, K. L. The Challenges in Recycling Post-Consumer Polyolefins for Food Contact Applications: A Review. *Resour. Conserv. Recycl.* **2021**, *167*, 105422. https://doi.org/10.1016/j.resconrec.2021.105422.

(76) Juan, R.; Paredes, B.; García-Muñoz, R. A.; Domínguez, C. Quantification of PP Contamination in Recycled PE by TREF Analysis for Improved the Quality and Circularity of Plastics. *Polym. Test.* **2021**, *100*, 107273. https://doi.org/10.1016/j.polymertesting.2021.107273.

(77) Hashemnejad, M. Composition Analysis of Post-consumer Recycled Blends of Linear Low- and Low-density Polyethylene Using a Solution-based Technique. *J. Appl. Polym. Sci.* **2023**, *140* (30), e54099. https://doi.org/10.1002/app.54099.

(78) Larsen, Å. G.; Olafsen, K.; Alcock, B. Determining the PE Fraction in Recycled PP. *Polym. Test.* **2021**, *96*, 107058. https://doi.org/10.1016/j.polymertesting.2021.107058.

(79) Curtzwiler, G. W.; Schweitzer, M.; Li, Y.; Jiang, S.; Vorst, K. L. Mixed Post-Consumer Recycled Polyolefins as a Property Tuning Material for Virgin Polypropylene. *J. Clean. Prod.* **2019**, *239*, 117978. https://doi.org/10.1016/j.jclepro.2019.117978.

(80) Gall, M.; Freudenthaler, P. J.; Fischer, J.; Lang, R. W. Characterization of Composition and Structure–Property Relationships of Commercial Post-Consumer Polyethylene and Polypropylene Recyclates. *Polymers* **2021**, *13* (10), 1574. https://doi.org/10.3390/polym13101574.

(81) Velásquez, E.; Patiño Vidal, C.; Copello, G.; López De Dicastillo, C.; Pérez, C. J.; Guarda, A.; Galotto, M. J. Developing Post-Consumer Recycled Flexible Polypropylene and Fumed Silica-Based Nanocomposites with Improved Processability and Thermal Stability. *Polymers* **2023**, *15* (5), 1142. https://doi.org/10.3390/polym15051142.

(82) Ye, L.; Liu, H.; Chen, D.; Li, Z.; Li, D.; Xiao, S.; Lao, Y.; Lu, S. Non-Isothermal Crystallization Analysis of Recycled High-Density Polyethylene/Black Shale Composites. *J. Therm. Anal. Calorim.* **2023**, *148* (12), 5719–5732. https://doi.org/10.1007/s10973-023-12075-7.

(83) Coba-Daza, S.; Carmeli, E.; Otaegi, I.; Aranburu, N.; Guerrica-Echevarria, G.; Kahlen, S.; Cavallo, D.; Tranchida, D.; Müller, A. J. Effect of Compatibilizer Addition on the Surface Nucleation of Dispersed Polyethylene Droplets in a Self-Nucleated Polypropylene Matrix. *Polymer* **2022**, *263*, 125511. https://doi.org/10.1016/j.polymer.2022.125511.

(84) Jubinville, D.; Esmizadeh, E.; Saikrishnan, S.; Tzoganakis, C.; Mekonnen, T. A Comprehensive Review of Global Production and Recycling Methods of Polyolefin (PO) Based Products and Their Post-Recycling Applications. *Sustain. Mater. Technol.* **2020**, *25*, e00188.

(85) *2050 long-term strategy*. https://climate.ec.europa.eu/eu-action/climate-strategies-targets/2050-long-term-strategy_en (accessed 2023-11-14).

(86) *Circular economy action plan*. https://environment.ec.europa.eu/strategy/circular-economy-action-plan_en (accessed 2023-11-14).

(87) Mitchell, J. M. Carbon Dioxide and Future Climate, 1977.

(88) Supran, G.; Rahmstorf, S.; Oreskes, N. Assessing ExxonMobil's Global Warming Projections. *Science* **2023**, *379* (6628), eabk0063. https://doi.org/10.1126/science.abk0063.

(89) Karlsson, S. Recycled Polyolefins. Material Properties and Means for Quality Determination. In *Long Term Properties of Polyolefins*; Albertsson, A.-C., Ed.; Advances in Polymer Science; Springer: Berlin, Heidelberg, 2004; pp 201–230. https://doi.org/10.1007/b94173.

(90) Sari, P. S.; Sharika, T.; Bicy, K.; Thomas, S. Recycling of Polyolefin Materials. In *Polyolefin Compounds and Materials: Fundamentals and Industrial Applications*; Al-Ali AlMa'adeed, M., Krupa, I., Eds.; Springer International Publishing: Cham, 2016; pp 315–339. https://doi.org/10.1007/978-3-319-25982-6_13.

(91) Al-Salem, S. M.; Lettieri, P.; Baeyens, J. Recycling and Recovery Routes of Plastic Solid Waste (PSW): A Review. *Waste Manag.* **2009**, *29* (10), 2625–2643. https://doi.org/10.1016/j.wasman.2009.06.004.

(92) Constantinescu, D.; Boata, B.; Iordache, M.; Stelescu, M. D.; Georgescu, M.; Sönmez, M. Technological Considerations Regarding the Mechanical Recycling of Waste from Polyethylene and Polypropylene Packaging. In *Proceedings of the 9th International Conference on Advanced Materials and Systems*; INCDTP - Leather and Footwear Research Institute (ICPI), Bucharest, Romania, 2022; pp 401–406. https://doi.org/10.24264/icams-2022.IV.3.

(93) Ragaert, K.; Delva, L.; Van Geem, K. Mechanical and Chemical Recycling of Solid Plastic Waste. *Waste Manag.* **2017**, *69*, 24–58. https://doi.org/10.1016/j.wasman.2017.07.044.

(94) Schyns, Z. O. G.; Shaver, M. P. Mechanical Recycling of Packaging Plastics: A Review. *Macromol. Rapid Commun.* **2021**, *42* (3), 2000415. https://doi.org/10.1002/marc.202000415.

(95) Akhras, M. H.; Freudenthaler, P. J.; Straka, K.; Fischer, J. From Bottle Caps to Frisbee—A Case Study on Mechanical Recycling of Plastic Waste towards a Circular Economy. *Polymers* **2023**, *15* (12), 2685. https://doi.org/10.3390/polym15122685.

(96) Pinheiro, L. A.; Chinelatto, M. A.; Canevarolo, S. V. The Role of Chain Scission and Chain Branching in High Density Polyethylene during Thermo-Mechanical Degradation. *Polym. Degrad. Stab.* **2004**, *86* (3), 445–453. https://doi.org/10.1016/j.polymdegradstab.2004.05.016.

(97) Ammala, A.; Bateman, S.; Dean, K.; Petinakis, E.; Sangwan, P.; Wong, S.; Yuan, Q.; Yu, L.; Patrick, C.; Leong, K. H. An Overview of Degradable and Biodegradable Polyolefins.

Prog. Polym. Sci. **2011**, *36* (8), 1015–1049. https://doi.org/10.1016/j.progpolymsci.2010.12.002.

(98) FBR Sustainable Chemistry & Technology; Alvarado Chacon, F.; Brouwer, M. T.; Thoden van Velzen, E. U.; Smeding, I. W. *A First Assessment of the Impact Ofimpurities in PP and PE Recycled Plastics*; Wageningen Food & Biobased Research: Wageningen, 2020. https://doi.org/10.18174/518299.

(99) Layman, J. M.; Gunnerson, M.; Bond, E. B.; NELTNER, A. E.; HOSMER, J. E. Articles of Reclaimed Polypropylene Compositions. WO2017003802A1, January 5, 2017. https://patents.google.com/patent/WO2017003802A1/en (accessed 2023-11-14).

(100) Layman, J. M.; Collias, D. I.; Schonemann, H.; Williams, K. Method For Purifying Reclaimed Polypropylene. US20180171094A1, June 21, 2018. https://patents.google.com/patent/US20180171094A1/en (accessed 2023-11-14).

(101) Huth-Fehre, Th.; Feldhoff, R.; Kantimm, Th.; Quick, L.; Winter, F.; Cammann, K.; van den Broek, W.; Wienke, D.; Melssen, W.; Buydens, L. NIR - Remote Sensing and Artificial Neural Networks for Rapid Identification of Post Consumer Plastics. *J. Mol. Struct.* **1995**, *348*, 143–146. https://doi.org/10.1016/0022-2860(95)08609-Y.

(102) *Artificial Intelligence poised to transform waste management & recycling industry*. https://www.wasterecyclingmea.com/top-stories/artificial-intelligence-poised-to-transform-waste-management-recycling-industry (accessed 2023-11-14).

(103) Rani, M.; Marchesi, C.; Federici, S.; Rovelli, G.; Alessandri, I.; Vassalini, I.; Ducoli, S.; Borgese, L.; Zacco, A.; Bilo, F.; Bontempi, E.; Depero, L. E. Miniaturized Near-Infrared (MicroNIR) Spectrometer in Plastic Waste Sorting. *Materials* **2019**, *12* (17), 2740. https://doi.org/10.3390/ma12172740.

(104) Voulvoulis, N.; Kirkman, R.; Giakoumis, T.; Metivier, P.; Kyle, C.; Vicky, M. *Veolia Plastic White Paper*; 2020. https://doi.org/10.13140/RG.2.2.12793.70241.

(105) *Plastic bags versus paper bags | letstalkplastics*. http://www.letstalkplastics.com/facts/plastic-bags-versus-paper-bags (accessed 2022-01-26).

(106) Ahamed, A.; Vallam, P.; Iyer, N. S.; Veksha, A.; Bobacka, J.; Lisak, G. Life Cycle Assessment of Plastic Grocery Bags and Their Alternatives in Cities with Confined Waste Management Structure: A Singapore Case Study. *J. Clean. Prod.* **2021**, *278*, 123956. https://doi.org/10.1016/j.jclepro.2020.123956.

(107) *FAQs on Plastics*. Our World in Data. https://ourworldindata.org/faq-on-plastics (accessed 2023-11-14).

(108) Devasahayam, S.; Bhaskar Raju, G.; Mustansar Hussain, C. Utilization and Recycling of End of Life Plastics for Sustainable and Clean Industrial Processes Including the Iron and Steel Industry. *Mater. Sci. Energy Technol.* **2019**, *2* (3), 634–646. https://doi.org/10.1016/j.mset.2019.08.002.

(109) *Advanced recycling: Opportunities for growth | McKinsey*. https://www.mckinsey.com/industries/chemicals/our-insights/advanced-recycling-opportunities-for-growth (accessed 2023-11-16).

(110) Vollmer, I.; Jenks, M. J. F.; Roelands, M. C. P.; White, R. J.; Harmelen, T.; Wild, P.; Laan, G. P.; Meirer, F.; Keurentjes, J. T. F.; Weckhuysen, B. M. Beyond Mechanical Recycling: Giving New Life to Plastic Waste. *Angew. Chem. Int. Ed.* **2020**, *59* (36), 15402–15423. https://doi.org/10.1002/anie.201915651.

(111) Jubinville, D.; Esmizadeh, E.; Saikrishnan, S.; Tzoganakis, C.; Mekonnen, T. A Comprehensive Review of Global Production and Recycling Methods of Polyolefin (PO) Based Products and Their Post-Recycling Applications. *Sustain. Mater. Technol.* **2020**, *25*, e00188. https://doi.org/10.1016/j.susmat.2020.e00188.

(112) *Advanced mechanical recycling: Enabling true circularity for plastics*. https://circular-economy.tomra.com/resources/amr-whitepaper-guide (accessed 2023-11-16).

(113) Faraca, G.; Astrup, T. Plastic Waste from Recycling Centres: Characterisation and Evaluation of Plastic Recyclability. *Waste Manag.* **2019**, *95*, 388–398. https://doi.org/10.1016/j.wasman.2019.06.038.

(114) Aschenbrenner, D.; Gros, J.; Fangerow, N.; Werner, T.; Colloseus, C.; Taha, I. Recyclebot – Using Robots for Sustainable Plastic Recycling. *Procedia CIRP* **2023**, *116*, 275–280. https://doi.org/10.1016/j.procir.2023.02.047.

(115) *Top 5 Challenges in Plastics Recycling – Seastainable*. https://www.seastainable.co/blogs/seastainable-blog/top-5-challenges-in-plastics-recycling (accessed 2023-11-16).

(116) *Post-shredder for waste - the FineCut series from WEIMA*. WEIMA Maschinenbau. https://weima.com/en/shredders/finecut/ (accessed 2024-02-09).

(117) Castaño, J. D.; Hauge, D. A.; Haag, A.; Severtson, S. J.; Zhang, J. Fungal Biodegradation of a Hybrid Adhesive Polymer Containing High-Biomass Content. *J. Polym. Environ.* **2023**, *31* (12), 5234–5244. https://doi.org/10.1007/s10924-023-02938-3.

(118) Stenvall, E.; Boldizar, A. Mechanical and Thermal Characterization of Melt-Filtered, Blended and Reprocessed Post-Consumer WEEE Thermoplastics. *Recycling* **2016**, *1* (1), 89–100. https://doi.org/10.3390/recycling1010089.

(119) GmbH, E. G. *EREMA's continuous high-performance filter with 50 percent more screen surface area | EREMA Group*. EREMA Group GmbH. https://www.erema-group.com/en/erema-s-continuous-high-performance-filter-with-50-percent-more-screen-surface-area (accessed 2023-12-14).

(120) Iyer, K. A.; Zhang, L.; Torkelson, J. M. Direct Use of Natural Antioxidant-Rich Agro-Wastes as Thermal Stabilizer for Polymer: Processing and Recycling. *ACS Sustain. Chem. Eng.* **2016**, *4* (3), 881–889. https://doi.org/10.1021/acssuschemeng.5b00945.

(121) *Recycled fishing nets*. https://www.bmwgroup.com/en/news/general/2022/recycled-plastics.html (accessed 2023-11-29).

(122) *Plastic Packaging Recycling and Clean Energy Manufacturing | Advanced Manufacturing Research | NREL*. https://www.nrel.gov/manufacturing/remade.html (accessed 2023-12-15).

(123) Hamaya, S. The Present Situation and Outlook on Plastic Waste Recycling in Japan. *Conserv. Recycl.* **1981**, *4* (3), 185–192. https://doi.org/10.1016/0361-3658(81)90023-0.

(124) Wilson, A.; Piepkorn, M. *Green Building Products, 3rd Edition: The GreenSpec¨ Guide to Residential Building Materials--3rd Edition*; New Society Publishers, 2008.

(125) Morgan, S. *Waste, Recycling and Reuse*; Evans Brothers, 2009.

(126) Zhu, Y.; Heo, T. W.; Rodriguez, J. N.; Weber, P. K.; Shi, R.; Baer, B. J.; Morgado, F. F.; Antonov, S.; Kweon, K. E.; Watkins, E. B. Hydriding of Titanium: Recent Trends and Perspectives in Advanced Characterization and Multiscale Modeling. *Curr. Opin. Solid State Mater. Sci.* **2022**, *26* (6), 101020.

(127) Nwabunma, D.; Kyu, T. *Polyolefin Blends*; John Wiley & Sons, 2008.

(128) Saikrishnan, S. Investigation of Thermo-Mechanical Degradation of Polypropylene-Low Density Polyethylene Blends Exposed to Simulated Recycling. Master's Thesis, University of Waterloo, 2020. https://uwspace.uwaterloo.ca/handle/10012/16168 (accessed 2023-11-17).

(129) Carmeli, E.; Fenni, S. E.; Caputo, M. R.; Müller, A. J.; Tranchida, D.; Cavallo, D. Surface Nucleation of Dispersed Polyethylene Droplets in Immiscible Blends Revealed by Polypropylene Matrix Self-Nucleation. *Macromolecules* **2021**, *54* (19), 9100–9112. https://doi.org/10.1021/acs.macromol.1c01430.

(130) Jasinska-Walc, L.; Bouyahyi, M.; Duchateau, R. Potential of Functionalized Polyolefins in a Sustainable Polymer Economy: Synthetic Strategies and Applications. *Acc. Chem. Res.* **2022**, *55* (15), 1985–1996. https://doi.org/10.1021/acs.accounts.2c00195.

(131) Colbeaux, A.; Fenouillot, F.; Gérard, J.-F.; Taha, M.; Wautier, H. Compatibilization of a Polyolefin Blend through Covalent and Ionic Coupling of Grafted Polypropylene and Polyethylene. I. Rheological, Thermal, and Mechanical Properties. *J. Appl. Polym. Sci.* **2005**, *95* (2), 312–320. https://doi.org/10.1002/app.21226.

(132) Graziano, A.; Jaffer, S.; Sain, M. Review on Modification Strategies of Polyethylene/Polypropylene Immiscible Thermoplastic Polymer Blends for Enhancing Their Mechanical Behavior. *J. Elastomers Plast.* **2019**, *51* (4), 291–336. https://doi.org/10.1177/0095244318783806.

(133) Delgado, C.; Barruetabeña, L.; Salas, O.; Wolf, O. Assessment of the Environmental Advantages and Drawbacks of Existing and Emerging Polymers Recovery Processes. *Inst. Prospect. Technol. Stud. Jt. Res. Cent. Eur. Comm.* **2007**.

(134) Pearson, J. R. *Mechanics of Polymer Processing*; Springer Science & Business Media, 1985.

(135) Cogswell, F. N. *Thermoplastic Aromatic Polymer Composites: A Study of the Structure, Processing and Properties of Carbon Fibre Reinforced Polyetheretherketone and Related Materials*; Elsevier, 2013.

(136) Monrabal, B. Polyolefin Characterization: Recent Advances in Separation Techniques. In *Polyolefins: 50 years after Ziegler and Natta I*; Kaminsky, W., Ed.; Advances in Polymer Science; Springer Berlin Heidelberg: Berlin, Heidelberg, 2013; Vol. 257, pp 203–251. https://doi.org/10.1007/12_2013_216.

(137) Evans, A. M.; Strauss, M. J.; Corcos, A. R.; Hirani, Z.; Ji, W.; Hamachi, L. S.; Aguilar-Enriquez, X.; Chavez, A. D.; Smith, B. J.; Dichtel, W. R. Two-Dimensional Polymers and Polymerizations. *Chem. Rev.* **2022**, *122* (1), 442–564. https://doi.org/10.1021/acs.chemrev.0c01184.

(138) Di Leo, P. A Nuclear Magnetic Resonance (NMR) and Fourier-Transform Infrared (FTIR) Study of Glycine Speciation on a Cd-Rich Montmorillonite. *Clays Clay Miner.* **2000**, *48* (5), 495–502. https://doi.org/10.1346/CCMN.2000.0480501.

(139) Workman, J. J.; Mobley, P. R.; Kowalski, B. R.; Bro, R. Review of Chemometrics Applied to Spectroscopy: 1985-95, Part I. *Appl. Spectrosc. Rev.* **1996**, *31* (1–2), 73–124. https://doi.org/10.1080/05704929608000565.

(140) Amamoto, Y. Data-Driven Approaches for Structure-Property Relationships in Polymer Science for Prediction and Understanding. *Polym. J.* **2022**, *54* (8), 957–967.
(141) Tian, Z.-Y.; Mbayachi, V. B.; Dai, W.-K.; Khalil, M.; Ayejoto, D. A. Thermal Analysis Methods. In *Advanced Diagnostics in Combustion Science*; Tian, Z.-Y., Ed.; Springer Nature Singapore: Singapore, 2023; pp 71–109. https://doi.org/10.1007/978-981-99-0546-1_3.
(142) Razumas, V.; Larsson, K.; Miezis, Y.; Nylander, T. A Cubic Monoolein−Cytochrome *c* −Water Phase: X-Ray Diffraction, FT-IR, Differential Scanning Calorimetric, and Electrochemical Studies. *J. Phys. Chem.* **1996**, *100* (28), 11766–11774. https://doi.org/10.1021/jp952613h.
(143) Schick, C. Differential Scanning Calorimetry (DSC) of Semicrystalline Polymers. *Anal. Bioanal. Chem.* **2009**, *395* (6), 1589–1611. https://doi.org/10.1007/s00216-009-3169-y.
(144) Müller, A. J.; Michell, R. M. Differential Scanning Calorimetry of Polymers. In *Polymer Morphology*; Guo, Q., Ed.; Wiley, 2016; pp 72–99. https://doi.org/10.1002/9781118892756.ch5.
(145) Ramesh, M.; Rajeshkumar, L.; Sasikala, G.; Balaji, D.; Saravanakumar, A.; Bhuvaneswari, V.; Bhoopathi, R. A Critical Review on Wood-Based Polymer Composites: Processing, Properties, and Prospects. *Polymers* **2022**, *14* (3), 589.
(146) Chakravarty, J. Characterization of Polyolefins by Temperature Rising Elution Fractionation (Tref). **1993**.
(147) Mushtaq, M. Y.; Choi, Y. H.; Verpoorte, R.; Wilson, E. G. Extraction for Metabolomics: Access to The Metabolome. *Phytochem. Anal.* **2014**, *25* (4), 291–306. https://doi.org/10.1002/pca.2505.
(148) Pérez-Camargo, R. A.; Cavallo, D.; Müller, A. J. Recent Applications of the Successive Self-Nucleation and Annealing Thermal Fractionation Technique. *Front. Soft Matter* **2022**, *2*, 1003500.
(149) Tong, R.-A.; Chen, L.; Fan, B.; Shao, G.; Liu, R.; Wang, C.-A. Solvent-Free Process for Blended PVDF-HFP/PEO and LLZTO Composite Solid Electrolytes with Enhanced Mechanical and Electrochemical Properties for Lithium Metal Batteries. *ACS Appl. Energy Mater.* **2021**, *4* (10), 11802–11812. https://doi.org/10.1021/acsaem.1c02566.
(150) Müller, A. J.; Michell, R. M.; Pérez, R. A.; Lorenzo, A. T. Successive Self-Nucleation and Annealing (SSA): Correct Design of Thermal Protocol and Applications. *Eur. Polym. J.* **2015**, *65*, 132–154.

(151) Ringsdorf, H.; Schlarb, B.; Venzmer, J. Molecular Architecture and Function of Polymeric Oriented Systems: Models for the Study of Organization, Surface Recognition, and Dynamics of Biomembranes. *Angew. Chem. Int. Ed. Engl.* **1988**, *27* (1), 113–158. https://doi.org/10.1002/anie.198801131.

(152) Striegel, A.; Yau, W. W.; Kirkland, J. J.; Bly, D. D. *Modern Size-Exclusion Liquid Chromatography: Practice of Gel Permeation and Gel Filtration Chromatography*; John Wiley & Sons, 2009.

(153) *Differential scanning calorimetry (DSC) of semicrystalline polymers | Analytical and Bioanalytical Chemistry*. https://link.springer.com/article/10.1007/s00216-009-3169-y (accessed 2023-11-16).

(154) Drzeżdżon, J.; Jacewicz, D.; Sielicka, A.; Chmurzyński, L. Characterization of Polymers Based on Differential Scanning Calorimetry Based Techniques. *TrAC Trends Anal. Chem.* **2019**, *110*, 51–56. https://doi.org/10.1016/j.trac.2018.10.037.

(155) Wunderlich, B. Glass Transition as a Key to Identifying Solid Phases. *J. Appl. Polym. Sci.* **2007**, *105* (1), 49–59. https://doi.org/10.1002/app.26110.

(156) Scoppio, A.; Cavallo, D.; Müller, A. J.; Tranchida, D. Temperature Modulated DSC for Composition Analysis of Recycled Polyolefin Blends. *Polym. Test.* **2022**, *113*, 107656.

(157) Zheng, Q.; Zhang, Y.; Montazerian, M.; Gulbiten, O.; Mauro, J. C.; Zanotto, E. D.; Yue, Y. Understanding Glass through Differential Scanning Calorimetry. *Chem. Rev.* **2019**, *119* (13), 7848–7939. https://doi.org/10.1021/acs.chemrev.8b00510.

(158) Riga, A.; Collins, R. Differential Scanning Calorimetry and Differential Thermal Analysis. In *Encyclopedia of Analytical Chemistry*; Meyers, R. A., Ed.; Wiley, 2000. https://doi.org/10.1002/9780470027318.a6602.

(159) Gill, P. S.; Sauerbrunn, S. R.; Reading, M. Modulated Differential Scanning Calorimetry. **1993**.

(160) Wunderlich, B. The Application of MTDSC to Polymer Melting. In *Modulated Temperature Differential Scanning Calorimetry*; Reading, M., Hourston, D. J., Eds.; Hot Topics in Thermal Analysis and Calorimetry; Springer Netherlands, 2006; Vol. 6, pp 217–319. https://doi.org/10.1007/1-4020-3750-3_4.

(161) Lacey, A. A.; Price, D. M.; Reading, M. Theory and Practice of Modulated Temperature Differential Scanning Calorimetry. In *Modulated Temperature Differential Scanning Calorimetry*; Reading, M., Hourston, D. J., Eds.; Hot Topics in Thermal Analysis and

Calorimetry; Springer Netherlands, 2006; Vol. 6, pp 1–81. https://doi.org/10.1007/1-4020-3750-3_1.

(162) Paffenbarger Jr, R. S.; Blair, S. N.; Lee, I.-M. A History of Physical Activity, Cardiovascular Health and Longevity: The Scientific Contributions of Jeremy N Morris, DSc, DPH, FRCP. *Int. J. Epidemiol.* **2001**, *30* (5), 1184–1192.

(163) Li, D.; Zhou, L.; Wang, X.; He, L.; Yang, X. Effect of Crystallinity of Polyethylene with Different Densities on Breakdown Strength and Conductance Property. *Materials* **2019**, *12* (11), 1746. https://doi.org/10.3390/ma12111746.

(164) Dorigato, A. Recycling of Polymer Blends. *Adv. Ind. Eng. Polym. Res.* **2021**, *4* (2), 53–69.

(165) Blundell, D. J.; Keller, A.; Kovacs, A. J. A New Self-Nucleation Phenomenon and Its Application to the Growing of Polymer Crystals from Solution. *J. Polym. Sci. [B]* **1966**, *4* (7), 481–486. https://doi.org/10.1002/pol.1966.110040709.

(166) Fillon, B.; Wittmann, J. C.; Lotz, B.; Thierry, A. Self-Nucleation and Recrystallization of Isotactic Polypropylene (α Phase) Investigated by Differential Scanning Calorimetry. *J. Polym. Sci. Part B Polym. Phys.* **1993**, *31* (10), 1383–1393. https://doi.org/10.1002/polb.1993.090311013.

(167) Müller, A. J.; Hernández, Z. H.; Arnal, M. L.; Sánchez, J. J. Successive Self-Nucleation/Annealing (SSA): A Novel Technique to Study Molecular Segregation during Crystallization. *Polym. Bull.* **1997**, *39* (4), 465–472. https://doi.org/10.1007/s002890050174.

(168) Gray, A.; Casey, K. J. Polym. Sci., Part B. *Polym Lett* **1964**, *2*, 381.

(169) Varga, J.; Tóth, F.; Hummel, D. Annealing of the β-Modification of Polypropylene. In *Makromolekulare Chemie. Macromolecular Symposia*; Wiley Online Library, 1986; Vol. 5, pp 213–223.

(170) Zhang, M.; Lynch, D. T.; Wanke, S. E. Characterization of Commercial Linear Low-Density Polyethylene by TREF-DSC and TREF-SEC Cross-Fractionation. *J. Appl. Polym. Sci.* **2000**, *75* (7), 960–967.

(171) Paolini, Y.; Ronca, G.; Luis Feijoo, J.; Da Silva, E.; Ramírez, J.; Müller, A. J. Application of the SSA Calorimetric Technique to Characterise an XLPE Insulator Aged under Multiple Stresses. *Macromol. Chem. Phys.* **2001**, *202* (9), 1539–1547.

(172) Zhang, M.; Wanke, S. E. Quantitative Determination of Short-Chain Branching Content and Distribution in Commercial Polyethylenes by Thermally Fractionated Differential

Scanning Calorimetry. *Polym. Eng. Sci.* **2003**, *43* (12), 1878–1888. https://doi.org/10.1002/pen.10159.

(173) Arnal, M.; Sanchez, J.; Müller, A. Miscibility of Linear and Branched Polyethylene Blends by Thermal Fractionation: Use of the Successive Self-Nucleation and Annealing (SSA) Technique. *Polymer* **2001**, *42* (16), 6877–6890.

(174) Arnal, M. L.; Cañizales, E.; Müller, A. J. Thermal and Morphological Evaluation of Very Low Density Polyethylene/High Density Polyethylene Blends. *Polym. Eng. Sci.* **2002**, *42* (10), 2048–2063.

(175) Virkkunen, V.; Laari, P.; Pitkänen, P.; Sundholm, F. Tacticity Distribution of Isotactic Polypropylene Prepared with Heterogeneous Ziegler–Natta Catalyst. 2. Application and Analysis of SSA Data for Polypropylene. *Polymer* **2004**, *45* (14), 4623–4631. https://doi.org/10.1016/j.polymer.2004.05.027.

(176) Kang, J.; Yang, F.; Wu, T.; Li, H.; Cao, Y.; Xiang, M. Polymerization Control and Fast Characterization of the Stereo-Defect Distribution of Heterogeneous Ziegler–Natta Isotactic Polypropylene. *Eur. Polym. J.* **2012**, *48* (2), 425–434.

(177) Chang, H.; Zhang, Y.; Ren, S.; Dang, X.; Zhang, L.; Li, H.; Hu, Y. Study on the Sequence Length Distribution of Polypropylene by the Successive Self-Nucleation and Annealing (SSA) Calorimetric Technique. *Polym Chem* **2012**, *3* (10), 2909–2919. https://doi.org/10.1039/C2PY20452E.

(178) Alamo, R. G.; Mandelkern, L. Thermodynamic and Structural Properties of Ethylene Copolymers. *Macromolecules* **1989**, *22* (3), 1273–1277. https://doi.org/10.1021/ma00193a045.

(179) Alamo, R. G.; Viers, B. D.; Mandelkern, L. Phase Structure of Random Ethylene Copolymers: A Study of Counit Content and Molecular Weight as Independent Variables. *Macromolecules* **1993**, *26* (21), 5740–5747. https://doi.org/10.1021/ma00073a031.

(180) Keating, M.; Lee, I.-H.; Wong, C. S. Thermal Fractionation of Ethylene Polymers in Packaging Applications. *Thermochim. Acta* **1996**, *284* (1), 47–56. https://doi.org/10.1016/0040-6031(96)02891-2.

(181) Lorenzo, A. T.; Arnal, M. L.; Müller, A. J.; Boschetti de Fierro, A.; Abetz, V. High Speed SSA Thermal Fractionation and Limitations to the Determination of Lamellar Sizes and Their Distributions. *Macromol. Chem. Phys.* **2006**, *207* (1), 39–49. https://doi.org/10.1002/macp.200500437.

(182) Pijpers, T. F. J.; Mathot, V. B. F.; Goderis, B.; Scherrenberg, R. L.; van der Vegte, E. W. High-Speed Calorimetry for the Study of the Kinetics of (De)Vitrification, Crystallization, and Melting of Macromolecules †. *Macromolecules* **2002**, *35* (9), 3601–3613. https://doi.org/10.1021/ma011122u.

(183) Varga, J.; Menczel, J.; Solti, A. Memory Effect of Low-Density Polyethylene Crystallized in a Stepwise Manner. *J. Therm. Anal.* **1976**, *10* (3), 433–440. https://doi.org/10.1007/BF01909895.

(184) Varga, J.; Menczel, J.; Solti, A. The Melting of High-Pressure Polyethylene Subjected to Stepwise Heat Treatment. *J. Therm. Anal.* **1979**, *17* (2), 333–342. https://doi.org/10.1007/BF01914024.

(185) Góra, M.; Tranchida, D.; Albrecht, A.; Müller, A. J.; Cavallo, D. Fast Successive Self-Nucleation and Annealing (SSA) Thermal Fractionation Protocol for the Characterization of Polyolefin Blends from Mechanical Recycling. *J. Polym. Sci. n/a* (n/a). https://doi.org/10.1002/pol.20220104.

(186) Juan, R.; Paredes, B.; García-Muñoz, R. A.; Domínguez, C. Quantification of PP Contamination in Recycled PE by TREF Analysis for Improved the Quality and Circularity of Plastics. *Polym. Test.* **2021**, *100*, 107273.

(187) Papkov, D.; Delpouve, N.; Delbreilh, L.; Araujo, S.; Stockdale, T.; Mamedov, S.; Maleckis, K.; Zou, Y.; Andalib, M. N.; Dargent, E.; Dravid, V. P.; Holt, M. V.; Pellerin, C.; Dzenis, Y. A. Quantifying Polymer Chain Orientation in Strong and Tough Nanofibers with Low Crystallinity: Toward Next Generation Nanostructured Superfibers. *ACS Nano* **2019**, *13* (5), 4893–4927. https://doi.org/10.1021/acsnano.8b08725.

(188) Malik, M. I.; Pasch, H. Characterization of Polyolefins. In *Molecular Characterization of Polymers*; Elsevier, 2021; pp 173–222.

(189) Fredrickson, G. H.; Liu, A. J.; Bates, F. S. Entropic Corrections to the Flory-Huggins Theory of Polymer Blends: Architectural and Conformational Effects. *Macromolecules* **1994**, *27* (9), 2503–2511. https://doi.org/10.1021/ma00087a019.

(190) Anantawaraskul, S.; Soares, J. B. P.; Wood-Adams, P. M. Fractionation of Semicrystalline Polymers by Crystallization Analysis Fractionationand Temperature Rising Elution Fractionation. In *Polymer Analysis Polymer Theory*; Abe, A., Dušek, K., Kobayashi, S., Eds.; Advances in Polymer Science; Springer Berlin Heidelberg: Berlin, Heidelberg, 2005; Vol. 182, pp 1–54. https://doi.org/10.1007/b135559.

(191) Favre, E.; Nguyen, Q. T.; Clement, R.; Neel, J. Application of Flory-Huggins Theory to Ternary Polymer-Solvents Equilibria: A Case Study. *Eur. Polym. J.* **1996**, *32* (3), 303–309.
(192) van Leuken, S. H.; van Benthem, R. A.; Tuinier, R.; Vis, M. Theoretically Predicting the Solubility of Polydisperse Polymers Using Flory–Huggins Theory. *J. Phys. Mater.* **2023**, *7* (1), 015005.
(193) Flory, P. J. *Principles of Polymer Chemistry*; Cornell university press, 1953.
(194) Wild, L.; Glöckner, G. Temperature Rising Elution Fractionation. In *Separation Techniques Thermodynamics Liquid Crystal Polymers*; Springer Berlin Heidelberg: Berlin, Heidelberg, 1991; pp 1–47.
(195) Wild, L.; Ryle, T. R.; Knobeloch, D. C.; Peat, I. R. Determination of Branching Distributions in Polyethylene and Ethylene Copolymers. *J. Polym. Sci. Polym. Phys. Ed.* **1982**, *20* (3), 441–455. https://doi.org/10.1002/pol.1982.180200307.
(196) Pochivalov, K. V.; Basko, A. V.; Lebedeva, T. N.; Ilyasova, A. N.; Yurov, M. Y.; Golovanov, R. Y.; Artemov, V. V.; Volkov, V. V.; Ezhov, A. A.; Volkov, A. V. Thermally Induced Phase Separation in Semicrystalline Polymer Solutions: How Does the Porous Structure Actually Arise? *Mater. Today Commun.* **2021**, *28*, 102558.
(197) Liu, W.; Wang, W.-J.; Fan, H.; Yu, L.; Li, B.-G.; Zhu, S. Structure Analysis of Ethylene/1-Octene Copolymers Synthesized from Living Coordination Polymerization. *Eur. Polym. J.* **2014**, *54*, 160–171. https://doi.org/10.1016/j.eurpolymj.2014.03.010.
(198) Pasch, H.; Malik, M. I.; Macko, T. Recent Advances in High-Temperature Fractionation of Polyolefins. In *Polymer Composites – Polyolefin Fractionation – Polymeric Peptidomimetics – Collagens*; Abe, A., Kausch, H.-H., Möller, M., Pasch, H., Eds.; Advances in Polymer Science; Springer Berlin Heidelberg: Berlin, Heidelberg, 2012; Vol. 251, pp 77–140. https://doi.org/10.1007/12_2012_167.
(199) Pasch, H.; Malik, M. I. *Advanced Separation Techniques for Polyolefins*; Springer Laboratory; Springer International Publishing: Cham, 2014. https://doi.org/10.1007/978-3-319-08632-3.
(200) Koenig, J. L. Chapter 3 - Experimental IR Spectroscopy of Polymers. In *Spectroscopy of Polymers (Second Edition)*; Koenig, J. L., Ed.; Elsevier Science: New York, 1999; pp 77–145. https://doi.org/10.1016/B978-044410031-3/50003-7.
(201) Aboagye, E. A.; Chea, J. D.; Yenkie, K. M. Systems Level Roadmap for Solvent Recovery and Reuse in Industries. *Iscience* **2021**, *24* (10).

(202) Aust, N.; Gahleitner, M.; Reichelt, K.; Raninger, B. Optimization of Run Parameters of Temperature-Rising Elution Fractionation with the Aid of a Factorial Design Experiment. *Polym. Test.* **2006**, *25* (7), 896–903. https://doi.org/10.1016/j.polymertesting.2006.05.008.

(203) Boborodea, A.; Mirabella, F. M. Elution Temperatures of Polyethylene Copolymers in Temperature Rising Elution Fractionation (TREF): Comparison in Xylene and Trichlorobenzene Diluents. *Int. J. Polym. Anal. Charact.* **2014**, *19* (5), 468–473. https://doi.org/10.1080/1023666X.2014.920661.

(204) Meunier, D. M.; Wade, J. H.; Janco, M.; Cong, R.; Gao, W.; Li, Y.; Mekap, D.; Wang, G. Recent Advances in Separation-Based Techniques for Synthetic Polymer Characterization. *Anal. Chem.* **2021**, *93* (1), 273–294. https://doi.org/10.1021/acs.analchem.0c04352.

(205) Cong, R.; Parrott, A.; Hollis, C.; Cheatham, M.; Hill, T.; Bailey, K.; Zhou, Z.; Bautista, J.; Balding, P.; Fan, J. Quantification of Chemical Composition Distribution of Polyolefin Materials for Improved Accuracy and Speed. *Macromolecules* **2023**, *56* (4), 1492–1502. https://doi.org/10.1021/acs.macromol.3c00020.

(206) Yu, Y.; Hildebrand, M. Development of an Integrated On-Line 2D Analytical TREF-High Throughput SEC Technique for Polyolefins Characterization. *Macromol. Symp.* **2020**, *390* (1), 1900015. https://doi.org/10.1002/masy.201900015.

(207) Chitta, R.; Steenbakkers, R.; Tacx, J.; Meppelder, A. Selective Experimental Parameters for Preparative TREF of Propylene-ethylene Random Copolymers: Limiting Undercooling of PP. *J. Appl. Polym. Sci.* **2021**, *138* (45), 51333. https://doi.org/10.1002/app.51333.

(208) Pasch, H.; Malik, M. I. Crystallization-Based Fractionation Techniques. In *Advanced Separation Techniques for Polyolefins*; Springer Laboratory; Springer International Publishing: Cham, 2014; pp 11–73. https://doi.org/10.1007/978-3-319-08632-3_2.

(209) Pasch, H.; Ndiripo, A.; Bungu, P. S. E. Multidimensional Analytical Protocols for the Fractionation and Analysis of Complex Polyolefins. *J. Polym. Sci.* **2022**, *60* (7), 1059–1078. https://doi.org/10.1002/pol.20210236.

(210) Deshmukh, S.; Brüll, R.; Macko, T.; Arndt, J.-H.; Bernardo, R.; Niessen, S. Characterization of Ethylene-Propylene-Diene Terpolymers Using High-Temperature Size Exclusion Chromatography Coupled with an Ultraviolet Detector. *Polymer* **2022**, *242*, 124585.

(211) Qian, C.; Zhao, Y.; Wang, Z.; Liu, L.; Wang, D. Probing the Difference of Crystalline Modifications and Structural Disorder of Isotactic Polypropylene via High-Resolution FTIR Spectroscopy. *Polymer* **2021**, *224*, 123722.

(212) Pasch, H.; Ndiripo, A.; Bungu, P. S. E. Multidimensional Analytical Protocols for the Fractionation and Analysis of Complex Polyolefins. *J. Polym. Sci.* **2022**, *60* (7), 1059–1078. https://doi.org/10.1002/pol.20210236.

(213) Pastor-García, M. T.; Suárez, I.; Expósito, M. T.; Coto, B.; García-Muñoz, R. A. Engineered PP Impact Copolymers in a Single Reactor as Efficient Method for Determining Their Structure and Properties. *Eur. Polym. J.* **2021**, *157*, 110642.

(214) Pérez-Camargo, R. A.; Cavallo, D.; Müller, A. J. Recent Applications of the Successive Self-Nucleation and Annealing Thermal Fractionation Technique. *Front. Soft Matter* **2022**, *2*, 1003500. https://doi.org/10.3389/frsfm.2022.1003500.

(215) Malpass, D. B.; Band, E. *Introduction to Industrial Polypropylene: Properties, Catalysts Processes*; John Wiley & Sons, 2012.

(216) Sigwinta, M. Ethylene-1-Octene Elastomers: Molecular Structure Characterization by Advanced Analytical Methods. PhD Thesis, Cape Peninsula University of Technology, 2019. https://etd.cput.ac.za/handle/20.500.11838/2993 (accessed 2023-11-30).

(217) Palali, S. N. Polymer Processing in a Circular Plastic Economy. PhD Thesis, The University of Manchester (United Kingdom), 2022. https://search.proquest.com/openview/26ead106d97a6a44e67967cb8d0efdcf/1?pq-origsite=gscholar&cbl=2026366&diss=y (accessed 2023-11-30).

(218) Wessels, A. Structure Property Relationships in Bimodal HDPEs. PhD Thesis, Stellenbosch: Stellenbosch University, 2021. https://scholar.sun.ac.za/handle/10019.1/123903 (accessed 2023-11-30).

(219) Striegel, A.; Yau, W. W.; Kirkland, J. J.; Bly, D. D. *Modern Size-Exclusion Liquid Chromatography: Practice of Gel Permeation and Gel Filtration Chromatography*; John Wiley & Sons, 2009.

(220) Moore, J. C. Gel Permeation Chromatography. I. A New Method for Molecular Weight Distribution of High Polymers. *J. Polym. Sci. A* **1964**, *2* (2), 835–843. https://doi.org/10.1002/pol.1964.100020220.

(221) Moore, J. C. Gel Permeation Chromatography: Its Inception. *J. Polym. Sci. Part C Polym. Symp.* **1968**, *21* (1), 1–3. https://doi.org/10.1002/polc.5070210103.

(222) Barth, H. The Early Development of Size Exclusion Chromatography: A Historical Perspective. *LCGC N. Am.* **2013**, *31*, 550–558.

(223) Striegel, A. M. Size-Exclusion Chromatography. In *Liquid chromatography*; Elsevier, 2023; pp 509–537.

(224) Held, D.; Kilz, P. Size-Exclusion Chromatography as a Useful Tool for the Assessment of Polymer Quality and Determination of Macromolecular Properties. *Chem. Teach. Int.* **2021**, *3* (2), 77–103. https://doi.org/10.1515/cti-2020-0024.

(225) Wang, H.; Liu, Y.; Li, J. Designer Metal–Organic Frameworks for Size-Exclusion-Based Hydrocarbon Separations: Progress and Challenges. *Adv. Mater.* **2020**, *32* (44), 2002603. https://doi.org/10.1002/adma.202002603.

(226) Lubomirsky, E.; Khodabandeh, A.; Preis, J.; Susewind, M.; Hofe, T.; Hilder, E. F.; Arrua, R. D. Polymeric Stationary Phases for Size Exclusion Chromatography: A Review. *Anal. Chim. Acta* **2021**, *1151*, 338244.

(227) Broeckhoven, K.; Desmet, G. Advances and Innovations in Liquid Chromatography Stationary Phase Supports. *Anal. Chem.* **2021**, *93* (1), 257–272. https://doi.org/10.1021/acs.analchem.0c04466.

(228) Sun, Z.; Ma, Y.; Ponge, D.; Zaefferer, S.; Jägle, E. A.; Gault, B.; Rollett, A. D.; Raabe, D. Thermodynamics-Guided Alloy and Process Design for Additive Manufacturing. *Nat. Commun.* **2022**, *13* (1), 4361.

(229) Hecht, E. S.; Obiorah, E. C.; Liu, X.; Morrison, L.; Shion, H.; Lauber, M. Microflow Size Exclusion Chromatography to Preserve Micromolar Affinity Complexes and Achieve Subunit Separations for Native State Mass Spectrometry. *J. Chromatogr. A* **2022**, *1685*, 463638.

(230) Hareland, C. A.; Guillemot, G.; Gandin, C.-A.; Voorhees, P. W. The Thermodynamics of Non-Equilibrium Interfaces during Phase Transformations in Concentrated Multicomponent Alloys. *Acta Mater.* **2022**, *241*, 118407.

(231) Li, M.; Lv, L.; Fang, T.; Hao, L.; Li, S.; Dong, S.; Wu, Y.; Dong, X.; Liu, H. Self-Consistent Implementation of a Solvation Free Energy Framework to Predict the Salt Solubilities of Six Alkali Halides. *J. Chem. Theory Comput.* **2023**, *19* (16), 5586–5601. https://doi.org/10.1021/acs.jctc.3c00083.

(232) Poole, C. F.; Atapattu, S. N. Determination of Physicochemical Properties of Small Molecules by Reversed-Phase Liquid Chromatography. *J. Chromatogr. A* **2020**, *1626*, 461427.

(233) Malik, M. I.; Berek, D. *Liquid Chromatography of Synthetic Polymers: Entropy/Enthalpy Compensation and Critical Conditions*; Springer Nature, 2023.

(234) Monrabal, B. Polystyrene Bonded Silica as GPC Packing: A Variable Pore Diameter Packing Concept in GPC. In *Liquid Chromatography of Polymers and Related Materials. III*; CRC Press, 2020; pp 79–98.

(235) Xiao, J.; Cao, H.; Cong, H.; Shen, Y.; Yu, B. Preparation and Modification of Monodisperse Large Particle Size Crosslinked Polystyrene Microspheres and Their Application in High Performance Liquid Chromatography. *React. Funct. Polym.* **2022**, *178*, 105357.

(236) Pogrebnyak, V. G.; Chudyk, I. I.; Perkun, I. V. Solutions of Polymers in the Oil and Gas Technologies. *PROSPECTS Dev. Resour.-Sav. Technol. Miner. Min. Process.* **2022**, 110.

(237) Ali, A. H. High-Performance Liquid Chromatography (HPLC): A Review. *Ann Adv Chem* **2022**, *6*, 010–020.

(238) Unger, K. K.; Lamotte, S.; Machtejevas, E. Column Technology in Liquid Chromatography. In *Liquid Chromatography*; Elsevier, 2017; pp 39–89.

(239) Berek, D. Coupled Liquid Chromatographic Techniques for the Separation of Complex Polymers. *Prog. Polym. Sci.* **2000**, *25* (7), 873–908.

(240) Lubomirsky, E.; Khodabandeh, A.; Preis, J.; Susewind, M.; Hofe, T.; Hilder, E. F.; Arrua, R. D. Polymeric Stationary Phases for Size Exclusion Chromatography: A Review. *Anal. Chim. Acta* **2021**, *1151*, 338244.

(241) Montaudo, G.; Garozzo, D.; Montaudo, M. S.; Puglisi, C.; Samperi, F. Molecular and Structural Characterization of Polydisperse Polymers and Copolymers by Combining MALDI-TOF Mass Spectrometry with GPC Fractionation. *Macromolecules* **1995**, *28* (24), 7983–7989. https://doi.org/10.1021/ma00128a003.

(242) de la Torre, J. G.; Bloomfield, V. A. Hydrodynamic Properties of Complex, Rigid, Biological Macromolecules: Theory and Applications. *Q. Rev. Biophys.* **1981**, *14* (1), 81–139.

(243) Harding, S. E. On the Hydrodynamic Analysis of Macromolecular Conformation. *Biophys. Chem.* **1995**, *55* (1–2), 69–93.

(244) Podzimek, S. Molar Mass Distribution by Size Exclusion Chromatography: Comparison of Multi-Angle Light Scattering and Universal Calibration. *J. Appl. Polym. Sci.* **2019**, *136* (21), 47561. https://doi.org/10.1002/app.47561.

(245) Podzimek, S. Importance of Multi-Angle Light Scattering in Polyolefin Characterization. *Macromol. Symp.* **2013**, *330* (1), 81–91. https://doi.org/10.1002/masy.201300014.

(246) Yau, W. W. Examples of Using 3D-GPC-TREF for Polyolefin Characterization. *Macromol. Symp.* **2007**, *257* (1), 29–45. https://doi.org/10.1002/masy.200751103.

(247) Ortín, A.; López, E.; Del Hierro, P.; Sancho-Tello, J.; Yau, W. W. Simplified Robust Triple Detection Methods for High Temperature GPC Analysis of Polyolefins. *Macromol. Symp.* **2018**, *377* (1), 1700044. https://doi.org/10.1002/masy.201700044.

(248) Pathaweeisariyakul, T.; Narkchamnan, K.; Thitisuk, B.; Yau, W. Methods of Long Chain Branching Detection in PE by Triple-Detector Gel Permeation Chromatography. *J. Appl. Polym. Sci.* **2015**, *132* (28), n/a-n/a. https://doi.org/10.1002/app.42222.

(249) Plüschke, L.; Mundil, R.; Sokolohorskyj, A.; Merna, J.; Sommer, J.-U.; Lederer, A. High Temperature Quadruple-Detector Size Exclusion Chromatography for Topological Characterization of Polyethylene. *Anal. Chem.* **2018**, *90* (10), 6178–6186. https://doi.org/10.1021/acs.analchem.8b00619.

(250) Hellgeth, J. W.; Taylor, L. T. Optimization of a Flow Cell Interface for Reversed-Phase Liquid Chromatography/Fourier Transform Infrared Spectrometry. *Anal. Chem.* **1987**, *59* (2), 295–300. https://doi.org/10.1021/ac00129a016.

(251) Wang, C. Po.; Sparks, D. T.; Williams, S. S.; Isenhour, T. L. Comparison of Methods for Reconstructing Chromatographic Data from Liquid Chromatography Fourier Transform Infrared Spectrometry. *Anal. Chem.* **1984**, *56* (8), 1268–1272. https://doi.org/10.1021/ac00272a017.

(252) DesLauriers, P. J.; Rohl, D. C. Quantifying Short Chain Branching Microstructures in Ethylene 1-Olefin Copolymers Using Size Exclusion Chromatography and Fourier Transform Infrared Spectroscopy (SEC±FTIR). **2002**.

(253) De Goede, E.; Mallon, P.; Pasch, H. Fractionation and Analysis of an Impact Poly(Propylene) Copolymer by TREF and SEC-FTIR: Fractionation and Analysis of an Impact Poly(Propylene) Copolymer by …. *Macromol. Mater. Eng.* **2010**, *295* (4), 366–373. https://doi.org/10.1002/mame.200900336.

(254) Macko, T.; Schulze, U.; Brüll, R.; Albrecht, A.; Pasch, H.; Fónagy, T.; Häussler, L.; Iván, B. Monitoring the Chemical Heterogeneity and the Crystallization Behavior of PP-g-PS Graft Copolymers Using SEC-FTIR and CRYSTAF. *Macromol. Chem. Phys.* **2008**, *209* (4), 404–409. https://doi.org/10.1002/macp.200700398.

(255) Hiller, W.; Pasch, H.; Macko, T.; Hofmann, M.; Ganz, J.; Spraul, M.; Braumann, U.; Streck, R.; Mason, J.; Van Damme, F. On-Line Coupling of High Temperature GPC and 1H NMR for the Analysis of Polymers. *J. Magn. Reson.* **2006**, *183* (2), 290–302. https://doi.org/10.1016/j.jmr.2006.09.004.

(256) Hiller, W.; Sinha, P.; Hehn, M.; Pasch, H. Online LC-NMR – From an Expensive Toy to a Powerful Tool in Polymer Analysis. *Prog. Polym. Sci.* **2014**, *39* (5), 979–1016. https://doi.org/10.1016/j.progpolymsci.2013.10.001.

(257) Yang, S.; Luo, C.; Lin, H.; Xu, P.-P.; Xu, L.; Lei, J.; Zhong, G.-J.; Li, Z.-M. Robust Propylene-Ethylene Copolymer/Polypropylene Films: Extensional Stress-Induced Orientation Realized at Low Temperature Processing. *Polymer* **2020**, *206*, 122848.

(258) Phala, A. C. Application of Multivariate Regression Techniques to Paint: For the Quantitive FTIR Spectroscopic Analysis of Polymeric Components. PhD Thesis, Cape Peninsula University of Technology, 2011. https://etd.cput.ac.za/handle/20.500.11838/733 (accessed 2023-11-17).

(259) Mülhaupt, R. Catalytic Polymerization and Post Polymerization Catalysis Fifty Years After the Discovery of Ziegler's Catalysts. *Macromol. Chem. Phys.* **2003**, *204* (2), 289–327. https://doi.org/10.1002/macp.200290085.

(260) Pigeon, M.; Prud'homme, R. E.; Pezolet, M. Characterization of Molecular Orientation in Polyethylene by Raman Spectroscopy. *Macromolecules* **1991**, *24* (20), 5687–5694. https://doi.org/10.1021/ma00020a032.

(261) Matsuoka, S. Relationship between Structure and Mechanical Properties of Polyolefins. *Polym. Eng. Sci.* **1965**, *5* (3), 142–147. https://doi.org/10.1002/pen.760050310.

(262) Randall, J. C. A Review of High Resolution Liquid 13carbon Nuclear Magnetic Resonance Characterizations of Ethylene-Based Polymers. *J. Macromol. Sci. Macromol. Chem. Phys.* **1989**, *29* (2–3), 201–317.

(263) Vignoli, A.; Ghini, V.; Meoni, G.; Licari, C.; Takis, P. G.; Tenori, L.; Turano, P.; Luchinat, C. High-Throughput Metabolomics by 1D NMR. *Angew. Chem. Int. Ed.* **2019**, *58* (4), 968–994. https://doi.org/10.1002/anie.201804736.

(264) Park, Y.; Jin, S.; Noda, I.; Jung, Y. M. Emerging Developments in Two-Dimensional Correlation Spectroscopy (2D-COS). *J. Mol. Struct.* **2020**, *1217*, 128405.

(265) Dencheva, N.; Stribeck, A.; Denchev, Z. Nanostructure Development in Multicomponent Polymer Systems Characterized by Synchrotron X-Ray Scattering. *Eur. Polym. J.* **2016**, *81*, 447–469.

(266) Michler, G. H.; Lebek, W. Electron Microscopy of Polymers. In *Polymer Morphology*; Guo, Q., Ed.; Wiley, 2016; pp 37–53. https://doi.org/10.1002/9781118892756.ch3.

(267) Hagège, R.; Bailly, J. C. SEM Image Analysis to Characterize the Shape of Catalyst and Polyethylene Prepolymer Particles in Olefinic Polymerization. *Polymer* **1993**, *34* (13), 2720–2725. https://doi.org/10.1016/0032-3861(93)90113-O.

(268) Park, J.; Eom, K.; Kwon, O. Characteristic Morphology and Its Properties of Melt-Crystallized Polyethylene Banded Spherulites on Scanning Electron Microscope. *Microsc. Microanal.* **2001**, *7* (S2), 500–501. https://doi.org/10.1017/S1431927600028579.

(269) Wilkes, G. L.; Samuels, S. L.; Crystal, R. Scanning and Transmission Electron Microscopy Studies on a Model Series of Spherulitic Segmented Polyurethanes. *J. Macromol. Sci. Part B* **1974**, *10* (2), 203–229. https://doi.org/10.1080/00222347408260827.

(270) Tagawa, T.; Mori, J.; Aita, S.; Ogura, K. Application of the High Resolution SEM to the Fine Structure Study of Polyethylene. *Micron 1969* **1978**, *9* (4), 215–221. https://doi.org/10.1016/0047-7206(78)90024-9.

(271) White, J. R.; Thomas, E. L. Advances in SEM of Polymers. *Rubber Chem. Technol.* **1984**, *57*, 457–506.

(272) Goldstein, J. I.; Newbury, D. E.; Michael, J. R.; Ritchie, N. W.; Scott, J. H. J.; Joy, D. C. *Scanning Electron Microscopy and X-Ray Microanalysis*; springer, 2017.

(273) Milicevic, D.; Micic, M.; Stamboliev, G.; Leskovac, A.; Mitric, M.; Suljovrujic, E. Microstructure and Crystallinity of Polyolefins Oriented via Solid-State Stretching at an Elevated Temperature. *Fibers Polym.* **2012**, *13* (4), 466–470. https://doi.org/10.1007/s12221-012-0466-4.

(274) Nogales, A.; Hsiao, B. S.; Somani, R. H.; Srinivas, S.; Tsou, A. H.; Balta-Calleja, F. J.; Ezquerra, T. A. Shear-Induced Crystallization of Isotactic Polypropylene with Different Molecular Weight Distributions: In Situ Small- and Wide-Angle X-Ray Scattering Studies. *Polymer* **2001**, *42* (12), 5247–5256. https://doi.org/10.1016/S0032-3861(00)00919-8.

(275) Santana, R. M. C.; Manrich, S. Morphology and Mechanical Properties of Polypropylene/High-impact Polystyrene Blends from Postconsumer Plastic Waste. *J. Appl. Polym. Sci.* **2003**, *88* (13), 2861–2867. https://doi.org/10.1002/app.11760.

(276) Teteris, G. Degradation of Polyolefines during Various Recovery Processes. *Macromol. Symp.* **1999**, *144* (1), 471–479. https://doi.org/10.1002/masy.19991440143.

(277) Baviskar, K. P.; Jain, D. V.; Pingale, S. D.; Wagh, S. S.; Gangurde, S. P.; Shardul, S. A.; Dahale, A. R.; Jain, K. S. A Review on Hyphenated Techniques in Analytical Chemistry. *Curr. Anal. Chem.* **2022**, *18* (9), 956–976.

(278) Awuchi, C. G.; Twinomuhwezi, H.; Awuchi, C. G. Hyphenated Techniques. In *Analytical Techniques in Biosciences*; Elsevier, 2022; pp 125–145.

(279) Schoonover, J. R.; Zhang, S. L.; Bridgewater, J. S.; Havrilla, G. J.; Fletcher, M. A.; Lightfoot, J. M. Polymer Degradation Study by Factor Analysis of GPC-FT-IR Data. *Appl. Spectrosc.* **2001**, *55* (7), 927–934.

(280) Wild, L.; Glöckner, G. Temperature Rising Elution Fractionation. In *Separation Techniques Thermodynamics Liquid Crystal Polymers*; Abe, A., Benoit, H., Cantow, H.-J., Corradini, P., Dušek, K., Edwards, S., Fujita, H., Glöckner, G., Höcker, H., Hörhold, H.-H., Kausch, H.-H., Kennedy, J. P., Koenig, J. L., Ledwith, A., Monnerie, L., Okamura, S., Overberger, C. G., Ringsdorf, H., Saegusa, T., Salamone, J. C., Schrag, J. L., Wegner, G., Series Eds.; Advances in Polymer Science; Springer Berlin Heidelberg: Berlin, Heidelberg, 1990; Vol. 98, pp 1–47. https://doi.org/10.1007/3-540-53135-1_4.

(281) Monrabal, B. Polyolefin Characterization: Recent Advances in Separation Techniques. In *Polyolefins: 50 years after Ziegler and Natta I*; Kaminsky, W., Ed.; Advances in Polymer Science; Springer Berlin Heidelberg: Berlin, Heidelberg, 2013; Vol. 257, pp 203–251. https://doi.org/10.1007/12_2013_216.

(282) Balke, S. T. Orthogonal Chromatography: Chromatographic Cross-Fractionation of Polymers. *Sep. Purif. Methods* **1982**, *11* (1), 1–28. https://doi.org/10.1080/03602548208066015.

(283) Danielsen, S. P. O.; Beech, H. K.; Wang, S.; El-Zaatari, B. M.; Wang, X.; Sapir, L.; Ouchi, T.; Wang, Z.; Johnson, P. N.; Hu, Y.; Lundberg, D. J.; Stoychev, G.; Craig, S. L.; Johnson, J. A.; Kalow, J. A.; Olsen, B. D.; Rubinstein, M. Molecular Characterization of Polymer Networks. *Chem. Rev.* **2021**, *121* (8), 5042–5092. https://doi.org/10.1021/acs.chemrev.0c01304.

(284) Awaja, F.; Zhang, S.; Tripathi, M.; Nikiforov, A.; Pugno, N. Cracks, Microcracks and Fracture in Polymer Structures: Formation, Detection, Autonomic Repair. *Prog. Mater. Sci.* **2016**, *83*, 536–573.

(285) Jacobsen, O.; Månsson, M.; Olsson, M. *Methods of Analysis for Trace Amounts of CFC in Polymeric Foams*; Nordic Council of Ministers, 1991.

(286) Cheruthazhekatt, S. Novel Multidimensional Fractionation Techniques for the Compositional Analysis of Impact Polypropylene Copolymers. PhD Thesis, Stellenbosch: Stellenbosch University, 2013. https://scholar.sun.ac.za/handle/10019.1/80118 (accessed 2023-12-01).

(287) Xu, J.; Feng, L. Application of Temperature Rising Elution Fractionation in Polyolefins. *Eur. Polym. J.* **2000**, *36* (5), 867–878.

(288) Glöckner, G. *Gradient HPLC of Copolymers and Chromatographic Cross-Fractionation*; Springer Science & Business Media, 2012.

(289) Orski, S. V.; Kassekert, L. A.; Farrell, W. S.; Kenlaw, G. A.; Hillmyer, M. A.; Beers, K. L. Design and Characterization of Model Linear Low-Density Polyethylenes (LLDPEs) by Multidetector Size Exclusion Chromatography. *Macromolecules* **2020**, *53* (7), 2344–2353. https://doi.org/10.1021/acs.macromol.9b02623.

(290) Nakano, S.; Goto, Y. Development of Automatic Cross Fractionation: Combination of Crystallizability Fractionation and Molecular Weight Fractionation. *J. Appl. Polym. Sci.* **1981**, *26* (12), 4217–4231. https://doi.org/10.1002/app.1981.070261222.

(291) Ortin, A.; Monrabal, B.; Sancho-Tello, J. Development of an Automated Cross-Fractionation Apparatus (TREF-GPC) for a Full Characterization of the Bivariate Distribution of Polyolefins. *Macromol. Symp.* **2007**, *257* (1), 13–28. https://doi.org/10.1002/masy.200751102.

(292) Albrecht, A.; Jayaratne, K.; Jeremic, L.; Sumerin, V.; Pakkanen, A. Describing and Quantifying the Chemical Composition Distribution in Unimodal and Multimodal ZN-Polyethylene Using CRYSTAF. *J. Appl. Polym. Sci.* **2016**, *133* (9), n/a-n/a. https://doi.org/10.1002/app.43089.

(293) Fan, Z.; Yu, Z.; Steuernagel, L.; Fischlschweiger, M. Thermomechanical Degradation of Polypropylene – Polystyrene Blends During Extrusion-Based Melt Blending – A First Survey of Shear-Induced Molecular Architecture Changes. *Macromol. Chem. Phys.* **2022**, *223* (22), 2200206. https://doi.org/10.1002/macp.202200206.

(294) Eselem Bungu, P. S.; Pasch, H. Comprehensive Analysis of Branched Polyethylene: The Multiple Preparative Fractionation Concept. *Polym. Chem.* **2017**, *8* (31), 4565–4575. https://doi.org/10.1039/C7PY00893G.

(295) Tadmor, Z.; Gogos, C. G. *Principles of Polymer Processing*; John Wiley & Sons, 2006.

(296) Pawlak, A.; Galeski, A. Crystallization of Polypropylene. In *Polypropylene Handbook*; Karger-Kocsis, J., Bárány, T., Eds.; Springer International Publishing: Cham, 2019; pp 185–242. https://doi.org/10.1007/978-3-030-12903-3_4.

(297) Kantz, M. R. The Effects of Melt Processing Variables on the Morphology and Properties of Injection Molded Polypropylene. *Int. J. Polym. Mater.* **1974**, *3* (3), 245–258. https://doi.org/10.1080/00914037408072355.

(298) Wang, K.; Chen, F.; Li, Z.; Fu, Q. Control of the Hierarchical Structure of Polymer Articles via "Structuring" Processing. *Prog. Polym. Sci.* **2014**, *39* (5), 891–920.

(299) Jabarin, S. A.; Majdzadeh-Ardakani, K.; Lofgren, E. A. Crystallization and Melting Behavior in Polymer Blends. In *Encyclopedia of Polymer Blends*; Isayev, A. I., Ed.; Wiley, 2016; pp 135–190. https://doi.org/10.1002/9783527653966.ch2.

(300) Shanks, R. A. Concepts and Classification of Compatibilization Processes. In *Compatibilization of polymer blends*; Elsevier, 2020; pp 31–56.

(301) Gopanna, A.; Rajan, K. P.; Thomas, S. P.; Chavali, M. Polyethylene and Polypropylene Matrix Composites for Biomedical Applications. In *Materials for biomedical engineering*; Elsevier, 2019; pp 175–216.

(302) Salakhov, I. I.; Shaidullin, N. M.; Chalykh, A. E.; Matsko, M. A.; Shapagin, A. V.; Batyrshin, A. Z.; Shandryuk, G. A.; Nifant'ev, I. E. Low-Temperature Mechanical Properties of High-Density and Low-Density Polyethylene and Their Blends. *Polymers* **2021**, *13* (11), 1821.

(303) Rana, S. K. Blend of High-density Polyethylene and a Linear Low-density Polyethylene with Compositional-invariant Mechanical Properties. *J. Appl. Polym. Sci.* **2002**, *83* (12), 2604–2608. https://doi.org/10.1002/app.10219.

(304) Hussein, I. A.; Hameed, T. Influence of Branching Characteristics on Thermal and Mechanical Properties of Ziegler–Natta and Metallocene Hexene Linear Low-density Polyethylene Blends with Low-density Polyethylene. *J. Appl. Polym. Sci.* **2005**, *97* (6), 2488–2498. https://doi.org/10.1002/app.21985.

(305) Fereydoon, M.; Tabatabaei, S. H.; Ajji, A. Properties of Co-Extruded Nanoclay-Filled Aliphatic Nylon (PA6)/Linear Low-Density Polyethylene and Aromatic Nylon (MXD6)/ Linear Low-Density Polyethylene Multilayer Films. *J. Plast. Film Sheeting* **2015**, *31* (1), 45–77. https://doi.org/10.1177/8756087914528348.

(306) Martuscelli, E. Influence of Composition, Crystallization Conditions and Melt Phase Structure on Solid Morphology, Kinetics of Crystallization and Thermal Behavior of Binary Polymer/Polymer Blends. *Polym. Eng. Sci.* **1984**, *24* (8), 563–586. https://doi.org/10.1002/pen.760240809.

(307) Sen, S. K.; Raut, S. Microbial Degradation of Low Density Polyethylene (LDPE): A Review. *J. Environ. Chem. Eng.* **2015**, *3* (1), 462–473.

(308) Mileva, D.; Tranchida, D.; Gahleitner, M. Designing Polymer Crystallinity: An Industrial Perspective. *Polym. Cryst.* **2018**, *1* (2). https://doi.org/10.1002/pcr2.10009.

(309) Parvin, N. Synthesis and Characterization of Talc and Carbon Black Reinforced High Density Polyethylene Composites. **2012**.

(310) Ndlovu, P. Z. Long Chain Branching Analysis of Polyethylene Using Advanced Fractionation Methods. PhD Thesis, Stellenbosch: Stellenbosch University, 2021. https://scholar.sun.ac.za/handle/10019.1/123767 (accessed 2023-11-30).

(311) De Rosa, C.; Auriemma, F. Structure and Physical Properties of Syndiotactic Polypropylene: A Highly Crystalline Thermoplastic Elastomer. *Prog. Polym. Sci.* **2006**, *31* (2), 145–237.

(312) Auriemma, F.; De Rosa, C.; Di Girolamo, R.; Malafronte, A.; Scoti, M.; Cioce, C. Molecular View of Properties of Random Copolymers of Isotactic Polypropylene. In *Polymer Crystallization I*; Auriemma, F., Alfonso, G. C., De Rosa, C., Eds.; Advances in Polymer Science; Springer International Publishing: Cham, 2016; Vol. 276, pp 45–92. https://doi.org/10.1007/12_2016_350.

(313) van Drongelen, M.; Van Erp, T. B.; Peters, G. W. M. Quantification of Non-Isothermal, Multi-Phase Crystallization of Isotactic Polypropylene: The Influence of Cooling Rate and Pressure. *Polymer* **2012**, *53* (21), 4758–4769.

(314) De Rosa, C.; Corradini, P. Crystal Structure of Syndiotactic Polypropylene. *Macromolecules* **1993**, *26* (21), 5711–5718. https://doi.org/10.1021/ma00073a028.

(315) Plazek, D. L.; Plazek, D. J. Viscoelastic Behavior of Atactic Polypropylene. *Macromolecules* **1983**, *16* (9), 1469–1475. https://doi.org/10.1021/ma00243a011.

(316) Tripathi, D. *Practical Guide to Polypropylene*; iSmithers Rapra Publishing, 2002.

(317) Wang, S.; Zhang, J.; Chen, S.; Zhu, H. Crystal Structure and Melting Behavior of Homo-Polypropylene and Heterophasic Ethylene–Propylene Copolymer after Long Time Heat Treatment. *J. Cryst. Growth* **2012**, *355* (1), 151–158.

(318) Gahleitner, M.; Tranninger, C.; Doshev, P. Polypropylene Copolymers. In *Polypropylene Handbook*; Karger-Kocsis, J., Bárány, T., Eds.; Springer International Publishing: Cham, 2019; pp 295–355. https://doi.org/10.1007/978-3-030-12903-3_6.

(319) Cui, K.; Ma, Z.; Tian, N.; Su, F.; Liu, D.; Li, L. Multiscale and Multistep Ordering of Flow-Induced Nucleation of Polymers. *Chem. Rev.* **2018**, *118* (4), 1840–1886. https://doi.org/10.1021/acs.chemrev.7b00500.

(320) Aksel, S. Nucleation and Clarification of Polyethylenes. PhD Thesis, ETH Zurich, 2015. https://www.research-collection.ethz.ch/bitstream/handle/20.500.11850/110945/1/eth-48528-01.pdf (accessed 2023-11-17).

(321) Vega, J. F.; Da Silva, Y.; Vicente-Alique, E.; Núñez-Ramírez, R.; Trujillo, M.; Arnal, M. L.; Müller, A. J.; Dubois, P.; Martínez-Salazar, J. Influence of Chain Branching and Molecular Weight on Melt Rheology and Crystallization of Polyethylene/Carbon Nanotube Nanocomposites. *Macromolecules* **2014**, *47* (16), 5668–5681. https://doi.org/10.1021/ma501269g.

(322) Gennes, P.-G. de; Gennes, P. P.-G. *Scaling Concepts in Polymer Physics*; Cornell University Press, 1979.

(323) Balzano, L.; Rastogi, S.; Peters, G. Self-Nucleation of Polymers with Flow: The Case of Bimodal Polyethylene. *Macromolecules* **2011**, *44* (8), 2926–2933. https://doi.org/10.1021/ma102662p.

(324) Kornfield, J. A.; Kumaraswamy, G.; Issaian, A. M. Recent Advances in Understanding Flow Effects on Polymer Crystallization. *Ind. Eng. Chem. Res.* **2002**, *41* (25), 6383–6392. https://doi.org/10.1021/ie020237z.

(325) Nagarajan, K.; Levon, K.; Myerson, A. S. Nucleating Agents in Polypropylene. **2000**.

(326) Mubarak, Y.; Martin, P. J.; Harkin-Jones, E. Effect of Nucleating Agents and Pigments on Crystallisation, Morphology, and Mechanical Properties of Polypropylene. *Plast. Rubber Compos.* **2000**, *29* (7), 307–315. https://doi.org/10.1179/146580100101541111.

(327) Ren, Q.; Fan, J.; Zhang, Q.; Yi, J.; Feng, J. Toughened Polypropylene Random Copolymer with Olefin Block Copolymer. *Mater. Des.* **2016**, *107*, 295–301.

(328) Fakirov, S. Nano-/Microfibrillar Polymer–Polymer and Single Polymer Composites: The Converting Instead of Adding Concept. *Compos. Sci. Technol.* **2013**, *89*, 211–225.

(329) Su, B.; Zhou, Y.-G.; Wu, H.-H. Influence of Mechanical Properties of Polypropylene/Low-Density Polyethylene Nanocomposites: Compatibility and Crystallization. *Nanomater. Nanotechnol.* **2017**, *7*, 184798041771592. https://doi.org/10.1177/1847980417715929.

(330) Brucato, V.; Piccarolo, S.; La Carrubba, V. An Experimental Methodology to Study Polymer Crystallization under Processing Conditions. The Influence of High Cooling Rates. *Chem. Eng. Sci.* **2002**, *57* (19), 4129–4143.

(331) Li, J.; Shanks, R. A.; Olley, R. H.; Greenway, G. R. Miscibility and Isothermal Crystallisation of Polypropylene in Polyethylene Melts. *Polymer* **2001**, *42* (18), 7685–7694.

(332) Birley, A. W. *Plastics Materials: Properties and Applications*; Springer Science & Business Media, 2012.

(333) Beck, H. N.; Ledbetter, H. D. DTA Study of Heterogeneous Nucleation of Crystallization in Polypropylene. *J. Appl. Polym. Sci.* **1965**, *9* (6), 2131–2142. https://doi.org/10.1002/app.1965.070090610.

(334) Le, M. C.; Belhabib, S.; Nicolazo, C.; Vachot, P.; Mousseau, P.; Sarda, A.; Deterre, R. Pressure Influence on Crystallization Kinetics during Injection Molding. *J. Mater. Process. Technol.* **2011**, *211* (11), 1757–1763.

(335) Galeski, A. Strength and Toughness of Crystalline Polymer Systems. *Prog. Polym. Sci.* **2003**, *28* (12), 1643–1699.

(336) Öktem, H.; Shinde, D. Determination of Optimal Process Parameters for Plastic Injection Molding of Polymer Materials Using Multi-Objective Optimization. *J. Mater. Eng. Perform.* **2021**, *30* (11), 8616–8632. https://doi.org/10.1007/s11665-021-06029-z.

(337) Teh, J. W.; Rudin, A.; Keung, J. C. A Review of Polyethylene–Polypropylene Blends and Their Compatibilization. *Adv. Polym. Technol.* **1994**, *13* (1), 1–23. https://doi.org/10.1002/adv.1994.060130101.

(338) Góra, M.; Coba-Daza, S.; Carmeli, E.; Tranchida, D.; Albrecht, A.; Müller, A. J.; Cavallo, D. Surface-Enhanced Nucleation in Immiscible Polypropylene and Polyethylene Blends: The Effect of Polyethylene Chain Regularity. *Polymer* **2023**, 126180. https://doi.org/10.1016/j.polymer.2023.126180.

(339) Ibar, J. P. Control of Polymer Properties by Melt Vibration Technology: A Review. *Polym. Eng. Sci.* **1998**, *38* (1), 1–20. https://doi.org/10.1002/pen.10161.

(340) Ouyang, Y.; Pourrahimi, A. M.; Lund, A.; Xu, X.; Gkourmpis, T.; Hagstrand, P.-O.; Müller, C. High-Temperature Creep Resistant Ternary Blends Based on Polyethylene and Polypropylene for Thermoplastic Power Cable Insulation. *J. Polym. Sci.* **2021**, *59* (11), 1084–1094. https://doi.org/10.1002/pol.20210147.

(341) Eslamian, M.; Bagheri, R.; Pircheraghi, G. Co-Crystallization in Ternary Polyethylene Blends: Tie Crystal Formation and Mechanical Properties Improvement: Co-Crystallization in Ternary Polyethylene Blends. *Polym. Int.* **2016**, *65* (12), 1405–1416. https://doi.org/10.1002/pi.5191.

(342) Pracella, M.; Benedetti, E.; Galleschi, F. A Study of Crystallisation Behaviour and Compatibility of High-Density Polyethylene/Linear Low-Density Polyethylene Blends. *Thermochim. Acta* **1990**, *162* (1), 163–177. https://doi.org/10.1016/0040-6031(90)80338-Y.

(343) Lovinger, A. J.; Williams, M. L. Tensile Properties and Morphology of Blends of Polyethylene and Polypropylene. *J. Appl. Polym. Sci.* **1980**, *25* (8), 1703–1713. https://doi.org/10.1002/app.1980.070250817.

(344) Wenig, W.; Meyer, K. Investigation of the Crystallization Behaviour of Polypropylene — Polyethylene Blends by Optical Microscopy. *Colloid Polym. Sci.* **1980**, *258* (9), 1009–1014. https://doi.org/10.1007/BF01382395.

(345) Kudláček, L.; Kaplanova, M.; Knap, F. Faserforsch. u. Textiltechnik. *Z Polym.* **1978**, *29*, 286–289.

(346) Last, A. G. M. Nucleation Effects in High Polymers. *J. Polym. Sci.* **1959**, *39* (135), 543–545. https://doi.org/10.1002/pol.1959.1203913555.

(347) Lotz, B.; Wittmann, J. C. Polyethylene–Isotactic Polypropylene Epitaxy: Analysis of the Diffraction Patterns of Oriented Biphasic Blends. *J. Polym. Sci. Part B Polym. Phys.* **1987**, *25* (5), 1079–1087. https://doi.org/10.1002/polb.1987.090250509.

(348) Wittmann, J. C.; Lotz, B. Epitaxial Crystallization of Polymers on Organic and Polymeric Substrates. *Prog. Polym. Sci.* **1990**, *15* (6), 909–948. https://doi.org/10.1016/0079-6700(90)90025-V.

(349) Yan, S.; Petermann, J.; Yang, D. Effect of Lamellar Thickness on the Epitaxial Crystallization of PE on Oriented iPP Films. *Polym. Bull.* **1997**, *38* (1), 87–94. https://doi.org/10.1007/s002890050023.

(350) Yan, S.; Lin, J.; Yang, D.; Petermann, J. Critical Epitaxial Layers of Different Kinds of Polyethylene on Highly Oriented Isotactic Poly(Propylene) Substrates. *Macromol. Chem. Phys.* **1994**, *195* (1), 195–201. https://doi.org/10.1002/macp.1994.021950117.

(351) Rybnikar, F.; Kaszonyiova, M. Epitaxial Crystallization of Linear Polyethylene in Blends with Isotactic Polypropylene. *J. Macromol. Sci. Part B* **2014**, *53* (2), 217–232. https://doi.org/10.1080/00222348.2013.808522.

(352) Nishio, Y.; Yamane, T.; Takahashi, T. Crystallization Behavior of High-Density Polyethylene in an Oriented Blend with Polypropylene. *J. Macromol. Sci. Part B* **1984**, *23* (1), 17–27. https://doi.org/10.1080/00222348408229360.

(353) Kojima, M.; Satake, H. Morphological and Structural Features of Heat-Treated Drawn Polypropylene/High-Density Polyethylene Blends. *J. Polym. Sci. Polym. Phys. Ed.* **1984**, *22* (2), 285–294. https://doi.org/10.1002/pol.1984.180220213.

(354) Samuel, C.; Parpaite, T.; Lacrampe, M.-F.; Soulestin, J.; Lhost, O. Melt Compatibility between Polyolefins: Evaluation and Reliability of Interfacial/Surface Tensions Obtained by

Various Techniques. *Polym. Test.* **2019**, *78*, 105995. https://doi.org/10.1016/j.polymertesting.2019.105995.

(355) Morgan, R. L.; Hill, M. J.; Barham, P. J. Morphology, Melting Behaviour and Co-Crystallization in Polyethylene Blends: The Effect of Cooling Rate on Two Homogeneously Mixed Blends. *Polymer* **1999**, *40* (2), 337–348. https://doi.org/10.1016/S0032-3861(98)00193-1.

(356) Li, J.; Shanks, R. A.; Long, Y. Isothermal Crystallization and Spherulite Structure of Partially Miscible Polypropylene–Linear Low-density Polyethylene Blends. *J. Appl. Polym. Sci.* **2001**, *82* (3), 628–639. https://doi.org/10.1002/app.1891.

(357) Alamo, R. G.; Glaser, R. H.; Mandelkern, L. The Cocrystallization of Polymers: Polyethylene and Its Copolymers. *J. Polym. Sci. Part B Polym. Phys.* **1988**, *26* (10), 2169–2195. https://doi.org/10.1002/polb.1988.090261011.

(358) Lee, H.; Cho, K.; Ahn, T.-K.; Choe, S.; Kim, I.-J.; Park, I.; Lee, B. H. Solid-State Relaxations in Linear Low-Density (1-Octene Comonomer), Low-Density, and High-Density Polyethylene Blends. *J. Polym. Sci. Part B Polym. Phys.* **1997**, *35* (10), 1633–1642. https://doi.org/10.1002/(SICI)1099-0488(19970730)35:10<1633::AID-POLB15>3.0.CO;2-B.

(359) Hill, M. J.; Barham, P. J. Absence of Phase Separation Effects in Blends of Linear Polyethylene Fractions of Differing Molecular Weight. *Polymer* **1995**, *36* (8), 1523–1530. https://doi.org/10.1016/0032-3861(95)98995-Y.

(360) Xu, J.; Eagan, J. M.; Kim, S.-S.; Pan, S.; Lee, B.; Klimovica, K.; Jin, K.; Lin, T.-W.; Howard, M. J.; Ellison, C. J.; LaPointe, A. M.; Coates, G. W.; Bates, F. S. Compatibilization of Isotactic Polypropylene (*i* PP) and High-Density Polyethylene (HDPE) with *i* PP–PE Multiblock Copolymers. *Macromolecules* **2018**, *51* (21), 8585–8596. https://doi.org/10.1021/acs.macromol.8b01907.

(361) Fortelný, I.; Kruliš, Z.; Michálková, D.; Horák, Z. Effect of EPDM Admixture and Mixing Conditions on the Morphology and Mechanical Properties of LDPE/PP Blends. *Angew. Makromol. Chem.* **1996**, *238* (1), 97–104. https://doi.org/10.1002/apmc.1996.052380109.

(362) Su, B.; Zhou, Y.-G.; Wu, H.-H. Influence of Mechanical Properties of Polypropylene/Low-Density Polyethylene Nanocomposites: Compatibility and Crystallization. *Nanomater. Nanotechnol.* **2017**, *7*, 1847980417715929. https://doi.org/10.1177/1847980417715929.

(363) Utracki, L. A. Compatibilization of Polymer Blends. *Can. J. Chem. Eng.* **2002**, *80* (6), 1008–1016. https://doi.org/10.1002/cjce.5450800601.

(364) Zeng, J.-B.; Li, K.-A.; Du, A.-K. Compatibilization Strategies in Poly(Lactic Acid)-Based Blends. *RSC Adv.* **2015**, *5* (41), 32546–32565. https://doi.org/10.1039/C5RA01655J.

(365) Ji, W.-Y. Development of a Concept of Reactive Compatibilizer-Tracer for Studying the Evolution of the Interfacial Reaction and Morphology of Reactive Polymer Blends.

(366) Koning, C.; Duin, M. V.; Pagnoulle, C.; Jerome, R. Strategies for Compatibilization of Polymer Blends. *Prog. Polym. Sci.* **1998**, *23* (4), 707–757. https://doi.org/10.1016/S0079-6700(97)00054-3.

(367) Jordan, A. M.; Kim, K.; Soetrisno, D.; Hannah, J.; Bates, F. S.; Jaffer, S. A.; Lhost, O.; Macosko, C. W. Role of Crystallization on Polyolefin Interfaces: An Improved Outlook for Polyolefin Blends. *Macromolecules* **2018**, *51* (7), 2506–2516. https://doi.org/10.1021/acs.macromol.8b00206.

(368) Farris, S.; Pozzoli, S.; Biagioni, P.; Duó, L.; Mancinelli, S.; Piergiovanni, L. The Fundamentals of Flame Treatment for the Surface Activation of Polyolefin Polymers–A Review. *Polymer* **2010**, *51* (16), 3591–3605.

(369) Liu, Y.-X.; Wang, X.-J.; Lu, J.; Ching, C.-B. Influence of the Roughness, Topography, and Physicochemical Properties of Chemically Modified Surfaces on the Heterogeneous Nucleation of Protein Crystals. *J. Phys. Chem. B* **2007**, *111* (50), 13971–13978. https://doi.org/10.1021/jp0741612.

(370) Vallejo-Montesinos, J.; Muñoz, U. M.; Gonzalez-Calderon, J. A. Mechanical Properties, Crystallization and Degradation of Polypropylene Due to Nucleating Agents, Fillers and Additives. *Polypropyl Prop. Uses Benefits* **2016**, *4*, 83–140.

(371) Bai, H.; Zhang, W.; Deng, H.; Zhang, Q.; Fu, Q. Control of Crystal Morphology in Poly(L -Lactide) by Adding Nucleating Agent. *Macromolecules* **2011**, *44* (6), 1233–1237. https://doi.org/10.1021/ma102439t.

(372) Wypych, G. *Handbook of Nucleating Agents*; Elsevier, 2021.

(373) Papageorgiou, D. G.; Papageorgiou, G. Z.; Bikiaris, D. N.; Chrissafis, K. Crystallization and Melting of Propylene–Ethylene Random Copolymers. Homogeneous Nucleation and β-Nucleating Agents. *Eur. Polym. J.* **2013**, *49* (6), 1577–1590.

(374) De Yoreo, J. J.; Vekilov, P. G. Principles of Crystal Nucleation and Growth. *Rev. Mineral. Geochem.* **2003**, *54* (1), 57–93.

(375) Das, A.; Bryant, J. S.; Williams, C. B.; Bortner, M. J. Melt-Based Additive Manufacturing of Polyolefins Using Material Extrusion and Powder Bed Fusion. *Polym. Rev.* **2023**, *63* (4), 895–960. https://doi.org/10.1080/15583724.2023.2220024.

(376) Ramel, P. R.; Campos, R.; Marangoni, A. G. Effects of Shear and Cooling Rate on the Crystallization Behavior and Structure of Cocoa Butter: Shear Applied During the Early Stages of Nucleation. *Cryst. Growth Des.* **2018**, *18* (2), 1002–1011. https://doi.org/10.1021/acs.cgd.7b01472.

(377) Saikrishnan, S.; Jubinville, D.; Tzoganakis, C.; Mekonnen, T. H. Thermo-Mechanical Degradation of Polypropylene (PP) and Low-Density Polyethylene (LDPE) Blends Exposed to Simulated Recycling. *Polym. Degrad. Stab.* **2020**, *182*, 109390.

(378) Jones, H.; McClements, J.; Ray, D.; Hindle, C. S.; Kalloudis, M.; Koutsos, V. Thermomechanical Properties of Virgin and Recycled Polypropylene—High-Density Polyethylene Blends. *Polymers* **2023**, *15* (21), 4200.

(379) Meenan, P. A.; Anderson, S. R.; Klug, D. L. The Influence of Impurities and Solvents on Crystallization. *Handb. Ind. Cryst.* **2002**, 67–100.

(380) Schyns, Z. O. G.; Shaver, M. P. Mechanical Recycling of Packaging Plastics: A Review. *Macromol. Rapid Commun.* **2021**, *42* (3), 2000415. https://doi.org/10.1002/marc.202000415.

(381) Hopewell, J.; Dvorak, R.; Kosior, E. Plastics Recycling: Challenges and Opportunities. *Philos. Trans. R. Soc. B Biol. Sci.* **2009**, *364* (1526), 2115–2126. https://doi.org/10.1098/rstb.2008.0311.

(382) Beghetto, V.; Sole, R.; Buranello, C.; Al-Abkal, M.; Facchin, M. Recent Advancements in Plastic Packaging Recycling: A Mini-Review. *Materials* **2021**, *14* (17), 4782. https://doi.org/10.3390/ma14174782.

(383) Eagan, J. M.; Xu, J.; Di Girolamo, R.; Thurber, C. M.; Macosko, C. W.; LaPointe, A. M.; Bates, F. S.; Coates, G. W. Combining Polyethylene and Polypropylene: Enhanced Performance with PE/ *i* PP Multiblock Polymers. *Science* **2017**, *355* (6327), 814–816. https://doi.org/10.1126/science.aah5744.

(384) Van Belle, A.; Demets, R.; Mys, N.; Van Kets, K.; Dewulf, J.; Van Geem, K.; De Meester, S.; Ragaert, K. Microstructural Contributions of Different Polyolefins to the Deformation Mechanisms of Their Binary Blends. *Polymers* **2020**, *12* (5), 1171. https://doi.org/10.3390/polym12051171.

(385) Xanthos, M. Recycling of the #5 Polymer. *Science* **2012**, *337* (6095), 700–702. https://doi.org/10.1126/science.1221806.

(386) Jones, H.; Saffar, F.; Koutsos, V.; Ray, D. Polyolefins and Polyethylene Terephthalate Package Wastes: Recycling and Use in Composites. *Energies* **2021**, *14* (21), 7306. https://doi.org/10.3390/en14217306.

(387) Alvarado Chacon, F.; Brouwer, M. T.; Thoden van Velzen, E. U.; Smeding, I. W. *A First Assessment of the Impact of Impurities in PP and PE Recycled Plastics*; Report / Wageningen Food & Biobased Research; Wageningen Food & Biobased Research, 2020. https://doi.org/10.18174/518299.

(388) Zhang, M.; Guo, B.-H.; Xu, J. A Review on Polymer Crystallization Theories. *Crystals* **2016**, *7* (1), 4. https://doi.org/10.3390/cryst7010004.

(389) Xu, J.; Reiter, G.; Alamo, R. Concepts of Nucleation in Polymer Crystallization. *Crystals* **2021**, *11* (3), 304. https://doi.org/10.3390/cryst11030304.

(390) Carraher, C. E.; Seymour, R. B. *Seymour/Carraher's Polymer Chemistry*, 6th ed., rev.expanded.; Undergraduate chemistry; M. Dekker: New York, 2003.

(391) Soares, J. B. P.; Hamielec, A. E. Temperature Rising Elution Fractionation of Linear Polyolefins. *Polymer* **1995**, *36* (8), 1639–1654. https://doi.org/10.1016/0032-3861(95)99010-R.

(392) Monrabal, B.; Sancho-Tello, J.; Mayo, N.; Romero, L. Crystallization Elution Fractionation. A New Separation Process for Polyolefin Resins. *Macromol. Symp.* **2007**, *257* (1), 71–79. https://doi.org/10.1002/masy.200751106.

(393) *CRYSTAF-TREF Analytical Instrument for Polyolefins*. Polymer Char. https://polymerchar.com/products/analytical-instruments/crystaf-tref (accessed 2021-12-02).

(394) Müller, A. J.; Michell, R. M.; Pérez, R. A.; Lorenzo, A. T. Successive Self-Nucleation and Annealing (SSA): Correct Design of Thermal Protocol and Applications. *Eur. Polym. J.* **2015**, *65*, 132–154. https://doi.org/10.1016/j.eurpolymj.2015.01.015.

(395) Chen, F. Crystallisation of Single-Site Polyethylene Blends Investigated by Thermal Fractionation Techniques. *Polymer* **2001**, *42* (10), 4579–4587. https://doi.org/10.1016/S0032-3861(00)00859-4.

(396) Arnal, M. L.; Balsamo, V.; Ronca, G.; Sánchez, A.; Müller, A. J.; Cañizales, E.; de Navarro, C. U. Applications of Successive Self-Nucleation and Annealing (SSA) to Polymer Characterization. **2000**, 20.

(397) Kontopoulou, M.; Wang, W.; Gopakumar, T. G.; Cheung, C. Effect of Composition and Comonomer Type on the Rheology, Morphology and Properties of Ethylene-α-Olefin

Copolymer/Polypropylene Blends. *Polymer* **2003**, *44* (24), 7495–7504. https://doi.org/10.1016/j.polymer.2003.08.043.

(398) Michell, R. M.; Mugica, A.; Zubitur, M.; Müller, A. J. Self-Nucleation of Crystalline Phases Within Homopolymers, Polymer Blends, Copolymers, and Nanocomposites. In *Polymer Crystallization I*; Auriemma, F., Alfonso, G. C., de Rosa, C., Eds.; Advances in Polymer Science; Springer International Publishing: Cham, 2015; Vol. 276, pp 215–256. https://doi.org/10.1007/12_2015_327.

(399) Sangroniz, L.; Cavallo, D.; Müller, A. J. Self-Nucleation Effects on Polymer Crystallization. *Macromolecules* **2020**, *53* (12), 4581–4604. https://doi.org/10.1021/acs.macromol.0c00223.

(400) Carmeli, E.; Fenni, S. E.; Caputo, M. R.; Müller, A. J.; Tranchida, D.; Cavallo, D. Surface Nucleation of Dispersed Polyethylene Droplets in Immiscible Blends Revealed by Polypropylene Matrix Self-Nucleation. *Macromolecules* **2021**, *54* (19), 9100–9112. https://doi.org/10.1021/acs.macromol.1c01430.

(401) Trujillo, M.; Arnal, M. L.; Müller, A. J.; Laredo, E.; Bredeau, St.; Bonduel, D.; Dubois, Ph. Thermal and Morphological Characterization of Nanocomposites Prepared by In-Situ Polymerization of High-Density Polyethylene on Carbon Nanotubes. *Macromolecules* **2007**, *40* (17), 6268–6276. https://doi.org/10.1021/ma071025m.

(402) Balsamo, V.; Paolini, Y.; Ronca, G.; Müller, A. J. Crystallization of the Polyethylene Block in Polystyrene-b-Polyethylene-b-Polycaprolactone Triblock Copolymers, 1. Self-Nucleation Behavior. *Macromol. Chem. Phys.* **2000**, *201* (18), 2711–2720. https://doi.org/10.1002/1521-3935(20001201)201:18<2711::AID-MACP2711>3.0.CO;2-6.

(403) Pijpers, M. F. J.; Mathot, V. B. F. Optimization of Instrument Response and Resolution of Standard- and High-Speed Power Compensation DSC: Benefits for the Study of Crystallization, Melting and Thermal Fractionation. *J. Therm. Anal. Calorim.* **2008**, *93* (1), 319–327. https://doi.org/10.1007/s10973-007-8924-8.

(404) Feng, Y.; Jin, X.; Hay, J. N. Evaluation of Multiple Melting Peaks of Propylene-Ethylene Copolymers. *Polym. J.* **1998**, *30* (3), 215–221. https://doi.org/10.1295/polymj.30.215.

(405) Kim, M.-H.; Alamo, R. G.; Lin, J. S. The Cocrystallization Behavior of Binary Blends of Isotactic Polypropylene and Propylene-Ethylene Random Copolymers. *Polym. Eng. Sci.* **1999**, *39* (11), 2117–2131. https://doi.org/10.1002/pen.11602.

(406) Anantawaraskul, S.; Soares, J. B. P.; Wood-Adams, P. M. Effect of Operation Parameters on Temperature Rising Elution Fractionation and Crystallization Analysis Fractionation. *J. Polym. Sci. Part B Polym. Phys.* **2003**, *41* (14), 1762–1778. https://doi.org/10.1002/polb.10537.

(407) Van Geem, K. M. Plastic Waste Recycling Is Gaining Momentum. *Science* **2023**, *381* (6658), 607–608. https://doi.org/10.1126/science.adj2807.

(408) Xu, Z.; Munyaneza, N. E.; Zhang, Q.; Sun, M.; Posada, C.; Venturo, P.; Rorrer, N. A.; Miscall, J.; Sumpter, B. G.; Liu, G. Chemical Upcycling of Polyethylene, Polypropylene, and Mixtures to High-Value Surfactants. *Science* **2023**, *381* (6658), 666–671. https://doi.org/10.1126/science.adh0993.

(409) Luijsterburg, B.; Goossens, H. Assessment of Plastic Packaging Waste: Material Origin, Methods, Properties. *Resour. Conserv. Recycl.* **2014**, *85*, 88–97. https://doi.org/10.1016/j.resconrec.2013.10.010.

(410) *ReShaping Plastics • Plastics Europe*. Plastics Europe. https://plasticseurope.org/changingplasticsforgood/reshaping-plastics/ (accessed 2023-08-23).

(411) Geyer, R.; Jambeck, J. R.; Law, K. L. Production, Use, and Fate of All Plastics Ever Made. *Sci. Adv.* **2017**, *3* (7), e1700782. https://doi.org/10.1126/sciadv.1700782.

(412) *Green Deal: key to a climate-neutral and sustainable EU | News | European Parliament*. https://www.europarl.europa.eu/news/en/headlines/society/20200618STO81513/green-deal-key-to-a-climate-neutral-and-sustainable-eu (accessed 2023-08-16).

(413) *European Green Deal: Putting an end to wasteful packaging*. European Commission - European Commission. https://ec.europa.eu/commission/presscorner/detail/en/ip_22_7155 (accessed 2023-08-16).

(414) *U.S. Actions to Address Plastic Pollution*. United States Department of State. https://www.state.gov/u-s-actions-to-address-plastic-pollution/ (accessed 2023-08-16).

(415) Environment, U. N. *TACKLING PLASTIC POLLUTION: Legislative Guide for the Regulation of Single-Use Plastic Products*. UNEP - UN Environment Programme. http://www.unep.org/resources/toolkits-manuals-and-guides/tackling-plastic-pollution-legislative-guide-regulation (accessed 2023-08-16).

(416) Freudenthaler, P. J.; Fischer, J.; Liu, Y.; Lang, R. W. Short- and Long-Term Performance of Pipe Compounds Containing Polyethylene Post-Consumer Recyclates from Packaging Waste. *Polymers* **2022**, *14* (8), 1581. https://doi.org/10.3390/polym14081581.

(417) Freudenthaler, P. J.; Fischer, J.; Lang, R. W. Assessment of Commercially Available Polyethylene Recyclates for Blow Molding Applications by a Novel Environmental Stress Cracking Method. *Polymers* **2022**, *15* (1), 46. https://doi.org/10.3390/polym15010046.

(418) Freudenthaler, P. J.; Fischer, J.; Liu, Y.; Lang, R. W. Polypropylene Post-Consumer Recyclate Compounds for Thermoforming Packaging Applications. *Polymers* **2023**, *15* (2), 345. https://doi.org/10.3390/polym15020345.

(419) Freudenthaler, P. J.; Fischer, J.; Liu, Y.; Lang, R. W. Polypropylene Pipe Compounds with Varying Post-Consumer Packaging Recyclate Content. *Polymers* **2022**, *14* (23), 5232. https://doi.org/10.3390/polym14235232.

(420) Pereda, M.; Gerber, E.; Sander, I.; Welle, F. How to Evaluate Post-Consumer Polyolefin Recyclates in Cosmetic Packaging?

(421) Freudenthaler, P.; Fischer, J.; Eder, M.; Lang, R. Effect of Chlorinated Water on the Fatigue Crack Growth Resistance of Polyethylene Compounds with Recyclate Content for Pipe Applications; 2021.

(422) Mastellone, M. L. A Feasibility Assessment of an Integrated Plastic Waste System Adopting Mechanical and Thermochemical Conversion Processes. *Resour. Conserv. Recycl. X* **2019**, *4*, 100017. https://doi.org/10.1016/j.rcrx.2019.100017.

(423) Gala, A.; Guerrero, M.; Serra, J. M. Characterization of Post-Consumer Plastic Film Waste from Mixed MSW in Spain: A Key Point for the Successful Implementation of Sustainable Plastic Waste Management Strategies. *Waste Manag.* **2020**, *111*, 22–33. https://doi.org/10.1016/j.wasman.2020.05.019.

(424) Vogt, B. D.; Stokes, K. K.; Kumar, S. K. Why Is Recycling of Postconsumer Plastics so Challenging? *ACS Appl. Polym. Mater.* **2021**, *3* (9), 4325–4346. https://doi.org/10.1021/acsapm.1c00648.

(425) Karaagac, E.; Jones, M. P.; Koch, T.; Archodoulaki, V.-M. Polypropylene Contamination in Post-Consumer Polyolefin Waste: Characterisation, Consequences and Compatibilisation. *Polymers* **2021**, *13* (16), 2618. https://doi.org/10.3390/polym13162618.

(426) Karaagac, E.; Koch, T.; Archodoulaki, V.-M. The Effect of PP Contamination in Recycled High-Density Polyethylene (rPE-HD) from Post-Consumer Bottle Waste and Their Compatibilization with Olefin Block Copolymer (OBC). *Waste Manag.* **2021**, *119*, 285–294. https://doi.org/10.1016/j.wasman.2020.10.011.

(427) Furushima, Y.; Hirota, N.; Nakada, M.; Masuda, A.; Okada, K.; Ohkura, M.; Schick, C. Determination of Mass Fractions in Polypropylene/Polyethylene Blends Using Fast Scanning Calorimetry. *J. Appl. Polym. Sci.* **2023**, e54556. https://doi.org/10.1002/app.54556.
(428) Boborodea, A.; O'Donohue, S. J.; Brookes, A. A New GPC/TREF/LinELSD Instrument to Determine the Molecular Weight Distribution and Chemical Composition: Application to Recycled Polymers. *Int. J. Polym. Anal. Charact.* **2021**, *26*, 721–734.
(429) Paulik, C.; Spiegel, G.; Jeremic, D. Bimodal Polyethylene: Controlling Polymer Properties by Molecular Design. In *Multimodal Polymers with Supported Catalysts*; Albunia, A. R., Prades, F., Jeremic, D., Eds.; Springer International Publishing: Cham, 2019; pp 243–265. https://doi.org/10.1007/978-3-030-03476-4_7.
(430) Piriyakulkit, P.; Kanoknukulchai, K.; Potisatityuenyong, A.; Anantawaraskul, S. Cocrystallization of Polyethylene Blends during TREF–GPC Cross-Fractionation Characterization. *Macromol. Chem. Phys.* **2022**, *223* (21), 2200200. https://doi.org/10.1002/macp.202200200.
(431) Yu, Y.; Hildebrand, M. Development of an Integrated On-Line 2D Analytical TREF-High Throughput SEC Technique for Polyolefins Characterization. *Macromol. Symp.* **2020**, *390* (1), 1900015. https://doi.org/10.1002/masy.201900015.
(432) Zhang, Z. Use of FT-IR Spectrometry for On-Line Detection in Temperature Rising Elution Fractionation. *Macromol. Symp.* **2009**, *282* (1), 111–127. https://doi.org/10.1002/masy.200950812.
(433) Faldi, A.; Soares, J. B. P. Characterization of the Combined Molecular Weight and Composition Distribution of Industrial Ethylene/α-Olefin Copolymers. *Polymer* **2001**, *42* (7), 3057–3066. https://doi.org/10.1016/S0032-3861(00)00664-9.
(434) Nakano, S.; Goto, Y. Development of Automatic Cross Fractionation: Combination of Crystallizability Fractionation and Molecular Weight Fractionation. *J. Appl. Polym. Sci.* **1981**, *26* (12), 4217–4231. https://doi.org/10.1002/app.1981.070261222.
(435) Worch, J. C.; Prydderch, H.; Jimaja, S.; Bexis, P.; Becker, M. L.; Dove, A. P. Stereochemical Enhancement of Polymer Properties. *Nat. Rev. Chem.* **2019**, *3* (9), 514–535. https://doi.org/10.1038/s41570-019-0117-z.
(436) Singh, G.; Kothari, A. V.; Gupta, V. K. Triad Sequence Determination of Ethylene–Propylene Copolymers – Application of Quantitative 13C NMR. *Polym. Test.* **2009**, *28* (5), 475–479. https://doi.org/10.1016/j.polymertesting.2009.02.008.

(437) Trathnigg, B.; Feichtenhofer, S.; Kollroser, M. Quantitation in Liquid Chromatography of Polymers: Size-Exclusion Chromatography with Dual Detection l. *J Chromatogr A* **1997**.

(438) Mager, M.; Berghofer, M.; Fischer, J. Polyolefin Recyclates for Rigid Packaging Applications: The Influence of Input Stream Composition on Recyclate Quality. *Polymers* **2023**, *15* (13), 2776. https://doi.org/10.3390/polym15132776.

(439) Pasch, H.; Brüll, R.; Wahner, U.; Monrabal, B. Analysis of Polyolefin Blends by Crystallization Analysis Fractionation. *Macromol. Mater. Eng.* **2000**, *279* (1), 46–51. https://doi.org/10.1002/1439-2054(20000601)279:1<46::AID-MAME46>3.0.CO;2-1.

(440) Monrabal, B.; del Hierro, P. Characterization of Polypropylene–Polyethylene Blends by Temperature Rising Elution and Crystallization Analysis Fractionation. *Anal. Bioanal. Chem.* **2011**, *399* (4), 1557–1561. https://doi.org/10.1007/s00216-010-4061-5.

(441) *ASTM D6474-99 - Standard Test Method for Determining Molecular Weight Distribution and Molecular Weight Averages of Polyolefins by High Temperature Gel Permeation Chromatography*. https://webstore.ansi.org/standards/astm/astmd647499 (accessed 2023-08-17).

(442) Wang, W.-J.; Zhu, S. Structural Analysis of Ethylene/Propylene Copolymers Synthesized with a Constrained Geometry Catalyst. *Macromolecules* **2000**, *33* (4), 1157–1162. https://doi.org/10.1021/ma991614v.

(443) Zhou, Z.; Kümmerle, R.; Qiu, X.; Redwine, D.; Cong, R.; Taha, A.; Baugh, D.; Winniford, B. A New Decoupling Method for Accurate Quantification of Polyethylene Copolymer Composition and Triad Sequence Distribution with 13C NMR. *J. Magn. Reson.* **2007**, *187* (2), 225–233. https://doi.org/10.1016/j.jmr.2007.05.005.

(444) Busico, V.; Carbonniere, P.; Cipullo, R.; Pellecchia, R.; Severn, J. R.; Talarico, G. Alk-1-Ene Polymerization in the Presence of a Monocyclopentadienyl Zirconium(IV) Acetamidinate Catalyst: Microstructural and Mechanistic Insights. *Macromol. Rapid Commun.* **2007**, *28* (10), 1128–1134. https://doi.org/10.1002/marc.200700098.

(445) Cheng, H. N. Carbon-13 NMR Analysis of Ethylene-Propylene Rubbers. *Macromolecules* **1984**, *17* (10), 1950–1955. https://doi.org/10.1021/ma00140a012.

(446) Scoppio, A.; Cavallo, D.; Müller, A. J.; Tranchida, D. Temperature Modulated DSC for Composition Analysis of Recycled Polyolefin Blends. *Polym. Test.* **2022**, *113*, 107656. https://doi.org/10.1016/j.polymertesting.2022.107656.

(447) Cheruthazhekatt, S.; Pijpers, T. F. J.; Mathot, V. B. F.; Pasch, H. Combination of TREF, High-Temperature HPLC, FTIR and HPer DSC for the Comprehensive Analysis of Complex

Polypropylene Copolymers. *Anal. Bioanal. Chem.* **2013**, *405* (28), 8995–9007. https://doi.org/10.1007/s00216-013-6955-5.

(448) Shirayama, K.; Okada, T.; Kita, S.-I. Distribution of Short-Chain Branching in Low-Density Polyethylene. *J. Polym. Sci. A* **1965**, *3* (3), 907–916. https://doi.org/10.1002/pol.1965.100030306.

(449) Floyd, W. H., S; Heiskanen, T; Ray. Solid Catalyzed Olefin Polymerization. *Chem. Eng. Prog.* **1988**.

(450) Zucchini, U.; Cecchin, G. Control of Molecular-Weight Distribution in Polyolefins Synthesized with Ziegler-Natta Catalytic Systems. In *Industrial Developments*; Advances in Polymer Science; Springer-Verlag: Berlin/Heidelberg, 1983; Vol. 51, pp 101–153. https://doi.org/10.1007/BFb0017586.

(451) Touloupidis, V. Catalytic Olefin Polymerization Process Modeling: Multi-Scale Approach and Modeling Guidelines for Micro-Scale/Kinetic Modeling: Catalytic Olefin Polymerization Process Modeling:…. *Macromol. React. Eng.* **2014**, *8* (7), 508–527. https://doi.org/10.1002/mren.201300188.

(452) *Multimodal Polymers with Supported Catalysts: Design and Production*; Albunia, A. R., Prades, F., Jeremic, D., Eds.; Springer International Publishing: Cham, 2019. https://doi.org/10.1007/978-3-030-03476-4.

(453) Gahleitner, M.; Tranninger, C.; Doshev, P. Heterophasic Copolymers of Polypropylene: Development, Design Principles, and Future Challenges. *J. Appl. Polym. Sci.* **2013**, *130* (5), 3028–3037. https://doi.org/10.1002/app.39626.

(454) Paukkeri, R.; Lehtinen, A. Thermal Behaviour of Polypropylene Fractions: 1. Influence of Tacticity and Molecular Weight on Crystallization and Melting Behaviour. *Polymer* **1993**, *34* (19), 4075–4082. https://doi.org/10.1016/0032-3861(93)90669-2.

(455) Bhati, S.; Macko, T.; Brüll, R. Quantification of Identical and Unique Segments in Ethylene-Propylene Copolymers Using Two Dimensional Liquid Chromatography with Infra-Red Detection. *Polyolefins J.* **2016**, *3* (2). https://doi.org/10.22063/poj.2016.1323.

(456) Swinehart, D. F. The Beer-Lambert Law. *J. Chem. Educ.* **1962**, *39* (7), 333. https://doi.org/10.1021/ed039p333.

(457) Frijns-Bruls, T.; Ortin, A.; Weusten, J.; Geladé, E. Studies on the Use of Filter-Based IR Detector for Short-Chain Branching Characterization of Polyolefin Copolymers with High Temperature Size Exclusion Chromatography. *Polymer* **2019**, *180*, 121600. https://doi.org/10.1016/j.polymer.2019.121600.

(458) Coto, B.; Escola, J. M.; Suárez, I.; Caballero, M. J. Determination of Dn/Dc Values for Ethylene–Propylene Copolymers. *Polym. Test.* **2007**, *26* (5), 568–575. https://doi.org/10.1016/j.polymertesting.2007.02.001.

(459) Frijns-Bruls, T.; Ortin, A.; Weusten, J.; Geladé, E. Studies on the Application of Filter-Based IR Detector for Polyolefin Characterization with HT-SEC. *Macromol. Symp.* **2015**, *356* (1), 87–94. https://doi.org/10.1002/masy.201500077.

(460) Eriksen, M. K.; Christiansen, J. D.; Daugaard, A. E.; Astrup, T. F. Closing the Loop for PET, PE and PP Waste from Households: Influence of Material Properties and Product Design for Plastic Recycling. *Waste Manag.* **2019**, *96*, 75–85. https://doi.org/10.1016/j.wasman.2019.07.005.

(461) Brachet, P.; Høydal, L. T.; Hinrichsen, E. L.; Melum, F. Modification of Mechanical Properties of Recycled Polypropylene from Post-Consumer Containers. *Waste Manag.* **2008**, *28* (12), 2456–2464. https://doi.org/10.1016/j.wasman.2007.10.021.

(462) Garcia-Vazquez, H. D.; Martinez-Hernandez, H. D.; Trujillo-Barragan, M.; Mondragon-Flores, E.; Rodriguez-Juarez, M. E.; Millan-Malo, B. M.; Villada-Villalobos, J. A.; Rodriguez-Garcia, M. E. Impact of Thermomechanical Reprocessing Conditions on Polypropylene Composites Made from Automotive Waste Parts: A Path to a Circular Economy. *Polym. Eng. Sci.* **2023**, *63* (7), 2031–2042. https://doi.org/10.1002/pen.26343.

(463) Tratzi, P.; Giuliani, C.; Torre, M.; Tomassetti, L.; Petrucci, R.; Iannoni, A.; Torre, L.; Genova, S.; Paolini, V.; Petracchini, F.; Di Carlo, G. Effect of Hard Plastic Waste on the Quality of Recycled Polypropylene Blends. *Recycling* **2021**, *6* (3), 58. https://doi.org/10.3390/recycling6030058.

(464) Price, F. P. Nucleation in Polymer Crystallization. *Nucleation* **1969**.

(465) Wunderlich, B. Structural Data on Crystalline Polymers by Thermal Analysis. *J. Polym. Sci. Polym. Symp.* **2007**, *43* (1), 29–42. https://doi.org/10.1002/polc.5070430106.

(466) Gahleitner, M.; Wolfschwenger, J.; Mileva, D. Polymer Crystal Nucleating Agents. In *Reference Module in Materials Science and Materials Engineering*; Elsevier, 2016; p B9780128035818037735. https://doi.org/10.1016/B978-0-12-803581-8.03773-5.

(467) Guo, Z.; Xin, R.; Hu, J.; Li, Y.; Sun, X.; Yan, S. Direct High-Temperature Form I Crystallization of Isotactic Poly(1-Butene) Assisted by Oriented Isotactic Polypropylene. **2019**, 8.

(468) Zhou, H.; Jiang, S.; Yan, S. Epitaxial Crystallization of Poly(3-Hexylthiophene) on a Highly Oriented Polyethylene Thin Film from Solution. *J. Phys. Chem. B* **2011**, *115* (46), 13449–13454. https://doi.org/10.1021/jp205755r.

(469) Lotz, B.; Wittmann, J. C. Structural Relationships in Blends of Isotactic Polypropylene and Polymers with Aliphatic Sequences. *J. Polym. Sci. Part B Polym. Phys.* **1986**, *24* (7), 1559–1575. https://doi.org/10.1002/polb.1986.090240713.

(470) Yan, S.; Yang, D.; Petermann, J. Controlling Factors for the Occurrence of Heteroepitaxy of Polyethylene on Highly Oriented Isotactic Polypropylene. *Polymer* **1998**, *39* (19), 4569–4578. https://doi.org/10.1016/S0032-3861(97)10137-9.

(471) Wang, W.; Buzzi, S.; Fenni, S. E.; Carmeli, E.; Wang, B.; Liu, G.; Müller, A. J.; Cavallo, D. Surface Nucleation of Dispersed Droplets in Double Semicrystalline Immiscible Blends with Different Matrices. *Macromol. Chem. Phys.* **2022**, 2200202. https://doi.org/10.1002/macp.202200202.

(472) Córdova, M. E.; Lorenzo, A. T.; Müller, A. J.; Gani, L.; Tencé-Girault, S.; Leibler, L. The Influence of Blend Morphology (Co-Continuous or Sub-Micrometer Droplets Dispersions) on the Nucleation and Crystallization Kinetics of Double Crystalline Polyethylene/Polyamide Blends Prepared by Reactive Extrusion: The Influence of Blend Morphology (Co-Continuous or Sub-Micrometer Droplets Dispersions) …. *Macromol. Chem. Phys.* **2011**, *212* (13), 1335–1350. https://doi.org/10.1002/macp.201100039.

(473) Wang, B.; Utzeri, R.; Castellano, M.; Stagnaro, P.; Müller, A. J.; Cavallo, D. Heterogeneous Nucleation and Self-Nucleation of Isotactic Polypropylene Microdroplets in Immiscible Blends: From Nucleation to Growth-Dominated Crystallization. *Macromolecules* **2020**, *53* (14), 5980–5991. https://doi.org/10.1021/acs.macromol.0c01167.

(474) Sangroniz, L.; Wang, B.; Su, Y.; Liu, G.; Cavallo, D.; Wang, D.; Müller, A. J. Fractionated Crystallization in Semicrystalline Polymers. *Prog. Polym. Sci.* **2021**, *115*, 101376. https://doi.org/10.1016/j.progpolymsci.2021.101376.

(475) Fenni, S. E.; Caputo, M. R.; Müller, A. J.; Cavallo, D. Surface Roughness Enhances Self-Nucleation of High-Density Polyethylene Droplets Dispersed within Immiscible Blends. *Macromolecules* **2022**, *55* (4), 1412–1423. https://doi.org/10.1021/acs.macromol.1c02487.

(476) Chaffin, K. A.; Bates, F. S.; Brant, P.; Brown, G. M. Semicrystalline Blends of Polyethylene and Isotactic Polypropylene: Improving Mechanical Performance by Enhancing the Interfacial Structure. *J. Polym. Sci. Part B Polym. Phys.* **2000**, *38* (1), 108–121. https://doi.org/10.1002/(SICI)1099-0488(20000101)38:1<108::AID-POLB14>3.0.CO;2-9.

(477) Poon, B. C.; Chum, S. P.; Hiltner, A.; Baer, E. Adhesion of Polyethylene Blends to Polypropylene. *Polymer* **2004**, *45* (3), 893–903. https://doi.org/10.1016/j.polymer.2003.11.018.

(478) Jordan, A. M.; Kim, K.; Soetrisno, D.; Hannah, J.; Bates, F. S.; Jaffer, S. A.; Lhost, O.; Macosko, C. W. Role of Crystallization on Polyolefin Interfaces: An Improved Outlook for Polyolefin Blends. *Macromolecules* **2018**, *51* (7), 2506–2516. https://doi.org/10.1021/acs.macromol.8b00206.

(479) International, A. D1601 - 20 Standard Test Method for Analysis of Ethylene Glycols and Propylene Glycols by Gas Chromatography, 2023. https://www.astm.org/standard/D1601.html.

(480) Sangroniz, L.; Cavallo, D.; Müller, A. J. Self-Nucleation Effects on Polymer Crystallization. *Macromolecules* **2020**, *53* (12), 4581–4604. https://doi.org/10.1021/acs.macromol.0c00223.

(481) Gee, D. R.; Melia, T. P. Thermal Properties of Melt and Solution Crystallized Isotactic Polypropylene. *Makromol. Chem.* **1970**, *132* (1), 195–201. https://doi.org/10.1002/macp.1970.021320117.

(482) Lanyi, F. J.; Wenzke, N.; Kaschta, J.; Schubert, D. W. On the Determination of the Enthalpy of Fusion of α-Crystalline Isotactic Polypropylene Using Differential Scanning Calorimetry, X-Ray Diffraction, and Fourier-Transform Infrared Spectroscopy: An Old Story Revisited. *Adv. Eng. Mater.* **2020**, *22* (9), 1900796. https://doi.org/10.1002/adem.201900796.

(483) Wunderlich, B.; Czornyj, G. A Study of Equilibrium Melting of Polyethylene. *Macromolecules* **1977**, *10* (5), 906–913. https://doi.org/10.1021/ma60059a006.

(484) Mirabella, F. M.; Bafna, A. Determination of the Crystallinity of Polyethylene/?-Olefin Copolymers by Thermal Analysis: Relationship of the Heat of Fusion of 100% Polyethylene Crystal and the Density. *J. Polym. Sci. Part B Polym. Phys.* **2002**, *40* (15), 1637–1643. https://doi.org/10.1002/polb.10228.

(485) H.M. Ayad, M. R. Ahmed; Abou-El-Enein, M. A. Crystallization Behavior and Thermal Properties of Polypropylene/High-Density Polyethylene Blends. *J. Appl. Polym. Sci.* **2011**, *119* (6), 3202–3210.

(486) Gill, J. K. Blends of Polypropylene and Polyethylene: Morphology and Properties. *Polymer* **1994**, *35* (4), 794–803.

(487) Balakrishnan, J.; Sadasivuni, S. S. Polypropylene/Polyethylene Blends: Structure, Properties, and Processing. *Polym.-Plast. Technol. Eng.* **2009**, *48* (4), 413–432.

(488) Fenni, S. E.; Spigno, M.; Wang, W.; Costanzo, A.; Müller, A. J.; Cavallo, D. How Nucleating Particles Migration Affects the Fractionated Crystallization of Isotactic Polypropylene/Polystyrene Immiscible Blends. *Thermochim. Acta* **2023**, *719*, 179407. https://doi.org/10.1016/j.tca.2022.179407.

(489) Gałeski, A.; Bartczak, Z.; Pracella, M. Spherulite Nucleation in Polypropylene Blends with Low Density Polyethylene. *Polymer* **1984**, *25* (9), 1323–1326. https://doi.org/10.1016/0032-3861(84)90384-7.

(490) *Polymer Blends: Preparation, Properties, and Applications*; Matyjaszewski, K., Möller, M., Eds.; John Wiley & Sons, 2006.

(491) *Handbook of Polymer Synthesis, Characterization, and Processing*; Nebe, B., Ed.; Springer, 2017.

(492) Arnal, M. L.; Matos, M. E.; Morales, R. A.; Santana, O. O.; Müuller, A. J. Evaluation of the Fractionated Crystallization of Dispersed Polyolefins in a Polystyrene Matrix. *Macromol. Chem. Phys.* **1998**, *199* (10), 2275–2288. https://doi.org/10.1002/(SICI)1521-3935(19981001)199:10<2275::AID-MACP2275>3.0.CO;2-#.

(493) Chandrasekhar, S. Stochastic Problems in Physics and Astronomy. *Rev Mod Phys* **1943**, *15* (1), 1–89. https://doi.org/10.1103/RevModPhys.15.1.

(494) Yan, S.; Yang, D. Critical Crystallization Temperature for the Occurrence of Epitaxy between High-Density Polyethylene and Isotactic Polypropylene. *J. Appl. Polym. Sci.* **1997**, *66* (10), 2029–2034. https://doi.org/10.1002/(SICI)1097-4628(19971205)66:10<2029::AID-APP20>3.0.CO;2-Y.

Publications

1. Góra, M.; Tranchida, D.; Albrecht, A.; Müller, A. J.; Cavallo, D.; Fast successive self-nucleation and annealing (SSA) thermal fractionation protocol for the characterization of polyolefin blends from mechanical recycling, J. Polym. Sci. **2022**, 1; https://doi.org/10.1002/pol.20220104.
2. Góra, M.; Coba-Daza, S.; Carmeli, E.; Tranchida, D.; Albrecht, A.; Müller, A.J.; Cavallo, D.; Surface-enhanced nucleation in immiscible polypropylene and polyethylene blends: The effect of polyethylene chain regularity, Polymer, **2023**;126180. https://doi.org/10.1016/j.polymer.2023.126180.
3. Góra, M.; Tranchida, D.; Albrecht, A.; Müller, A. J.; Cavallo, D.; A novel approach for accurate determination of polyethylene and polypropylene content in polyolefin blends and recyclates by cross-fractionation chromatography, Polym. Test. **2024**, 131, 108351; https://doi.org/10.1016/j.polymertesting.2024.108351.

Appendix A: Supporting information to Chapter 3

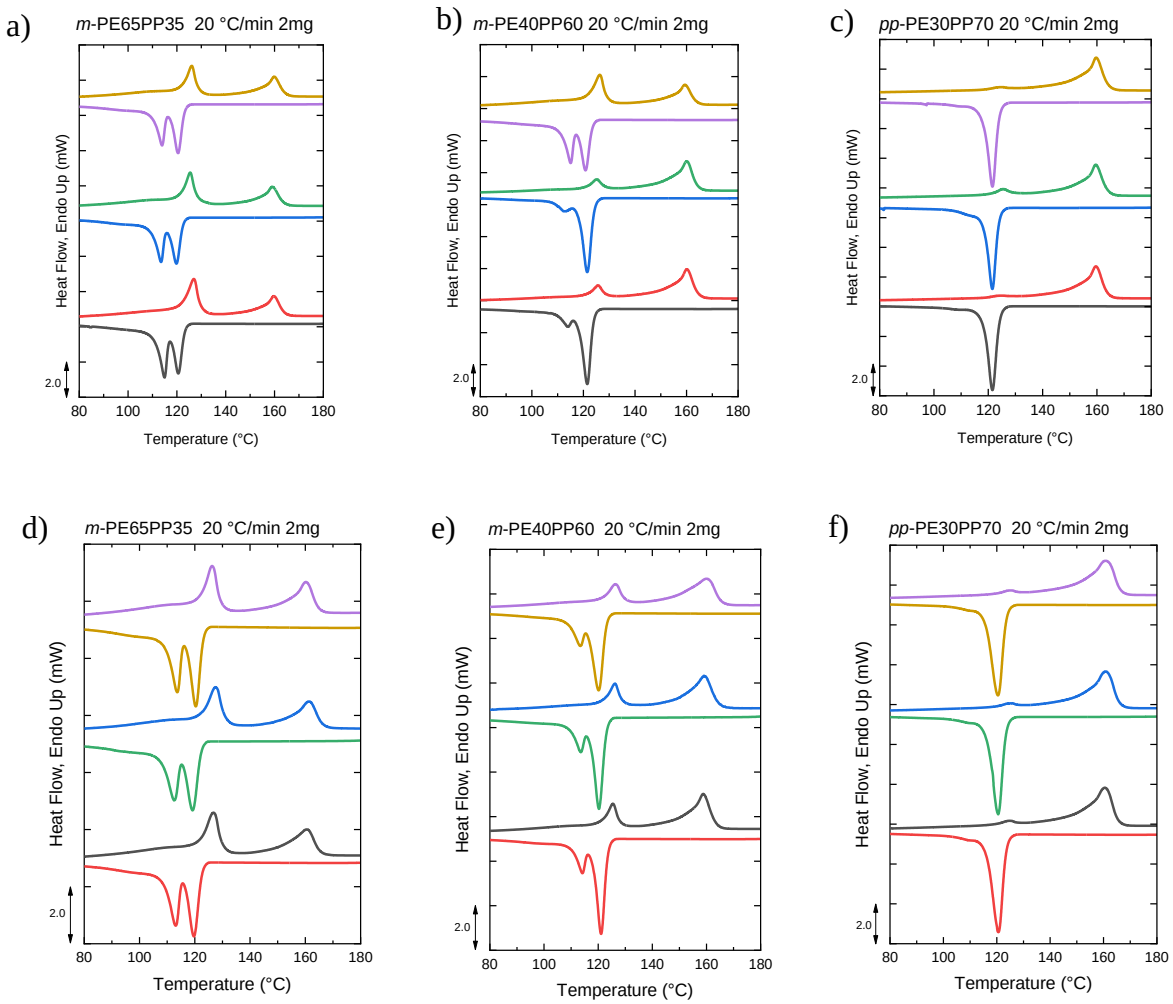

Figure S1 Blends employed in this work, which needed to be homogenized; scans rate: 20°C/min DSC cooling scans from the melt and a subsequent DSC heating scan, before homogenization: a) m-PE65PP35 b) m-PE40PP60 c) pp-PE30PP70 after homogenization: d) m-PE65PP35 e) m-PE40PP60 f) pp-PE30PP70.

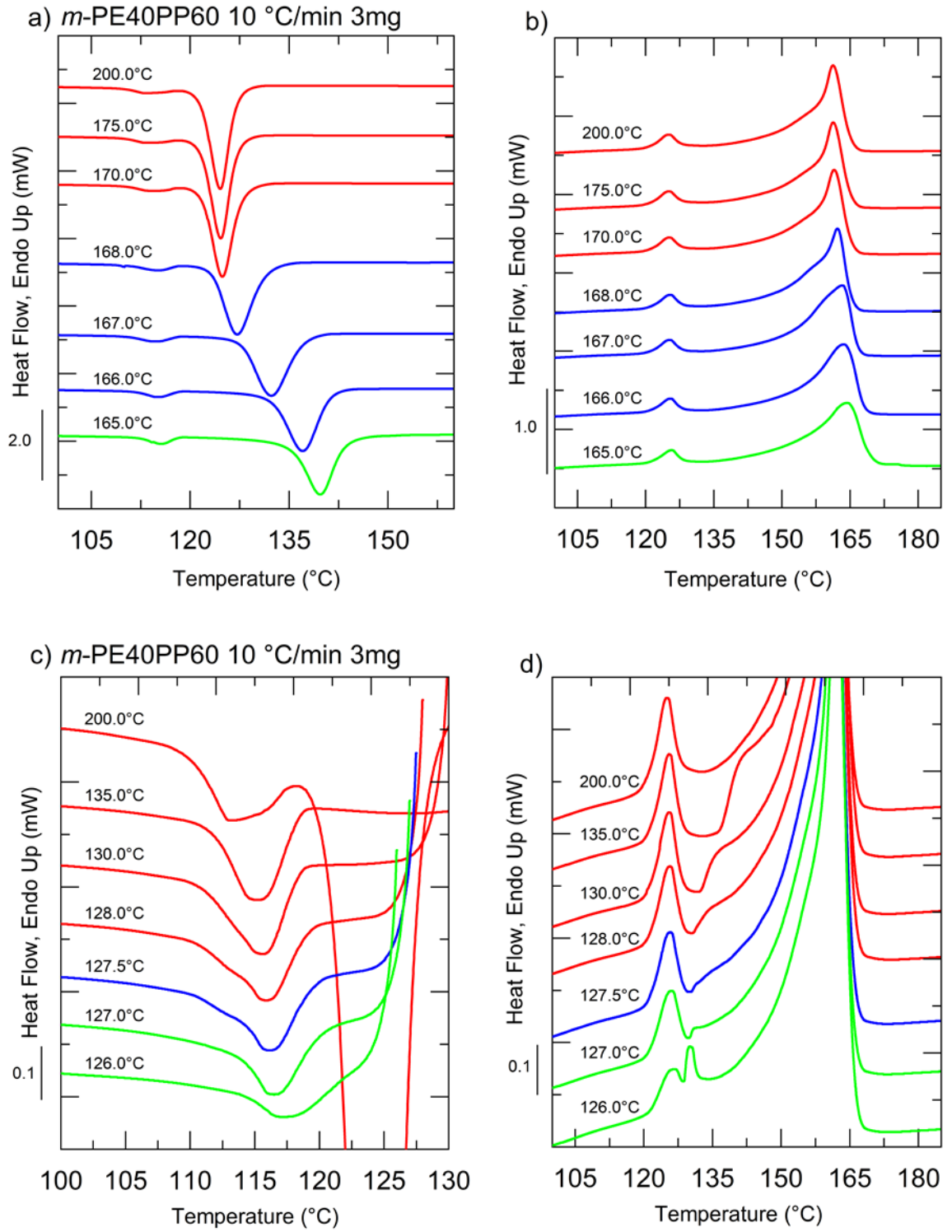

Figure S2 Ts ideal selection form m-PE40PP60 a) DSC cooling scans at 10°C/min after 5 min at the indicated Ts for polypropylene in recycled polyolefin blend b) subsequent heating scans (at 10 °C/min) after cooling runs shown in a). c) DSC cooling scans at 10°C/min after 5 min at the indicated Ts for polyethylene in recycled polyolefin blend d) subsequent heating scans (at 10 °C/min) after cooling runs shown in c) Colors of the lines in the graphs indicating material under certain domains: red lines - Domain I, blue lines- Domain II, green lines - Domain III. The occurrence of an annealing peak in the PE and PP phase is highlighted as a separate inset next to the corresponding curve.

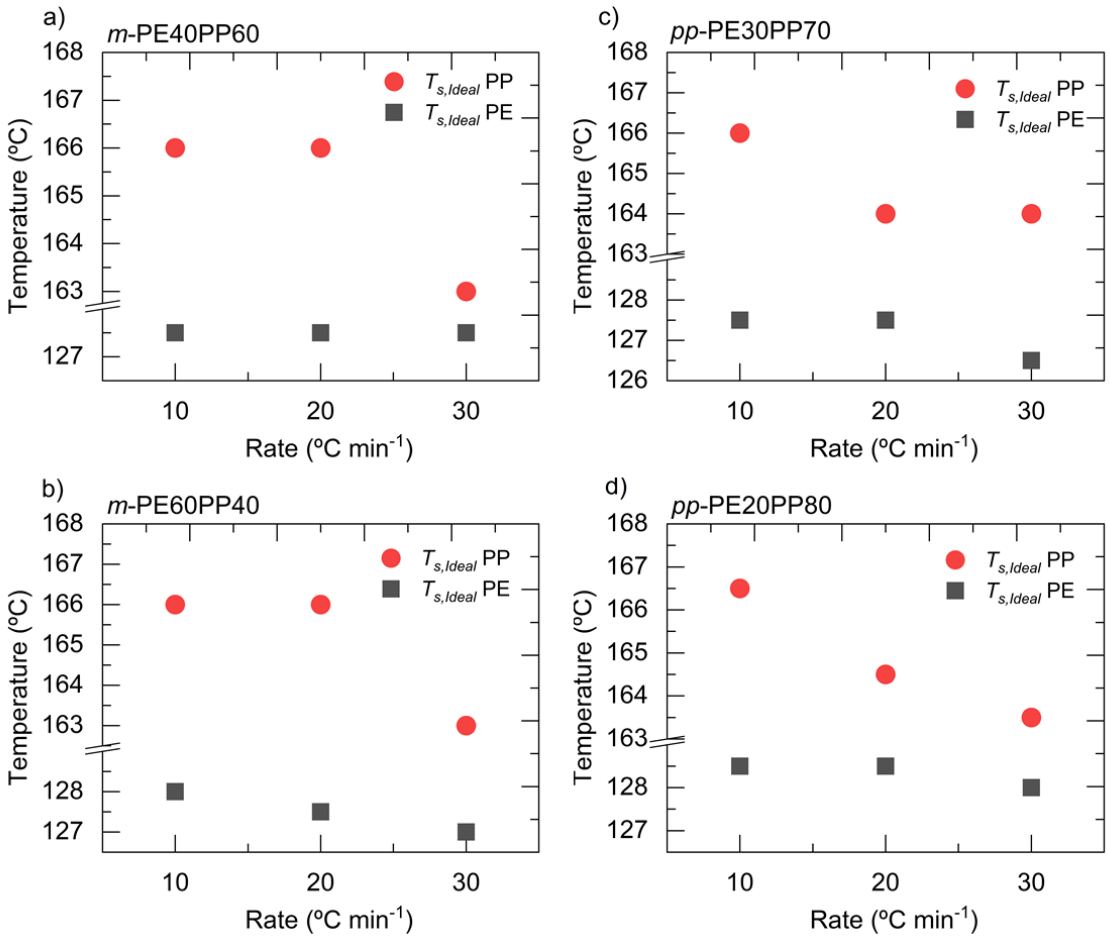

Figure S3 Different $T_{s,Ideal}$ vs rate used during the measurement starting front the upper-left m-PE60PP40 (a), top-right m-PE40PP60 (b), bottom-left pp-PE30PP70 (c) and bottom-right pp-PE20PP80 (d).

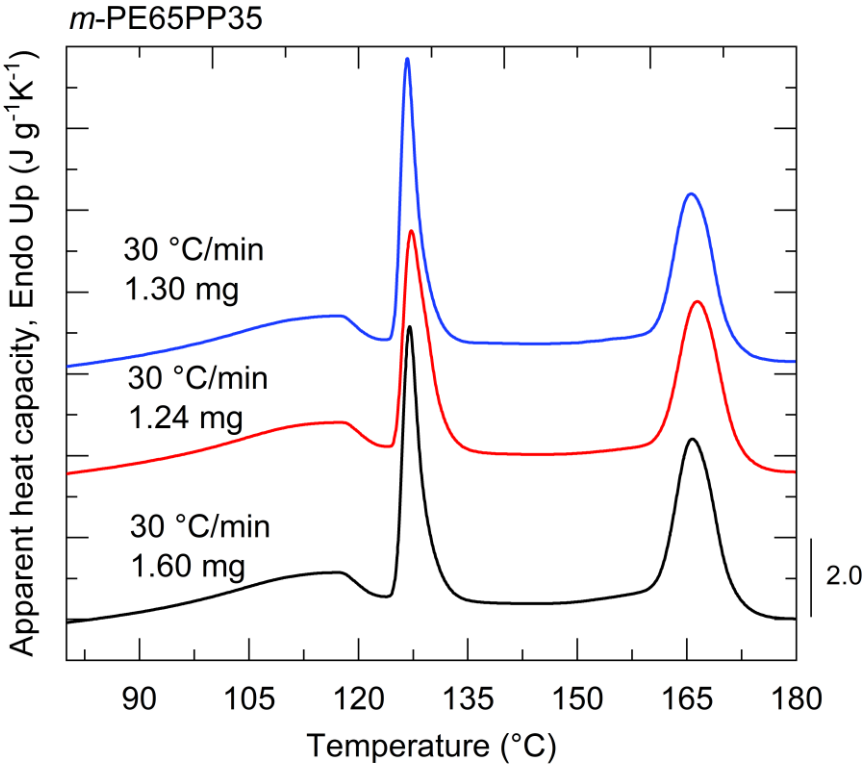

Figure S4 Three runs of m-PE65PP35 at 30 °C/min for the error calculation.

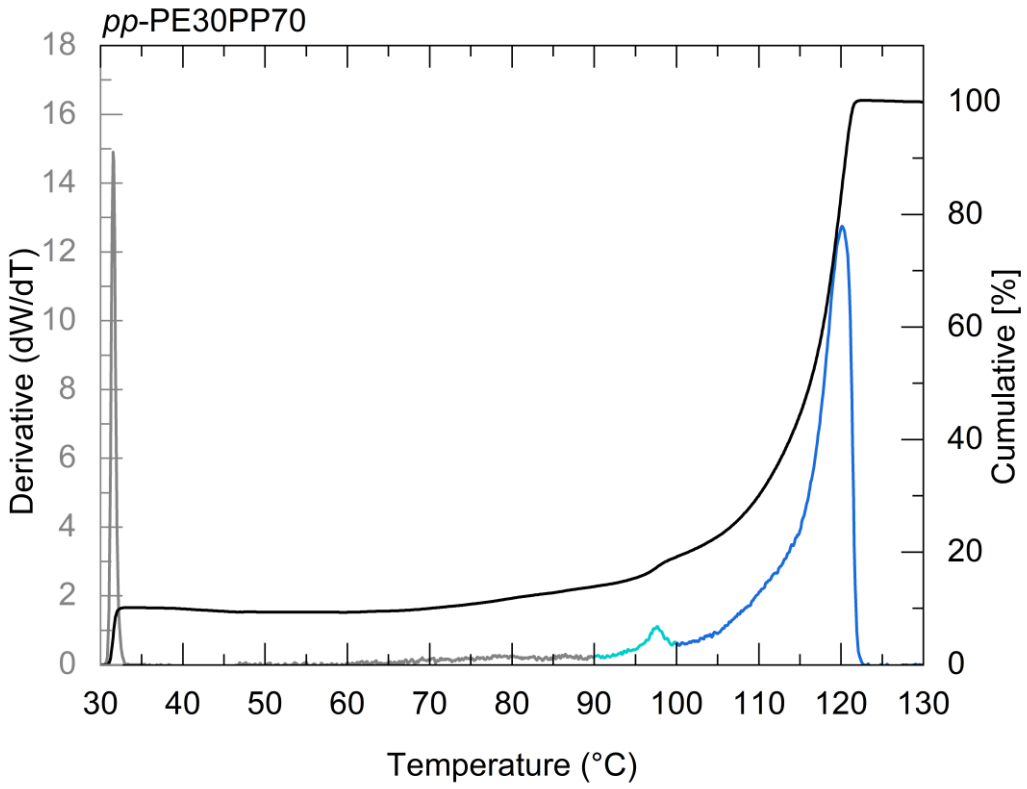

Figure S5 TREF analysis of pp-PE30PP70 for composition calculations as an industrial standard method.

Appendix B: Supporting information to Chapter 4

Table S1 Gathered data of the 17 blends and neat PP and PE, which shows the basic thermal properties, measured by DSC.

Name	Tm PP [ºC]	Tm PE [ºC]	ΔHm PP [J/g]	ΔHm PE [J/g]	Tc [ºC]	PP [wt%]	PE [wt%]
PE	-	127.5	-	173.3	115.7	-	100.0
PP/PE - 1.7/98.3	161.1	127.8	1.0	171.0	115.6	0.9	99.1
PP/PE - 2.2/97.8	161.2	127.9	1.7	171.1	115.6	1.6	98.4
PP/PE - 3.2/96.8	161.5	127.8	2.2	171.9	115.7	2.0	98.0
PP/PE - 4.2/95.8	161.7	127.7	3.1	168.4	115.6	2.9	97.1
PP/PE - 5.2/94.8	161.6	127.7	3.1	166.0	115.6	3.0	97.0
PP/PE - 6.2/93.8	161.9	128.3	4.7	158.5	115.2	4.6	95.4
PP/PE - 11.2/88.8	161.9	128.1	8.2	147.9	115.5	8.3	91.7
PP/PE - 21.3/78.7	160.7	128.2	15.6	133.5	114.7/116.4	16.0	84.0
PP/PE - 61.4/38.6	160.9	127.6	44.7	57.8	116.6	55.7	44.3
PP/PE - 81.4/18.6	160.9	126.9	61.4	24.0	116.2	80.6	19.4
PP/PE - 91.5/8.5	161.9	126.6	72.2	8.4	116.1	93.4	6.6
PP/PE - 96.5/3.5	161.2	126.3	73.7	2.9	115.9	97.6	2.4
PP/PE - 97.5/2.5	160.4	126.6	74.0	1.6	115.2	98.7	1.3
PP/PE - 98.5/1.5	160.6	126.7	78.3	0.9	114.7	99.3	0.7
PP/PE - 99.5/0.5	161.0	128.7	79.8	0.3	114.9	99.7	0.3
PP/PE - 99.3/0.7	161.5	126.6	78.8	0.6	114.4	99.5	0.5
PP/PE - 99.8/0.2	162.1	126.4	79.1	0.2	115.7	99.9	0.1
PP	161.1	-	106.6	-	112.9	100.0	

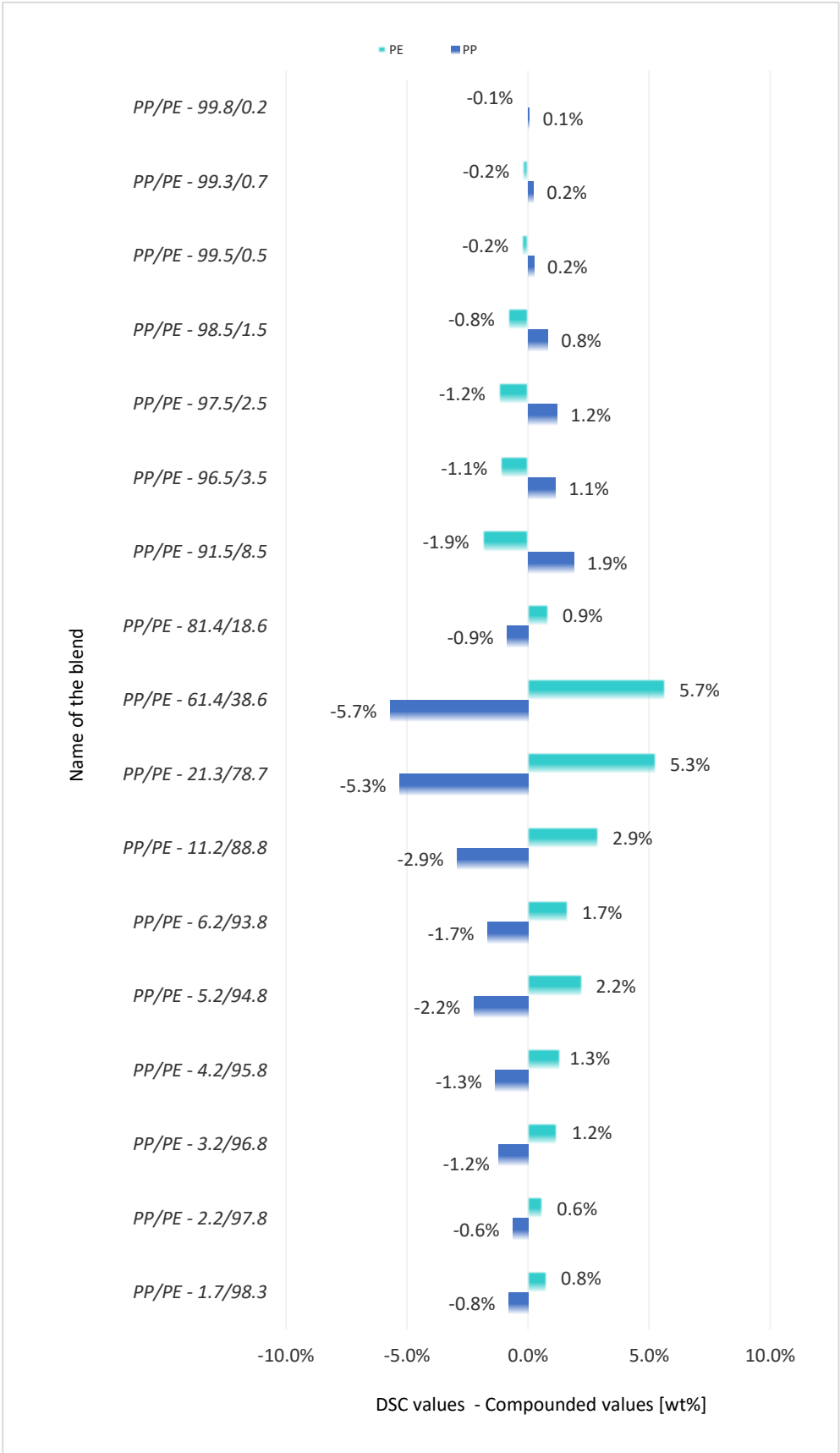

Figure S1 Bar chart illustrating differences between DSC values and compounded PP and PE content across 17 blends. The y-axis enumerates the 17 different blends, labelled by their respective PP and PE percentages, such as PP/PE - 1.7/98.3. The x-axis quantifies the percentage differences. The bars are distinguished by color, with polyethylene (PE) in light blue and polypropylene (PP) in blue.

Table S2 Data obtained from the series of the measurement of the 17 blends from processing, NMR, TREF before compensation and accordingly, values after detector factor and PP elution in the PE temperature range compensation.

	Processing		NMR		TREF(CFC)		TREF(CFC) d ^{mat} correction		TREF(CFC) d ^{mat} correction + PP in PE range correction	
Name	**PP [wt%]**	**PE [wt%]**	**PP [wt%]**	**PE [wt%]**	**PP [wt%]**	**PE[wt%]**	**PP [wt%]**	**PE [wt%]**	**PP [wt%]**	**PE [wt%]**
PP/PE - 1.7/98.3	1.7	98.3	1.8	98.2	0.7	99.3	0.7	99.3	0.7	99.3
PP/PE - 2.2/97.8	2.2	97.8	2.4	97.6	1.7	98.3	1.9	98.1	2.0	98.0
PP/PE - 3.2/96.8	3.2	96.8	3.1	96.9	2.4	97.6	2.7	97.3	2.8	97.2
PP/PE - 4.2/95.8	4.2	95.8	4.5	95.5	2.9	97.1	3.3	96.7	3.4	96.6
PP/PE - 5.2/94.8	5.2	94.8	4.9	95.1	3.5	96.5	3.8	96.2	4.0	96.0
PP/PE - 6.2/93.8	6.2	93.8	6.0	94.0	4.6	95.4	5.0	95.0	5.2	94.8
PP/PE - 11.2/88.8	11.2	88.8	11.0	89.0	7.8	92.2	8.5	91.5	8.8	91.2
PP/PE - 21.3/78.7	21.3	78.7	21.6	78.4	17.4	82.6	18.8	81.2	19.6	80.4
PP/PE - 61.4/38.6	61.4	38.6	61.5	38.5	54.1	45.9	56.5	43.5	58.9	41.1
PP/PE - 81.4/18.6	81.4	18.6	81.7	18.3	76.6	23.4	78.5	21.5	81.8	18.2
PP/PE - 91.5/8.5	91.5	8.5	91.8	8.2	85.5	14.5	86.8	13.2	90.7	9.3
PP/PE - 96.5/3.5	96.5	3.5	96.6	3.4	90.2	9.8	91.1	8.9	95.2	4.8
PP/PE - 97.5/2.5	97.5	2.5	97.9	2.1	91.7	8.3	92.5	7.5	96.4	3.6
PP/PE - 98.5/1.5	98.5	1.5	98.7	1.3	92.9	7.1	93.7	6.3	97.9	2.1

PP/PE - 99.5/0.5	99.5	0.5	99.5	0.5	93.5	6.5	94.2	5.8	98.3	1.7
PP/PE - 99.3/0.7	99.3	0.7	99.3	0.8	93.5	6.5	94.1	5.9	98.1	1.9
PP/PE - 99.8/0.2	99.8	0.2	99.8	0.2	93.9	6.1	94.5	5.5	98.6	1.4

Table S3 Gathered values of the PP elution in the PE temperature range and the viscosity-average molecular weight (M_v) of those PP, which were investigated in this study.

Sample name	PP in PE range [wt%]	Mv [g/mol] 103 -130ºC
PP-1	48.6	31000
PP-2	12.9	80000
PP-3	15.5	97000
PP-4	10.5	105000
PP-5	9.5	113000
PP-6	8.6	117000
PP-7	9.1	118000
PP-8	10.3	127000
PP-9	8.4	128000
PP-10	5.8	244000
PP-11	4.3	318000
PP-12	4.3	325000
PP-13	3.0	412000

Table S4 Ethylene-Propylene Copolymers (EPC) utilized for detector factor validation in this study.

Sample name	**CH_3/1000TC**
EPC-1	326.7
EPC-2	316.6
EPC-3	308.5
EPC-4	304.9
EPC-5	286.4
EPC-6	271.1
EPC-7	171.5
EPC-8	148.3
EPC-9	103.3
EPC-10	0

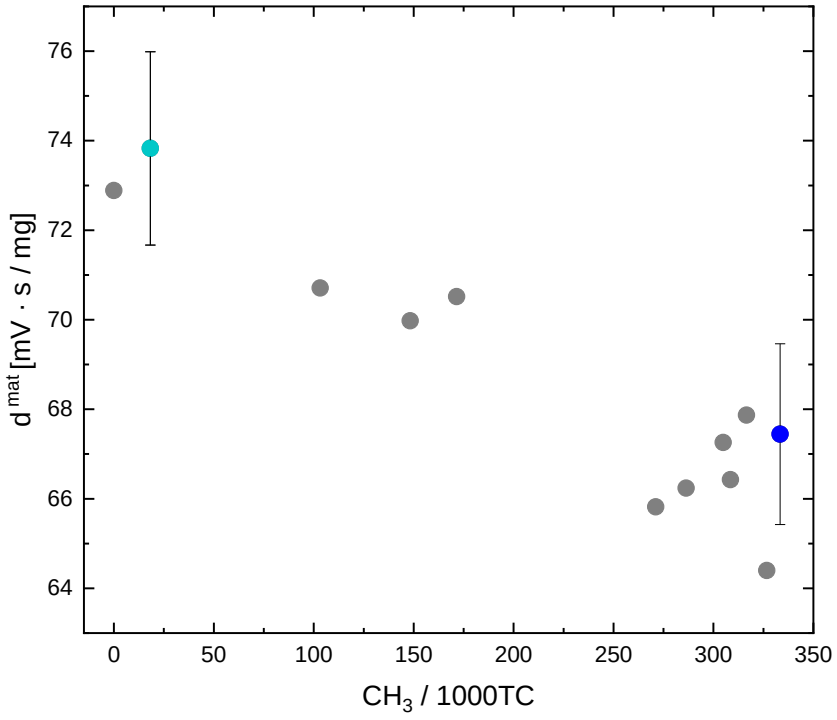

Figure S2 Scatter plot illustrating the correlation between detector factor (d^{mat}) and CH3/1000TC ratio for various ethylene-propylene copolymers. Polymers with a higher proportion of methyl groups correspondingly exhibit lower detector factors.

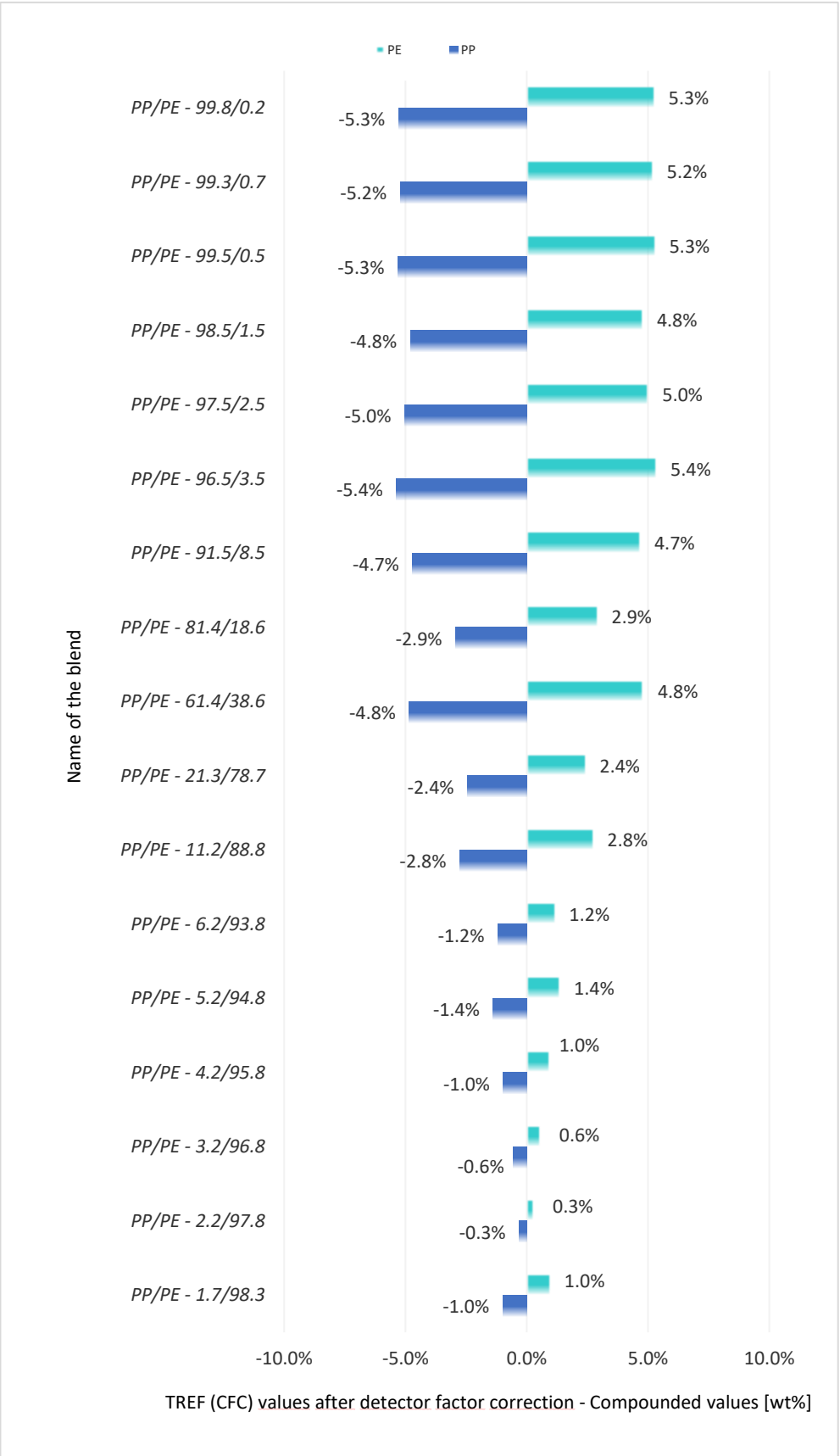

Figure S3 Bar chart comparing TREF (CFC) values after application of detector factor correction vs. compounded values. The y-axis categorizes 17 different blends, designated by their respective PP and PE contents. The x-axis displays the percentage differences. The bars are color-coded, with polyethylene (PE) shown in light blue and polypropylene (PP) in blue.

Table S5 Data obtained from the series of the measurement of 3 validation blends from processing, TREF before compensation and accordingly, values after detector factor and PP elution in the PE temperature range compensation.

	Processing		TREF(CFC)		TREF(CFC) d ^{mat} correction		TREF(CFC) d ^{mat} correction + PP in PE range correction	
Name	**PP [wt%]**	**PE [wt%]**	**PP [wt%]**	**PE[wt%]**	**PP [wt%]**	**PE [wt%]**	**PP [wt%]**	**PE [wt%]**
V1-PP/PE	51.8	48.2	49.2	50.8	51.4	48.6	53.4	46.6
V2-PP/PE	50.5	49.5	48.5	51.5	50.8	49.2	52.6	47.4
V3-PP/PE	53.7	46.3	46.2	53.8	48.4	51.6	52.8	47.2

Table S6 Data obtained from the series of the measurement of the 3 post-consumer recycled blends from NMR, TREF before compensation and accordingly, values after detector factor and PP elution in the PE temperature range compensation.

	NMR		TREF(CFC)		TREF(CFC) d ^{mat} correction		TREF(CFC) d ^{mat} correction + PP in PE range correction	
Name	**PP [wt%]**	**PE [wt%]**	**PP [wt%]**	**PE[wt%]**	**PP [wt%]**	**PE [wt%]**	**PP [wt%]**	**PE [wt%]**
PCR-1	72.1	27.9	63.9	36.1	66.0	34.0	70.8	29.2
PCR-2	51.3	48.7	44.2	55.8	46.5	53.5	49.4	50.6
PCR-3	92.2	7.8	85.0	15.0	86.1	13.9	92.1	7.9

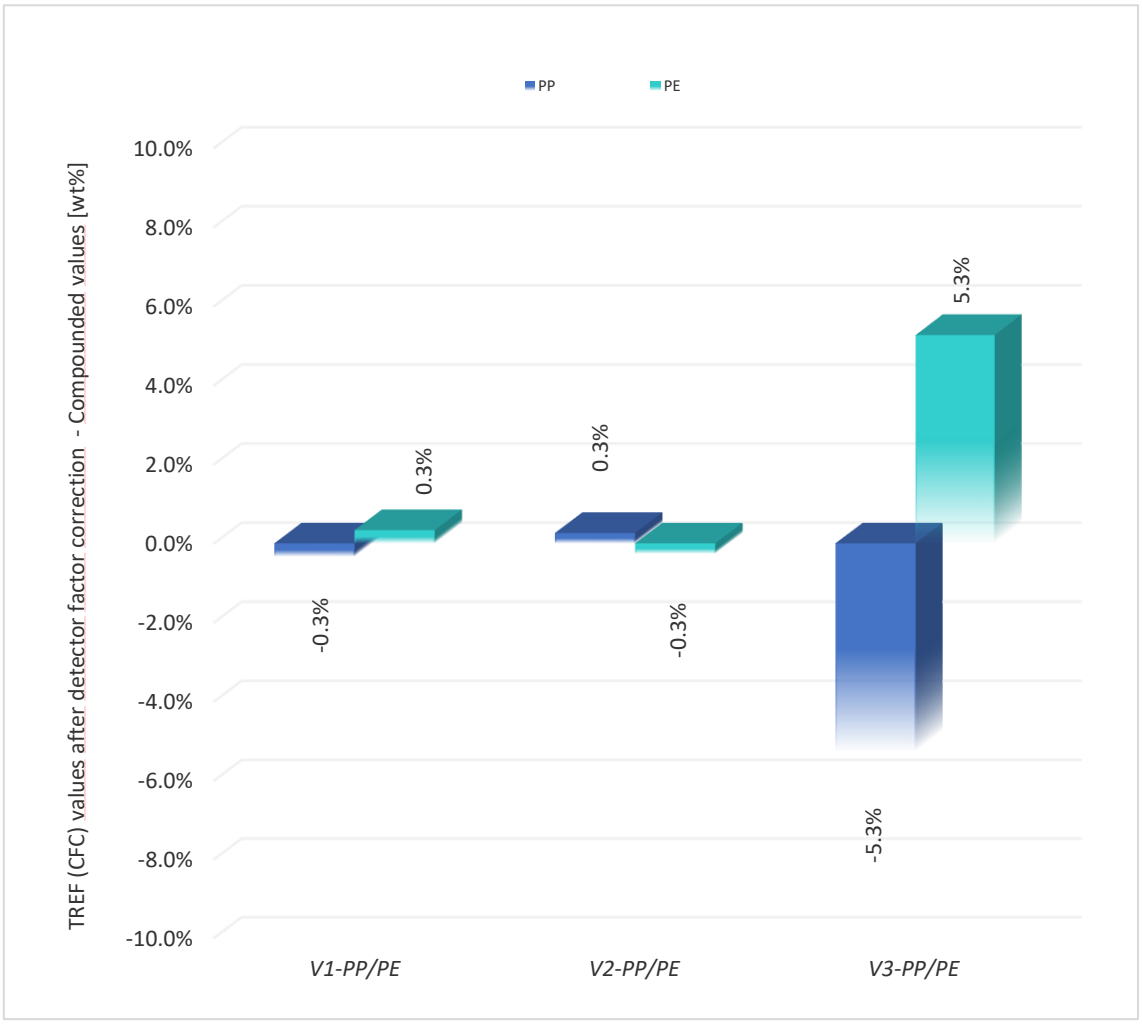

Figure S3 Bar chart comparing TREF (CFC) values after application of detector factor correction vs. compounded values. The x-axis categorizes 3 different validation blends. The y-axis displays the percentage differences. The bars are color-coded, with polyethylene (PE) shown in light blue and polypropylene (PP) in blue.

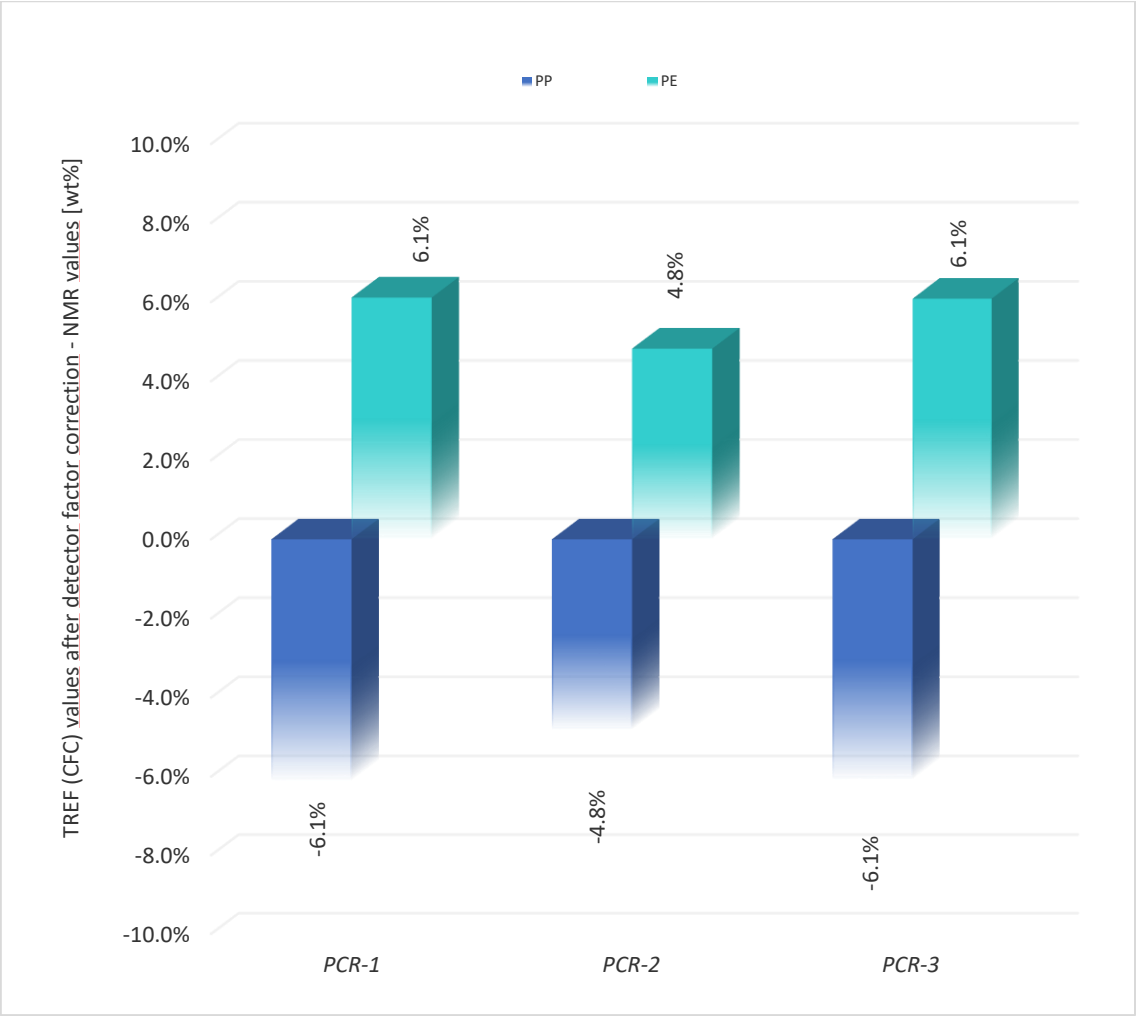

Figure S4 Bar chart comparing TREF (CFC) values after applying detector factor vs. the amount of the PE and PP calculated by NMR. The x-axis categorizes 3 different PCR blends. The y-axis displays the percentage differences. The bars are color-coded, with polyethylene (PE) shown in light blue and polypropylene (PP) in blue.

Appendix C: Supporting information to Chapter 5

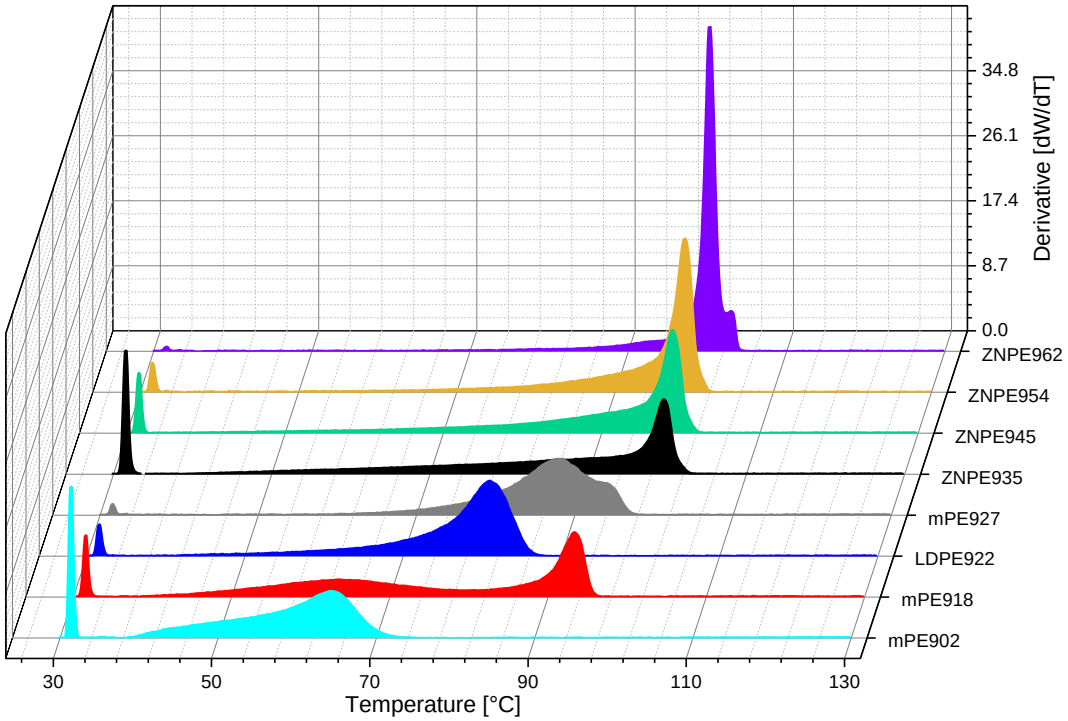

Figure S1 Neat PE grades employed in this work, and their TREF elution profiles (materials with high density on the top, materials with low density on the bottom).

Table S7 TREF elution detained information extracted from the Polymer Char device software for data analysis.

Material	SF 30-35°C [%]	T1 35-90°C [%]	T2 90-95°C [%]	T3 95-110°C [%]	Mp [°C]
ZNPE962	0.4	5.5	4.6	89.5	100.3
ZNPE954	2.7	22.8	15.2	59.2	98.8
ZNPE945	5.6	34.8	14.7	44.9	98.9
ZNPE935	12.0	43.4	10.8	33.7	99.5
mPE927	1.0	72.3	23.4	3.3	88.4
LDPE922	2.9	97.1	0.0	0.0	80.9
mPE918	5.7	63.8	29.3	1.2	93.3
mPE902	12.3	87.7	0.0	0.0	64.7

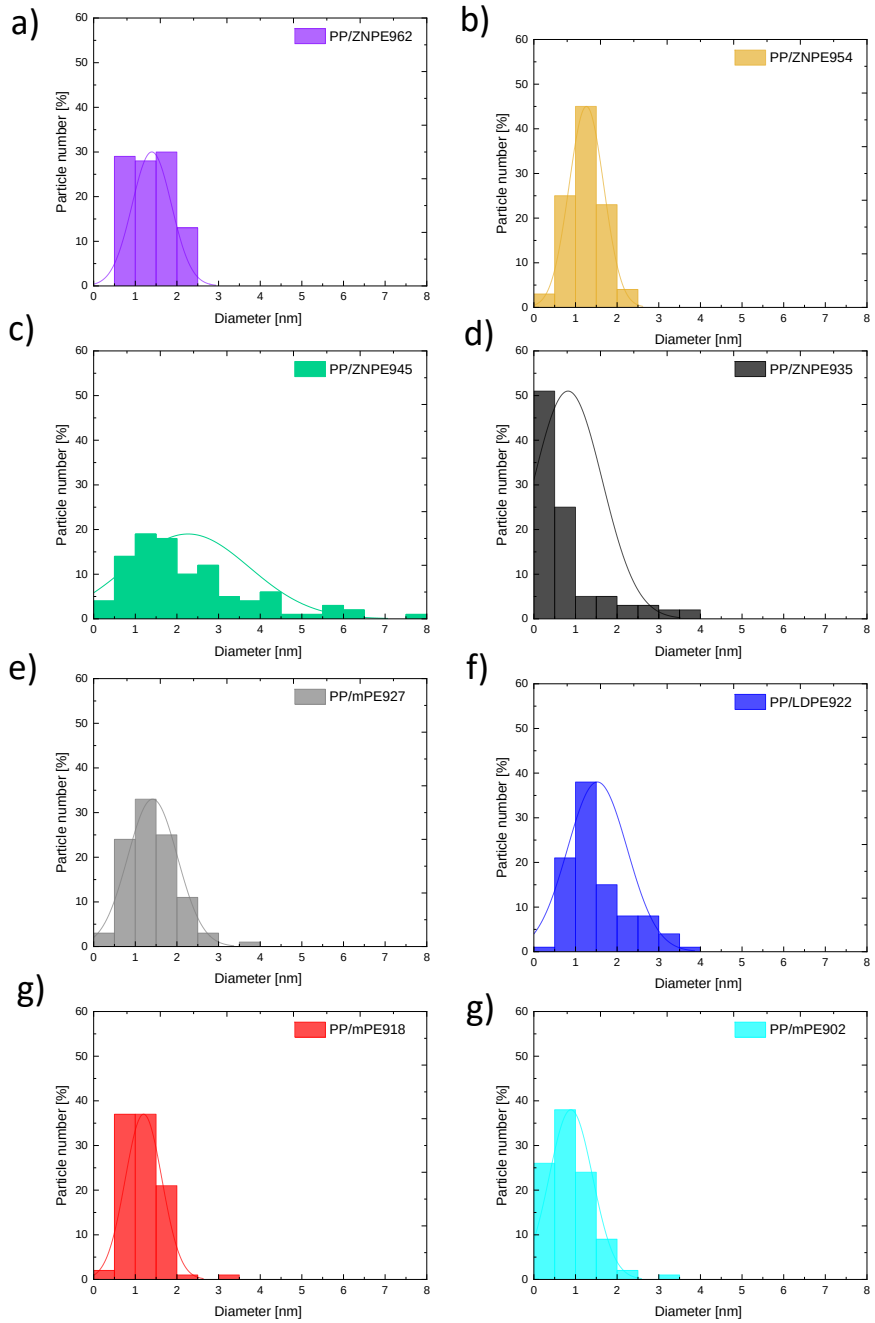

Figure S2 Particle size distribution of the PE dispersed in the PP matrix for all PE grades used in this study.

Table S2 Number-average (d_n) and volume-average (d_v) diameters, particle size distribution (D) of the blends.

Material	d_n **[µm]**	d_v **[µm]**	***D***
PP/ZNPE962	1.8	1.5	1.2
PP/ZNPE954	1.6	1.3	1.3
PP/ZNPE945	4.8	2.0	2.4
PP/ZNPE935	2.9	1.0	3.0
PP/mPE927	2.1	1.4	1.5
PP/LDPE922	2.9	1.5	1.9
PP/mPE918	1.7	1.2	1.5
PP/mPE902	1.9	0.9	2.2

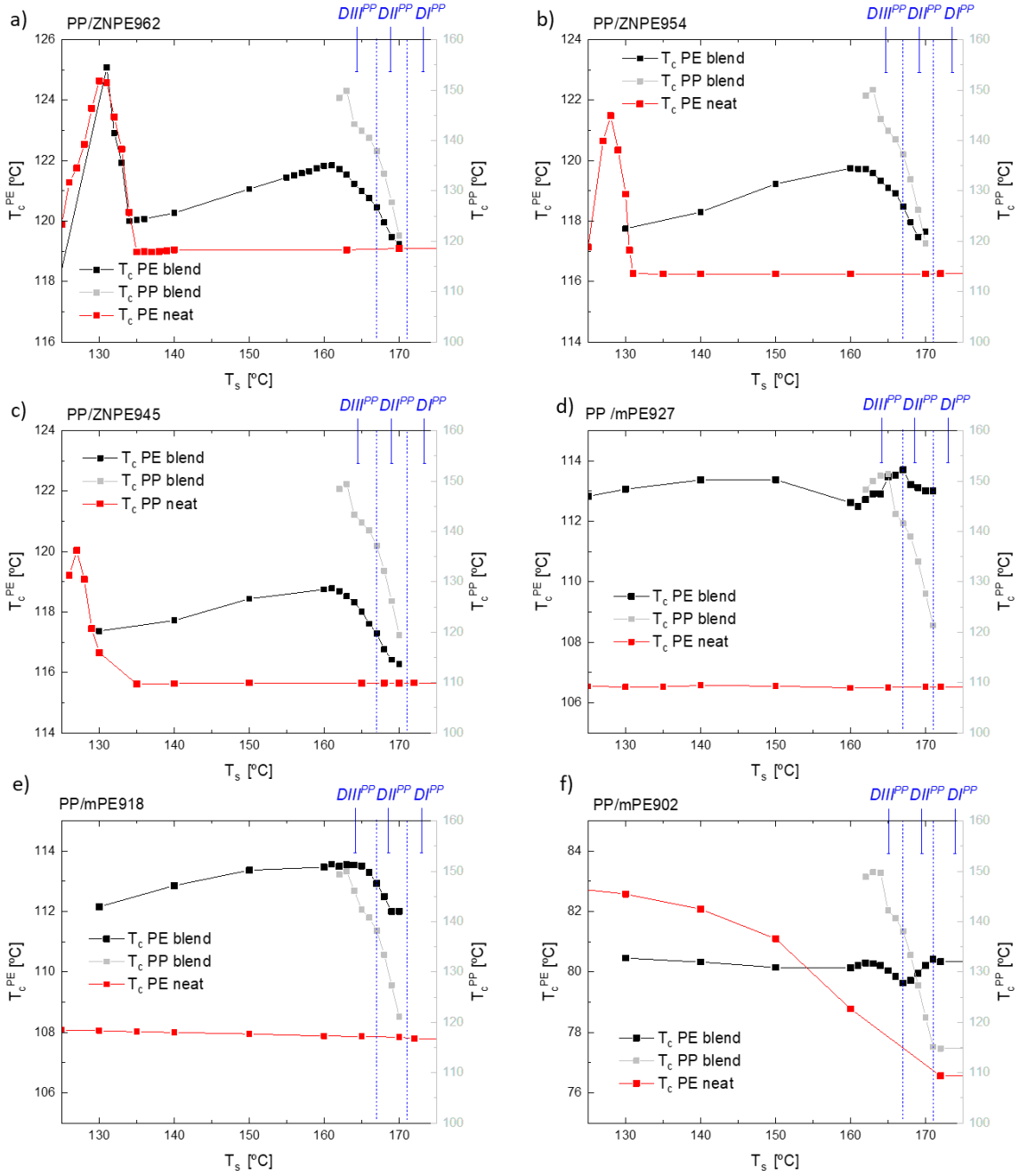

Figure S3 Crystallization temperature (T_c) values of PE phase in the blend (black dots, left y-axis) and PP phase (grey dots, right y-axis) and of neat PE (red symbols) as a function of T_s for a) PP/ZNPE962; b) PP/ZNPE954 c) PP/ZNPE945 d) PP/PE927 e) PP/mPE918 f) PP/mPE902; The different self- nucleation Domains of PP are also indicated.

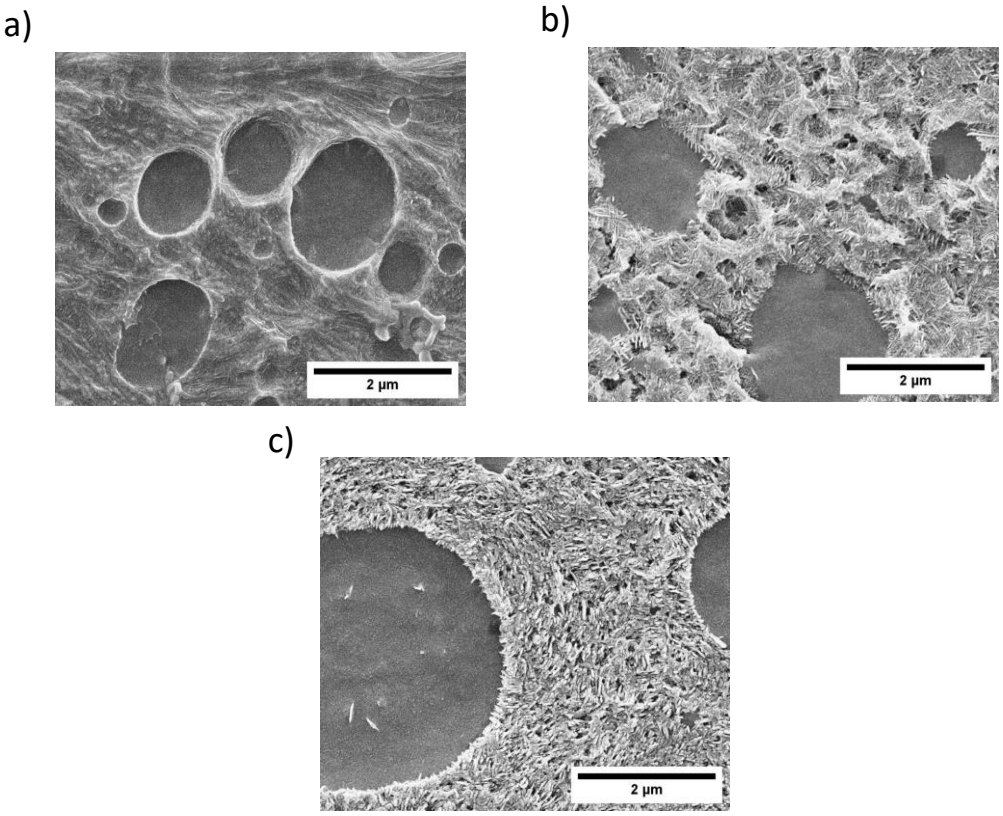

Figure S4 SEM images of the PP/mPE902 blend after cooling from selected T_s a) 225°C; b) 167°C; c) 161°C.

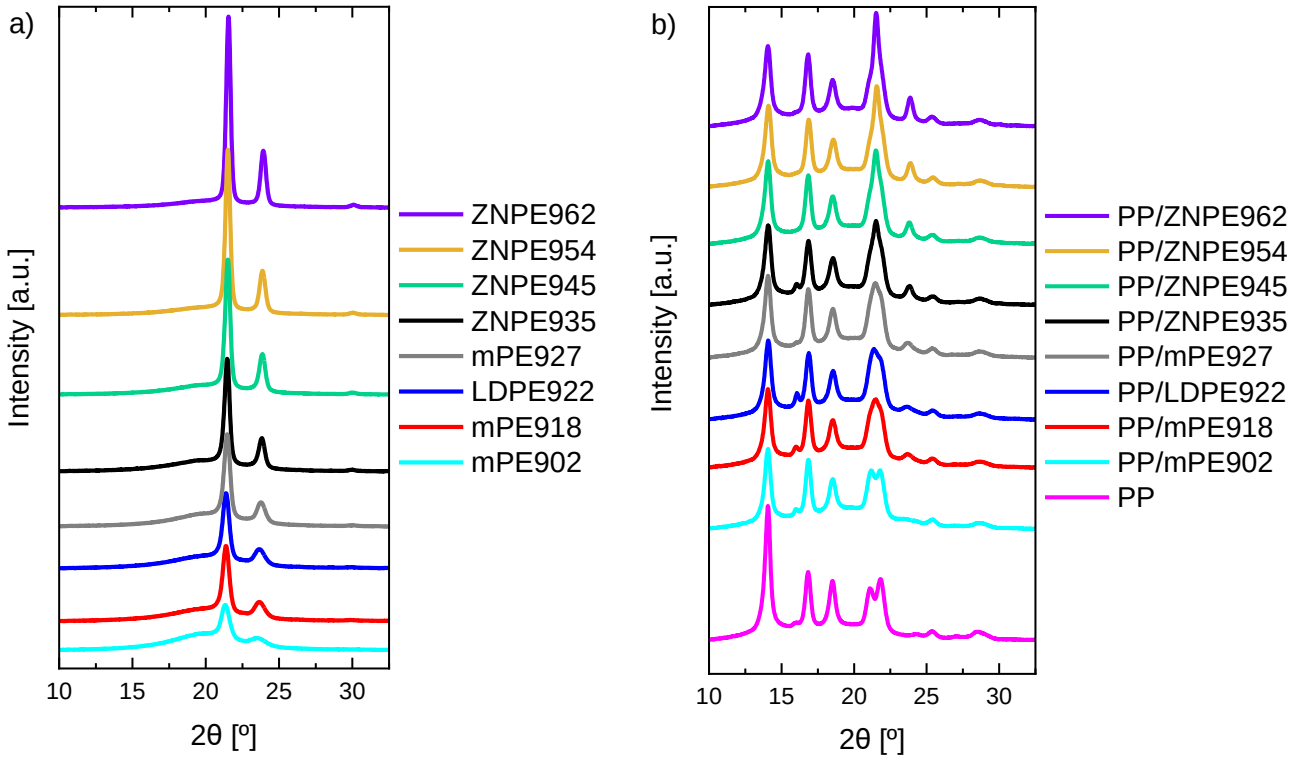

Figure S5 WAXD profiles of PE grades a) and iPP and PP/PE 80:20 blend from the respective PE and iPP grades.